

UNCLASSIFIED

WT-115

Copy 202 A

OPERATION

GREENHOUSE

SCIENTIFIC DIRECTOR'S REPORT

ANNEX 4.1 CLOUD STUDIES

PARTS I, II, AND III

NUCLEAR
EXPLOSIONS

1951

DECLASSIFIED BY DNA (ISTS)
DISTRIBUTION STATEMENT A APPLIES

DATE

Reproduced From
Best Available Copy

UNCLASSIFIED

20000202 080

DISTRIBUTION STATEMENT
Approved for Public Release
Distribution Unlimited



Defense Special Weapons Agency
6801 Telegraph Road
Alexandria, Virginia 22310-3398

UNCLASSIFIED

TRC

24 October 1997

MEMORANDUM FOR DEFENSE TECHNICAL INFORMATION CENTER
ATTENTION: OMI/Mr. William Bush

SUBJECT: Submission of WT-511 to DTIC

The Defense Special Weapons Agency has declassified the following report:

WT-115
OPERATION GREENHOUSE, Scientific Director's Report,
Annex 4.1, Cloud Studies, Parts I, II, and III, Nuclear
Explosions, 1951.

Distribution statement "A" now applies.

Since DTIC does not appear on the distribution of this report, this office is submitting a copy for entry into the system.

Attachment:
A/S

Arduith Jarrett
ARDITH JARRETT
Chief, Technical Research Center

UNCLASSIFIED

UNCLASSIFIED

If this report is no longer needed, return it to
AEC Technical Information Service
P. O. Box 401
Oak Ridge, Tennessee

UNCLASSIFIED

UNCLASSIFIED

WT-115

This document consists of 188 plus 4 pages
(counting preliminary pages)

No. 202 of 245 copies, Series A

**Scientific Director's Report
of Atomic Weapon Tests
at Eniwetok, 1951**

Annex 4.1

Cloud Studies

Parts I, II, and III

UNCLASSIFIED



CLOUD STUDIES

PARTS I, II, AND III

Approved by: PETER H. WYCKOFF
Director, Program 4

Approved by: ALVIN C. GRAVES
Scientific Director

Air Force Cambridge Research Center
University of California at Los Angeles
Edgerton, Germeshausen & Grier, Inc.

CONTENTS

	Page
PART I — CLOUD PHYSICS	
ACKNOWLEDGMENTS	3
ABSTRACT	5
CHAPTER 1 INTRODUCTION	7
1.1 Purpose of Project 4.1A	7
1.2 Basic Theory	7
CHAPTER 2 MEASUREMENT PROGRAM	11
2.1 Aircraft Instruments	11
2.2 Aerograph System	11
2.3 Aircraft Aerograph Installation	14
CHAPTER 3 EXPERIMENTAL PROCEDURE	20
3.1 Calibration of Aerograph	20
3.1.1 Static Errors	20
3.1.2 Dynamic Errors	20
3.1.3 Over-all Accuracy	22
3.2 Data Analysis	25
3.2.1 Preflight Operations	25
3.2.2 Postflight Analysis	27
CHAPTER 4 TEST RESULTS	29
4.1 General Operations Procedures	29
4.2 Aerograph-data Reduction Problems	29
4.3 Dog Shot	30
4.4 Easy Shot	30
4.5 George Shot	41
CHAPTER 5 DISCUSSION OF RESULTS	42
5.1 Introduction	42
5.2 Dog Shot Cloud	42
5.2.1 General Description of Cloud	42
5.2.2 Microstructure of the Dog Cloud Stem	43
5.2.3 Effect of Aging on Dog Cloud Properties	46

CONTENTS (Continued)

	Page
5.3 Easy Shot Cloud	48
5.3.1 General Description of Cloud	48
5.3.2 Microstructure of Easy Cloud	49
5.3.3 Aging of Easy Cloud	54
5.4 George Shot Cloud	54
5.4.1 General Description of George Cloud	54
5.4.2 Microstructure of the George Cloud Stem	55
5.4.3 Effect of Aging on George Cloud	60
CHAPTER 6 CONCLUSIONS	62
6.1 Summary of Aerograph Results	62
6.1.1 Relation of Traverses to Cloud Geometry	62
6.1.2 Effect of State of Atmosphere on the Properties of the Atomic Cloud	62
6.1.3 Temperatures Inside the Atomic Cloud	62
6.1.4 Turbulence Inside the Atomic Cloud	62
6.2 Formation of Rain in an Atomic Cloud	62
CHAPTER 7 RECOMMENDATIONS	64
7.1 Future Instrumentation	64
7.2 Additional Studies on the Atomic Cloud	64

PART II — DEVELOPMENT OF THE ATOMIC CLOUD

PREFACE	67
ACKNOWLEDGMENTS	69
ABSTRACT	71
CHAPTER 1 OBSERVATIONAL DATA	73
1.1 Objectives of Greenhouse Project 4.1B	73
1.2 Surface Visual Observations at Greenhouse	73
1.3 Surface Photographic Network at Greenhouse	74
1.3.1 Location of Sites	74
1.3.2 Description of the Cameras	75
1.3.3 Photographic Exposures	75
1.4 Aerial Observations at Greenhouse	76
1.5 Auxiliary Meteorological Data	76
1.6 Data from Previous Atomic Explosions	76
CHAPTER 2 RISE OF THE ATOMIC CLOUD	78
2.1 Main Features of the Initial Growth and Rise of a Tower Burst	78
2.2 Rate of Rise	79
2.3 Maximum Altitude	79
2.4 Internal Circulation of the Cloud	83

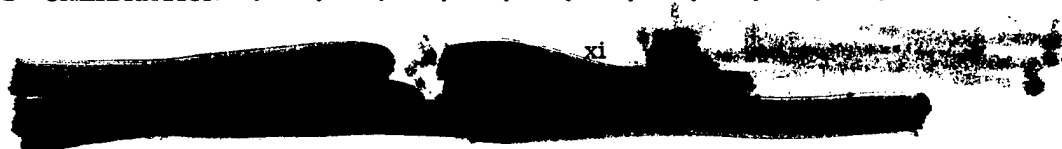


CONTENTS (Continued)

	Page
CHAPTER 3 DISPERSION OF THE ATOMIC CLOUD	87
3.1 Effects of Wind, Wind Shear, and Diffusion	87
3.2 Dog Shot	88
3.2.1 General	88
3.2.2 Meteorological Conditions	88
3.2.3 Rise and Development	88
3.3 Easy Shot	98
3.3.1 General	98
3.3.2 Meteorological Conditions	98
3.3.3 Rise and Development	99
3.4 George Shot	101
3.4.1 General	101
3.4.2 Meteorological Conditions	111
3.4.3 Rise and Development	112
3.5 Item Shot	115
3.5.1 General	115
3.5.2 Meteorological Conditions	128
3.5.3 Rise and Development	130
CHAPTER 4 SUMMARY AND CONCLUSIONS	133
4.1 Summary	133
4.2 Conclusions and Recommendations	133
APPENDIX A RECORD OF CAMERA EXPOSURES, ORIENTATIONS, AND OPERATING RESULTS	136
APPENDIX B METHOD OF DETERMINING DISTANCES AND HEIGHTS FROM THE PHOTOGRAPHS	141
B.1 Determining Angles from the Photographs	141
B.2 Determining Heights from the Angles	141
B.3 Obtaining Fixes on the Cloud	143
APPENDIX C TENTATIVE EXPLANATION OF THE HOVER OF AN ATOMIC CLOUD	144
C.1 Observations	144
C.2 General Considerations	144
C.3 Estimates of the Internal Accelerations in a Fireball	146
APPENDIX D CALCULATIONS ON THE RISE AND GROWTH OF AN ATOMIC CLOUD	148
D.1 Assumptions and Derivations of the Equations	148
D.2 Calculations of Temperatures Inside the Cloud	149

PART III - CLOUD-TRACKING PHOTOGRAPHY

1 DOCUMENTATION OF THE CLOUD	153
2 CALIBRATION	153



CONTENTS (Continued)

	Page
3 ASPECTS OF CLOUD-TRACKING ANALYSIS	153
4 OPERATION	161
5 DATA AND DISCUSSION	161
5.1 Dog Shot	161
5.2 Easy Shot	161
5.3 George Shot	172

ILLUSTRATIONS

PART I - CLOUD PHYSICS

CHAPTER 1 INTRODUCTION

1.1 Collection-efficiency Dependence on the Reynolds Number	8
1.2 Collection Efficiency of Falling Raindrops	9

CHAPTER 2 MEASUREMENT PROGRAM

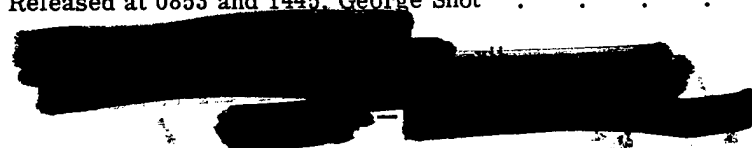
2.1 Block Diagram of Aerograph	12
2.2 Aerograph Probe	12
2.3 Probe Installation, TB-17	15
2.4 Cathode Follower, TB-17	15
2.5 Temperature-Humidity Transmitter, TB-17	16
2.6 Pressure-Airspeed Transmitter, TB-17	16
2.7 Recorder, TB-17	17
2.8 Recorder with Cover Removed, TB-17	17
2.9 Probe Installation, T-33	18
2.10 Temperature-Humidity Transmitter Mounting, T-33	18
2.11 Recorder, T-33	19

CHAPTER 3 EXPERIMENTAL PROCEDURE

3.1 Dynamic Heating in the Probe	23
3.2 Calibration Flight of H-drone Compared with Raob of the Same Day	24
3.3 Calibration Flight of K-drone Compared with Raob of the Same Day	24
3.4 Calibration Flight of B-drone Compared with Radiosonde of the Same Day.	24
3.5 Relative Humidity Reported on Calibration Flights of H-, B-, and K-drones Compared with Raob of the Same Day.	25
3.6 Aerograph Record of Relative Humidity, Flight Through Cumulus Clouds	25
3.7 Effect of Exposure on Carbon Element	26
3.8 Temperature-Humidity Test Chamber	26

CHAPTER 4 TEST RESULTS

4.1 Comparison of Drone Data Just Prior to Cloud Entry with Radiosondes Released at 0034 and 0900, Dog Shot	33
4.2 Comparison of Drone Data Just Prior to Cloud Entry with Radiosondes Released at 0551 and 0845, Easy Shot	34
4.3 Comparison of Drone Data Just Prior to Cloud Entry with Radiosondes Released at 0853 and 1445, George Shot	40



ILLUSTRATIONS (Continued)

Page

CHAPTER 5 DISCUSSION OF RESULTS

5.1	Cross Section of Dog Cloud at 16,000 Ft, First Pass	44
5.2	Cross Section of Dog Cloud at 18,000 Ft, First Pass	44
5.3	Cross Section of Dog Cloud at 20,000 Ft, First Pass	44
5.4	Cross Section of Dog Cloud at 22,000 Ft, First Pass	44
5.5	Cross Section of Dog Cloud at 24,000 Ft, First Pass	45
5.6	Cross Section of Dog Cloud at 26,000 Ft, First Pass	45
5.7	Cross Section of Dog Cloud at 28,000 Ft, First Pass	45
5.8	Cross Section of Dog Cloud at 30,000 Ft, First Pass	45
5.9	Cross Section of Dog Cloud at 16,000 Ft, Second Pass	47
5.10	Cross Section of Dog Cloud at 18,000 Ft, Second Pass	47
5.11	Cross Section of Dog Cloud at 20,000 Ft, Second Pass	47
5.12	Cross Section of Dog Cloud at 24,000 Ft, Second Pass	47
5.13	Cross Section of Dog Cloud at 28,000 Ft, Second Pass	48
5.14	Cross Section of Dog Cloud at 30,000 Ft, Second Pass	48
5.15	Altitude Distribution of Relative Humidity As a Function of Time of Penetration, Dog Cloud	48
5.16	Cross Section of Easy Cloud at 18,000 Ft, First Pass	49
5.17	Cross Section of Easy Cloud at 20,000 Ft, First Pass	50
5.18	Cross Section of Easy Cloud at 22,000 Ft, First Pass	50
5.19	Cross Section of Easy Cloud at 24,000 Ft, First Pass	51
5.20	Cross Section of Easy Cloud at 26,000 Ft, First Pass	51
5.21	Cross Section of Easy Cloud at 28,000 Ft, First Pass	51
5.22	Cross Section of Easy Cloud at 30,000 Ft, First Pass	51
5.23	Cross Section of Easy Cloud at 16,000 Ft, Second Pass	52
5.24	Cross Section of Easy Cloud at 18,000 Ft, Second Pass	52
5.25	Cross Section of Easy Cloud at 20,000 Ft, Second Pass	52
5.26	Cross Section of Easy Cloud at 22,000 Ft, Second Pass	52
5.27	Cross Section of Easy Cloud at 24,000 Ft, Second Pass	53
5.28	Cross Section of Easy Cloud at 26,000 Ft, Second Pass	53
5.29	Cross Section of Easy Cloud at 28,000 Ft, Second Pass	53
5.30	Cross Section of Easy Cloud at 30,000 Ft, Second Pass	53
5.31	Altitude Distribution of Relative Humidity As a Function of Time of Penetration, Easy Cloud	54
5.32	Cross Section of George Cloud at 16,000 Ft, First Pass	56
5.33	Cross Section of George Cloud at 18,000 Ft, First Pass	56
5.34	Cross Section of George Cloud at 20,000 Ft, First Pass	57
5.35	Cross Section of George Cloud at 22,000 Ft, First Pass	57
5.36	Cross Section of George Cloud at 24,000 Ft, First Pass	57
5.37	Cross Section of George Cloud at 26,000 Ft, First Pass	57
5.38	Cross Section of George Cloud at 28,000 Ft, First Pass	58
5.39	Cross Section of George Cloud at 16,000 Ft, Second Pass	58
5.40	Cross Section of George Cloud at 18,000 Ft, Second Pass	58
5.41	Cross Section of George Cloud at 20,000 Ft, Second Pass	58
5.42	Cross Section of George Cloud at 22,000 Ft, Second Pass	59
5.43	Cross Section of George Cloud at 24,000 Ft, Second Pass	59
5.44	Cross Section of George Cloud at 26,000 Ft, Second Pass	59
5.45	Cross Section of George Cloud at 28,000 Ft, Second Pass	59
5.46	Altitude Distribution of Liquid Water As a Function of Time of Penetration, George Cloud	60
5.47	Altitude Distribution of Relative Humidity As a Function of Time of Penetration, George Cloud	60

ILLUSTRATIONS (Continued)

Page

PART II - DEVELOPMENT OF THE ATOMIC CLOUD

CHAPTER 1 OBSERVATIONAL DATA

1.1 Map of Eniwetok Atoll, Showing Observational and Camera Sites and Their Relation to the Shot Points	73
1.2 Nomenclature of the Atomic Cloud	74

CHAPTER 2 RISE OF THE ATOMIC CLOUD

2.1 Height of Tops of Clouds As a Function of Time, Operation Greenhouse	80
2.2 Height of Tops of Clouds As a Function of Time, Operations Sandstone and Trinity.	80
2.3 Rate of Rise of Tops of Clouds As a Function of Time	81
2.4 Diameter and Depth of Mushroom Clouds As a Function of Time	82
2.5 Ratio of Observed Radius to Observed Depth of Mushrooms As a Function of Time	82
2.6 Rise and Vertical Growth of the Easy and George Clouds	83
2.7 Schematic Representation of the Velocity Field of a Rising Atomic Cloud	85

CHAPTER 3 DISPERSION OF THE ATOMIC CLOUD

3.1 Wind Diagram for Dog Shot (8 April 1951)	89
3.2 Radiosonde for Dog Shot (8 April 1951, 0900M)	90
3.3 Sequence of Photographs of the Rising Atomic Cloud, Dog Shot	91
3.4 Shape of Dog Cloud at One-half Hour	96
3.5 Detail of the Development of Dog Cloud Between 35,000 and 40,000 Ft	97
3.6 Wind Diagram for Easy Shot (21 April 1951, 0600M and 0900M)	99
3.7 Radiosonde for Easy Shot (21 April 1951, 0600M)	100
3.8 Sequence of Photographs of the Rising Atomic Cloud, Easy Shot	102
3.9 Shape of Easy Cloud at One-half Hour	111
3.10 Comparison Between the Actual Movement of the Top of Easy Cloud and the Movement Predicted on the Basis of the Upper-wind Observations	112
3.11 Wind Diagram for George Shot (9 May 1951, 0900M and 1000M)	113
3.12 Radiosonde for George Shot (9 May 1951, 0900M)	114
3.13 Sequence of Photographs of the Rising Atomic Cloud, George Shot	116
3.14 Shape of George Cloud at One-half Hour	127
3.15 Detail of the Development of the Skirt, George Shot	128
3.16 Wind Diagram for Item Shot (25 May 1951, 0600M and 0845M)	129
3.17 Radiosonde for Item Shot (25 May 1951, 1500M)	130
3.18 Shape of Item Cloud at One-half Hour	131

APPENDIX A RECORD OF CAMERA EXPOSURES, ORIENTATIONS, AND OPERATING RESULTS

A.1 Diagram of Camera Orientations	139
--	-----

APPENDIX B METHOD OF DETERMINING DISTANCES AND HEIGHTS FROM THE PHOTOGRAPHS

B.1 Diagram of the Optical System of a Camera, Showing the Relation Between the Various Angles and Distances	142
--	-----

Distribution

Military Distribution Categories 5-40, 5-70, 5-80 and 5-90

ARMY ACTIVITIES

Asst. Chief of Staff, G-3, D/A, Washington 25, D.C. ATTN: Dep. CofS, G-3 (RR&SW)	1
Chief of Research and Development, D/A, Washington 25, D.C. ATTN: Special Weapons and Air Defense Division	2
Chief of Ordnance, D/A, Washington 25, D.C. ATTN: ORDTX-AR	3
Chief Signal Officer, D/A, P&O Division, Washington 25, D.C. ATTN: SIGOP	4-6
The Surgeon General, D/A, Washington 25, D.C. ATTN: Chief, R&D Division	7
Chief Chemical Officer, D/A, Washington 25, D.C.	8-9
The Quartermaster General, CBR, Liaison Officer, Research and Development Div., D/A, Washington 25, D.C.	10-11
Chief of Engineers, D/A, Washington 25, D.C. ATTN: ENGNB	12-16
Chief of Transportation, Military Planning and Intelligence Div., Washington 25, D.C.	17
Commanding General, Continental Army Command, Ft. Monroe, Va.	18-20
President, Board #1, Headquarters, Continental Army Command, Ft. Bragg, N.C.	21
President, Board #2, Headquarters, Continental Army Command, Ft. Knox, Ky.	22
President, Board #3, Headquarters, Continental Army Command, Ft. Benning, Ga.	23
President, Board #4, Headquarters, Continental Army Command, Ft. Bliss, Tex.	24
Commanding General, First Army, Governor's Island, New York 4, N.Y.	25
Commanding General, Second Army, Ft. George G. Meade, Md.	26
Commanding General, Third Army, Ft. McPherson, Ga. ATTN: ACofS, G-3	27
Commanding General, Fourth Army, Ft. Sam Houston, Tex. ATTN: G-3 Section	28
Commanding General, Fifth Army, 1660 E. Hyde Park Blvd., Chicago 15, Ill.	29
Commanding General, Sixth Army, Presidio of San Francisco, Calif. ATTN: AMGCT-4	30
Commanding General, U.S. Army Caribbean, Ft. Amador, C.Z. ATTN: Cml. Off.	31
Commanding General, USARFANT & MDP, Ft. Brooke, Puerto Rico	32
Commanding General, U.S. Forces Austria, APO 168, c/o PM, New York, N.Y. ATTN: ACofS, G-3	33
Commander-in-Chief, Far East Command, APO 500, c/o PM, San Francisco, Calif. ATTN: ACofS, J-3	34-35
Commanding General, U.S. Army Forces Far East (Main), APO 343, c/o PM, San Francisco, Calif. ATTN: ACofS, G-3	36
Commanding General, U.S. Army Alaska, APO 942, c/o PM, Seattle, Wash.	37
Commanding General, U.S. Army Europe, APO 403, c/o PM, New York, N.Y. ATTN: OPOT Div., Combat Dev. Br.	38-39
Commanding General, U.S. Army Pacific, APO 958, c/o PM, San Francisco, Calif. ATTN: Cml. Off.	40-41
Commandant, Command and General Staff College, Ft. Leavenworth, Kan. ATTN: ALLLS(AS)	42-43
Commandant, Army War College, Carlisle Barracks, Pa. ATTN: Library	44
Commandant, The Artillery and Guided Missile School, Ft. Sill, Okla.	45
Secretary, The Antiaircraft Artillery and Guided Missile School, Ft. Bliss, Texas. ATTN: Lt. Col. Albert D. Epley, Dept. of Tactics and Combined Arms	46
Commanding General, Medical Field Service School, Brooke Army Medical Center, Ft. Sam Houston, Tex.	47

Director, Special Weapons Development Office, Headquarters, CONARC, Ft. Bliss, Tex.	
ATTN: Lt. Arthur Jaskierny	48
Commandant, Army Medical Service Graduate School, Walter Reed Army Medical Center, Washington 25, D.C.	49
Superintendent, U.S. Military Academy, West Point, N.Y. ATTN: Prof. of Ordnance	50
Commandant, Chemical Corps School, Chemical Corps Training Command, Ft. McClellan, Ala.	51
Commanding General, Research and Engineering Command, Army Chemical Center, Md.	
ATTN: Deputy for RW and Non-Toxic Material	52-53
Commanding General, Aberdeen Proving Grounds, Md. (inner envelope) ATTN: RD Control Officer (for Director, Ballistics Research Laboratory)	54-55
Commanding General, The Engineer Center, Ft. Belvoir, Va. ATTN: Asst. Commandant, Engineer School	56-58
Commanding Officer, Engineer Research and Development Laboratory, Ft. Belvoir, Va.	
ATTN: Chief, Technical Intelligence Branch	59
Commanding Officer, Picatinny Arsenal, Dover, N.J. ATTN: ORDBB-TK	60
Commanding Officer, Frankford Arsenal, Philadelphia 37, Pa. ATTN: Col. Tewes Kundel	61
Commanding Officer, Army Medical Research Laboratory, Ft. Knox, Ky.	62
Commanding Officer, Chemical Corps Chemical and Radiological Laboratory, Army Chemical Center, Md. ATTN: Tech. Library	63-64
Commanding Officer, Transportation R&D Station, Ft. Eustis, Va.	65
Commandant, The Transportation School, Ft. Eustis, Va. ATTN: Security and Information Officer	66
Director, Technical Documents Center, Evans Signal Laboratory, Belmar, N.J.	67
Director, Waterways Experiment Station, PO Box 631, Vicksburg, Miss. ATTN: Library	68
Director, Operations Research Office, Johns Hopkins University, 7100 Connecticut Ave., Chevy Chase, Md., Washington 15, D.C. ATTN: Library	69
Technical Information Service, Oak Ridge, Tenn. (Surplus)	70-76

NAVY ACTIVITIES

Chief of Naval Operations, D/N, Washington 25, D.C. ATTN: OP-36	77-78
Chief of Naval Operations, D/N, Washington 25, D.C. ATTN: OP-03EG	79
Director of Naval Intelligence, D/N, Washington 25, D.C. ATTN: OP-922V	80
Chief, Bureau of Medicine and Surgery, D/N, Washington 25, D.C. ATTN: Special Weapons Defense Div.	81
Chief, Bureau of Ordnance, D/N, Washington 25, D.C.	82
Chief of Naval Personnel, D/N, Washington 25, D.C.	83
Chief, Bureau of Ships, D/N, Washington 25, D.C. ATTN: Code 348	84-85
Chief, Bureau of Yards and Docks, D/N, Washington 25, D.C. ATTN: D-440	86
Chief, Bureau of Supplies and Accounts, D/N, Washington 25, D.C.	87
Chief, Bureau of Aeronautics, D/N, Washington 25, D.C.	88-89
Chief of Naval Research, Department of the Navy Washington 25, D.C. ATTN: LT(jg) F. McKee, USN	90
Commander-in-Chief, U.S. Pacific Fleet, Fleet Post Office, San Francisco, Calif.	91
Commander-in-Chief, U.S. Atlantic Fleet, U.S. Naval Base, Norfolk 11, Va.	92
Commandant, U.S. Marine Corps, Washington 25, D.C. ATTN: Code A03H	93-96
President, U.S. Naval War College, Newport, R.I.	97
Superintendent, U.S. Naval Postgraduate School, Monterey, Calif.	98
Commanding Officer, U.S. Naval Schools Command, U.S. Naval Station, Treasure Island, San Francisco, Calif.	99
Commanding Officer, U.S. Fleet Training Center, Naval Base, Norfolk 11, Va. ATTN: Special Weapons School	100
Commanding Officer, U.S. Fleet Training Center, Naval Station, San Diego 36, Calif. ATTN: (SPWP School)	101-102
Commanding Officer, Air Development Squadron 5, VX-5, U.S. Naval Air Station, Moffett Field, Calif.	103
Commanding Officer, U.S. Naval Damage Control Training Center, Naval Base, Philadelphia 12, Pa. ATTN: ABC Defense Course	104
Commanding Officer, U.S. Naval Unit, Chemical Corps School, Army Chemical Training Center, Ft. McClellan, Ala.	105
Commander, U.S. Naval Ordnance Laboratory, Silver Spring 19, Md. ATTN: EH	106
Commander, U.S. Naval Ordnance Laboratory, Silver Spring 19, Md. ATTN: R	107

Commander, U.S. Naval Ordnance Test Station, Inyokern, China Lake, Calif.	108
Officer-in-Charge, U.S. Naval Civil Engineering Res. and Evaluation Lab., U.S. Naval Construction Battalion Center, Port Hueneme, Calif. ATTN: Code 753	109
Commanding Officer, U.S. Naval Medical Research Inst., National Naval Medical Center, Bethesda 14, Md.	110
Director, U.S. Naval Research Laboratory, Washington 25, D.C. ATTN: Code 2029	111
Director, The Material Laboratory, New York Naval Shipyard, Brooklyn, N.Y.	112
Commanding Officer and Director, U.S. Navy Electronics Laboratory, San Diego 52, Calif. ATTN: Code 4223	113
Commanding Officer, U.S. Naval Radiological Defense Laboratory, San Francisco 24, Calif. ATTN: Technical Information Division	114-117
Officer-in-Charge, Special Weapons Supply Depot, U.S. Naval Supply Center, Norfolk 11, Va.	118
Commanding Officer and Director, David W. Taylor Model Basin, Washington 7, D.C. ATTN: Library	119
Commanding Officer, U.S. Naval Photographic Center, Anacostia, D.A.	120-121
Commander, U.S. Naval Air Development Center, Johnsville, Pa.	122
Director, Office of Naval Research Branch Office, 1000 Geary St., San Francisco, Calif.	123
Commanding Officer, Clothing Supply Office, Code 1D-0, 3rd Avenue and 29th St., Brooklyn, N.Y.	124
Commandant, U.S. Coast Guard, 1300 E. St. N.W., Washington 25, D.C. ATTN: Capt. J. R. Stewart	125
Technical Information Service, Oak Ridge, Tenn. (Surplus)	126-132

AIR FORCE ACTIVITIES

Asst. for Atomic Energy, Headquarters, USAF, Washington 25, D.C. ATTN: DCS/O	133
Director of Operations, Headquarters, USAF, Washington 25, D.C. ATTN: Operations Analysis	134
Director of Plans, Headquarters, USAF, Washington 25, D.C. ATTN: War Plans Div.	135
Director of Research and Development, Headquarters, USAF, Washington 25, D.C. ATTN: Combat Components Div.	136
Director of Intelligence, Headquarters, USAF, Washington 25, D.C. ATTN: AFOIN-IB2	137-138
The Surgeon General, Headquarters, USAF, Washington 25, D.C. ATTN: Bio. Def. Br., Pre. Med. Div.	139
Deputy Chief of Staff, Intelligence, Headquarters, U.S. Air Forces Europe, APO 633, c/o PM, New York, N.Y. ATTN: Directorate of Air Targets	140
Commander, 497th Reconnaissance Technical Squadron (Augmented), APO 633, c/o PM, New York, N.Y.	141
Commander, Far East Air Forces, APO 925, c/o PM, San Francisco, Calif.	142
Commander-in-Chief, Strategic Air Command, Offutt Air Force Base, Omaha, Nebraska. ATTN: Special Weapons Branch, Inspection Div., Inspector General	143
Commander, Tactical Air Command, Langley AFB, Va. ATTN: Documents Security Branch	144
Commander, Air Defense Command, Ent AFB, Colo.	145
Commander, Wright Air Development Center, Wright-Patterson AFB, Dayton, O. ATTN: WCCRN, Blast Effects Research	146-147
Commander, Air Training Command, Scott AFB, Belleville, Ill. ATTN: DCS/O GTP	148
Assistant Chief of Staff, Installations, Headquarters, USAF, Washington 25, D.C. ATTN: AFCIE-E	149
Commander, Air Research and Development Command, PO Box 1395, Baltimore, Md. ATTN: RDDN	150
Commander, Air Proving Ground Command, Eglin AFB, Fla. ATTN: AG/TRB	151
Director, Air University Library, Maxwell AFB, Ala.	152-153
Commander, Flying Training Air Force, Waco, Tex. ATTN: Director of Observer Training	154-161
Commander, Crew Training Air Force, Randolph Field, Tex. ATTN: 2GTS, DCS/O	162
Commander, Headquarters, Technical Training Air Force, Gulfport, Miss. ATTN: TA&D	163
Commandant, Air Force School of Aviation Medicine, Randolph AFB, Tex.	164-165
Commander, Wright Air Development Center, Wright-Patterson AFB, Dayton, O. ATTN: WCOSI	166-168
Commander, Air Force Cambridge Research Center, 230 Albany Street, Cambridge 39, Mass. ATTN: CRQST-2	169-170
Commander, Air Force Special Weapons Center, Kirtland AFB, N. Mex. ATTN: Library	171-173

Commandant, USAF Institute of Technology, Wright-Patterson AFB, Dayton, O. ATTN: Resident College	174
Commander, Lowry AFB, Denver, Colo. ATTN: Department of Armament Training	175
Commander, 1009th Special Weapons Squadron, Headquarters, USAF, Washington 25, D.C.	176
The RAND Corporation, 1700 Main Street, Santa Monica, Calif. ATTN: Nuclear Energy Division	177-178
Commander, Second Air Force, Barksdale AFB, Louisiana. ATTN: Operations Anal. Office	179
Commander, Eighth Air Force, Westover AFB, Mass. ATTN: Operations Anal. Office	180
Commander, Fifteenth Air Force, March AFB, Calif. ATTN: Operations Anal. Office	181
Technical Information Service, Oak Ridge, Tenn. (Surplus)	182-188
 OTHER DEPARTMENT OF DEFENSE ACTIVITIES	
Asst. Secretary of Defense, Research and Development, D/D, Washington 25, D.C. ATTN: Tech. Library	189
U.S. Documents Officer, Office of the U.S. National Military Representative—SHAPE, APO 55, New York, N.Y.	190
Director, Weapons Systems Evaluation Group, OSD, Rm 2E1006, Pentagon, Washington 25, D.C.	191
Commandant, Armed Forces Staff College, Norfolk 11, Va. ATTN: Secretary	192
Commanding General, Field Command, Armed Forces, Special Weapons Project, PO Box 5100, Albuquerque, N. Mex.	193-198
Commanding General, Field Command, Armed Forces, Special Weapons Project, PO Box 5100, Albuquerque, N. Mex. ATTN: Technical Training Group	199-200
Chief, Armed Forces Special Weapons Project, Washington 25, D.C. ATTN: Document Library Branch	201-209
Commanding General, Military District of Washington, Room 1543, Building T-7, Gravelly Point, Va.	210
Technical Information Service, Oak Ridge, Tenn. (Surplus)	211-217
 ATOMIC ENERGY COMMISSION ACTIVITIES	
U.S. Atomic Energy Commission, Classified Technical Library, 1901 Constitution Ave., Washington 25, D.C. ATTN: Mrs. J. M. O'Leary (For DMA)	218-220
Los Alamos Scientific Laboratory, Report Library, PO Box 1663, Los Alamos, N. Mex. ATTN: Helen Redman	221-222
Sandia Corporation Classified Document Division, Sandia Base, Albuquerque, N. Mex. ATTN: Martin Lucero	223-227
University of California Radiation Laboratory, PO Box 808, Livermore, Calif. ATTN: Margaret Edlund	228-230
Weapon Data Section, Technical Information Service, Oak Ridge, Tenn.	231
Technical Information Service, Oak Ridge, Tenn. (Surplus)	232-245

ILLUSTRATIONS (Continued)

	Page
B.2 Trajectories of the Tops of the Rising Clouds Determined from the Observed Heights and the Observed Upper Winds	142
B.3 Idealized Sketch of the Atomic Cloud, Showing the Method of Correcting for the Angle of View.	143
APPENDIX C TENTATIVE EXPLANATION OF THE HOVER OF AN ATOMIC CLOUD	
C.1 Schematic Representation of Fields of Temperature, Pressure, and Circulation in the Fireball	145

PART III - CLOUD-TRACKING PHOTOGRAPHY

1 Cloud-tracking Stations	154
2 Horizontal Angular Coverage	155
3 Vertical Angular Coverage.	155
4 Stereo Nearness Limits	156
5 Composite Visibility Diagram	157
6 K-24 Camera	158
7 K-8A-B Camera Station	158
8 K-8A-B Camera	159
9 Standard-speed Mitchell 35-mm Camera	159
10 Positioning of Camera Banks	160
11 Cloud-tracking Wiring Diagram.	162
12 Cloud-tracking Control Panel	165
13 Remote Station 192 on Rigili	168

TABLES

PART I - CLOUD PHYSICS

CHAPTER 2 MEASUREMENT PROGRAM

2.1 Calibration of Temperature Channel	13
2.2 Calibration of Humidity Channel	14

CHAPTER 3 EXPERIMENTAL PROCEDURE

3.1 Temperature Correction for True Airspeed from 140 to 308 Mph	22
3.2 Pressure Increments for Calibrated Airspeed from 140 to 300 Mph	23
3.3 Relative-humidity Calibration	24
3.4 Time Comparisons	28

CHAPTER 4 TEST RESULTS

4.1 Cloud Traverses, Dog Shot	31
4.2 Shock-wave Intercept, Dog Shot	34
4.3 Cloud Traverses, Easy Shot	35
4.4 Shock-wave Intercept, Easy Shot	37
4.5 Cloud Traverses, George Shot	38

TABLES (Continued)

Page

CHAPTER 5 DISCUSSION OF RESULTS

5.1	Time Lapse Between Cloud-top Passage and Cloud Penetration, Dog Cloud	42
5.2	Dog Shot Cloud Penetration Times	46
5.3	Time Lapse Between Cloud Passage and Penetration, Easy Cloud	49
5.4	Easy Shot Cloud Penetration Times	50
5.5	Time Lapse Between Cloud Passage and Penetration, George Cloud	55
5.6	George Shot Cloud Penetration Times	56

PART II - DEVELOPMENT OF THE ATOMIC CLOUD

CHAPTER 2 RISE OF THE ATOMIC CLOUD

2.1	Maximum Heights of Atomic Clouds	84
-----	--	----

APPENDIX A RECORD OF CAMERA EXPOSURES, ORIENTATIONS, AND OPERATING RESULTS

A.1	Camera Data for Dog Shot	137
A.2	Camera Data for Easy Shot	138
A.3	Camera Data for George Shot	139

APPENDIX C TENTATIVE EXPLANATION OF THE HOVER OF AN ATOMIC CLOUD

C.1	Accelerations Inside the Fireball	147
-----	---	-----

APPENDIX D CALCULATIONS ON THE RISE AND GROWTH OF AN ATOMIC CLOUD

D.1	Expansion and Entrainment of Easy and George Shots	150
D.2	Expansion of the Trinity Cloud	150

PART III - CLOUD-TRACKING PHOTOGRAPHY

1	Airborne Cloud-tracking Photography, Dog Shot	169
2	Airborne Cloud-tracking Photography, Dog Shot	169
3	Airborne Cloud-tracking Photography, Easy Shot	170
4	Airborne Cloud-tracking Photography, Easy Shot	171
5	Airborne Cloud-tracking Photography, George Shot	171

Part I

CLOUD PHYSICS

by
CHARLES E. ANDERSON
and
PHILIP E. GUSTAFSON

Atmospheric Physics Laboratory
Air Force Cambridge Research Center
Cambridge, Massachusetts

August 1951

Acknowledgments

The success of Project 4.1A depended on reliable operation of the aerograph systems in the drone aircraft. The efforts of the military crew assigned to the installation and maintenance of this equipment cannot be underestimated. Their diligent attention to their jobs resulted in 100 per cent performance of the aerograph systems in all three shots. Much of the credit is due to the spirited cooperation and initiative of Maj H. P. Livingstone, their leader. The men were S/Sgt D. A. Rose, S/Sgt J. E. Wilson, S/Sgt P. E. Renwick, and S/Sgt C. L. Simmons, all from the 3200 Drone Squadron, 550th G. M. Wing, Eglin Air Force Base, Fla. Eugene

Heaney, field representative from the Kollsman Instrument Corp., was extremely helpful in assisting in the maintenance of the aerograph systems.

Finally, acknowledgment is made of the all-round assistance of Paul G. Goldberg, Geophysics Research Directorate, Air Force Cambridge Research Center, Air Research and Development Command, in the procurement and follow-up testing of the aerographs.

The postanalysis of the raw data was accomplished with the assistance of Albert Chmela, who was responsible for reducing most of the data to a more assimilable form.

Abstract

The cloud-physics project was primarily intended to fulfill a requirement for detailed information on the meteorological microstructure of atomic clouds. This requirement arose from the speculation that radioactive material could be deposited by the scavenging action of rain falling from the atomic cloud. More factual information was required on the properties of atomic clouds before definite answers could be given to these questions.

With the time available, advantage had to be taken of existing equipment rather than wait for the development of more suitable gear. Aerographs were chosen as the test equipment since they offered the best solution to the many conditions. These devices were installed in the drone aircraft, and they operated satisfactorily in each of the aircraft on all tests. The equipment measured and recorded the airspeed, air-temperature, relative-humidity, and static-pressure parameters. Inspection of the records led to the conclusion that the majority of the drones penetrated the stem cloud beneath the main mushroom cloud. Confirmation of this conclusion was obtained from the Director of Program 4, who stated that the flights were planned this way since it was feared that se-

vere turbulence in the main cloud would cause a high loss of drone aircraft.

Analyses of data obtained by the aerograph equipment revealed the following conclusions concerning the meteorological properties of atomic clouds.

1. The cloud properties depended greatly on the conditions in the environment air, particularly the moisture content. The stems of both Dog and Easy clouds were found to be dry. George cloud, which was formed in air having high humidities up to 10,000 ft, had a stem cloud composed of water drops.
2. The temperatures inside the stems, even at relatively short times after the explosions, differed very little from ambient temperatures.
3. The circulation of air inside the stem was similar, perhaps, to the circulation inside the core of intense cumulo-nimbus clouds.
4. The possibility of rain falling from an atomic cloud was extremely remote, even in the event of seeding. The root clouds associated with the lower end of the stem clouds could develop as natural convective clouds into shower clouds, but this development depends greatly on the properties of the atmosphere at the time of explosion.



Chapter 1

Introduction

1.1 PURPOSE OF PROJECT 4.1A

The cloud-physics program was initiated to fulfill the requirement for detailed information on the meteorological characteristics of the particulate cloud ensuing from an atomic explosion. This requirement arose from consideration of the important possibility that radioactive matter could be deposited on surface objects by the scavenging action of rain falling through an atomic cloud. Preliminary calculations indicated that this possibility was not too remote. Speculations then arose as to the production of artificial rainfall by appropriate seeding of an atomic cloud. It was strongly felt by some in Air Force Headquarters that a thorough investigation of the susceptibility of an atomic cloud to artificial seeding should be carried out.

In addition, graphic documentation of the atomic clouds of the Crossroads and Sandstone tests was restricted to sketches made by artists. No serious effort had been made to photographically record the development of the cloud throughout its visible history. It was felt that such a photographic documentation would be a valuable adjunct to the other meteorological measurements. This phase was therefore included in the over-all experimental meteorology program to be prosecuted by the Air Force Cambridge Research Center (AFCRC).

1.2 BASIC THEORY

The production of rain by artificial seeding has been a controversial topic among meteorologists since its introduction. This lack of agreement on the merits of cloud seeding has

come about mainly by the absence of a clear, well-defined, and experimentally verified theory of the formation of precipitation in general. The primary problem regarding the origin of precipitation is one of formulating an acceptable hypothesis whereby cloud droplets are converted into raindrops. This involves a transition in mean size of particles from $25\ \mu$ to 1 mm in diameter, a 100-fold increase.

Two theories have been advanced in recent years which qualitatively account for this growth. The first was the Bergeron-Findeisen theory, which has as its basis the concept of a mixed cloud. A mixed cloud is one in which water drops and ice particles coexist. At temperatures below 0°C the vapor pressure over water is greater than that over ice. Consequently evaporation of the water drops and a subsequent sublimation of the vapor on the ice particle occur, resulting in the development of a large particle with a considerable falling speed. As the ice particle or snowflake thus formed falls into air where melting can occur (above 0°C), the water particle resulting is of raindrop size.

The second theory is an extension of the Bergeron-Findeisen theory to include the known fact that larger particles are capable of collecting smaller water drops by an accretion mechanism. This view has been advanced by Langmuir¹ on the basis of theoretical calculations performed by him. He considers the trajectories of drops moving near the surface of other drops with various relative velocities and shows that the collection efficiency (probability that a given-size drop will strike the collector if it is contained in the conical volume swept out by the collector) is a function of several aerodynamic parameters. Chief among these are the fall velocity, the diameter, the vis-

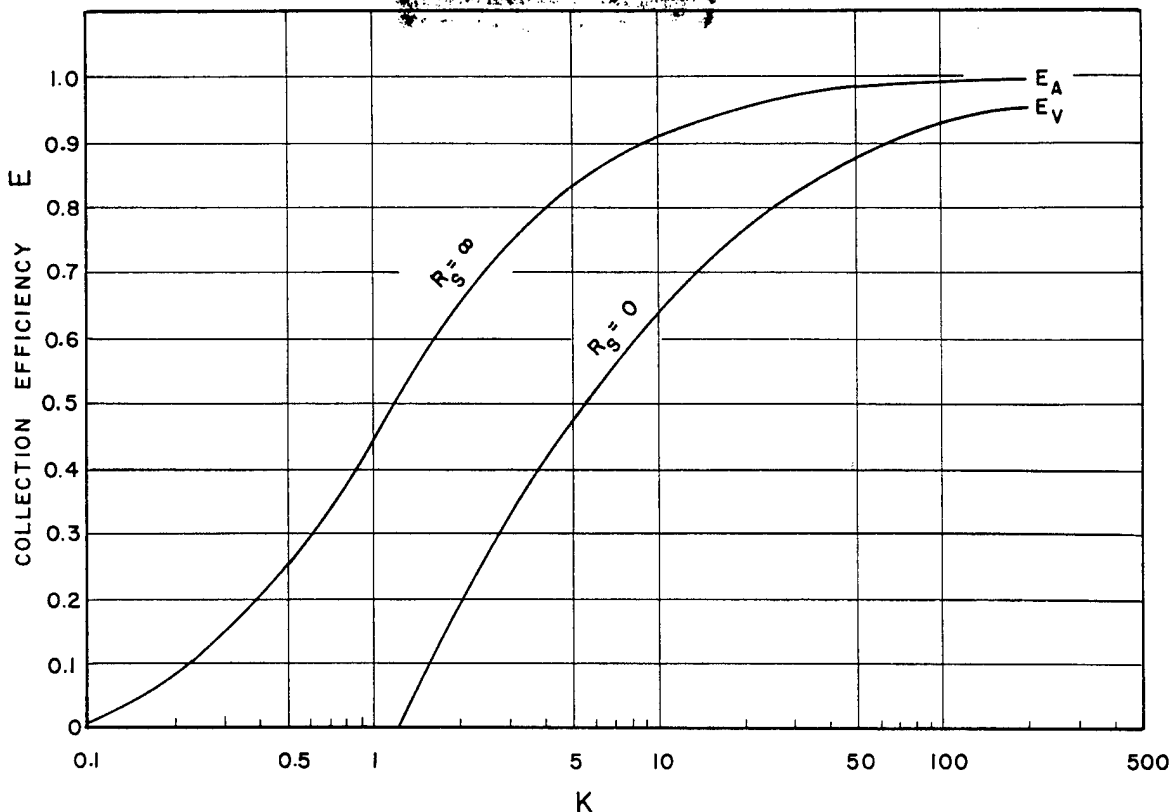


Fig. 1.1 Collection-efficiency Dependence on the Reynolds Number

cosity of the medium, and the density of the particles. Without entering into a detailed discussion of the derivation of the formulas, it can be shown that the efficiency of collection, E , can be equated as

$$E = \frac{(E_V + E_A)(R_s/60)}{1 + (R_s/60)} \quad (1.1)$$

where E_V = the collection efficiency for viscous-type flow

E_A = the collection efficiency for aerodynamic flow

R_s = the Reynolds number for falling sphere

E_V and E_A in turn are related to a dimensionless parameter, K , which is defined as

$$K = \frac{2\rho_s r^2}{9} \frac{U}{S\eta} \quad (1.2)$$

where ρ_s = the density of the spherical droplet
 r = the radius of the droplet

U = the velocity of fall of the collector drop

S = the radius of the collector sphere

η = the viscosity of air

The critical dependence of E upon the fall velocity or upon the Reynolds number of the collector is shown in Fig. 1.1. For small values of K the difference between the E values is considerable, depending on the type of flow involved.

The K values for intermediate Reynolds numbers can be obtained by an interpolation formula.

Figure 1.2 shows the results of the application of this theory to the case of raindrops and cloud droplets. It can be seen that no appreciable collection (synonymous to growth) occurs below collector sizes of 40μ radius.

It can be seen from Fig. 1.2 that coalescence of cloud drops (in the range 5 to 20μ radius) will be unlikely. However, by acceptance of the concept of rapid ice-particle growth by the Bergeron-Findeisen theory, a reasonable method for the formation of cloud particles of

suitable size is available. This growth process can lead to initial collector sizes of greater than 40μ radius in a short time. These particles in turn can grow rapidly by accreting cloud droplets since each increase in collector size leads to an increased efficiency of

The basic purpose of cloud seeding is to take advantage of this phenomenon by introducing appropriate chemicals into the cloud to convert it from a supercooled cloud into one containing a mixture of ice particles and water drops. It is then hoped that a favorable succession of

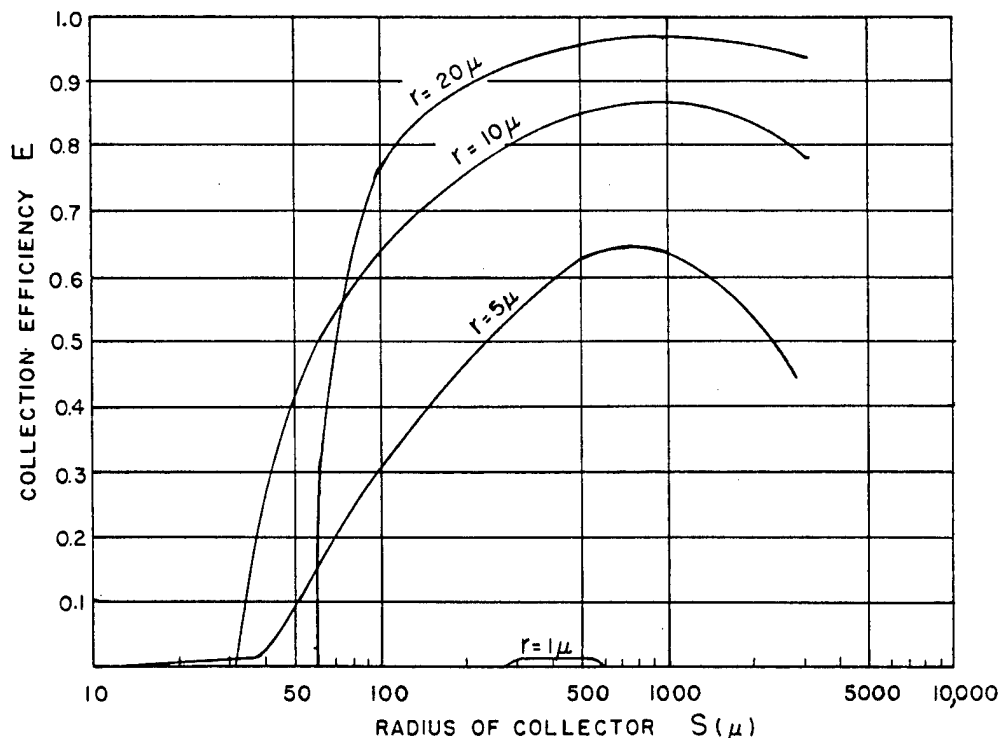


Fig. 1.2 Collection Efficiency of Falling Raindrops

collection (sizes less than 700μ). The collection of cloud droplets on ice particles leads to the formation of hydrometeors called "graupels."

It is evident then, if the graupel theory for significant rain production is a representative model of the true process, that the thermodynamic state of the cloud has a most important bearing on the probability of rainfall.

It is a recognized fact that water is capable of being rather easily supercooled in the atmosphere. The formation of ice on the aircraft stems directly from this phenomenon. In the winter, clouds composed of supercooled water droplets are frequent. This occurs to a slight extent in the summer in deep, thick clouds such as swelling cumulus, or cumulonimbus. Reports of heavy icing in these clouds confirm the presence of supercooled droplets.

events, such as those discussed previously, will occur, leading finally to rainfall from the cloud.

It has been demonstrated conclusively that solid carbon dioxide, by virtue of its low temperature, can cause the formation of ice particles in a supercooled cloud.² It has also been shown that certain chemicals, such as silver iodide³ and cadmium iodide,⁴ can act to produce similar effects.

The actual production of rainfall from natural clouds has met with varying, claimed success. The U. S. Weather Bureau undertook extensive field trials from which little or no success in rainfall stimulation resulted.^{5,6} Other trials reported marked success.^{7,8} According to the proponents of cloud seeding, success can be attained only when the proper synoptic conditions are present.⁸ These con-

sist of all the favorable conditions, i.e., supercooled clouds, a high liquid-water content, and a large mass of cloud, with the exception of sufficient ice-producing nuclei. Seeding will be beneficial in only these instances.

Consideration of the basic problem of precipitation production from an atomic cloud by artificial seeding in light of the above discussion makes it imperative that a knowledge of the physical state of the cloud be available. It is difficult to predict the possibility of rainfall generation if the necessary elements are present. However, no argument can be raised against the statement that no precipitation will result if none of the necessary conditions are present.

The first task is to determine the magnitude of the favorable parameters in the cloud. If the measurements indicate a lack of liquid water or supercooled cloud or an overabundance of ice-forming nuclei, it can be concluded with certainty that seeding will be useless.

There was considerable doubt as to the composition of the cloud. In some quarters it was felt that the cloud was mainly a smoke and dust cloud. Visual observation of the clouds produced at Crossroads and Sandstone certainly indicated little possibility of a deep mass of supercooled cloud being present.

This question was discussed thoroughly in a conference with I. Langmuir and V. J. Schaefer of the General Electric Research Laboratories at AFCRC on 3 August 1950. The conclusion of this meeting was that the type of cloud likely to result from an explosion in the Pacific Proving Grounds would be unsuitable for seeding. This view was predicated mainly on an examination of the meteorological soundings in the vicinity. These soundings show a very definite deficiency

of water vapor above the trade-wind inversion. This dryness aloft will lead to rapid evaporation of a water cloud. In addition, sketches of atomic clouds made at the site indicated that these clouds were tenuous columns with little likelihood of possessing characteristics similar to cumulus congestus clouds.

Nevertheless, a decision to go ahead with the program was made since there were no measurements to substantiate these predictions.

REFERENCES

1. I. Langmuir, The Production of Rain by a Chain Reaction in Cumulus Clouds at Temperatures Above Freezing, *J. Meteorol.*, 5: 175 (1948).
2. V. J. Schaefer, The Production of Clouds Containing Supercooled Water Droplets or Ice Crystals Under Laboratory Conditions, *Bull. Am. Meteorol. Soc.*, 29: 175 (1948).
3. B. Vonnegut, Nucleation of Ice Formation by Silver Iodide, *J. Appl. Phys.*, 18: 593 (1947).
4. E. M. Fournier D'Albe, Some Experiments on the Condensation of Water Vapour Below 0°C, *Quart. J. Roy. Meteorol. Soc.*, 75: 1 (1949).
5. First Partial Report on the Artificial Production of Precipitation, Research Paper No. 30, U. S. Department of Commerce, Weather Bureau, Washington, D. C., 1948.
6. Second Partial Report on the Artificial Production of Precipitation, Research Paper No. 31, U. S. Department of Commerce, Weather Bureau, Washington, D. C., 1949.
7. E. B. Kraus and P. Squires, Experiments on the Stimulation of Clouds To Produce Rain, *Nature*, 159: 489 (1947).
8. I. Langmuir, Progress in Cloud Modification by Project Cirrus, General Electric Research Laboratory Report RL-357, Schenectady, N. Y., April 1950.

Chapter 2

Measurement Program

2.1 AIRCRAFT INSTRUMENTS

When it became apparent in October 1949 that the cloud-physics section of the AFCRC would be responsible for conducting the necessary measurements in the 1951 tests, a survey of instruments was undertaken. Visits were made to various groups that were engaged in aircraft meteorological measurement to determine the availability of developed equipment. The National Advisory Committee for Aeronautics (NACA) Laboratories in Cleveland, Ohio, the Ice Research Base of Ypsilanti, Mich., the General Electric Research Laboratories "Project Cirrus," the Evans Signal Laboratories (ESL), and the Meteorological Group at the Massachusetts Institute of Technology were among those canvassed.

This extensive survey revealed a decided deficiency in developed equipment that was readily applicable to the measurement program. This lack was more acute because the mock-up date for the drone aircraft had been set for 1 January 1950. A compromise was reached wherein the measurement program would be limited to those parameters for which equipment was available. This eliminated consideration of liquid- or solid-water-content measuring devices and more accurate temperature and relative-humidity measuring instruments. The cloud-physics program was left with the only possibility of securing aerographs for the aircraft.

2.2 AEROGRAPH SYSTEM

Some research on aerograph equipment had been accomplished by the Geophysical Sciences Branch, Directorate of Research and Devel-

opment, Air Force Headquarters (AFMRS), prior to the entrance of this group into Program 4. They had recommended the reconditioning of 30 AN/AMQ-2 aerographs to be loaned by the Air Weather Service. Investigation showed that the Signal Corps was developing a much better aerograph system, the AN/AMQ-7, but production had not been started. AFMRS recommended that the recorder units from the AN/AMQ-2 be utilized in conjunction with the Signal Corps Engineering Laboratories probe and electronic transmitting system. The Kollsman Instrument Division of Square D Company (now Kollsman Instrument Corp.) had the development contract for this unit.

A series of conferences was held among representatives of the AFCRC, the ESL, and Kollsman to determine the most expedient and yet practicable procurement of aerograph equipment. It was decided that the time limitation dictated the choice of the complete Kollsman instrument. An estimate of costs involved in either alternative (the modified AN/AMQ-2 and AN/AMQ-7 type or the complete AN/AMQ-7 type) showed that there was no advantage to be gained by attempting to salvage and recondition the AN/AMQ-2 recorders.

The AFCRC aerograph system produced by Kollsman consisted of the following components:

Item	Kollsman type No.
Bridge indicator	1302
Four amplifiers	1351
Cathode-follower amplifier	1586
Recorder	1301
Airspeed transmitter	1346
Pressure transmitter	1587-01

In addition to these items suitable probes and sensing elements had to be incorporated into the

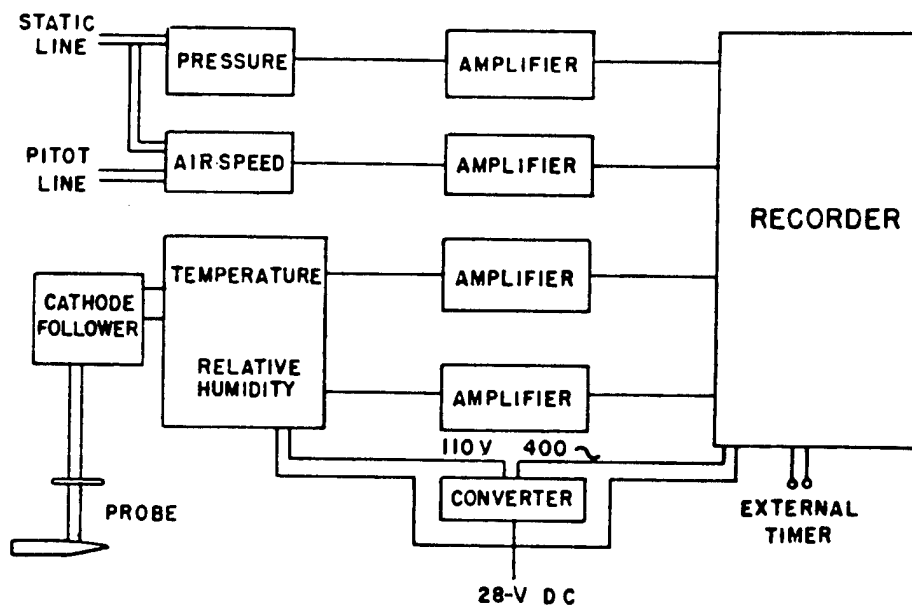


Fig. 2.1 Block Diagram of Aerograph

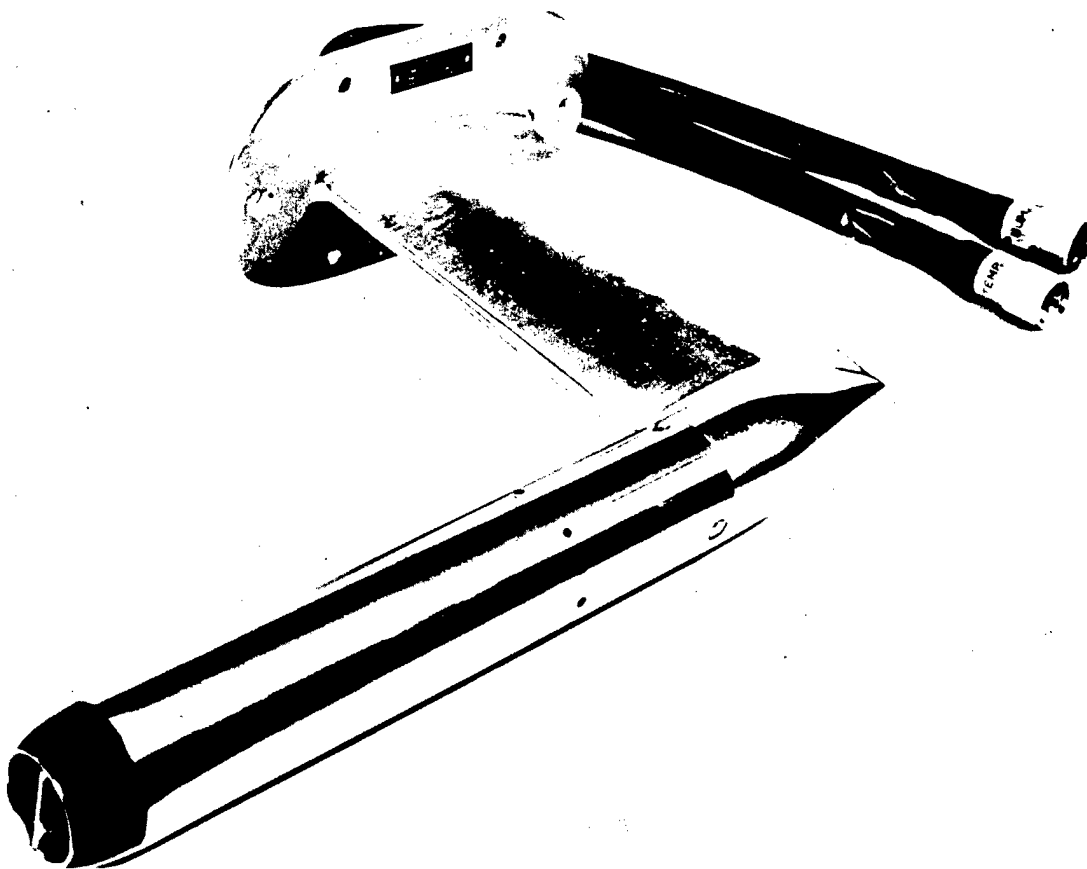


Fig. 2.2 Aerograph Probe

system. The Meteorological Branch of ESL was actively investigating probe designs and was thus in a position to offer advice concerning them. The latest design temperature- and humidity-sensing elements were also available from the Signal Corps.

The block diagram in Fig. 2.1 depicts the AFCRC system.

The AFCRC aerograph was designed to operate two direct-reading dials that give temperature and relative-humidity readings as sensed by an externally mounted probe. The pressure and airspeed data necessary for obtaining ambient values of these two parameters are obtained from the pressure and airspeed synchrotels. All four variables are recorded on a five-channel recorder having a chart drive speed of 0.6 in./min. The fifth channel is spare and can be utilized for any of the four variables.

In March 1950 the necessary authorization was granted to enable a contract to be placed with the Kollsman Instrument Corp. for the fabrication of 22 complete AFCRC aerograph systems including the Signal Corps designed probe and field maintenance kits. In addition, Kollsman agreed to conduct a two-week training course for the Air Force personnel and to furnish a company representative for field maintenance. Complete delivery by 1 January 1951 was specified.

The probe is shown in Fig. 2.2. The temperature-sensing element is a carefully selected Western Electric thermistor bead No. 6-14B having a range of resistance of about 1000 to 300,000 ohms. Originally the humidity was to be measured by the change in resistance of a lithium chloride strip manufactured by the Friez Instrument Division, Bendix Aviation Corp. This strip, called ML-379/AM, is a standard component of the radiosonde. A new type of humidity element with a carbon coating, under development by Arthur D. Little, Inc., with Signal Corps sponsorship, which has operating characteristics superior to the lithium chloride strip was actually used in the tests.

The temperature and humidity transmitter is a self-balancing bridge indicator which measures the resistance of the thermistor and the humidity element in accordance with U. S. Army Specification No. 74-109-A. It has two direct-reading dials for temperature and relative humidity, respectively. The unit consists of two motor follow-up Wheatstone bridge circuits, including mechanisms so designed that the relation between the dial indication and

resistance follows Tables 2.1 and 2.2 for temperature and humidity. Each channel of the transmitter positions a synchro equivalent to Bendix AY 201-3-B to transmit the values of temperature and humidity to the recorder.

TABLE 2.1 CALIBRATION OF TEMPERATURE CHANNEL

Temperature (°C)	Resistance of standard thermistor (ohms)	Tolerance, unit to unit (scale div.)	Repeatability to individual calibration (scale div.)
-70	339,500	1.0	0.5
-65	239,400	1.0	0.5
-60	171,800	0.4	0.3
-55	124,200	0.4	0.3
-50	90,230	0.3	0.2
-45	66,600	0.3	0.2
-40	49,450	0.2	0.2
-35	37,040	0.2	0.2
-30	28,060	0.2	0.2
-25	21,400	0.2	0.2
-20	16,490	0.2	0.2
-15	12,800	0.2	0.2
-10	10,020	0.4	0.2
-5	7,898	0.4	0.2
0	6,265	0.6	0.3
5	5,009	0.6	0.3
10	4,030	0.6	0.3
15	3,263	0.6	0.3
20	2,660	0.8	0.4
25	2,182	0.8	0.4
30	1,800	0.8	0.4
35	1,492	0.8	0.4
40	1,244	1.0	0.5
45	1,044	1.0	0.5
50	877.1	1.0	0.6

A cathode-follower amplifier is placed between the transmitter and the probe to reduce the input impedance to the bridge and to reduce stray capacitance effects of the cables connecting the sensitive elements and the bridge.

The airspeed transmitter consists of a synchrotel and diaphragm unit, which is coupled to the aircraft pitot and static pressure lines. The synchrotel converts movements of this diaphragm into electrical signals, which are transmitted to the recorder.

The pressure transmitter is likewise a synchrotel and aneroid unit, which converts mechanical movement of the aneroid into elec-

trical variations and transmits them to the recorder.

The recorder is designed to receive these synchro rotation inputs and to position a stylus on a lead screw in proportion to the electrical angles of the transmitting synchros. This is accomplished by means of a servomechanism

TABLE 2.2 CALIBRATION OF HUMIDITY CHANNEL

Humidity (%)	Resistance (ohms)	Tolerance, unit to unit (scale div.)	Repeatability to individual calibration (scale div.)
0	3,000,000	0.4	0.3
10	920,000	0.3	0.2
20	310,000	0.2	0.2
30	113,000	0.2	0.2
40	47,500	0.2	0.2
50	23,000	0.3	0.2
60	12,200	0.4	0.3
70	7,400	0.6	0.4
80	4,650	0.8	0.6
90	3,050	1.0	0.6
100	2,000	1.0	0.6

consisting of a two-phase motor, a synchro equivalent to Bendix AY 201-3-B, the lead screw and stylus, suitable gearing, and a servoamplifier.

The speed of response of each recording channel is such as to cover the full range of the chart in 15 sec. The stability of each channel is such that it responds to step changes in the input of one-quarter of full scale with an overshoot of not more than 1 per cent of the chart range.

The accuracy of the recorder is such that the displacement of the pen marker from its theoretical position shall not be greater than 0.5 per cent of the full range of the chart. The chart is driven by a governor-controlled d-c motor operating on 24 to 28 volts direct current at 36 in./hr with an accuracy of ± 2 per cent.

The aerograph is designed to operate between temperature limits of -70 to $+50^{\circ}\text{C}$ without damage. The total weight of the system is 80 lb. Power requirements are 138 va at 115 volts, 400 cycles/sec, and 75 watts, 28 volts direct current.

The following table gives measuring characteristics of the system.

Variable	Range	Sensitivity
Airspeed	60 to 550 knots	3 knots
Pressure	1060 to 150 mb	5 mb
Temperature	-70 to $+50^{\circ}\text{C}$	0.1°C
Humidity	0 to 100 per cent	0.1 per cent

2.3 AIRCRAFT AEROGRAPH INSTALLATION

The preliminary plans for the aircraft program called for installation of aerograph systems in twelve TB-17 drone aircraft. These ships were assigned to AEC testing projects. The plan was later changed to include six T-33 jet drone aircraft.

The drone aircraft would be vectored into the cloud at various levels to record pertinent data. The decisions regarding the precise flight patterns of the drone aircraft rested with the AEC, which had the primary requirements.

Mounting provisions were such that the major components of the system could be taken out very easily. Tray assemblies were used wherever possible.

The TB-17 installation was as follows: The probe was located on the portside forward about 18 in. below the center line, as shown in Fig. 2.3.

The cathode follower rested on the navigator's table in the nose portside (Fig. 2.4). The light, foreground object is part of the temperature-humidity transmitter. The forward edge of the navigator's table was utilized for the temperature-humidity transmitter shown in Fig. 2.5. Two of the three cables coming from this unit go to the recorder, and the third goes to the cathode follower. The synchrotels for pressure and airspeed transmission were located in the nose portside above the cathode follower (Fig. 2.6). The pitot pressure line visible in Fig. 2.6 was connected to a probe similar to that shown in Fig. 2.3 mounted on the starboard side. The static pressure was obtained from two parallel, flush static heads mounted on opposite sides of the aircraft just aft of and about 40 deg below the wing root.

Figures 2.7 and 2.8 show the mounting of the recorder. This unit was located in the waist by the port window. The entire assembly is held by spring fasteners to enable quick removal for testing.

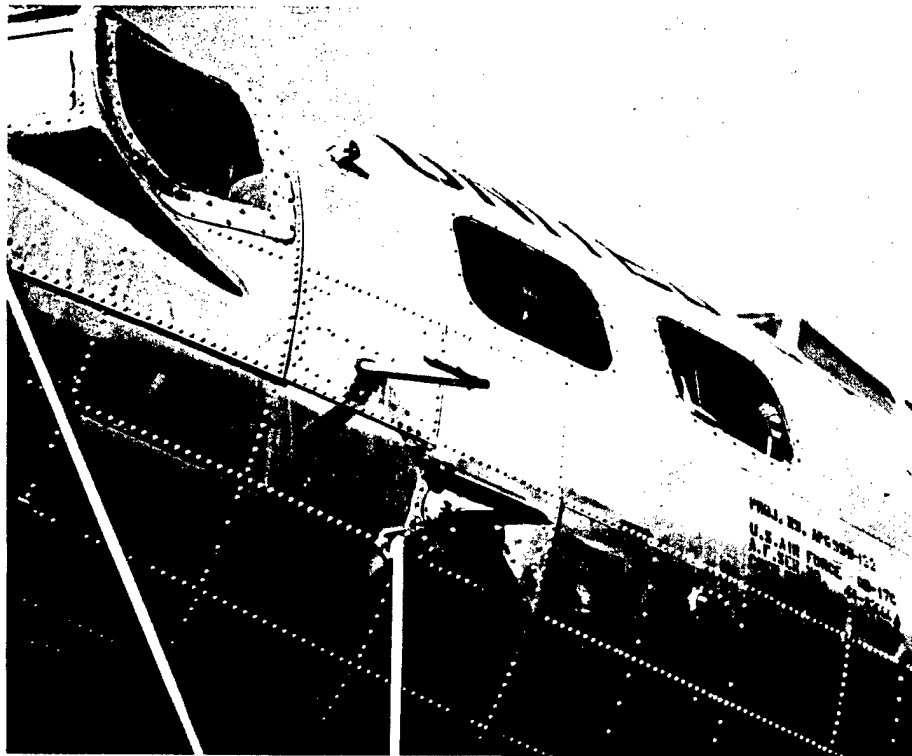


Fig. 2.3 Probe Installation, TB-17

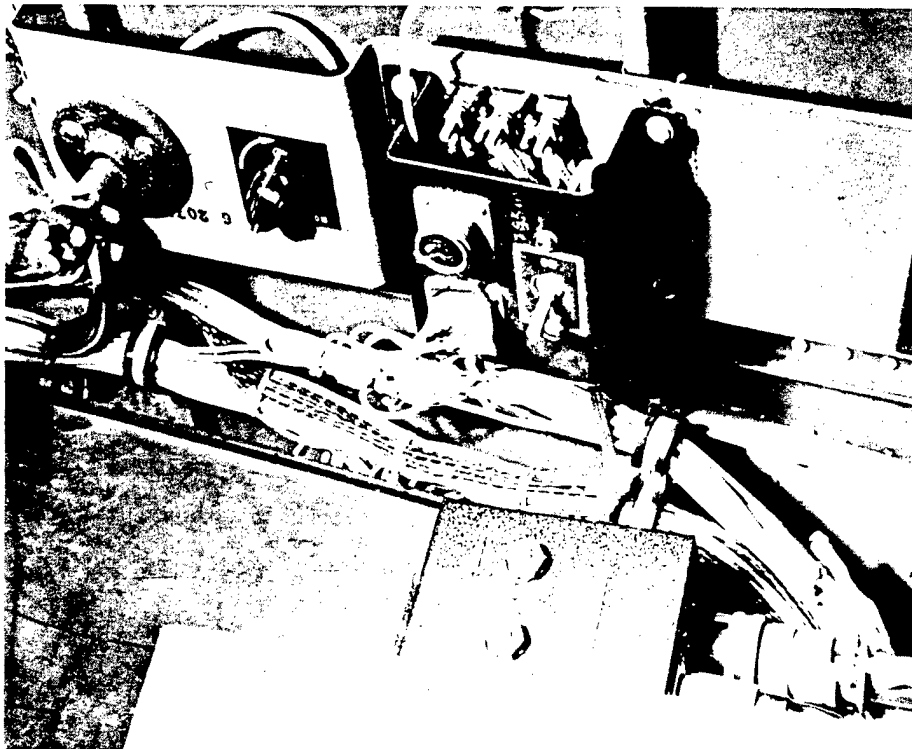
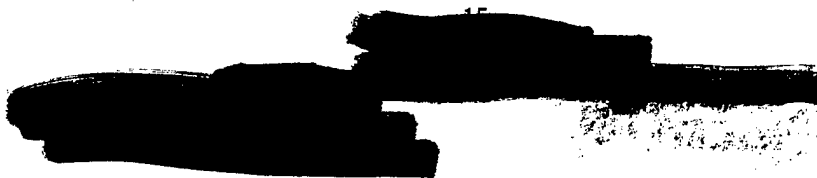


Fig. 2.4 Cathode Follower, TB-17



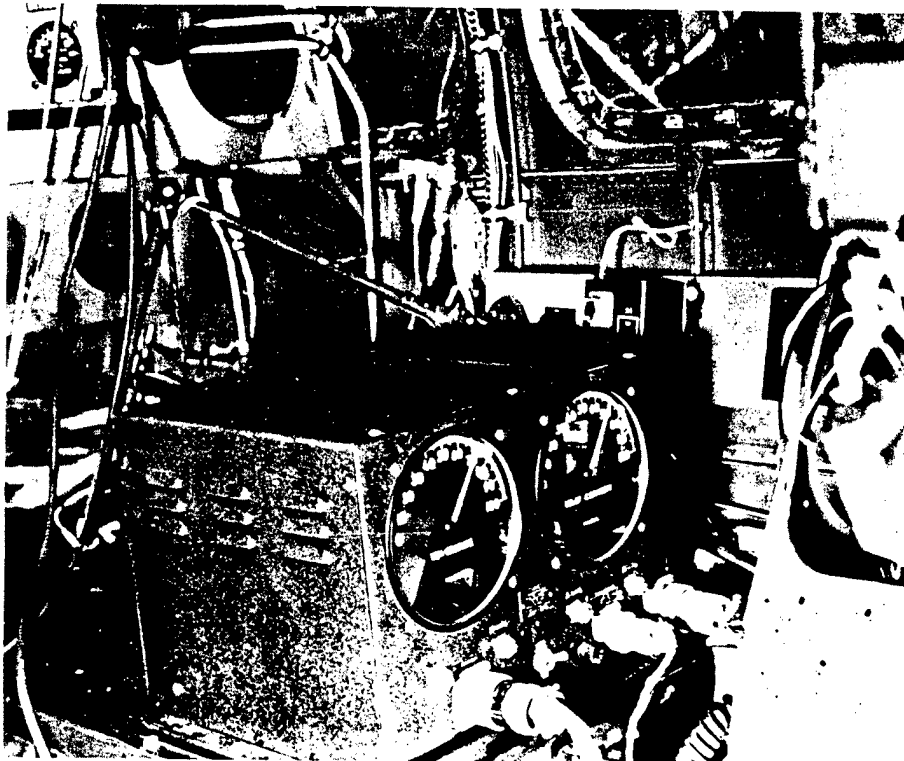


Fig. 2.5 Temperature-Humidity Transmitter, TB-17

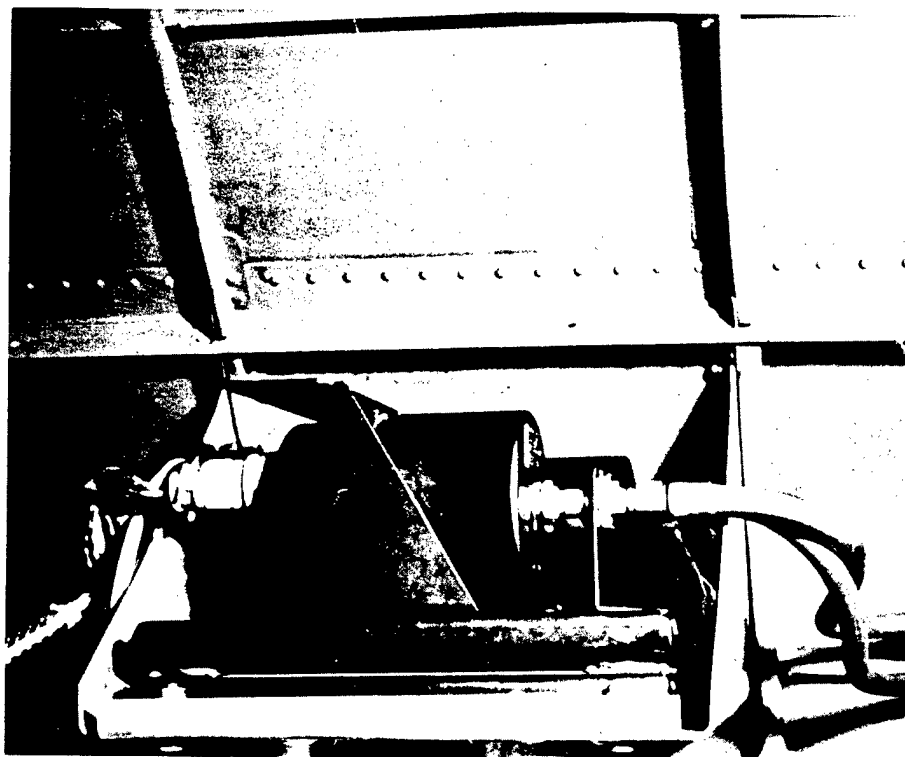
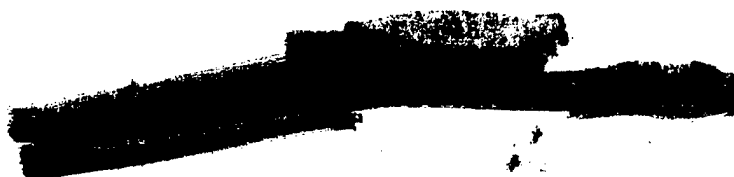


Fig. 2.6 Pressure-Airspeed Transmitter, TB-17



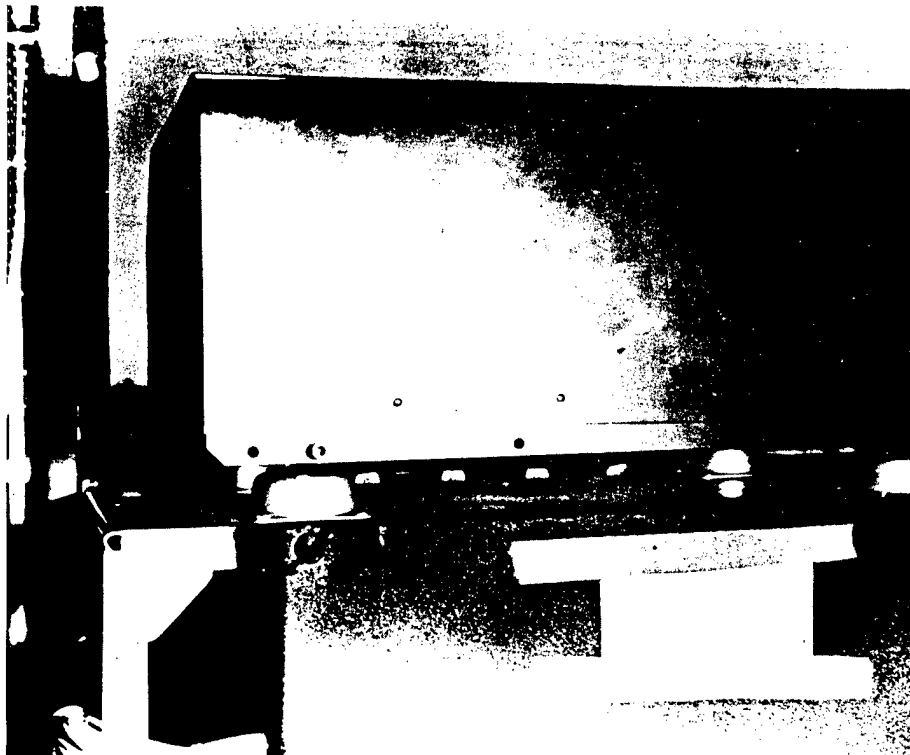


Fig. 2.7 Recorder, TB-17



Fig. 2.8 Recorder with Cover Removed, TB-17

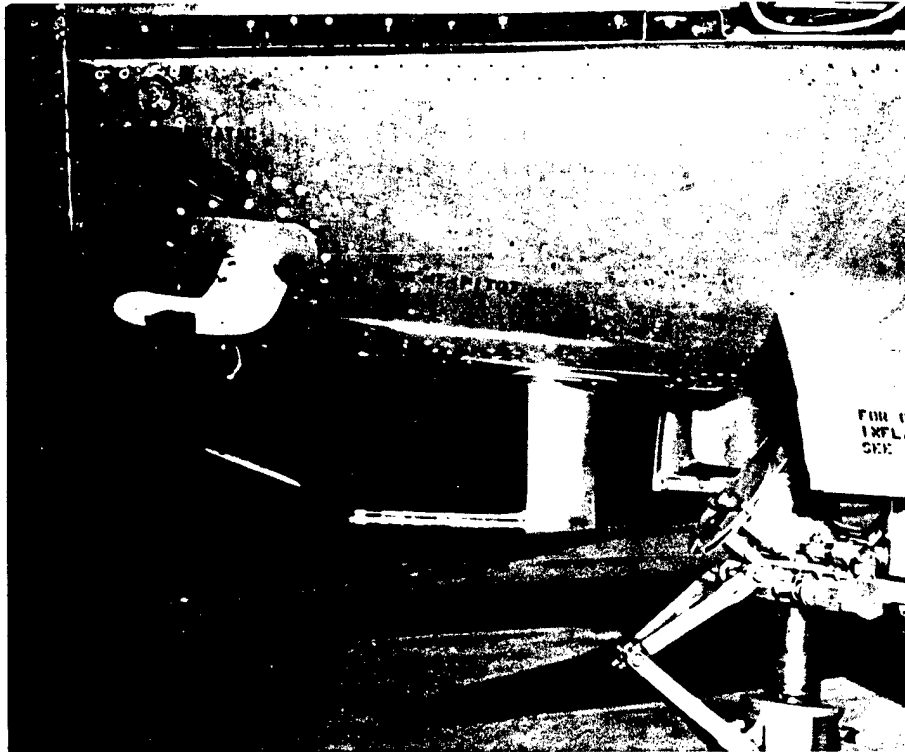


Fig. 2.9 Probe Installation, T-33

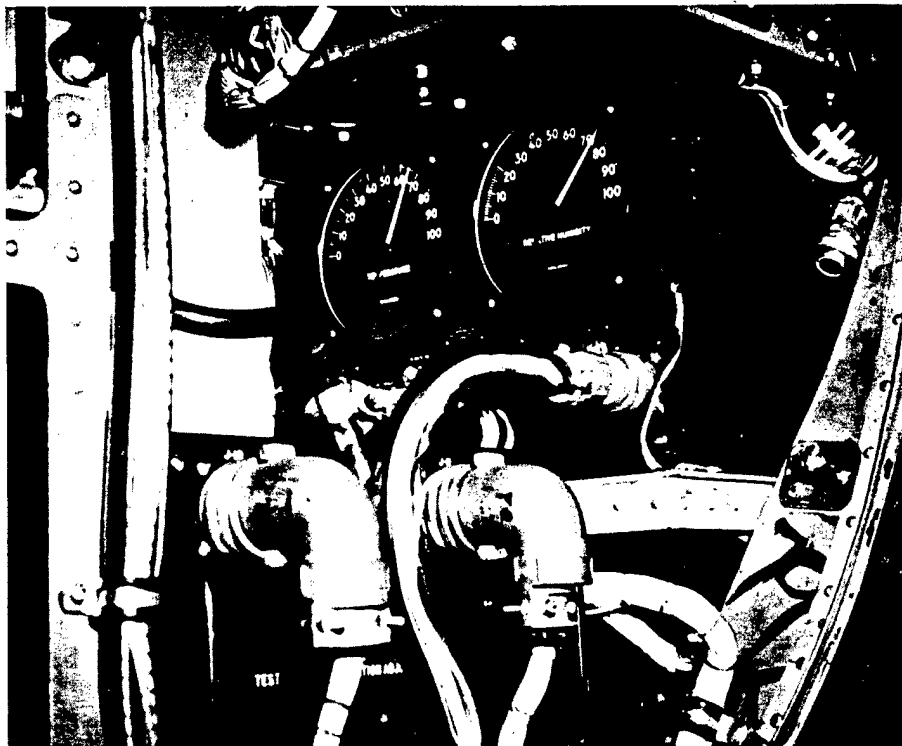


Fig. 2.10 Temperature-Humidity Transmitter Mounting, T-33

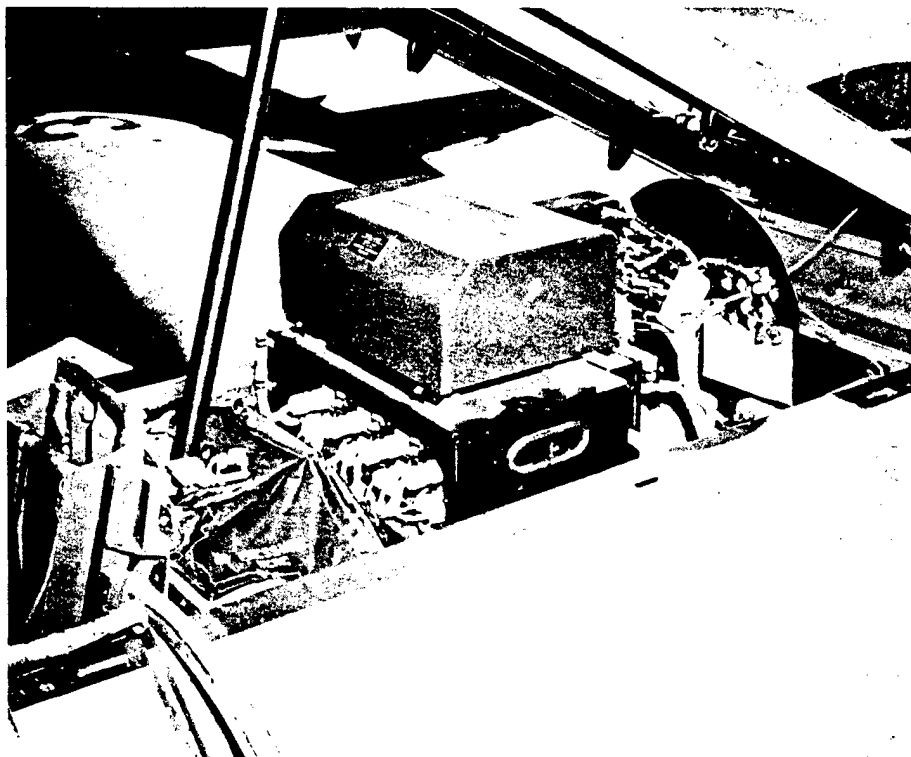


Fig. 2.11 Recorder, T-33

The probe unit was mounted on the underside of the T-33, forward of the nose landing gear, as is seen in Fig. 2.9. The cathode follower and the temperature-humidity transmitter were placed in the nose compartment. A view of the bridge indicator is contained in Fig. 2.10.

The airspeed and pressure transmitters located on the floor beneath the rear pilot's in-

strument panel were connected to the pitot and static pressure heads visible in Fig. 2.9.

The recorder and four amplifiers were mounted on a removable plate fastened to brackets high on each side of the aft cockpit. This allowed ready accessibility to replace chart rolls and otherwise service the instrument. The installation is shown in Fig. 2.11.

Chapter 3

Experimental Procedure

3.1 CALIBRATION OF AEROGRAPH

Errors of two distinct classes are inherent in the construction and operation of the aerograph equipment. The so-called "static errors" are errors due to the unavoidable mechanical deviation from desired response. When the aircraft is in flight, dynamic errors occur owing to airflow distortion by the sensing elements. An analysis of the methods of compensation for these errors follows.

3.1.1 Static Errors

Each complete aerograph system was subjected to bench calibration tests to determine the recorder response to known conditions at the sensing elements. The difference between the imposed conditions and the recorder indication was the sum of the mechanical and the electrical irregularities in the channel. This difference (scale error) was noted at related points over the complete range and was used to correct the subsequent records.

A vacuum pump supplied the reduced pressures necessary to check the pressure channel. The pump, a carefully calibrated aneroid barometer, and the pressure transmitter under test were connected with hydraulic tubing. Pressures of 100-mb decrements in the range 1060 to 150 mb were produced and maintained until the recorder-index position was recorded. Full-scale cycle of the pressure showed a hysteresis effect of 3 mb or less. For small pressure changes the effect was negligible. Bench checks for friction errors were of the same order.

Similarly, a compressed-air source was adjusted to give equivalents of pitot pressures

necessary to move the recorder index over the full range from 60 to 550 knots with stops at the extremes and each intermediate 50-knot multiple. Hysteresis and friction effects for a full-scale cycle were about 2 knots.

The reproducibility of the temperature and relative-humidity channels was checked by substituting known resistances for the sensing elements. The recorder indication was compared with the design values listed in Tables 2.1 and 2.2. Deviations from the standard values were recorded as scale errors.

3.1.2 Dynamic Errors

The fact that aerograph measurements are made under flight conditions necessitates corrections for heating due to the impact of air on the exposed sensing elements and for heating due to pressure changes caused by disruption of the airflow. This aerodynamic heating affects the measured temperature and relative humidity to cause a higher than ambient value for the former and a lower than ambient value for the latter.

The probe used in Project 4.1 was designed to permit as high a recovery factor as possible and to minimize heating due to radiation. A high recovery factor is desired since one would like to approximate adiabatic conditions within the probe for reasons seen below.

The Bernoulli equation for the conservation of energy of a fluid can be used to express the theoretical temperature increase due to an adiabatic conversion of the kinetic energy of air motion into heat:

$$\int \frac{dP}{\rho} + \frac{1}{2} q^2 = C \quad (3.1)$$

where P = pressure
 ρ = density
 q = velocity
 C = a constant

For adiabatic flow¹

$$\int_1^2 \frac{dP}{\rho} = \frac{\gamma}{\gamma-1} \frac{P_1}{\rho_1} \left(\frac{T_2}{T_1} - 1 \right) \quad (3.2)$$

where γ is C_p/C_v and T_2 and T_1 are temperatures in degrees Kelvin; the Bernoulli equation becomes

$$\frac{\gamma}{\gamma-1} \frac{P_1}{\rho_1} \left(\frac{T_2}{T_1} - 1 \right) + \frac{q_2^2 - q_1^2}{2} = 0 \quad (3.3)$$

Rearranging and making the substitution

$$P_1 = \rho_1 R T_1 \quad (3.4)$$

$$T_2 - T_1 = \frac{\gamma-1}{\gamma R} \frac{q_1^2 - q_2^2}{2} \quad (3.5)$$

Since the ratio of inlet area to outlet area was quite high for the probe used, the exit velocity of the air can be considered negligible when compared to the free-stream velocity. If q_1 represents the free-stream velocity and q_2 represents the exit velocity, the equation reduces to

$$T_2 - T_1 = \Delta T = \frac{\gamma-1}{\gamma R} \frac{q_1^2}{2} \quad (3.6)$$

or, alternately,

$$\Delta T = \frac{q_1^2}{2C_p} \quad (3.7)$$

When q is expressed in miles per hour and C_p is taken for moist air,

$$\Delta T (^{\circ}\text{C}) \cong \left(\frac{\text{mph}}{100} \right)^2 \quad (3.8)$$

In the usual case the temperature increase in the probe will not be strictly adiabatic owing to heat loss to the moving air, heat transfer through the probe housing, frictional and radiation effects, etc. In other words, the recovery may be less than 100 per cent, and therefore its value must be found experimentally. If

$$\Delta T = \alpha \left(\frac{q}{100} \right)^2 \quad (3.9)$$

where α is the correction factor, it has been found experimentally^{2,3} that α varies between 0.6 and 0.99 when q is measured in miles per hour and T is measured in degrees centigrade. It is cautioned that this formula is valid for speeds up to 400 mph only.

The value of α for a particular instrument depends not only on the design of the probe but also on the location of the probe on an aircraft. The probe employed in the tests was designed by the Meteorological Branch of the ESL, Belmar, N. J. The values of α for various airspeeds were experimentally determined by a series of flights with a B-25 type aircraft. The aircraft was flown at constant altitude for varying airspeeds, and the indicated temperature was plotted against $(q/100)^2$. The resulting curves were extrapolated to zero airspeed to get the ambient temperature. Table 3.1 shows the results of these trials. The probe was also tested for dynamic-pressure dependence on airspeed by mounting a small static pressure unit with a sensitive aneroid. The difference between the total pressure and the static pressure is the dynamic-pressure increment. Table 3.2 gives the results of this investigation.

Since B-17 and T-33 aircraft were utilized in Project 4.1, it was felt that further calibration flights would be necessary to establish the magnitude of the correction factor for these aircraft.

Three flights were made in B-17 aircraft in the Eniwetok area. Two of the flights were made at constant altitudes varying from 300 to 8000 ft, determined by radar altimeter. The flights were made over a known course at velocities ranging from 130 to 235 mph true airspeed. An additional flight was accomplished by flying one of the ships by the Engebi tower. An observer stationed at 300 ft on the tower measured the ambient temperature and relative humidity. The results of these calibration flights are shown in Fig. 3.1. The Signal Corps values for comparison purposes are plotted here also.

The combined data give a curve having a slope of approximately 1.0. It was therefore assumed that the temperature rise within the probe was adiabatic, which facilitated computations of true temperatures and true airspeeds. From this it was reasonable to assume the correction for aerodynamic heating in clouds to approximate a moist, adiabatic temperature rise. The question of the dependence of the final tem-

TABLE 3.1 TEMPERATURE CORRECTION* FOR TRUE AIRSPEED FROM 140 TO 308 MPH†

True airspeed (mph)	Temp. corr. (°C)	True airspeed (mph)	Temp. corr. (°C)	True airspeed (mph)	Temp. corr. (°C)	True airspeed (mph)	Temp. corr. (°C)
140	2.2	184	3.4	226	4.9	268	6.6
142	2.3	186	3.5	228	5.0	270	6.7
144	2.3	188	3.5	230	5.0	272	6.8
146	2.4	190	3.6	232	5.1	274	6.9
148	2.4	192	3.7	234	5.2	276	7.0
150	2.5	194	3.7	236	5.2	278	7.1
152	2.5	196	3.8	238	5.3	280	7.2
154	2.6	198	3.9	240	5.4	282	7.3
156	2.6	200	3.9	242	5.5	284	7.4
158	2.7	202	4.0	244	5.6	286	7.4
160	2.7	204	4.1	246	5.7	288	7.5
162	2.8	206	4.1	248	5.7	290	7.6
164	2.9	208	4.2	250	5.8	292	7.7
166	2.9	210	4.3	252	5.9	294	7.8
168	3.0	212	4.4	254	6.0	296	7.9
170	3.0	214	4.4	256	6.1	298	8.0
172	3.1	216	4.5	258	6.2	300	8.1
174	3.1	218	4.6	260	6.3	302	8.2
176	3.2	220	4.6	262	6.3	304	8.3
178	3.3	222	4.7	264	6.4	306	8.4
180	3.3	224	4.8	266	6.5	308	8.5
182	3.4						

* Indicated temperature - temperature correction = true temperature.

† The data in this table are given by courtesy of the U. S. Signal Corps.

perature on the amount of liquid water evaporated within the probe was avoided by reasoning that the protective screen prevented actual wetting of either the thermistor bead or the carbon element and that, regardless of the liquid-water content, saturation conditions were always maintained within the probe.

Aerodynamic heating affected the measured values of relative humidity since the saturation vapor pressure of water is highly dependent on the temperature and to a slight extent on the total pressure. The observed relative humidities were corrected for a temperature rise as obtained from the true airspeed (Table 3.1) and for a pressure rise as given by Table 3.2. The validity of this procedure was substantiated by comparison of computed and directly measured values of the ambient relative humidity on the occasion of the tower flights, as shown in Table 3.3.

3.1.3 Over-all Accuracy

It was desirable to have a measure of the over-all performance of the aerograph system.

The accuracy and reliability were two indexes which could best be studied by comparing the aerograph measurements to some primary standard. Furthermore, the standard should pertain to the conditions under which the aerographs were to operate, i.e., to the atmosphere itself.

Fortunately, the Eniwetok Weather Central conducted routine radiosonde flights which were available for comparison purposes. Since the rate of rise of the sounding balloons was relatively slow, aerodynamic heating of the sensing elements was negligible. Ambient temperatures and humidities could be obtained without introducing a correction for dynamic effects. It is customary to treat the radiosonde trace as a standard when studying the local thermodynamic or meteorological structure of the atmosphere.

In Figs. 3.2, 3.3, and 3.4, aerograph temperature soundings are compared against the local radiosonde flight. It is seen that remarkably good agreement prevails despite the numerous corrections that must be applied before the aerograph raw data can be reduced to ambient

TABLE 3.2 PRESSURE INCREMENTS* FOR CALIBRATED AIRSPEED FROM 140 TO 300 MPH†

Cal. airspeed (mph)	ΔP , (mb)	Cal. airspeed (mph)	ΔP , (mb)	Cal. airspeed (mph)	ΔP , (mb)	Cal. airspeed (mph)	ΔP , (mb)
140	23	184	40	226	59	268	83
142	24	186	41	228	60	270	84
144	25	188	42	230	61	272	85
146	25	190	43	232	62	274	87
148	26	192	43	234	63	276	88
150	27	194	44	236	64	278	89
152	27	196	45	238	65	280	90
154	28	198	46	240†	66	282	92
156	29	200	47	242	68	284	93
158	30	202	48	244	69	286	94
160	30	204	49	246	70	288	96
162	31	206	50	248	71	290	97
164	32	208	51	250	72	292	99
166	33	210	52	252	73	294	100
168	33	212	52	254	74	296	102
170	34	214	53	256	76	298	103
172	35	216	54	258	77	300	105
174	36	218	55	260	78		
176	37	220	56	262	79		
178	38	222	58	264	80		
180	38	224	58	266	82		
182	39						

* True pressure + pressure increment = probe effective pressure.

† The data in this table are given by courtesy of the U. S. Signal Corps.

‡ Pressures at speeds over 240 mph are estimated.

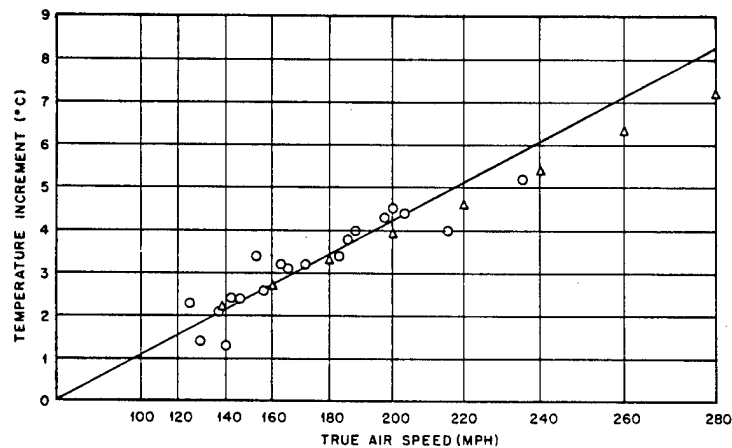


Fig. 3.1 Dynamic Heating in the Probe. —, theoretical.

O, B-17 installation. Δ, B-25 installation.

conditions. The average difference between the Raob and the aerograph soundings is less than 1°C.

The agreement between relative humidities is not so good. Two factors that may contribute to

the disparity are (1) the more sensitive, accurate, and reliable carbon element was used as opposed to the lithium chloride strip of the radiosonde and (2) inhomogeneities exist in the horizontal distribution of relative humidity.

TABLE 3.3 RELATIVE-HUMIDITY CALIBRATION*

True airspeed (mph)	Relative humidity (%)	
	Aerograph	Tower
126	77	73
144	76	73
164	80	73
186	79	72
203	80	72
154	76	72

* Ambient relative humidity was measured by aerograph and by tower observer during the calibration flight.

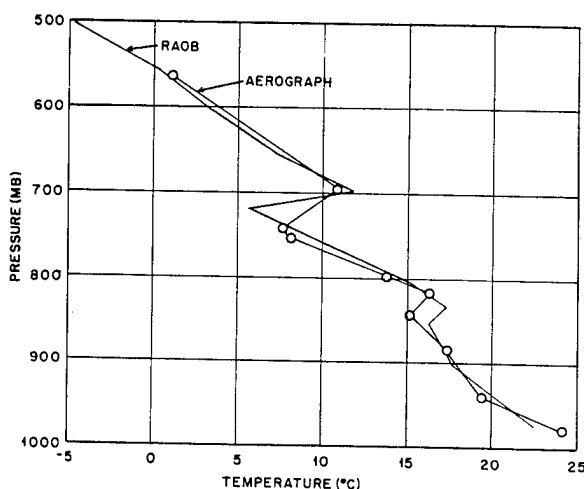


Fig. 3.2 Calibration Flight of H-drone Compared with Raob of the Same Day

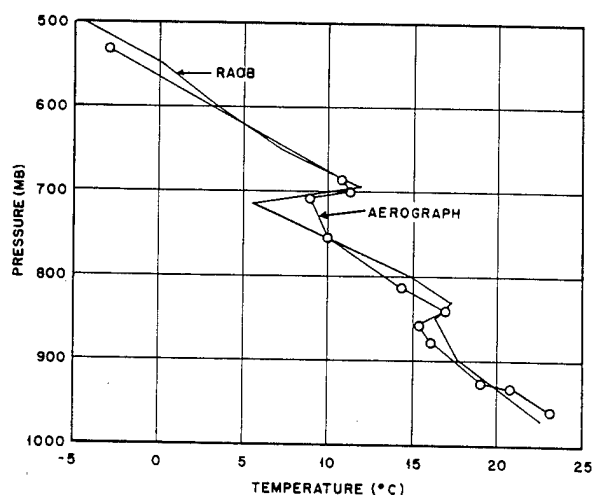


Fig. 3.3 Calibration Flight of K-drone Compared with Raob of the Same Day

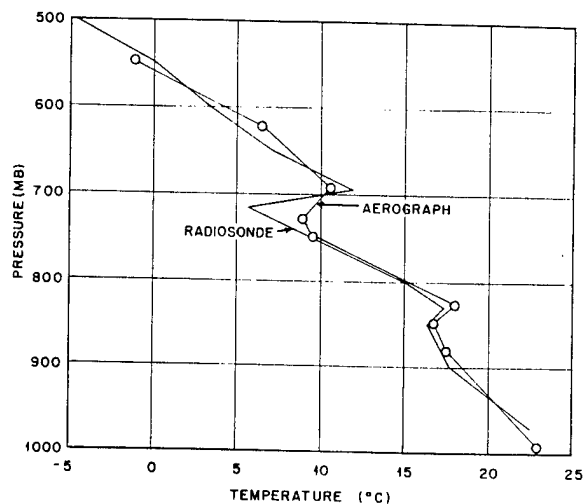


Fig. 3.4 Calibration Flight of B-drone Compared with Radiosonde of the Same Day

Figure 3.5 illustrates the difference in relative humidity as measured by the two methods. The response of the carbon element under actual cloud conditions is shown in Fig. 3.6. It is seen that the aerograph does faithfully indicate saturation conditions when they are truly present.

The accuracy with which the data can be presented is a measure of the validity of the various corrections applied. The purpose of this section is to present the maximum errors that may be present.

In the evaluation of the airspeed record, the trace can easily be read to 1 knot. The application of the scale error is about the same and may not be additive. The dynamic correction as applied is good to 0.5 knot. Allowing 0.5 mph possible error in using the true airspeed computer, the maximum error then is less than 4 or 5 mph.

The pressure trace can be read to 1 mb. The scale correction is no larger than this, and the dynamic error is negligible. The pressures are accurate within 2 mb.

The largest probable error in evaluating the temperature trace is in the determination of the preflight correction. Postoperational recalibration of the thermistors in the laboratory shows that the change of calibration is small and that the thermistors indicated higher than true temperatures. The preflight corrections determined in the field were adjusted to conform to the laboratory values if large discrepancies occurred. The final value used is accurate to ± 0.3 scale unit. The application of

scale correction is good to ± 0.3 scale unit, and the trace can be easily read to 0.1 scale unit. The sum corresponds to 0.7°C . The magnitude

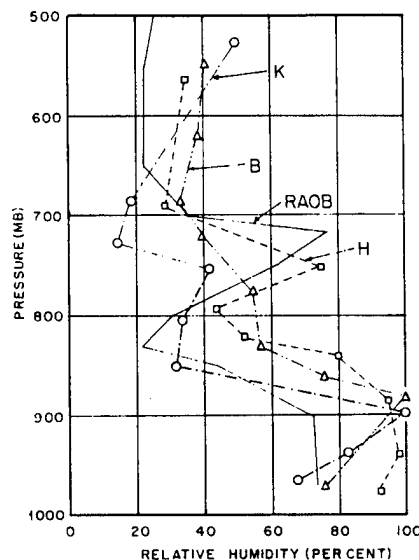


Fig. 3.5 Relative Humidity Reported on Calibration Flights of H-, B-, and K-drones Compared with Raob of the Same Day

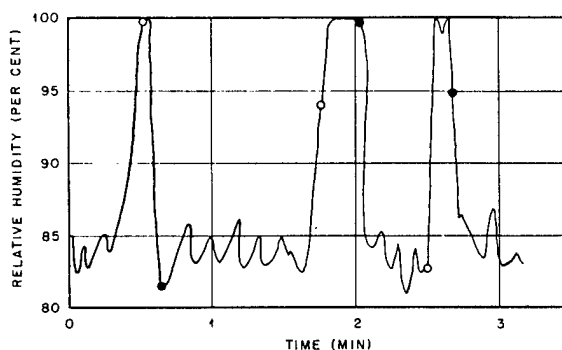


Fig. 3.6 Aerograph Record of Relative Humidity, Flight Through Cumulus Clouds.
O, cloud entry. ●, cloud exit.

of the dynamic correction error is based on the true airspeed accuracy, 0.2°C for 5 mph. The maximum error in the reported temperature is not larger than 1.0°C .

Unfortunately, laboratory recalibrations of the humidity elements could not be accomplished, and therefore the data obtained at the site were used to correct the records. The pre-flight correction is accurate to within 5.0 scale units. The application of dynamic and scale corrections should not be greater than the

equivalent of 0.5 unit. Allowing a similar amount for reading of the trace, the total error is no larger than 6.0 scale units. This corresponds to about 10 and 15 per cent at high and low relative humidities, respectively.

3.2 DATA ANALYSIS

In addition to the scale and dynamic corrections, the scale-unit vs temperature and relative-humidity curves were necessary. The 400 cycle/sec impedance of each thermistor bead at selected temperatures had been supplied by the contractor. By use of this information and that contained in Table 2.1, the required curve was produced.

A similar curve was drawn for the relative-humidity sensitive strips from the data of Table 2.2 and resistance vs relative humidity information. The average response of a number of the carbon elements was furnished through the courtesy of the Signal Corps. It was assumed that any one element would have a curve of the same shape although usually displaced.

The effect of age and exposure on the strips was unknown, and therefore an experiment was run to note any deviation with time. The strip was exposed in a closed, circulating airflow with water bath for controlling the relative humidity. A thermocouple measured the temperature near the strip. The true relative humidity was computed to 1 per cent accuracy from continuously recorded dew-point data. The resistance was measured on a 400 cycle/sec bridge with about 0.04 volt across the strip. This voltage was applied for a total of 52 hr over a period of seven days. The carbon element was continuously exposed to varying humidities for this period. A graph of true relative humidity and that indicated by the carbon element against elapsed current on time is shown in Fig. 3.7. The carbon element consistently indicated lower humidities than those computed from dew-point data. The maximum deviation was noted at about 16 hr. There was no apparent deterioration within the time of the experiment.

3.2.1 Preflight Operations

Prior to each flight a calibration of the thermistor and carbon element was accomplished with use of the device shown in Fig. 3.8. This is a test chamber designed to fit over the probe. A centrifugal blower circulates the air enclosed in the vessel. A pan for containing

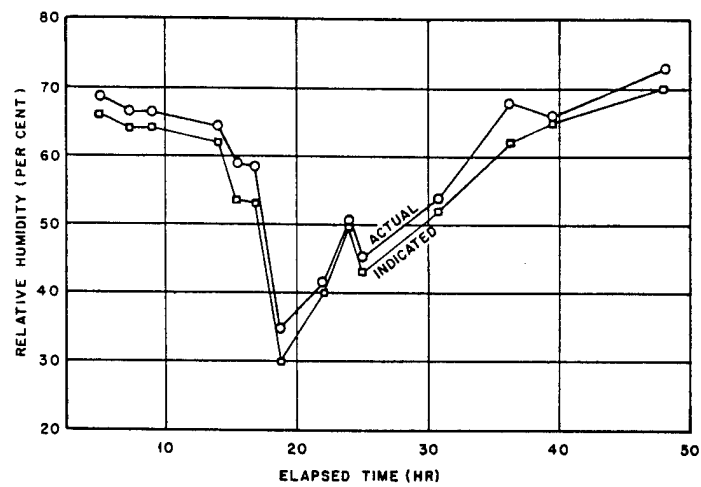


Fig. 3.7 Effect of Exposure on Carbon Element. Relative humidity is indicated by the carbon element as a function of actual humidity and exposure time.

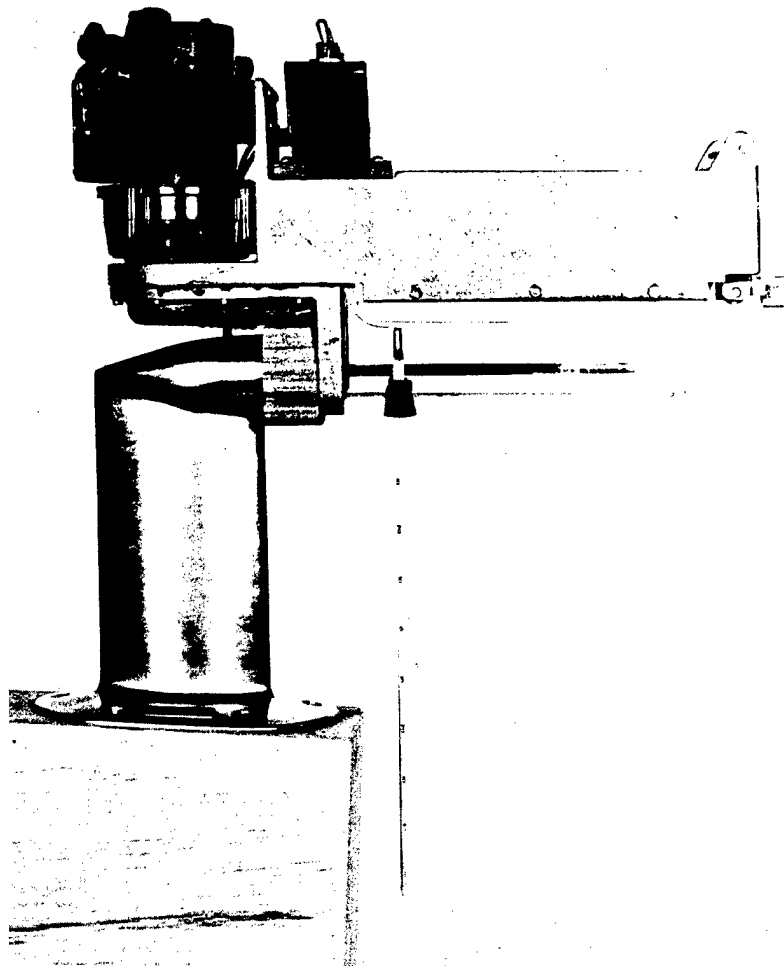


Fig. 3.8 Temperature-Humidity Test Chamber

water or salt solutions and a group of heaters gave some control over the temperature and relative humidity within the chamber. The dry- and wet-bulb temperatures and recorder indications were read when equilibrium was achieved in the chamber. The difference between the chamber temperature and the evaluated recorder reading was called the "preflight correction." This correction is an indication of thermistor-calibration drift from the original calibration curve.

The preflight correction for the relative-humidity strip was determined analogously. This correction is the measure of the deviation of the particular sensing element from the average. A new carbon element was used on each flight.

Since a drift of scale errors of the temperature and relative-humidity channels had been noted, part of the preflight procedure involved recalibration of these channels by noting recorder indication for fixed resistance input values. The drift was very small for times as short as a few days, but it was significant after about a week. The apparent cause was increased contact resistance at component junctions due to corrosion. The balancing potentiometers in the bridges were the chief offenders.

3.2.2 Postflight Analysis

The analysis of the records to obtain true values of the temperature, pressure, and relative humidity at selected times was straightforward. Some difficulty was encountered in constructing the time scale because the chart speed was found to differ in some cases from the printed scale. However, there were several signatures clearly identifiable on the aerograph trace, i.e., the take-off, T-5 sec signal, the shock wave, and cloud entry. The times of these occurrences were known from other sources, and so the actual length of record from take-off to whatever mark seemed to be most compatible with other data was measured and divided by the time difference to give the chart travel per minute. A scale was then constructed. Table 3.4 lists the times of some easily identifiable occurrences as measured from the constructed scale and the times of the same phenomena as reported by other test participants.

The indicated values of the four measured parameters were read from the record at times that appeared to be significant from the point of view of steady background or rapidly changing

indications. An effort was made to have the selected times correspond to those times for which the navigator's position report was available. Positions at other times were obtained by interpolation.

The scale correction was added to each selected indicated value. The aerodynamic correction of 2 knots was subtracted from the indicated airspeed to give calibrated airspeed. Methods of obtaining the true airspeed are given below.

The indicated pressure plus the scale correction yielded the true pressure. Using the calibrated airspeed as the argument, the pressure increment was selected from Table 3.2 and added to the true pressure to give the pressure within the temperature probe.

Addition of the preflight correction to the scale-corrected indicated temperature gave the calibrated temperature, in recorder units, which was converted to degrees centigrade by utilization of the calibration curve. The calibrated temperature is the temperature in the compressed atmosphere of the probe. The ambient temperature was found by application of the law of adiabatic expansion. The standard meteorological adiabatic charts were found useful for this step. An alternate method of ambient-temperature computation involved the calculation of the true airspeed. Here, unfortunately, two unknowns appear in the same equation, and so a method of successive approximation was utilized. The calibrated airspeed was assumed to be the true airspeed as the first guess. The aerodynamic correction for this airspeed was subtracted from the probe temperature to give the first approximation of the ambient temperature. Using this value and the true pressure, a second approximation of true airspeed was computed. The temperature correction for this new airspeed was subtracted from the probe temperature to find the second approximate ambient temperature. The process was continued until successive approximations of the true airspeed were identical, as would be the corresponding ambient temperatures. The actual determination can be accomplished very easily and quickly. Ambient temperatures computed by the two different methods agreed within a few tenths of a degree; therefore the procedures were used interchangeably except for those cases where the relative humidity was high. If the air sample reaches saturation during the computed expansion, correction must be made for the change in temperature-

TABLE 3.4 TIME COMPARISONS*

Aircraft identity	Shock wave		T-5 sec signal		Cloud penetration	
	Aerograph	Position plot	Aerograph	Actual time	Aerograph	Navigator
Dog Shot						
D	0634:52†	0634:52	Missing	0633:55	0637:45	0637:42
E	0634:35†	0634:35	0633:40	0633:55	0637:05	0637:30
K	0634:57†	0634:57	0634:08	0633:55	0639:20	0638:30
J	0634:45	0634:40	0633:55†	0633:55	0637:45	0637:45
A	0634:15	0635:02	0633:55†	0633:55	0637:45	0637:50
B	0635:40	0634:53	0633:55†	0633:55	0637:15	0637:05
C	0634:58†	0634:58	0633:50	0633:55	0638:10	0638:15
Easy Shot						
D	0627:56	0627:44	0627:00	0626:55	0630:35†	0630:50
I	0627:50	0627:43	0626:55†	0626:55	0630:20	0630:30
K	0627:43	0627:42	0626:55†	0626:55	0630:15	0630:50
B	0628:04	0627:59	0626:55†	0626:55	0631:45	0631:30
L	0627:44	0627:38	0626:55†	0626:55	0630:35	0630:25
C	0627:47	0627:43	0626:55†	0626:55	0629:45	Missing
A	0627:53	0627:47	0626:55†	0626:55	0630:40	Missing
J	0628:25	0628:02	0626:55†	0626:55	0632:30	0632:00
George Shot						
J	0931:06	0931:02	0929:15	0929:55	0935:13†	0935:13
C	0931:10	0931:08	0929:40	0929:55	0935:15†	0935:15
K	0930:45	0930:48	0929:55	0929:55	0934:40†	0934:40
L	0931:05	0930:52	0931:00	0929:55	0935:08†	0935:08
D	0931:00	0930:41	0928:35	0929:55	0934:47†	0934:47
B	0930:45	0930:59	0929:10	0929:55	0935:00†	0935:00
I	0931:05	0930:54	0929:55	0929:55	0934:35†	0934:35

* Time as read from constructed aerograph scale and from other sources.

† Base for aerograph time-scale construction.

decrease rate due to the liberation of heat of vaporization. In such cases the graphical method first described was used to find the ambient temperature since the saturated adiabatic expansion rate was printed on the chart.

The addition of scale and preflight corrections to the indicated relative-humidity value gave the relative humidity of the probe atmosphere in scale units, which was converted to per cent by the use of the calibration curve. Since the temperature and pressure of both the probe sample and the ambient air were known, the ambient relative humidity could be computed. Psychrometric Calculator ML-322/UM, a circular slide rule device, was used to make the computation.

The reported relative humidities at temperatures below the freezing point are computed with respect to the saturation vapor pressure over ice.

REFERENCES

1. N. A. V. Piercy, "Aerodynamics," 2d ed., English Universities Press, Ltd., London, 1947, p. 37.
2. W. L. Howland, Measurement of Ambient Temperatures in Flight, Reprint 106, Institute of Aeronautical Sciences, New York, p. 3.
3. The Correction of Aircraft Observations of Air Temperature and Humidity for the Effect of Aircraft Speed, Meteorological Office Index 2047, Great Britain Air Ministry, April 1942.

Chapter 4

Test Results

4.1 GENERAL OPERATIONS PROCEDURES

For each test shot the aerograph equipment was checked and preflighted, as discussed in Sec. 3.2.1, in each of the aircraft participating in the measurement program. Inasmuch as the drone aircraft had to take off as long as 4 hr before actual shot time in order to arrive at assigned positions, the aerograph equipment was turned on before take-off.

The time between take-off and actual cloud penetration was consumed in predetermined flight patterns designed to maneuver the test aircraft in proper positions for the blast. Following the cloud penetration, the aircraft had to remain aloft for an additional 1 to 2 hr before landing. The aerograph equipment operated satisfactorily throughout the period between take-off and landing in all the aircraft for each of the first three shots. The aerographs were not included in the fourth shot program.

4.2 AEROGRAPH-DATA REDUCTION PROBLEMS

Since the aerograph record for each aircraft was taken over a number of hours, a great deal of information had to be screened out. In the case of the AEC drone aircraft, attention was fixed on that portion of the record starting immediately before cloud penetration and continuing for some minutes after exit from the cloud. This portion was worked up in detail, and these results are presented in this chapter and in Chap. 5.

Selecting a 3- or 4-min period to the nearest second from a record of several hours in length posed a problem in ascertaining the time base accurately. The procedure discussed in Sec.

3.2.2 was followed, and Table 3.4 shows the time scale actually employed. Comparison of the aerograph trace, the navigator's log, and the results of Project 6.8 for time of cloud entry and cloud exit showed fair agreement. This point is discussed in greater detail in Sec. 5.2.2.

Another problem became apparent when the cloud-traverse records were analyzed. In all cases the true airspeed underwent a change, sometimes a violent fluctuation of 40 to 50 mph. The rapidity and amplitude of this fluctuation was such that a revision had to be made in the method of correcting the measured temperature and humidity for dynamic heating. When the ambient temperature and humidity were obtained as outlined in Sec. 3.2.2 and then plotted along with the true airspeed on a time cross section, it was immediately evident that changes in temperature and humidity were in phase with the true airspeed. Since the true airspeed and the ambient temperature are independent, there would be no natural reason for such closely correlated behavior.

The relation between indicated airspeed and ambient temperature was investigated, and it was concluded that (1) a change in ambient temperature of a few degrees has practically no effect on the indicated airspeed and (2) the density correction that must be employed to convert indicated airspeed to true airspeed takes into consideration changes in ambient temperature and pressure.

It was suspected, therefore, that the dynamic correction for airspeed was the source of the spurious phase agreement. The aerograph records were reexamined to determine how the indicated probe temperature fluctuated with true airspeed. It was found that no agreement between these latter two parameters existed and

that, for the majority of the traces, the probe temperature showed very little variation.

The fictitious oscillation in ambient temperature was due to the inability of the thermistor to follow the extremely rapid changes in temperature that would be produced inside the probe housing by violent changes in true airspeed. The probe employed a Western Electric type 14B thermistor bead covered with $\frac{1}{8}$ in. plastic coating. Although no data were available on the lag of this type bead, Jehn¹ reported a lag time of 2.8 sec for a Western Electric type D-177703. The 14B thermistor is larger in size than this bead and, therefore, would be expected to have a greater lag. When oscillating phenomena are measured, the period of the oscillations should be at least four times the lag constant to ensure measuring within 2 per cent of the true value, according to accepted practice. This would mean that oscillations in true airspeed having a period of less than 10 to 12 sec would not be followed by the thermistor. Inspection of the flight traces revealed that the true airspeed fluctuations occurred over a time interval of 5 sec or less in many cases.

It was decided to ignore the true airspeed fluctuation inside the cloud and to apply an airspeed correction based on the average true airspeed before cloud entry. This procedure was adopted for all temperatures measured inside the cloud on all shots.

4.3 DOG SHOT

The aerograph systems were operative in the 12 drone aircraft participating in Dog Shot. Records from the eight AEC flights and from the Air Force planes at 7800 and 15,000 ft were analyzed. The two other blast aircraft records were retrieved but not reduced since the planes were unable to participate as scheduled.

The eight AEC planes designated as Yellow A, Yellow B, etc., or as Yellow 16, Yellow 18, etc., were assigned the mission of penetrating the atomic cloud. Penetrations were made at the 16,000-, 18,000-, 20,000-, 22,000-, 24,000-, 26,000-, 28,000-, and 30,000-ft levels. The plan was to have two passes flown through the cloud by each aircraft. Yellow 26 was lost by the mother ship after the first penetration and was found too late to permit a second penetration. Yellow 22 actually made three passes through the cloud, but only the first two passes were analyzed in detail. The values of the aerograph

parameters (temperature, relative humidity, true airspeed, and static pressure) for each of the Dog Shot cloud traverses except as already noted are given in Table 4.1. The position of the aircraft as a function of time is given in the table in terms of bearing and range with respect to Ground Zero. Azimuths are measured clockwise from true north in degrees. The range is the projection of the slant range on the surface and is given in nautical miles. The remarks pertain to the relation of the drones to the atomic cloud.

The temperature and pressure reported by each drone aircraft immediately before entering the cloud are shown in Fig. 4.1. The radiosonde data as received from the Eniwetok Weather Central are plotted also for comparison. The radiosondes were made at about H-6 and H+3:30 hr. It is seen that the aerograph temperature compared very closely to the Raob and may be taken as good indication of well functioning aerograph equipment. This agreement lends weight to the validity of the cloud-traverse data in Table 4.1.

The records of the two Air Force blast aircraft at 7800 and 15,000 ft, respectively, are given in Table 4.2. The data pertain to the time of intercept of the shock wave at these altitudes. The aerograph data showed marked changes in pressure and true airspeed but little change in temperature and relative humidity. The small temperature change even for the low-level ship indicates that the aerograph probe is well protected from radiation effects.

4.4 EASY SHOT

Eight AEC drones and two Air Force drones were equipped with aerographs. An additional two Air Force drones were flown, but the aerographs were removed from these two because there was little chance of a successful return of these ships.

As in the Dog Shot mission the eight AEC aircraft were to penetrate the atomic cloud at the previous levels. Aerograph records were obtained for all aircraft, and the cloud-penetration data are shown in Table 4.3.

Some questions arose about the 24,000-, 26,000-, 28,000-, and 30,000-ft penetrations. According to the navigator's log the 24,000- and 26,000-ft aircraft failed to penetrate the cloud on their first pass. Yet Greenhouse Report, Annex 6.8, indicates definite penetration.

TABLE 4.1 CLOUD TRAVERSES, DOG SHOT

Time	Azimuth (deg)	Range (nautical miles)	True airspeed (TAS) (mph)	Pressure (mb)	Temp. (°C)	Relative humidity (%)	Remarks
Aircraft L, 16,000-ft Elevation							
0637:00	192	1.05	213	567	-0.2	21	Free air near cloud
0637:15	210	0.4	204	565	-0.6	52	Entry
0637:28	006	0.3	188	560	-0.8	94	Min. TAS
0637:35	355	0.75	255	557	-0.7	50	Max. TAS
0637:40	010	1.0	247	561	-0.2	Missing	Exit
0638:00	010	2.0	242	564	-0.3	Missing	Free air
0646:00	200	3.5	185	568	-1.1	Missing	Free air
0646:15	199	3.75	181	566	+0.9	16	Second entry
0647:00	198	4.5	207	567	+0.7	33	Exit
0647:03	198	4.65	214	566	+0.3	27	Free air
0647:10	198	4.6	215	566	+0.3	21	Free air
0648:00	198	7.5	206	567	-0.1	Missing	Free air
Aircraft K, 18,000-ft Elevation							
0638:00	358	1.5	205	530	-1.9	38	Free air
0638:30	000	0.0	203	529	-2.2	38	Entry
0638:45	180	0.65	202	527	-3.0	72	Min. TAS
0638:50	175	0.25	230	527	-3.7	97	In cloud
0639:10	175	3.2	212	529	-4.4	34	Exit
0639:30	175	3.0	210	528	-3.8	30	Free air
0651:00	205	1.7	199	529	-1.7	31	Free air
0651:20	240	1.2	201	530	-1.9	32	Free air
0651:25	246	1.2	205	529	-2.0	30	Free air
0651:40	264	1.25	201	529	-2.0	30	Second entry
0652:00	310	1.6	201	530	-2.5	50	In cloud
0652:40	338	2.8	201	530	-2.2	38	Exit
0653:45	350	5.2	202	530	-2.1	35	Free air
Aircraft J, 20,000-ft Elevation							
0637:30	180	1.05	206	483	-6.1	30	Free air
0637:45	180	7.4	215	485	-6.8	29	Near edge of cloud
0637:58	180	0.06	192	482	-7.0	36	Min. TAS
0638:00	180	6.7	198	486	-7.5	36	In cloud
0638:15	360	0.90	227	480	-7.6	34	Max. TAS
0638:23	180	5.6	231	485	-5.8	28	Exit
0639:45	335	3.0	222	486	-5.9	30	Free air
0645:00	001	0.06	206	483	-5.8	30	Free air near cloud
0645:03	182	1.6	210	480	-5.2	28	Second entry
0645:18	182	1.25	204	483	-6.2	34	Min. TAS
0645:21	182	1.43	208	484	-6.0	30	Max. TAS
0645:23	182	2.7	210	485	-6.2	29	Exit
0647:00	182	6.95	203	486	-6.2	28	Free air

TABLE 4.1 (Continued)

Time	Azimuth (deg)	Range (nautical miles)	True airspeed (TAS) (mph)	Pressure (mb)	Temp. (°C)	Relative humidity (%)	Remarks
Aircraft E, 22,000-ft Elevation							
0637:00	187	2.0	207	446	-8.3	50	Free air
0637:10	187	2.25	208	446	-8.4	50	Entry
0637:12	187	2.4	205	446	-7.9	50	Min. TAS
0637:15	185	2.4	245	446	-9.3	59	In cloud
0637:16	192	3.1	245	444	-10.0	63	Max. TAS
0637:35	185	3.1	227	448	-10.3	64	Exit
0638:10	198	5.5	229	445	-8.7	50	Free air
0643:30	360	0.1	220	446	-8.8	52	Second entry
0646:10	360	8.25	220	447	-7.3	50	Free air
Aircraft D, 24,000-ft Elevation							
0637:18	359	2.28	234	413	-13.1	48	Free air
0637:52	360	2.4	237	413	-13.7	49	Entry
0637:55	330	0.28	229	414	-13.1	48	Min. TAS
0637:58	300	0.17	272	414	-13.1	47	Max. TAS
0638:00	270	0.15	264	414	-13.5	51	In cloud
0638:07	270	0.3	261	413	-13.0	52	Exit
0640:00	295	3.7	259	415	-12.7	49	Free air
0644:00	335	5.5	227	414	-13.0	49	Free air
0644:45	351	4.4	226	414	-13.3	49	Second entry
0645:05	360	4.0	227	414	-13.4	49	Exit
Aircraft B, 26,000-ft Elevation							
0637:00	350	2.0	230	376	-18.8	27	Free air
0637:05	350	1.7	223	376	-18.7	24	Entry
0637:12	350	1.3	221	378	-18.3	28	Min. TAS
0637:33	350	0.13	279	376	-18.7	29	Max. TAS
0637:50	170	0.9	266	374	-18.2	24	Exit
0638:00	170	1.5	229	376	-18.7	28	Free air
0638:30	170	3.25	220	376	-18.7	29	Free air
Aircraft C, 28,000-ft Elevation							
0637:30	180	3.4	238	358	-21.2	42	Free air
0638:15	180	1.45	231	359	-20.8	43	Entry
0638:20	180	1.3	238	358	-21.2	45	In cloud
0638:30	180	1.0	231	357	-21.4	53	In cloud
0638:32	180	0.85	268	358	-21.8	44	Max. TAS
0638:50	180	0.3	269	358	-21.8	50	Exit
0640:00	332	3.0	250	357	-21.1	40	Free air
0644:30	030	2.38	239	359	-20.8	41	Free air
0644:58	046	1.10	227	358	-21.1	42	Second entry
0645:13	061	1.63	226	358	-21.1	43	Min. TAS
0645:28	066	2.5	244	358	-20.8	43	Max. TAS
0645:30	067	2.5	236	358	-21.2	43	In cloud
0645:35	067	1.7	237	358	-21.3	43	Exit
0646:00	070	4.0	245	356	-21.6	48	Free air
0647:00	090	7.0	241	358	-21.1	42	Free air

TABLE 4.1 (Continued)

Time	Azimuth (deg)	Range (nautical miles)	True airspeed (TAS) (mph)	Pressure (mb)	Temp. (°C)	Relative humidity (%)	Remarks
Aircraft A, 30,000-ft Elevation							
0637:00	358	3.0	241	329	-24.0	41	Free air
0637:40	290	0.4	249	328	-23.9	40	New cloud
0638:00	180	2.0	251	325	-23.9	43	Entry
0638:10	187	1.82	255	323	-23.9	44	Min. TAS
0638:12	187	1.97	274	323	-23.9	43	Max. TAS
0638:15	177	1.8	273	320	-24.0	50	In cloud
0638:45	171	3.8	234	316	-24.3	51	Exit
0639:00	190	5.0	233	318	-25.9	48	Free air
0644:30	184	5.5	247	325	-24.2	49	Second entry
0644:40	184	5.5	241	313	-24.9	44	In cloud
0644:52	180	1.98	226	326	-23.9	46	Min. TAS
0644:55	180	1.8	248	327	-23.9	45	Max. TAS
0645:10	180	0.9	244	327	-23.9	46	Exit

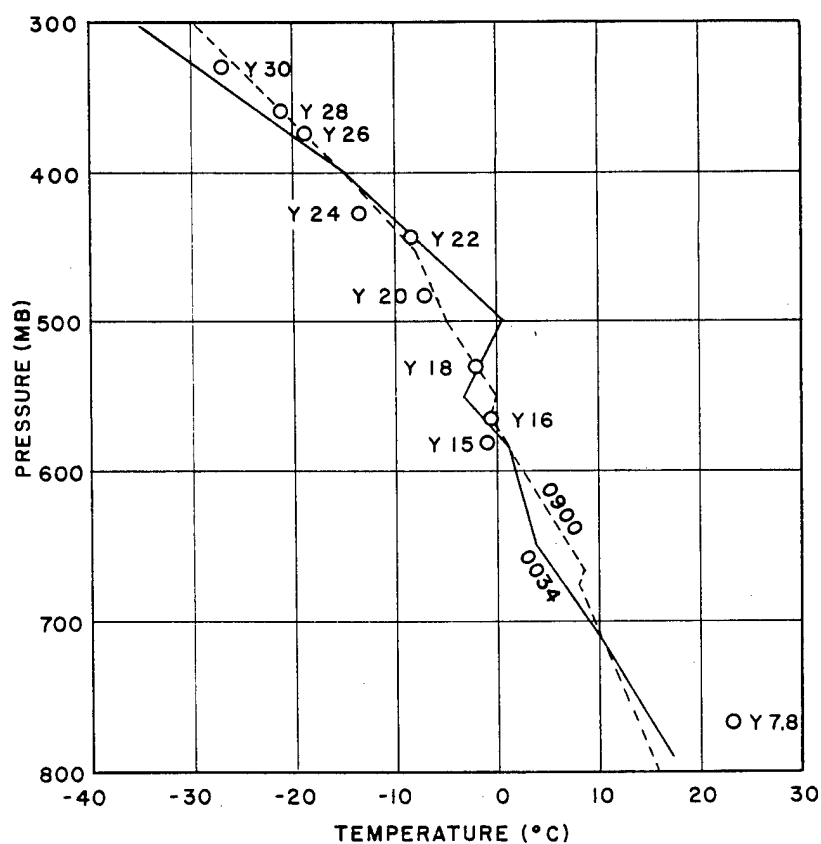


Fig. 4.1 Comparison of Drone Data Just Prior to Cloud Entry with Radiosondes Released at 0034 and 0900, Dog Shot

TABLE 4.2 SHOCK-WAVE INTERCEPT, DOG SHOT

True airspeed (mph)	Pressure (mb)	Temperature (°C)	Relative humidity (%)	Remarks
7,800-ft Elevation				
214	767	23.1	29	Prior to shock
265	770	20.8	33	Max. airspeed
167	750	25.0	27	Min. airspeed
15,000-ft Elevation				
197	582	-0.9	60	Prior to shock
223	582	-1.0	61	Max. airspeed
100	547	Missing	Missing	Min. airspeed

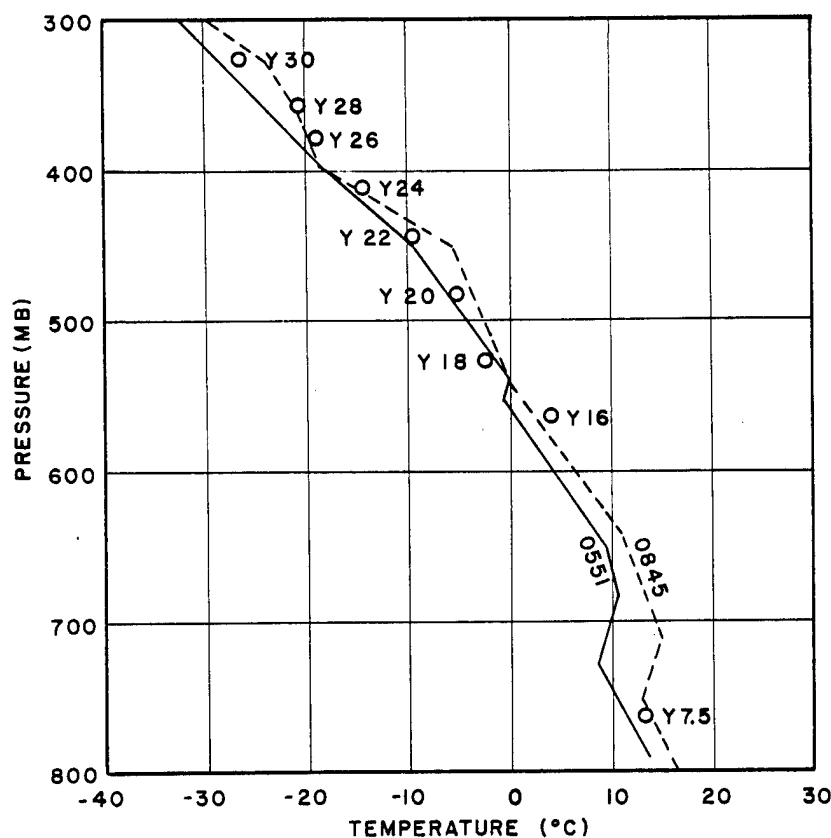


Fig. 4.2 Comparison of Drone Data Just Prior to Cloud Entry with Radiosondes Released at 0551 and 0845, Easy Shot

The aerograph record underwent a fluctuation of a nature similar to that of the lower altitudes; these data are included in Table 4.3. It is felt that these aircraft must have been very near the cloud, if not actually immersed, in order to record the fluctuation in measured parameters as found.

In the case of the 28,000- and 30,000-ft aircraft, the navigator's log does not state clearly if these aircraft actually penetrated the cloud on the first pass. Annex 6.8 claimed, on the basis of the lack of jet impactor samples, that no penetration was made. The aerograph data for these

TABLE 4.3 CLOUD TRAVERSES, EASY SHOT

Time	Azimuth (deg)	Range (nautical miles)	True airspeed (TAS) (mph)	Pressure (mb)	Temp. (°C)	Relative humidity (%)	Remarks
Aircraft L, 16,000-ft Elevation							
0637:45	215	0.25	197	561	-0.5	57	Free air
0638:15	215	1.65	198	561	-0.2	68	Entry
0638:30	215	2.75	199	561	-0.2	69	In cloud
0639:45	215	5.75	201	560	-0.8	56	Exit
Aircraft K, 18,000-ft Elevation							
0629:55	350	1.6	204	525	-2.7	52	Free air
0630:00	350	1.35	204	522	-2.6	52	Free air
0630:10	350	0.85	209	523	-2.8	53	Entry
0630:22	350	0.25	225	524	-3.1	56	Max. TAS
0630:25	000	0.0	206	524	-3.6	64	Max. RH
0630:32	170	0.50	189	524	-3.6	55	Min. TAS
0630:55	170	1.5	187	525	-3.5	52	Exit
0635:40	180	4.5	205	525	-3.6	52	Free air
0641:40	168	3.3	206	525	-3.1	52	Free air
0642:00	168	2.3	209	524	-3.0	51	Second entry
0642:10	168	1.3	216	525	-2.9	53	Max. TAS
0642:20	168	1.4	205	525	-3.0	52	In cloud
0642:22	168	1.2	203	525	-2.6	55	Min. TAS
0642:30	168	0.8	203	525	-2.6	55	Exit
0643:40	348	2.5	206	524	-3.0	52	Free air
0647:40	348	14.1	206	524	-2.9	52	Third entry
0648:50	348	11.0	207	524	-3.0	55	In cloud
0650:40	350	5.6	205	525	-3.0	52	Exit
Aircraft J, 20,000-ft Elevation							
0632:00	180	1.25	212	481	-5.0	46	Free air
0632:30	000	0.0	216	481	-5.1	46	Entry
0632:35	340	0.25	220	480	-5.2	48	Max. TAS
0632:55	340	1.25	183	485	-5.5	53	Min. TAS
0633:00	340	1.5	184	489	-5.5	52	Max. RH
0633:10	340	2.0	184	486	-5.6	48	Exit
0633:30	340	3.0	184	481	-6.0	46	Free air
0637:30	360	3.8	215	481	-5.1	46	Free air
0638:00	360	1.9	210	481	-5.5	45	Free air
0638:05	360	1.6	212	481	-5.0	46	Free air
0638:20			204	480	-5.0	48	Second entry
0638:25	360	0.3	201	480	-5.0	49	Min. TAS
0638:30	000	0.0	215	481	-4.4	51	In cloud
0638:50	180	0.95	230	481	-4.9	51	Max. TAS
0639:00	180	1.5	225	481	-3.8	47	Exit
0640:30	180	6.0	215	481	-5.0	46	Free air
Aircraft I, 22,000-ft Elevation							
0630:00	360	0.75	209	443	-9.9	21	Free air
0630:05	360	0.7	208	444	-9.9	32	Edge of cloud
0630:38	183	0.83	258	441	-10.5	57	Max. TAS
0630:45	184	1.2	232	444	-10.6	58	Min. TAS
0630:50	185	1.2	257	442	-10.6	60	In cloud

TABLE 4.3 (Continued)

Time	Azimuth (deg)	Range (nautical miles)	True airspeed (TAS) (mph)	Pressure (mb)	Temp. (°C)	Relative humidity (%)	Remarks
Aircraft I, 22,000-ft Elevation							
0631:05	185	1.8	236	443	-9.9	34	Exit
0633:05	200	7.7	220	445	-9.3	33	Free air
0636:00	180	1.05	215	445	-10.5	35	Free air
0636:05	180	1.0	215	443	-10.3	35	Free air
0636:15	180	0.5	220	444	-10.1	37	Second entry
0636:20	000	0.0	224	445	-10.0	39	Max. TAS
0636:30	360	0.6	209	444	-10.1	44	In cloud
0636:35	360	0.75	197	445	-10.0	39	Min. TAS
0637:05	360	2.05	214	445	-10.4	35	Exit
0640:05	360	11.05	209	444	-10.7	35	Free air
Aircraft D, 24,000-ft Elevation							
0630:30	360	0.4	222	414	-14.6	51	Free air
0630:35	180	0.6	224	412	-14.6	51	Near cloud
0630:55	360	1.73	203	414	-14.8	55	Min. TAS
0631:10	360	2.3	237	410	-16.3	56	In cloud
0631:15	357	2.35	271	413	-15.7	52	Max. TAS
0632:00	350	3.5	237	412	-14.5	52	Exit
0635:00	360	6.7	216	412	-14.9	51	Free air
0636:30	360	1.6	229	414	-14.4	50	Free air
0637:00	180	0.1	229	412	-14.8	50	Second entry
0637:10	180	0.7	227	414	-14.4	50	Max. TAS
0637:25	180	1.75	200	415	-14.3	50	In cloud
0637:28		1.78	176	415	-14.8	50	Exit
0637:32	180	1.82	172	415	-14.4	50	Free air
0639:00	180	6.9	222	413	-14.9	50	Free air
Aircraft B, 26,000-ft Elevation							
0631:00	005	2.1	221	376	-18.9	60	Free air
0631:20	001	1.3	224	377	-19.1	60	Edge of cloud
0631:45	260	0.3	208	376	-18.9	57	Min. TAS
0632:10	207	1.43	279	376	-18.4	54	Max. TAS
0632:12	207	1.5	240	376	-19.1	63	In cloud
0632:25	207	2.1	251	376	-18.1	50	Exit
0637:50	180	0.9	229	376	-18.4	57	Second entry
0638:00	180	0.7	225	376	-18.8	58	In cloud
0638:10	180	0.1	220	377	-18.9	62	In cloud
0638:20	360	0.3	250	376	-18.5	48	Exit
0638:40	360	0.14	214	377	-18.1	52	Free air
0638:50	360	1.85	198	378	-18.0	54	Free air
0639:00	360	0.3	208	377	-18.5	58	Free air
0641:00	360	8.9	220	377	-18.9	59	Free air
Aircraft C, 28,000-ft Elevation							
0629:00	180	3.8	239	355	-20.6	67	Free air
0629:20	180	2.7	239	354	-20.7	69	Free air
0629:37	180	1.75	250	354	-20.6	69	Entry
0629:47	180	1.2	250	352	-20.6	67	Max. RH
0629:50	180	1.05	250	353	-20.6	69	Exit

TABLE 4.3 (Continued)

Time	Azimuth (deg)	Range (nautical miles)	True airspeed (TAS) (mph)	Pressure (mb)	Temp. (°C)	Relative humidity (%)	Remarks
Aircraft C, 28,000-ft Elevation							
0636:45	358	4.9	236	354	-20.6	70	Free air
0636:50	358	1.5	242	356	-20.5	67	Second entry
0637:08	358	3.7	234	354	-20.6	70	Min. TAS
0637:13	358	3.4	238	354	-20.6	70	Max. TAS
0637:15	358	3.3	248	355	-20.5	68	In cloud
0637:20	358	3.2	249	355	-20.5	68	Exit
0639:45	178	6.4	232	355	-20.7	67	Free air
0642:45	170	7.65	238	354	-20.7	68	Free air
0643:00	170	7.0	250	355	-20.6	69	Third entry
0643:01	168	7.1	234	354	-20.7	70	Min. TAS
0643:02	168	7.0	250	354	-20.7	69	Max. TAS
0643:20	160	6.2	245	355	-20.6	69	In cloud
0644:45	160	19.5	243	355	-20.6	69	Exit
0645:30	340	.95	242	355	-20.6	69	Free air
Aircraft A, 30,000-ft Elevation							
0630:01	360	1.0	252	317	-27.0	54	Free air
0630:35	180	0.9	262	316	-26.9	53	Entry
0630:50	180	1.33	247	315	-27.1	55	Min. TAS
0631:00	180	2.6	273	315	-27.7	55	In cloud
0631:10	188	1.8	288	320	-27.0	52	Exit
0632:00	215	4.2	265	315	-26.9	53	Free air
0634:00	193	6.7	253	317	-27.0	54	Free air
0636:00	180	2.4	246	318	-27.0	53	Free air
0637:00	360	1.0	257	316	-27.0	56	Second entry
0637:05	360	1.3	292	317	-26.9	55	Max. TAS
0637:10	360	1.6	247	317	-26.9	56	Min. TAS
0637:45	360	3.6	275	317	-26.7	59	In cloud
0638:10	357	4.6	268	318	-26.8	57	Exit
0639:00	333	6.2	250	318	-27.0	56	Free air
0641:00	354	6.6	243	316	-27.5	56	Free air

TABLE 4.4 SHOCK-WAVE INTERCEPT, EASY SHOT

True airspeed (mph)	Pressure (mb)	Temperature (°C)	Relative humidity (%)	Remarks
7,500-ft Elevation				
159	761	16.0	68	Prior to shock
230	805	13.2	73	Max. airspeed
85	730	17.2	60	Min. airspeed
12,000-ft Elevation				
199	659	11.7	51	Prior to shock
211	693	12.5	49	Max. airspeed
184	664	12.6	52	Min. airspeed

TABLE 4.5 CLOUD TRAVERSES, GEORGE SHOT

Time	Azimuth (deg)	Range (nautical miles)	True airspeed (TAS) (mph)	Pressure (mb)	Temp. (°C)	Relative humidity (%)	Remarks
Aircraft L, 16,000-ft Elevation							
0935:00	048	0.75	206	563	-0.3	43	Free air
0935:02	046	0.81	204	563	-0.2	45	Free air
0935:08	032	0.98	196		-0.5	93	Entry
0935:13	024	1.17	193	564	-0.6	100	Min. TAS
0935:15	020	1.3	213	559	-1.3	100	Max. T-RH peak
0935:27	011	1.69	260	550	-3.8	100	Max. TAS
0935:30	010	1.9	263	550	-0.2	97	Max. RH, min. press.
0935:50	004	2.8	254	562	-1.3	92	Exit
0936:00	002	3.2	244	562	-1.8	88	Free air
0937:00	352	5.8	205	562	-1.6	46	Free air
0939:00	050	8.9	198	563	-0.6	46	Free air
0942:00	051	2.9	197	563	-0.1	45	Free air
0942:11	060	2.7	193	565	-0.1	46	Free air
0942:15	063	2.6	190	566	-0.1	49	Second entry
0942:38	085	2.4	164	568	-0.3	92	Min. TAS
0942:41	088	2.4	181	568	-0.4	88	Max. TAS
0943:00	107	2.6	172	564	-2.0	99	In cloud
0943:10	113	2.7	171	564	-2.7	85	Exit
0944:00	141	4.3	192	565	-1.6	54	Free air
Aircraft K, 18,000-ft Elevation							
0934:35	360	0.35	203	524	-3.1	45	Free air
0934:40	000	0.10	201	523	-3.4	47	Entry
0934:48	360	0.02	187	523	-1.1	100	Min. TAS
0934:50	177	2.4	199	524	-0.5	100	Max. RH
0934:55	177	2.8	206	518	-0.1	100	In cloud
0934:58	180	0.4	227	506	-0.3	100	Max. TAS
0935:20	177	1.4	219	508	-1.8	100	Exit
0935:45	177	3.4	214	508	-3.1	100	Free air
0937:45	175	4.9	218	521	-5.2	45	Free air
0940:00	005	0.95	203	522	-1.1	51	Free air
0940:05	005	1.4	203	521	-5.1	60	Near cloud
0940:10	005	1.5	224	522	-1.2	100	Max. TAS
0940:15	005	1.6	204	521	-1.0	100	In cloud
0940:20	005	1.95	204	521	-3.8	100	Min. TAS
0940:25	005	2.8	216	524	-3.5	100	Exit
0940:40	005	3.1	200	522	-4.4	95	Free air
Aircraft J, 20,000-ft Elevation							
0935:10	180	0.85	217	485	-3.7	44	Free air
0935:13	180	0.7	218	485	-3.7	45	Entry
0935:18	180	0.44	213	485	-3.2	86	Min. TAS
0935:40	360	0.8	250	481	-2.5	100	In cloud
0935:43	360	0.9	276	482	-2.2	100	Max. TAS
0935:53	360	1.4	250	487	-3.7	100	Exit
0937:00	350	4.2	221	485	-6.8	74	Free air
0940:00	357	8.2	207	485	-5.6	42	Free air
0943:15	005	2.67	198	486	-3.9	27	Free air
0943:18	005	2.5	198	485	-3.8	30	Free air

TABLE 4.5 (Continued)

Time	Azimuth (deg)	Range (nautical miles)	True airspeed (TAS) (mph)	Pressure (mb)	Temp. (°C)	Relative humidity (%)	Remarks
Aircraft J, 20,000-ft Elevation							
0943:40	005	1.71	195	486	-4.1	61	Second entry
0944:05	005	0.82	218	487	-5.5	86	Max. TAS
0944:20	185	0.3	218	486	-5.2	76	Exit
0944:58	185	2.5	217	485	-4.0	20	Free air
0946:00	185	5.5	211	485	-2.3	24	Free air
Aircraft I, 22,000-ft Elevation							
0934:00	016	3.8	218	448	-10.0	40	Free air
0934:30	027	2.7	230	445	-10.1	36	Entry
0934:40	032	2.3	227	451	-10.4	100	In cloud
0934:43	036	2.15	272	441	-6.7	100	Max. TAS
0934:45	038	2.05	213	437	-6.8	100	Min. TAS
0934:50	040	2.0	232	436	-6.7	100	Max. RH and temp.
0935:10	060	1.4	249	436	-8.4	100	Exit
0936:00	151	1.6	270	445	-12.5	82	Free air
0938:00	050	6.7	213	448	-10.6	49	Free air
0941:00	064	3.6	201	447	-9.8	41	Free air
0941:52	064	3.7	205	448	-9.6	49	Second entry
0942:10	054	4.3	219	446	-9.7	84	Max. TAS
0942:20	048	4.8	187	446	-10.2	84	Min. TAS
0942:45	039	5.7	193	448	-10.1	92	Max. RH
0943:00	036	6.4	195	449	-9.6	33	Exit
0944:00	026	9.2	203	448	-10.6	34	Free air
Aircraft D, 24,000-ft Elevation							
0934:40	173	0.3	246	414	-14.6	72	Free air
0934:47	353	0.1	240	412	-14.2	41	Entry
0934:49	353	0.15	225	414	-12.1	100	Min. TAS
0934:50	353	0.2	305	406	-12.3	100	In cloud
0934:55	353	0.5	320	400	-13.3	100	Max. TAS
0935:20	353	1.95	243	409	-15.1	100	Exit
0935:35	353	2.8	238	410	-14.1	100	Free air
0941:00	353	0.57	239	413	-14.6	78	Free air
0941:16	171	0.5	240	409	-15.0	92	Edge of cloud
0941:30	171	1.25	236	410	-14.3	70	Min. TAS
0941:40	171	1.35	246	411	-13.7	97	Max. TAS
0941:45	171	1.4	244	410	-14.7	87	Min. temp.
0941:55	171	1.5	229	411	-14.5	100	Max. RH
0942:25	171	4.05	205	411	-14.6	85	Exit
0942:35	171	4.6	207	412	-14.8	59	Free air
Aircraft B, 26,000-ft Elevation							
0934:55	008	0.26	233	380	-16.2	100	Free air
0935:00	000	0.0	229	381	-16.9	49	Entry
0935:15	198	0.77	186	381	-16.0	100	Min. TAS
0935:22	198	1.37	247	381	-16.1	100	Max. TAS
0935:50	198	2.5	234	379	-16.6	100	Exit

TABLE 4.5 (Continued)

Time	Azimuth (deg)	Range (nautical miles)	True airspeed (TAS) (mph)	Pressure (mb)	Temp. (°C)	Relative humidity (%)	Remarks
Aircraft B, 26,000-ft Elevation							
0936:00	198	3.2	234	379	-17.9	100	Free air
0943:30	200	2.0	207	382	-16.1	Missing	Free air
0943:35	200	2.3	203	382	-16.0	Missing	Second entry
0944:00	000	0.0	207	383	-15.9	30	In cloud
0944:05	020	0.3	192	386	-15.7	Missing	Min. TAS
0944:30	020	1.75	235	383	-16.0	87	Exit
0945:00	020	3.5	233	382	-16.0	Missing	Free air
Aircraft C, 28,000-ft Elevation							
0935:00	000	0.0	245	357	-18.0	32	Free air
0935:10	360	0.68	250	358	-18.6	46	Entry
0935:17	360	1.02	233	358	-18.5	100	Min. TAS
0935:33	360	1.98	312	348	-15.7	100	Max. TAS
0935:35	360	2.7	306	345	-17.0	100	In cloud
0936:15	354	4.1	258	357	-19.5	100	Exit
0937:00	330	7.4	250	357	-20.2	37	Free air
0940:55	180	3.4	240	358	-19.4	27	Free air
0941:00	180	3.7	241	358	-19.4	27	Second entry
0941:13	180	4.5	225	358	-19.2	80	Min. TAS
0941:15	180	4.6	238	358	-18.4	85	In cloud
0941:18	180	4.8	254	358	-19.2	32	Max. TAS
0941:40	180	6.1	174	360	-18.7	25	Exit
0942:00	180	7.4	174	365	-18.7	23	Free air
0944:00	180	14.8	188	366	-18.7	47	Free air

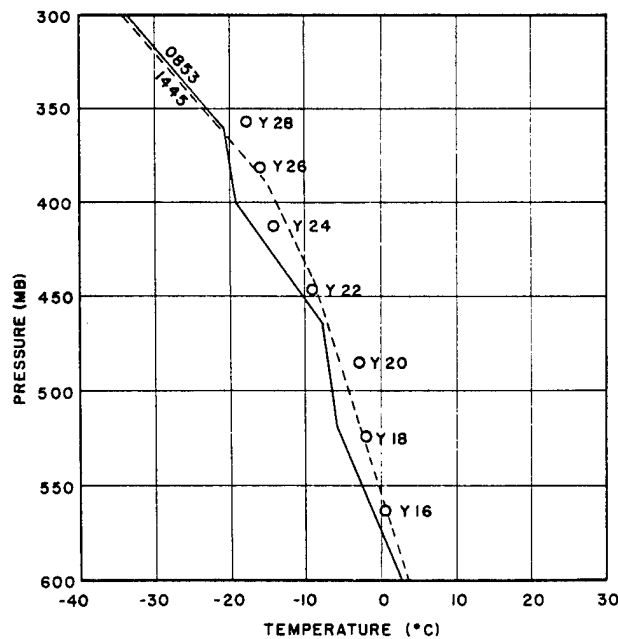


Fig. 4.3 Comparison of Drone Data Just Prior to Cloud Entry with Radiosondes Released at 0853 and 1445, George Shot

two aircraft are given at the time when the ships should have intercepted the cloud. Yellow 18, Yellow 28, and Yellow 30 made three passes. The data were worked up for all three passes for Yellow 18 and Yellow 28. The cloud had diffused so greatly by the time of the third pass of Yellow 30 that no indication of penetration could be picked up by the aerograph. Consequently only data pertaining to the first two passes are given.

The low-level aircraft, Yellow 7.5 and Yellow 12, were blast aircraft. Thus only the shock-wave intercept data, given in Table 4.4, are provided for these ships. It is interesting to note that Yellow 7.5 was the jet that crashed and burned on Bogallua Island. The aerograph record was recovered and worked up as is shown in Table 4.4.

The pre-cloud entry air temperatures compared well with the nearest Raob data, as shown in Fig. 4.2. As before, this

agreement bolsters the reliability of the aerograph data obtained during the cloud traverses.

4.5 GEORGE SHOT

Only seven drone aircraft participated in George Shot. These were the AEC cloud-sampling aircraft placed at the same levels as in Dog and Easy Shots. No ship was placed at 30,000 ft for George Shot. Table 4.5 summarizes the results of the cloud traverses.

Meteorologically speaking, George Shot provided the most interesting set of records. Figure 4.3 is given to illustrate the apparently well operating equipment at the time of cloud entry.

REFERENCE

1. K. H. Jehn, Rev. Sci. Instr., 20: 668 (1949).

Chapter 5

Discussion of Results

5.1 INTRODUCTION

The aerograph data provide the only measurements that reveal direct information regarding the microstructure of the atomic cloud. These data have been analyzed to determine the small-scale variation of temperature, moisture, and turbulence along a constant altitude cross section through the cloud.

In discussing the result of these analyses, it will be helpful to appreciate the circumstances under which the measurements were made. The state of development of the cloud when it was penetrated will be particularly important to the interpretation of these data.

Although the aerograph data cannot furnish this information, the photographic documentation of the atomic cloud contained in Part II of this report provides an excellent background on the over-all appearance and development of the visible cloud for each of the shots. Recourse will be made to this source in order to place the cloud traverses within the proper geometric relation to the cloud as they would have appeared to an observer.

In addition, the photographic documentation revealed some general features of interest, which, when combined, form a suitable model of the over-all atomic-cloud evolution. The logical consequences demanded by this model will be compared against the findings of the aerograph in an effort to arrive at a picture of the atomic cloud which is consistent with the different types of observations.

5.2 DOG SHOT CLOUD

5.2.1 General Description of Cloud

The detonation occurred at 0634 local time with a yield of about 90 kt.

From the photographic record given in Part II of this report, it appears that the Dog cloud reached a ceiling of about 56,000 ft after some 8 min. Thus at 0642 the cloud was stabilized with the top near 56,000 ft and the base of the mushroom (the main mass of cloud resembled a mushroom) at 40,000 ft. The mushroom had the characteristic stem cloud protruding downward from its base. The stem cloud appeared to have considerable motion within it and terminated in a root cloud at the base of the stem.

TABLE 5.1 TIME LAPSE BETWEEN CLOUD-TOP PASSAGE AND CLOUD PENETRATION, DOG CLOUD

Altitude (ft)	Time (min : sec)
16,000	2:25
18,000	3:30
20,000	2:35
22,000	1:55
24,000	2:22
26,000	1:20
28,000	2:15
30,000	1:30

The time of passage of the main mass of the mushroom cloud at a given altitude was not available for Dog cloud owing to the obscuring effect of a low strato-cumulus deck. The top of the cloud was followed, however, and the time lapse between cloud-top passage and cloud penetration is given in Table 5.1.

It is seen that the top of the cloud cleared the various penetration altitudes by more than a full minute in each instance. It is assumed that the time of passage of the main mass followed closely that of the top and that the actual penetrations took place through the stem cloud only.

Since each of the first penetrations occurred before the cloud stabilized, it would be expected that some severe air motions would be encoun-

tered. Part II presents a model of the rising cloud in which the main mass is undergoing a toroidal motion and expanding while rising. Presumably the expansion is accompanied by an inrush of air into the base of the mushroom, this inflow taking place up through the stem cloud.

Such a forced updraft as described would result in the air in the "chimney" having a lower temperature than its surroundings owing to adiabatic expansion. Superposed on these adiabatic temperature changes are temperature changes due to mixing of cloud air with surrounding air by turbulence. The resulting temperature difference between cloud and environment would be somewhat less than that given by a strictly adiabatic temperature drop and the environment temperature.

The photographic results also noted a characteristic twist in the stem. It was surmised that this twisted appearance was caused by a vortex motion in the stem. A consequence of this vortex motion would be a low-pressure region in the stem (see Part II).

5.2.2 Microstructure of the Dog Cloud Stem

The aerograph data on cloud penetrations, presented in Table 4.1, have been plotted as time cross sections for each of the passes. These first penetrations are shown in Figs. 5.1 to 5.8. The region between the two vertical lines on each trace represents the interval when the aircraft was inside the cloud. The vertical lines mark the entrance and exit times of the cloud penetrations.

The navigator's reported times were taken as a first reference in fixing the entrance and exit times. The time scale constructed from the best fit of known events (Table 3.4) was followed directly, and the values of the parameters (airspeed, temperature, etc.) at the navigator's entrance and exit times were noted. Usually the entrance to the cloud was marked by an extremely rapid and sometimes severe change in true airspeed. This effect was undoubtedly due to turbulence within the cloud. Thus the airspeed record served as a check on the time of entrance. Furthermore, in some of the penetrations the relative humidity increased toward 100 per cent. When this change was available, it too served as a good reference to cloud entrance.

If, on comparison, a wide difference seemed to exist between the aerograph time and the

navigator's time for entrance, the aerograph time was used. The time of exit from the cloud was much more difficult to determine. The relative-humidity trace decreased when the aircraft left the water cloud, but, owing to a lag in evaporation in the probe (as in George Shot), the time of return to ambient conditions could not always be relied on as representing the emergence of the plane from the cloud. Likewise, the airspeed recovery was not well enough defined for use as a definite reference. The time finally selected was that which seemed to be the most reasonable after comparing the aerograph and the navigator's records.

Annex 6.8, Operation Greenhouse Report, reported entrance and exit times based on jet impactor samples and turbulence-induced fluctuations in the dosage-rate recorder. The entrance and exit times from three independent sources, the aerograph, Annex 6.8, and the navigator's log, are compared in Table 5.2. Presumably, there should have been excellent agreement between Annex 6.8 and the aerograph since the sensing instruments were on the same planes. It is felt that any difference in reported entrance times is due to a difference in setting up the time-scale base for the recorders. The navigator's log had to be relied on for most of the exit times since the aerograph data were too vague. In general, there appears to be fair over-all agreement among the three methods and excellent agreement in some of the passes. The second penetration compared more poorly than the first, but this is to be expected since the cloud itself was becoming diffuse in dimensions and internal properties. Finally, it might be noted that a more positive identification for exit time would be helpful in future drone work.

As a whole, the individual soundings on the first penetration resembled each other closely. Each trace showed an increase in relative humidity, although only the 16,000- and 18,000-ft passes came close to a value suggestive of water clouds. This is puzzling since photographs of the stem cloud would lead one to expect this cloud to be composed of water droplets. It is well known that the stem has much debris composed of dirt, rock, coral, and metallic residues of both radioactive and non-radioactive nature. Perhaps the debris was present in amount and size range to give a light scattering effect similar to a water cloud. Nevertheless, above 18,000 ft the stem cloud appeared to be dry on the basis of the aerograph data.

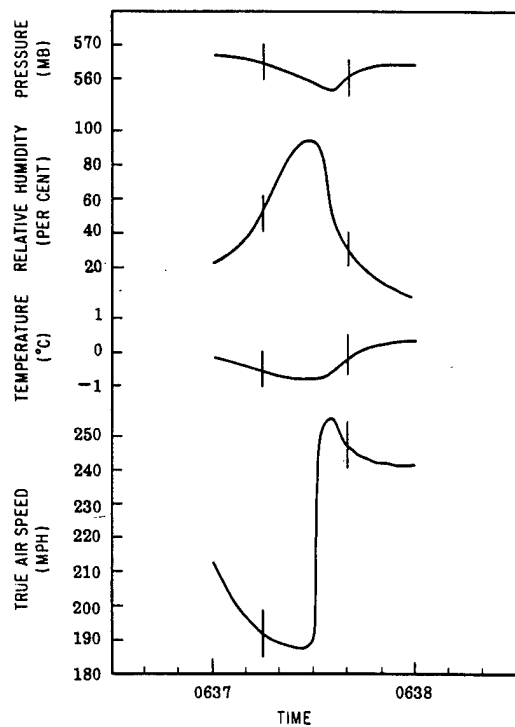


Fig. 5.1 Cross Section of Dog Cloud at 16,000 Ft, First Pass

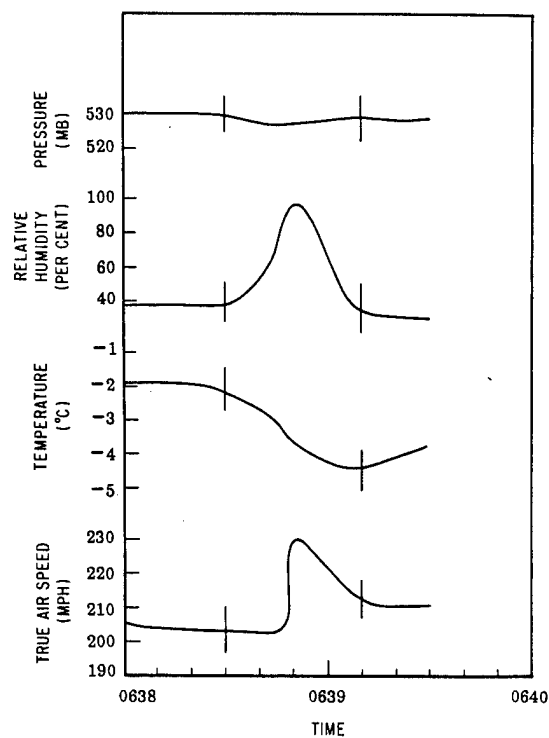


Fig. 5.2 Cross Section of Dog Cloud at 18,000 Ft, First Pass

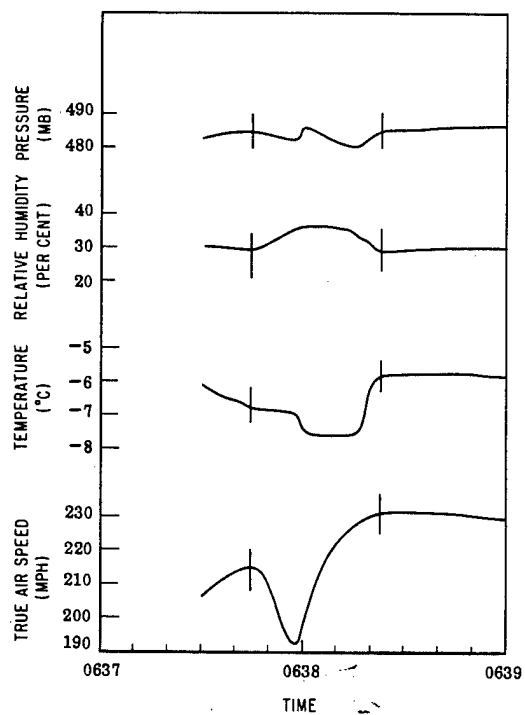


Fig. 5.3 Cross Section of Dog Cloud at 20,000 Ft, First Pass

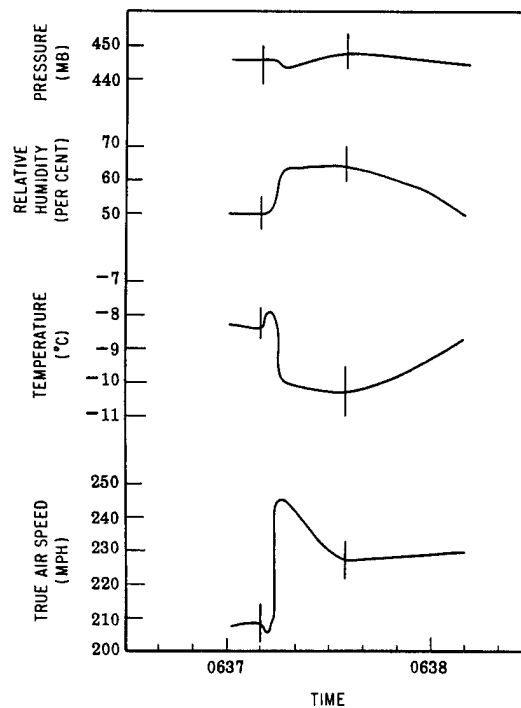


Fig. 5.4 Cross Section of Dog Cloud at 22,000 Ft, First Pass

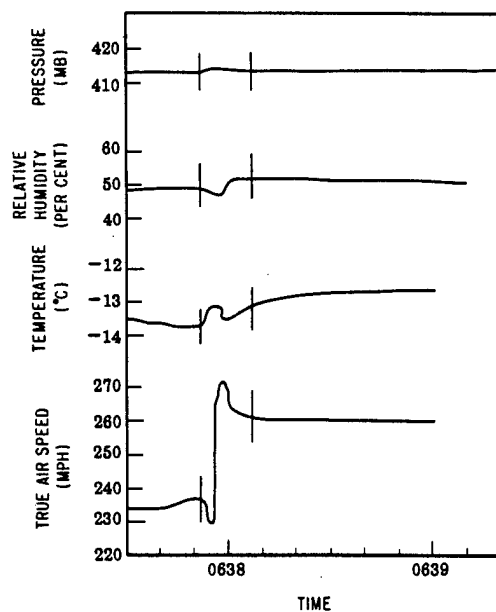


Fig. 5.5 Cross Section of Dog Cloud at 24,000 Ft, First Pass

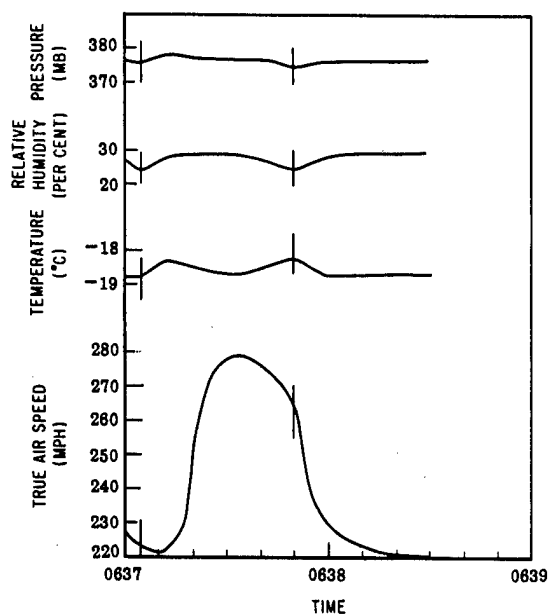


Fig. 5.6 Cross Section of Dog Cloud at 26,000 Ft, First Pass

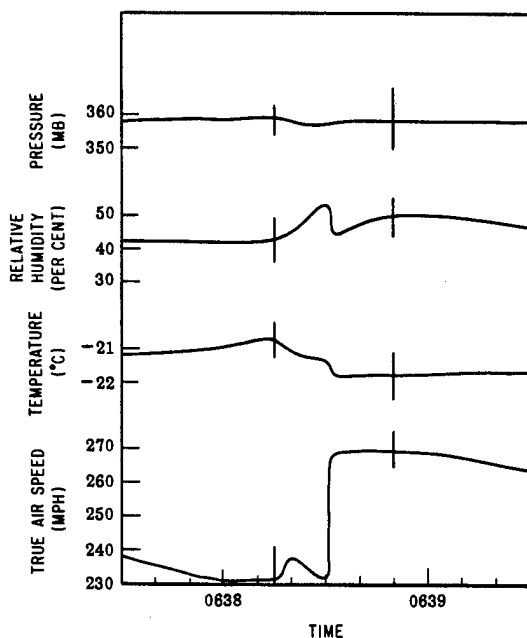


Fig. 5.7 Cross Section of Dog Cloud at 28,000 Ft, First Pass

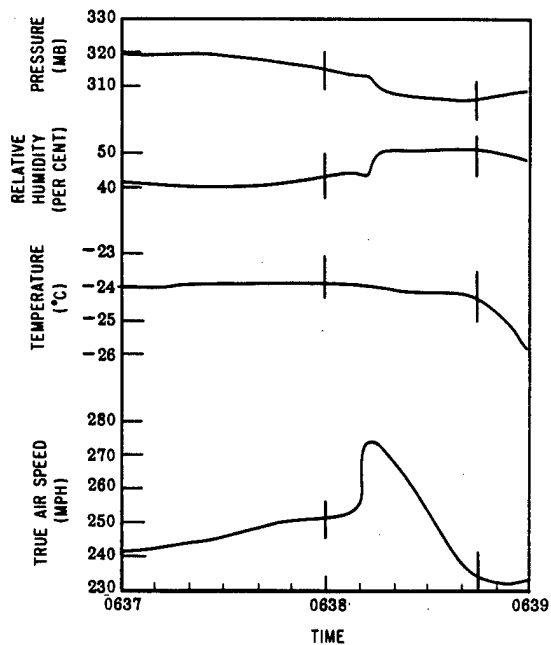


Fig. 5.8 Cross Section of Dog Cloud at 30,000 Ft, First Pass

TABLE 5.2 DOG SHOT CLOUD PENETRATION TIMES

Altitude (ft)	Pass	Time of entry			Time of exit		
		4.1A*	P.L.†	6.8‡	4.1A*	P.L.†	6.8‡
16,000	First	0637:15	0637:15	0637:14	0637:40		0637:28
	Second	0646:15	0646:15	0646:08	0647:00	0647:00	0647:05
18,000	First	0638:30	0638:30	0638:44	0639:10	0638:46	0639:09
	Second	0651:40	0651:20	0652:05	0652:40	0651:45	0652:34
20,000	First	0637:45	0637:45	0637:51	0638:23	0638:23	0638:16
	Second	0645:03	0645:03	0644:42	0645:23	0645:23	0645:08
22,000	First	0637:10	0637:30	0637:02	0637:35	0637:43	0637:22
	Second	0643:30	0643:30	0642:45		0643:45	0643:12
24,000	First	0637:52	0637:52		0637:07	0638:07	
	Second	0644:45	0644:45		0645:05	0645:05	
26,000	First	0637:05	0637:05	0637:24	0637:50	0637:50	0637:44
28,000	First	0638:15	0638:15	0638:23	0638:50	0639:00	0638:44
	Second	0644:58	0644:58	0645:30	0645:35	0645:18	0642:02
30,000	First	0638:00	0637:50		0638:45	0638:20	
	Second	0644:30	0644:50		0645:10	0645:10	

* 4.1A refers to aerograph data.

† P.L. refers to times given in the pilot's or navigator's log.

‡ 6.8 refers to times reported in Annex 6.8.

The first penetrations showed a characteristic decrease in temperature at each altitude except 24,000 ft. The temperature decrease may be accounted for by assuming a forced updraft model, as discussed in Sec. 5.2.1. Likewise, each pass had a sharp increase in airspeed the moment the cloud was penetrated. This sharp increase in airspeed may be attributed to gusts or drafts in the cloud. Unfortunately, the aerograph data alone are not sufficient to compute the value of the gusts encountered. Some qualitative idea may be gained from considering the fluctuation in the airspeed as being due to a vertical gust acting on the ship. Tolefson¹ points out that this is a perfectly acceptable procedure. Thus a sharp increase in true airspeed may be the result of a strong updraft, and, conversely, a decrease in true airspeed is due to a downdraft. In most of the passes the airspeed went through a rather sharp maximum, which could be interpreted as evidence of both updrafts and downdrafts in the stem.

Rounding out the measurements, the pressure behavior was consistent with the model adopted in Sec. 5.2.1. The pressure decreased through all traverses except at 24,000 and 26,000 ft. In some cases this drop amounted to 8 to 10 mb. Comparison of the time to the pressure change

makes it fairly clear that the time available was not sufficient for the aircraft to be carried to higher altitudes by an updraft and thereby account for the pressure drop. The pressure drop seems to be due primarily to a genuine low-pressure region inside the stem.

5.2.3 Effect of Aging on Dog Cloud Properties

The time cross sections for the second penetrations are presented in Figs. 5.9 to 5.14. As is seen in Table 5.2, the second passes were made some 6 to 10 min after the first pass. By this time the cloud had stabilized and was in a state of deterioration brought about by the shearing and spreading actions of winds.

It would be expected that eddy diffusion would serve to mix the cloud air with the environment and thus render the internal properties indistinguishable from those of the environment. That this is the case is clear on comparing the second passes with the first. All parameters show less fluctuation through the cloud, and in many little or no change from the free-air value is evident on the second pass. The 30,000-ft pass is the only one that showed any marked changes inside the cloud. This run was made about 2 min after the top stabilized, and, presumably,

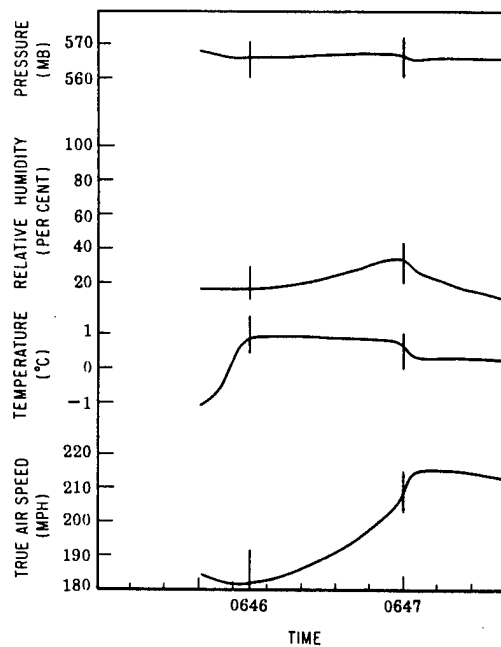


Fig. 5.9 Cross Section of Dog Cloud at 16,000 Ft, Second Pass

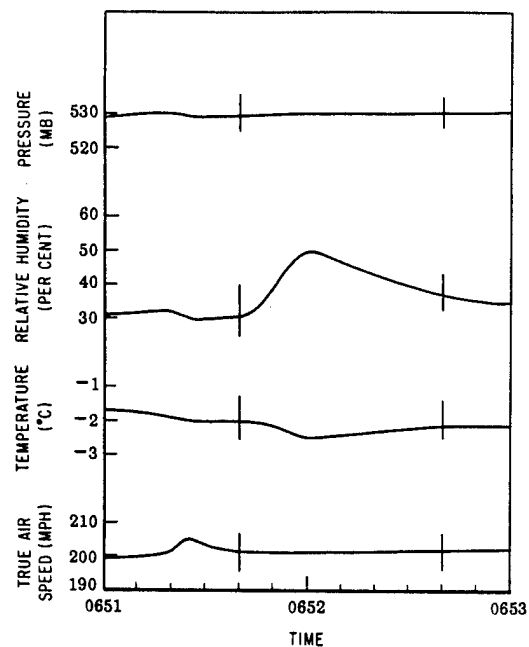


Fig. 5.10 Cross Section of Dog Cloud at 18,000 Ft, Second Pass

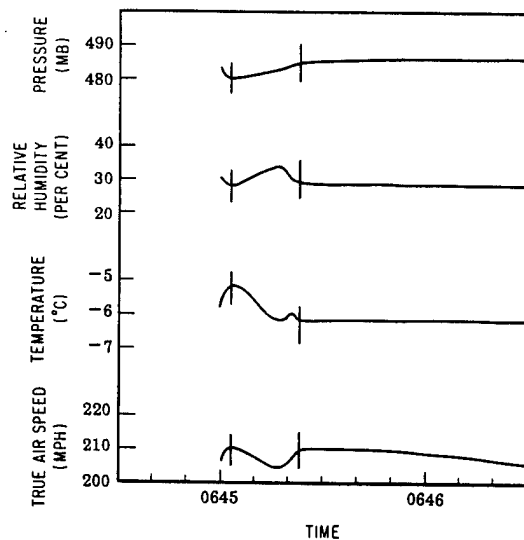


Fig. 5.11 Cross Section of Dog Cloud at 20,000 Ft, Second Pass

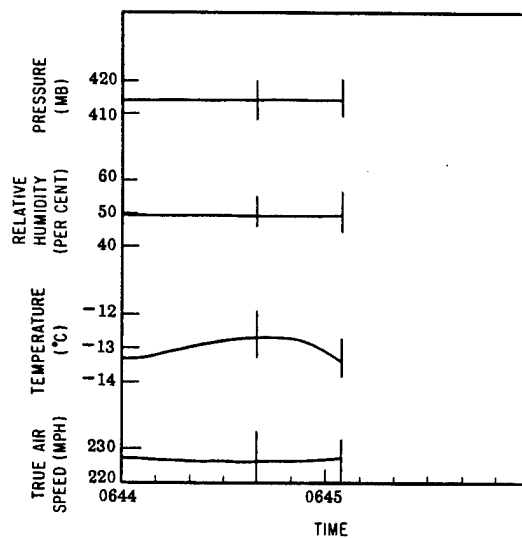
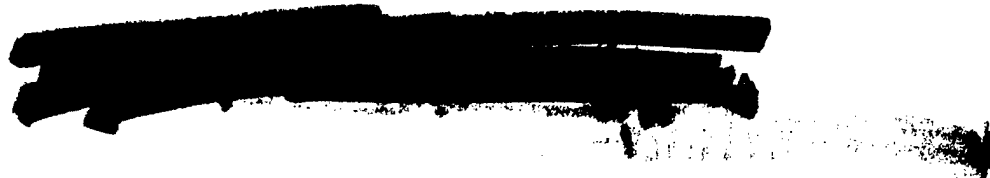


Fig. 5.12 Cross Section of Dog Cloud at 24,000 Ft, Second Pass



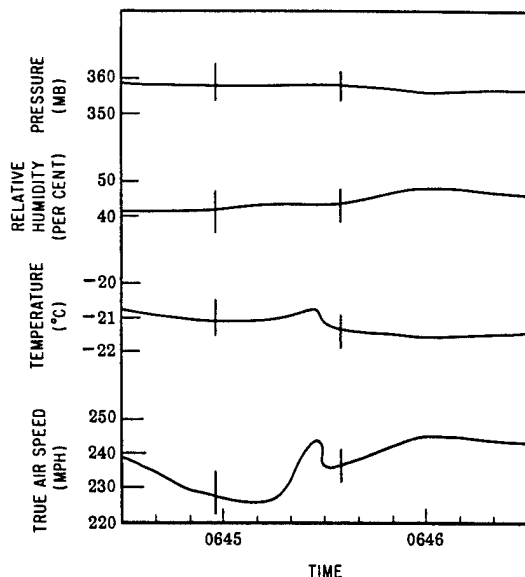


Fig. 5.13 Cross Section of Dog Cloud at 28,000 Ft, Second Pass

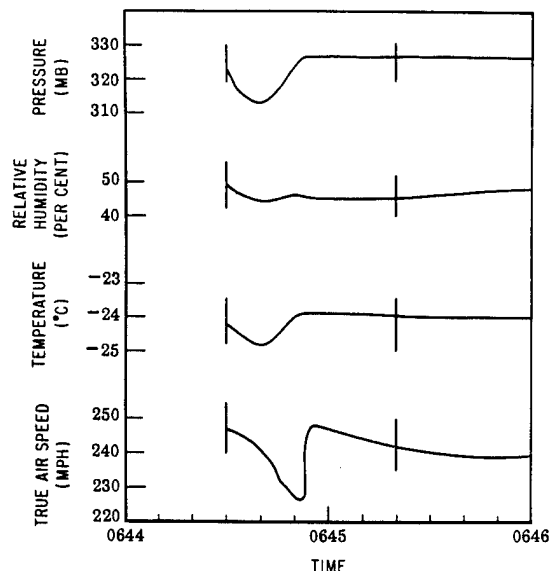


Fig. 5.14 Cross Section of Dog Cloud at 30,000 Ft, Second Pass

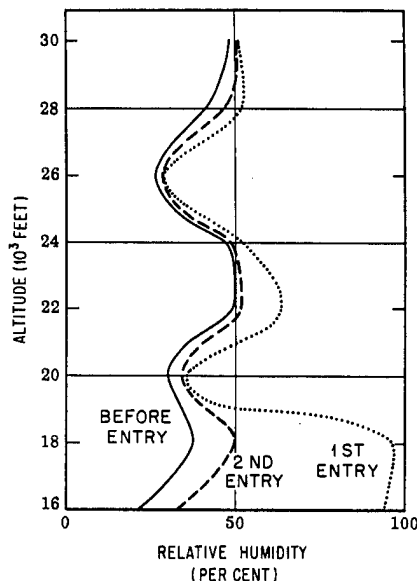


Fig. 5.15 Altitude Distribution of Relative Humidity As a Function of Time of Penetration, Dog Cloud

there was still some air intake into the base at this time.

A good illustration of the effect of aging on the cloud properties may be seen in Fig. 5.15, where the relative humidity is used as the subject. The relative humidities encountered on the second passes had almost returned to the ambient values.

5.3 EASY SHOT CLOUD

5.3.1 General Description of Cloud

The yield of Easy Shot was about one-half that of Dog Shot, and the resulting cloud was the least spectacular of the three clouds photographed. Detonation occurred at 0627, and after 6½ min the cloud had reached its maximum altitude of 41,000 ft. As early as 2½ min after detonation, the rising cloud began to shear away from the stem. The mushroom top began to lose its sharply defined outlines after about 5 min. The stem cloud at this time appeared diffuse, and it terminated in cumulus root clouds.

Despite its weaker comparison in physical attributes, the Easy cloud was the best observed of the Greenhouse tests. Excellent photographs were obtained during its ascension and later dissipating stages, and these records correlated quite well with ground and aerial visual observations. Thus the times of arrival of the cloud mass at various altitudes, as compiled in Part II, were considered to be quite representative of the actual case. The elapsed time between cloud passage and drone penetration is given for the various altitudes in Table 5.3.

Since the yield of Easy Shot was rather low, the cloud base stabilized near 30,000 ft. However, the definition of the base from the photographs is extremely difficult since the base

is indistinct and the stem cloud seems to extend almost to the top of the mushroom. From Table 5.3 it appears that the 28,000- and 30,000 ft aircraft were over Ground Zero before the

TABLE 5.3 TIME LAPSE BETWEEN CLOUD PASSAGE AND PENETRATION, EASY CLOUD

Altitude (ft)	Time (min : sec)	
	Cloud top	Cloud base
16,000	No penetration	
18,000	1:30	0:30
20,000	3:45	2:45
22,000	1:05	-0:15
24,000	1:15	-0:25
26,000	2:05	0:15
28,000	-0:17	-2:53
30,000	-0:08	

atomic cloud reached these altitudes at the time of the first pass. It also appears that the 22,000- and 24,000-ft first penetrations were made through the mushroom portion since the time of passage of the cloud base was after the pass was made.

It seems that the remainder of the passes were through the stem cloud. However, at the time of most of the second passes, the whole mass could be called stem cloud. The cloud at this time was rapidly undergoing shearing action and accompanying deterioration.

5.3.2 Microstructure of Easy Cloud

As in the case of Dog cloud, the aerograph data in Table 4.3 have been plotted as time cross sections in Figs. 5.16 to 5.30. Table 5.4 compares the entrance and exit times obtained by the three independent means as in Table 5.2. The aerograph times were selected as explained in Sec. 5.2.2. However, owing to the lack of significant increase in relative humidity, it was also impossible to tell from the aerograph alone when the planes entered or left the cloud. Consequently reliance on the navigator's log was frequently made in the Easy cloud data.

It is also noticed that some discrepancy exists on the 28,000- and 30,000-ft first penetrations since Annex 6.8 and the pilot's log reported no contact with the cloud; yet the aerograph reported entrance and exit times. Examination of the Annex 6.8 data gives convincing evidence that these drones did not pass through the clouds. The aerograph times are simply points when the fluctuation in the measured param-

eters seemed to justify contact with the cloud. Although the pilot's log indicates no penetrations on the first passes for the 24,000- and 26,000-ft levels, the aerograph and Annex 6.8 clearly show penetrations. It is believed that the asterisk notation in the pilot's log was incorrectly placed beside the 24,000- and 26,000-ft data when it was intended to be placed beside the 28,000- and 30,000-ft data to indicate no penetration.

The first penetrations are shown in Figs. 5.16 to 5.22. As is pointed out above, it is fairly certain that both the 30,000- and the 28,000-ft drones passed over the top of the cloud. If the aircraft passed close to the top of the rising mushroom, the traverse according to the model adopted in Sec. 5.2.1 and Part II would be marked by the effect of the plug of air being pushed upward by the mushroom. Figure 5.21, the 28,000-ft traverse, shows little or no change in all four parameters. Figure 5.22, however, indicates fluctuations of the same type that definite cloud penetrations exhibit. This difference in behavior can be attributed to the proximity of the aircraft to the cloud. Reference to Table 5.3 makes it apparent that the 30,000-ft aircraft must have been much closer to the cloud than the 28,000-ft drone since the time between air-

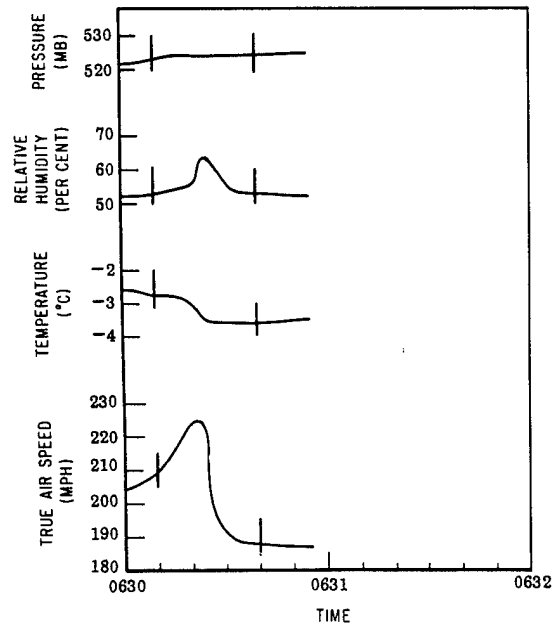


Fig. 5.16 Cross Section of Easy Cloud at 18,000 Ft, First Pass

TABLE 5.4 EASY SHOT CLOUD PENETRATION TIMES

Altitude (ft)	Pass	Time of entry			Time of exit		
		4.1A*	P.L.†	6.8‡	4.1A*	P.L.†	6.8‡
16,000	First		0630:25			0630:45	
	Second	0638:15	0638:40	0638:06	0639:45	0638:45	0638:34
18,000	First	0630:10	0630:50	0631:13	0630:40		0631:27
	Second	0642:00	0644:20	0644:34	0642:30	0644:38	0645:05
20,000	First	0632:30	0632:00	0632:14	0633:10	0633:00	0632:37
	Second	0638:20	0638:45	0637:42	0639:00	0639:00	0638:33
22,000	First	0630:05	0630:30	0630:43	0631:05	0630:45	0631:00
	Second	0636:15	0636:15	0636:11	0637:05	0637:00	0637:04
24,000	First	0630:35	0630:50	0630:58	0632:00	0631:50	0631:23
	Second	0637:00	0636:50	0637:14	0637:28	0637:28	0637:38
26,000	First	0631:20	0631:30	0631:26	0632:25	0631:50	0631:42
	Second	0637:50	0637:50	0637:56	0638:20	0638:20	0638:30
28,000	First	0629:37			0629:50		
	Second	0636:50	0638:05	0638:08	0637:20	0638:50	0638:31
30,000	First	0630:35			0630:10		
	Second	0637:00	0636:21	0636:21	0638:10	0636:57	0637:06

* 4.1A refers to times picked from the aerograph data.

† P.L. refers to times reported by the pilot's or navigator's log.

‡ 6.8 refers to times reported in Annex 6.8.

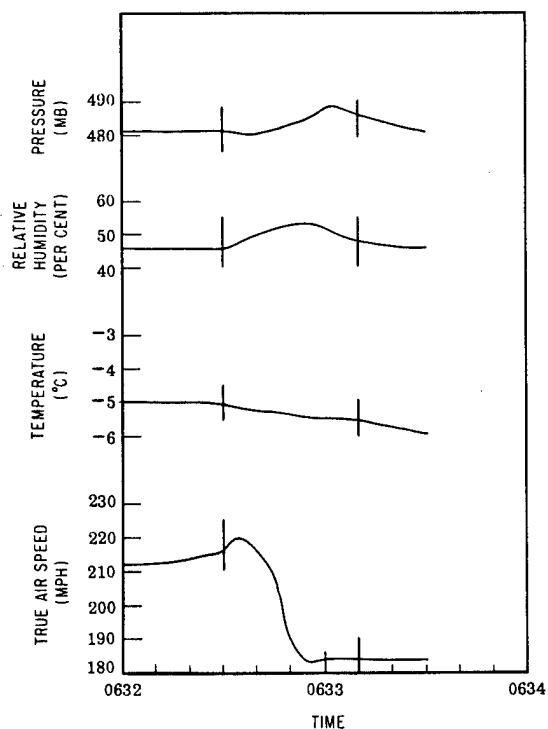


Fig. 5.17 Cross Section of Easy Cloud at 20,000 Ft, First Pass

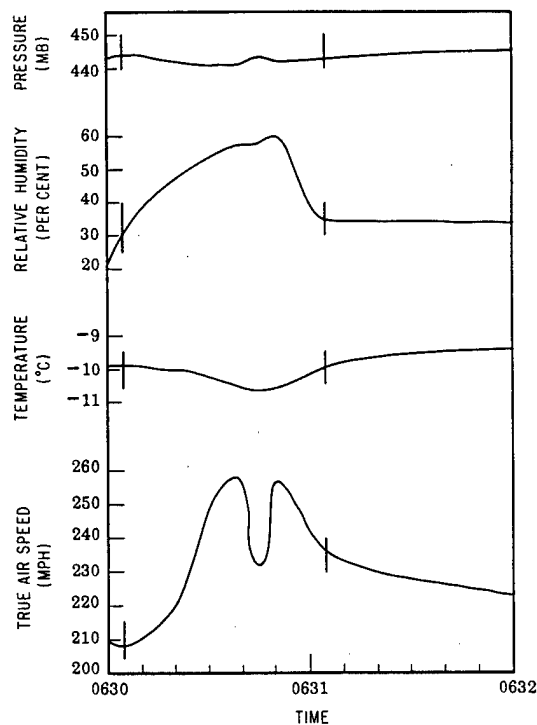


Fig. 5.18 Cross Section of Easy Cloud at 22,000 Ft, First Pass

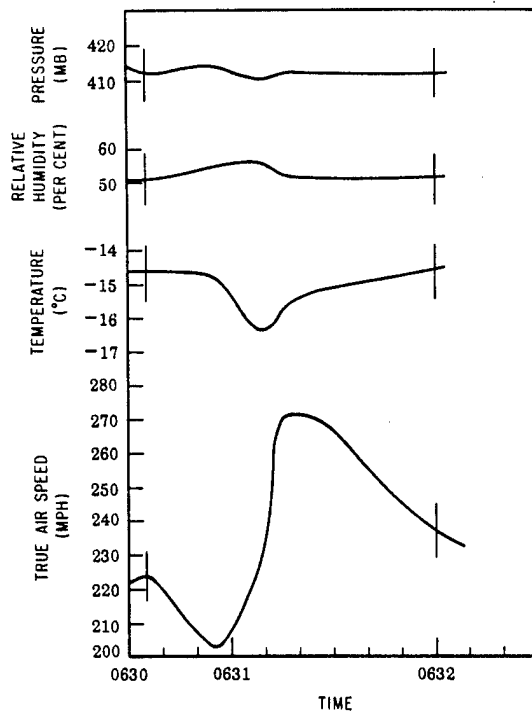


Fig. 5.19 Cross Section of Easy Cloud at 24,000 Ft,
First Pass

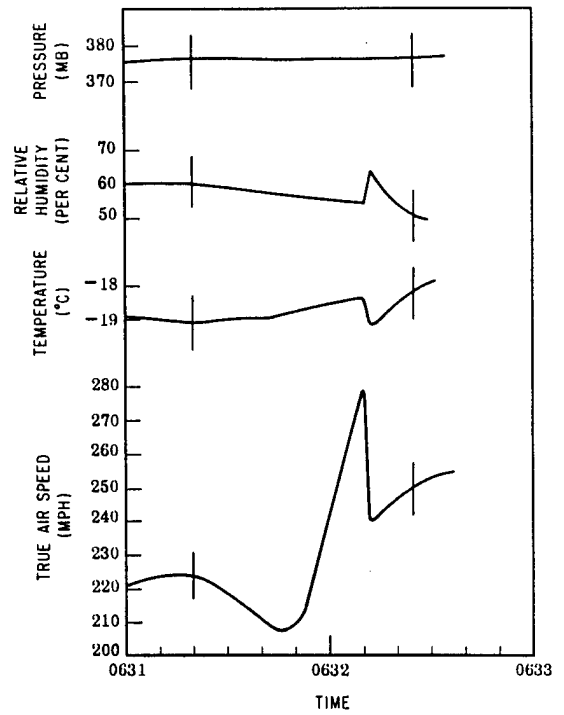


Fig. 5.20 Cross Section of Easy Cloud at 26,000 Ft,
First Pass

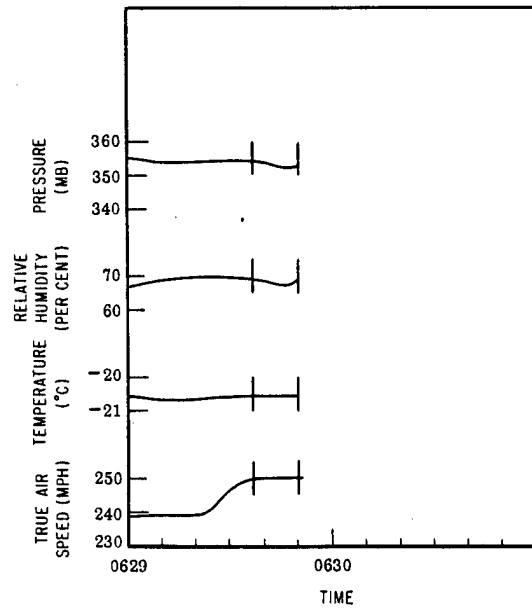


Fig. 5.21 Cross Section of Easy Cloud at 28,000 Ft,
First Pass

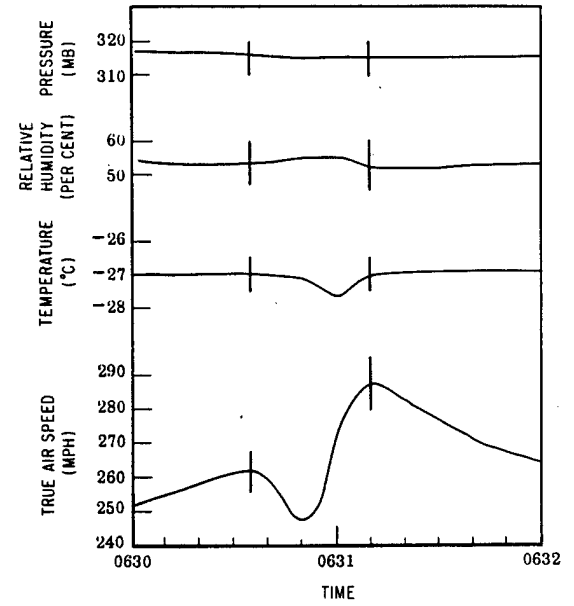


Fig. 5.22 Cross Section of Easy Cloud at 30,000 Ft,
First Pass

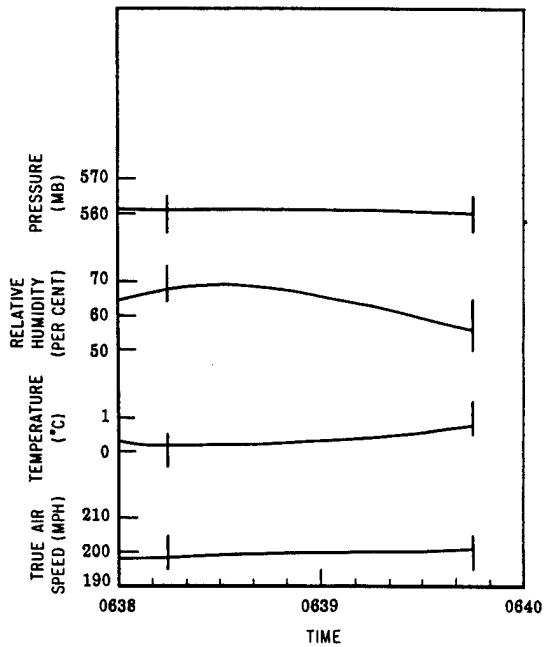


Fig. 5.23 Cross Section of Easy Cloud at 16,000 Ft, Second Pass

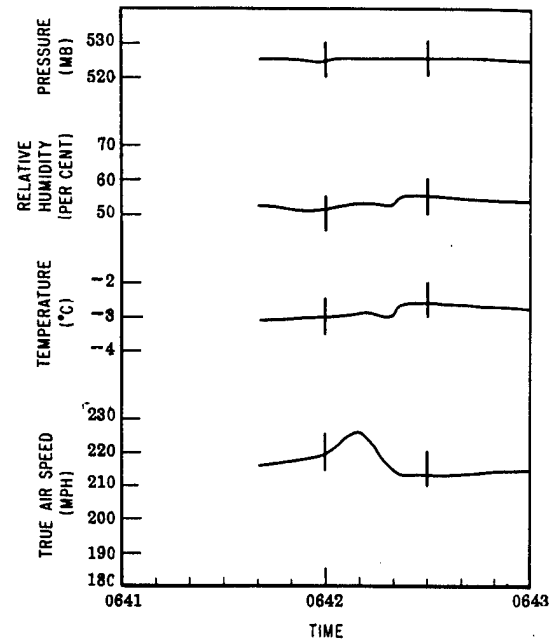


Fig. 5.24 Cross Section of Easy Cloud at 18,000 Ft, Second Pass

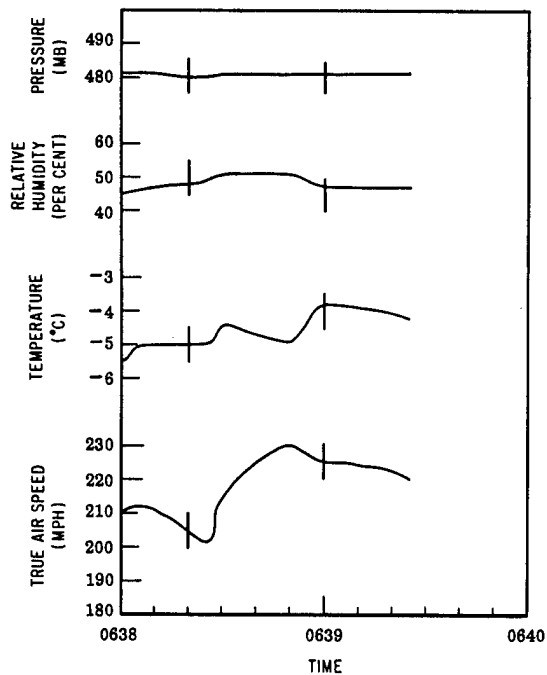


Fig. 5.25 Cross Section of Easy Cloud at 20,000 Ft, Second Pass

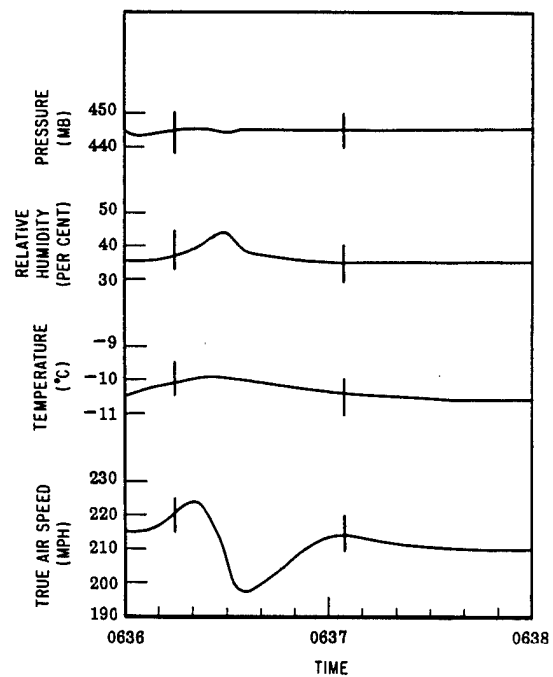


Fig. 5.26 Cross Section of Easy Cloud at 22,000 Ft, Second Pass

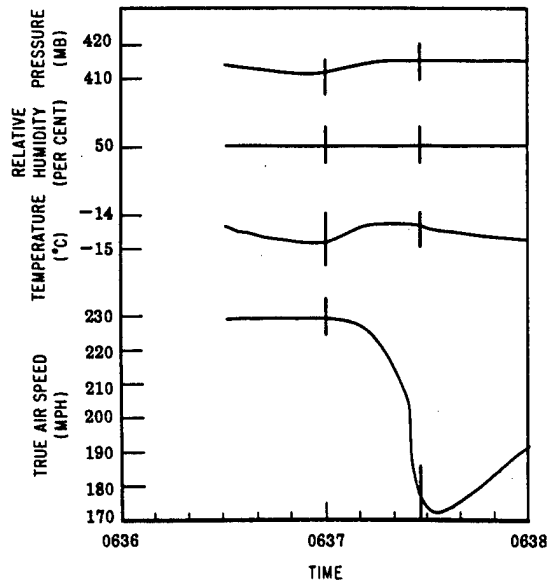


Fig. 5.27 Cross Section of Easy Cloud at 24,000 Ft, Second Pass

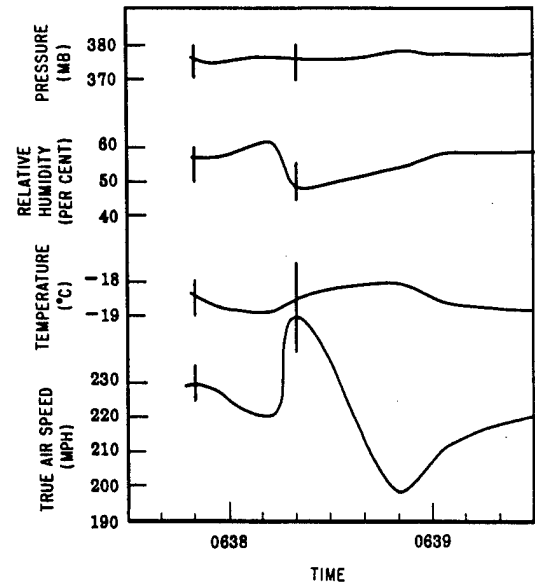


Fig. 5.28 Cross Section of Easy Cloud at 26,000 Ft, Second Pass

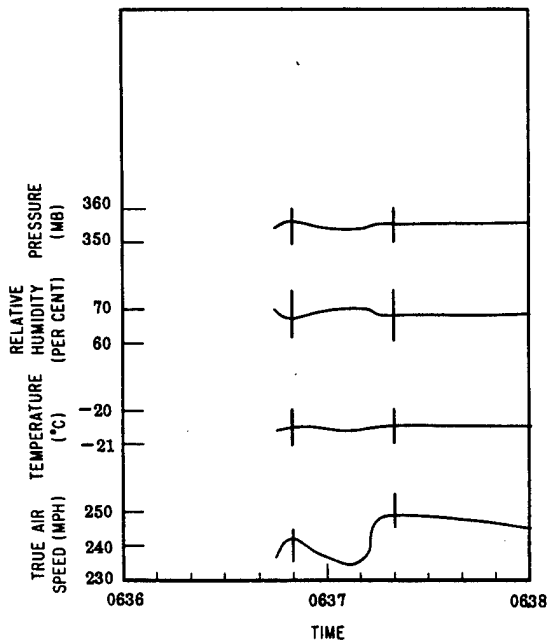


Fig. 5.29 Cross Section of Easy Cloud at 28,000 Ft, Second Pass

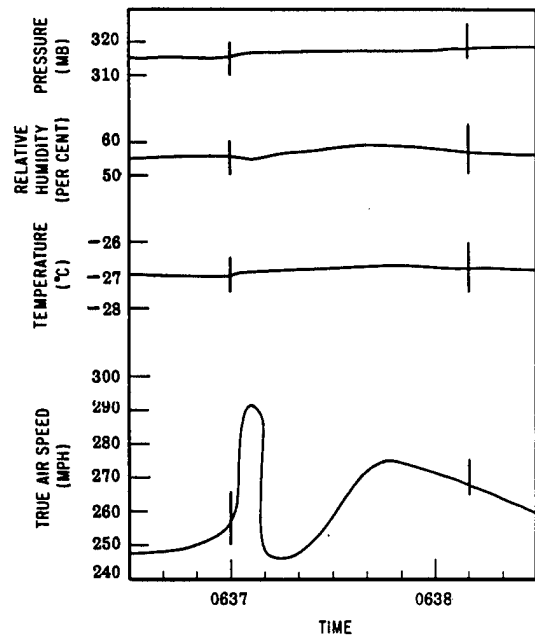


Fig. 5.30 Cross Section of Easy Cloud at 30,000 Ft, Second Pass

craft and cloud passage at 30,000 ft is one-half that for the 28,000-ft traverse.

The 30,000-ft traverse data fits quite nicely into the model of Part II. The pressure was relatively unchanged, as would be expected if the aircraft flew into the region just above the main mushroom cloud. The humidity shows only a slight increase. Air being forcibly lifted would undergo a decrease in temperature and an accompanying increase in relative humidity. The temperature decrease is obvious. Likewise the airspeed trace corresponds to those traces where a turbulent updraft is suspected.

The traverses at all other levels except 20,000 ft were very similar. All showed little or no change in static pressure, a slight increase in relative humidity to about 60 per cent, a temperature drop from 0.5 to 1°, and a sharp increase in true airspeed. It is surprising that the humidity remained so uniformly low despite the presence of a cloud. As in the case of Dog cloud, the scattering centers must have been material other than water droplets to account for the low humidity. In other respects the traverses were in keeping with the already proposed model.

The pass at 20,000 ft differed from the others in that a sharp decrease in true airspeed was found. Also, a gradual rise in pressure of some 8 mb was reported. According to Table 5.3 this pass was made much later than the others, and from the photographic record (Part II) at this time the cloud stem was in a mature stage. The aerograph traces and the photographs combine to suggest that the drone was flown into a cold downdraft. Cold downdrafts are usual in the case of thunderstorms in the mature stage.² The colder-than-ambient air, no longer being lifted or sustained by updraft into a growing mushroom, must sink when the growth stops since it is denser than air at the same level.

No penetration was made at 16,000 ft according to Annex 6.8, although the pilot's log gives a time. The aerograph data were not worked up at this time and consequently are not available to confirm the Annex 6.8 finding.

5.3.3 Aging of Easy Cloud

The aging of Easy cloud as determined from the aerograph traces is shown by the second penetration in Figs. 5.23 to 5.30. Since these traverses were made 10 min or more after detonation, they would be expected to reflect the state of deterioration of the cloud. Accord-

ing to the photographs in Part II, at 10 min the top still looked active but the stem was being sheared away, whereas at 15 min the whole cloud appeared dead and elongated greatly by the shearing winds.

The passes at 16,000 and 18,000 ft (Figs. 5.23 and 5.24) show little difference over the environment. The remainder of the passes indicate convective activity still residing in the cloud. Figures 5.26 to 5.28 suggest downdrafts at the 22,000-, 24,000-, and 26,000-ft levels, respectively. Figures 5.25, 5.29, and 5.30, which give data for altitudes of 20,000, 28,000, and 30,000 ft, respectively, indicate that little change outside of turbulent mixing is occurring at these altitudes.

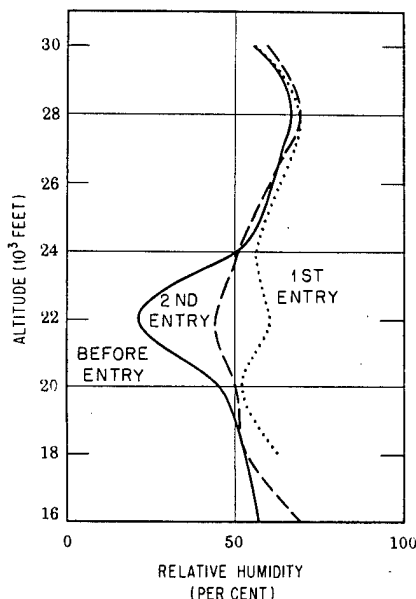


Fig. 5.31 Altitude Distribution of Relative Humidity As a Function of Time of Penetration, Easy Cloud

A comparison of humidity distribution as a function of time may be obtained from Fig. 5.31. Although the humidities were uniformly low before entry and during the traverses, a change with time can be noted. This is more pronounced at 22,000 ft than at the other levels. Above 24,000 ft little change was noted at all, indicating that the cloud had stabilized early, perhaps even before the traverses were made.

5.4 GEORGE SHOT CLOUD

5.4.1 General Description of George Cloud

On examination of the photographs in Part II, it is immediately apparent that George cloud

was much grander than the clouds from the preceding two shots. The yield of George Shot was more than twice that of Dog Shot, and about five times the yield of Easy Shot. This tremendous energy resulted in a huge mushroom, which boiled upward, sucking air into its base. The stem cloud that resulted was extremely dense and thick, with all manner of skirts and protuberances which indicated the violence of the air currents within. A twist in the stem, interpreted as gyratory motion in the stem, was noticeable (see Part II).

TABLE 5.5 TIME LAPSE BETWEEN CLOUD PASSAGE AND PENETRATION, GEORGE CLOUD

Altitude (ft)	Time (min: sec)	
	Cloud top	Cloud base
16,000	4:20	3:53
18,000	3:45	2:10
20,000	4:08	3:28
22,000	3:18	2:30
24,000	3:29	2:32
26,000	3:30	2:25
28,000	3:30	2:25

In addition to the extraordinary energy available, the rising air had the good fortune to find an environment nearly saturated with water vapor up to 10,000 ft. Thus the ambient air needed little lifting to reach condensation.

According to the photographic record in Part II, George cloud stabilized after about 6 min. The top reached 60,000 ft and then spread outward, and the base stabilized near 40,000 ft. The cloud stem remained intact as long as 21 min after the detonation, with evidence of convective activity still present. It was noticed that the stem had a light-brownish tinge, due probably to oxides of nitrogen.

In Table 5.5, the delay time between arrival of the cloud at a particular altitude and the time of drone penetration makes it clear that all drone passes must have been through the stem.

5.4.2 Microstructure of the George Cloud Stem

The internal properties of the George cloud stem are shown in the traverses of Figs. 5.32 to 5.45. Little difficulty was experienced in locating on the record the point of entrance to the cloud since the relative humidity increased to 100 per cent on all first penetrations. The second pene-

tration time was marked also by a strong increase in relative humidity, although not all reached 100 per cent. As is seen in Table 5.6, the aerograph entrance and exit times agree extremely well with the pilot's log. The agreement with the jet impactor data of Annex 6.8 was not so good; yet it was generally better than that on the two previous shots.

The first set of passes is shown in Figs. 5.32 to 5.38. According to Part II, the cloud stabilized about 6 min after detonation, or at about 0936. From Table 5.6 it is seen that all the first penetrations must have occurred before the cloud stabilized. This means that the stem should have been marked by upward currents in the still growing, expanding mushroom. Although the time lapse before penetrations (Table 5.5) was much longer than that for Dog or Easy Shot, the magnitude of the yield was so great that marked turbulence in the stem would be expected.

It is apparent immediately, referring to Figs. 5.32 to 5.38, that George cloud was entirely different from Dog or Easy cloud. The fact that George cloud was composed of water drops is obvious from the 100 per cent relative-humidity values obtained in each of the first passes. When the measured relative humidity was corrected for the effects of ram pressure and temperature rise inside the probe, it was noticed that in the George Shot data the humidity was very often 100 per cent before correction. Thus a correction would yield a true value of 100 per cent also, but the temperature and pressure change could be interpreted to get values of liquid-water contents as well. This procedure was followed, and it was found that, even in the case where the measured humidity was 70 per cent, on reduction a liquid-water content could be determined. George was the only shot to yield a liquid-water content in this manner. The values obtained are shown in Fig. 5.46. The magnitude of these values compares very well with that found in cumulus type clouds.³

The pattern of relative-humidity change through the George cloud stem was fairly constant for all the first passes. It is noticed that the exit point was not placed at the time the relative humidity returned to the value it had before cloud entrance. To do this, one would have to assume cloud diameters much greater than those seen in the photographs of Part II. It is believed that the existence of liquid water in the stem caused the humidity strip to be wetted despite the protective screen. Hence

TABLE 5.6 GEORGE SHOT CLOUD PENETRATION TIMES

Altitude (ft)	Pass	Time of entry			Time of exit		
		4.1A*	P.L.†	6.8‡	4.1A*	P.L.†	6.8‡
16,000	First	0935:08	0935:08	0935:11	0935:50	0935:30	0935:30
	Second	0942:15	0942:15	0942:20	0943:10	0942:50	0942:36
18,000	First	0934:40	0934:40	0934:04	0935:20	0934:55	0934:32
	Second	0940:05	0940:05	0940:16	0940:25	0940:25	0940:50
20,000	First	0935:13	0935:13	0935:27	0935:53	0935:53	0935:58
	Second	0943:40	0943:18	0943:33	0944:20	0944:58	0944:40
22,000	First	0934:30	0934:35	0934:28	0935:10	0935:10	0934:51
	Second	0941:52	0941:52	0942:10	0943:00	0943:15	0942:40
24,000	First	0934:47	0934:47	0934:53	0935:20	0935:20	0935:13
	Second	0941:16	0941:16	0941:14	0942:25	0942:25	0941:55
26,000	First	0935:00	0935:00	0935:35	0935:50	0935:50	0935:50
	Second	0943:35	0943:35	0944:20	0944:30	0944:30	0944:58
28,000	First	0935:10	0935:15	0935:37	0936:15	0936:00	0935:53
	Second	0941:00	0941:00	0941:02	0941:40	0941:40	0941:22

*4.1A refers to times picked from the aerograph data.

† P.L. refers to times reported by the pilot's or navigator's log.

‡ 6.8 refers to times reported in Annex 6.8.

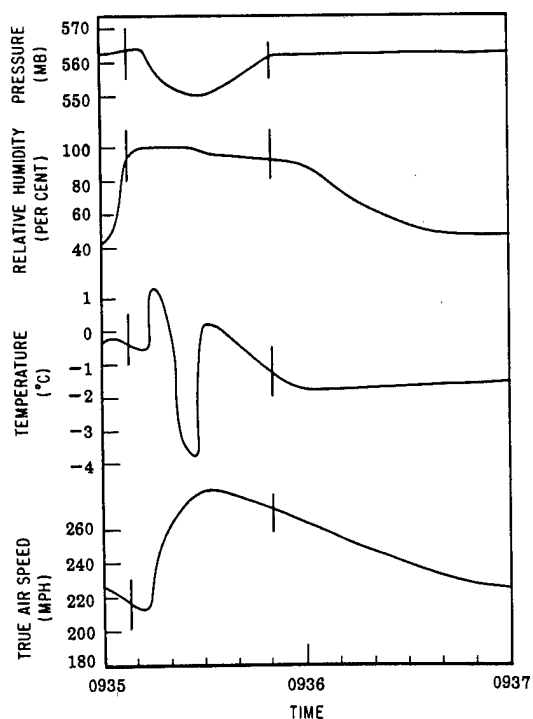


Fig. 5.32 Cross Section of George Cloud at 16,000 Ft.

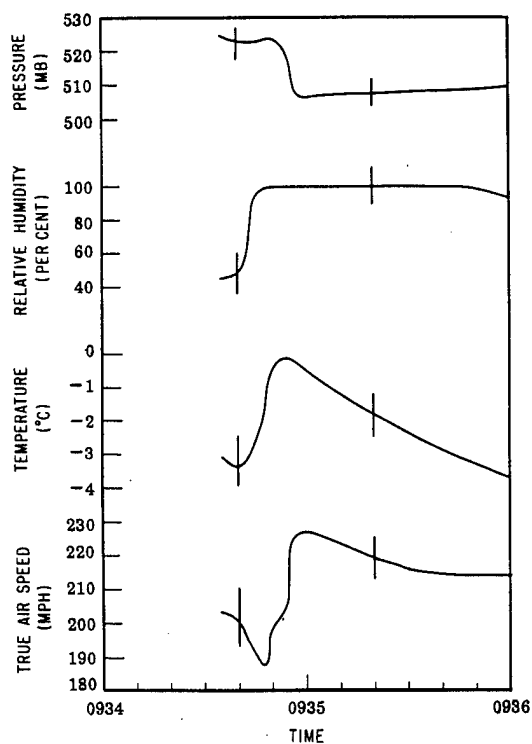


Fig. 5.33 Cross Section of George Cloud at 18,000 Ft, First Pass

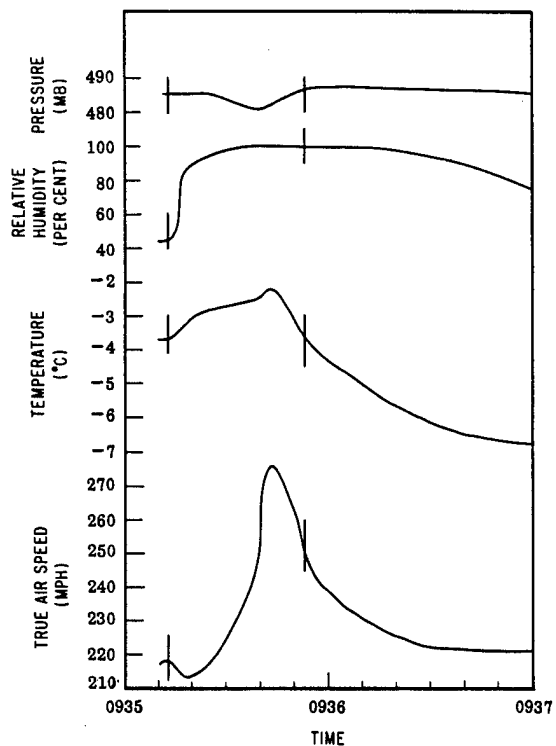


Fig. 5.34 Cross Section of George Cloud at 20,000 Ft, First Pass

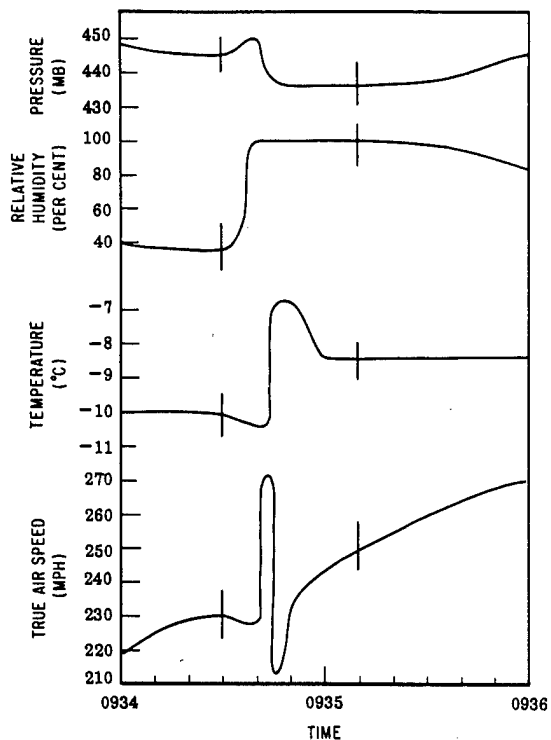


Fig. 5.35 Cross Section of George Cloud at 22,000 Ft, First Pass

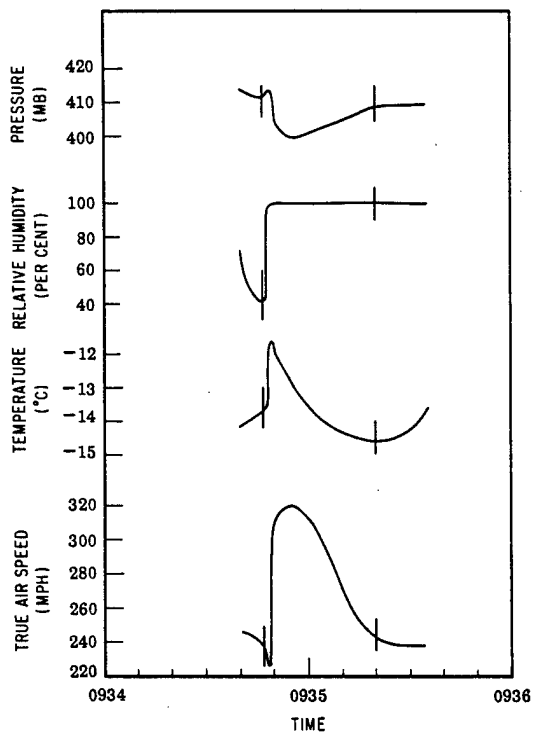


Fig. 5.36 Cross Section of George Cloud at 24,000 Ft, First Pass

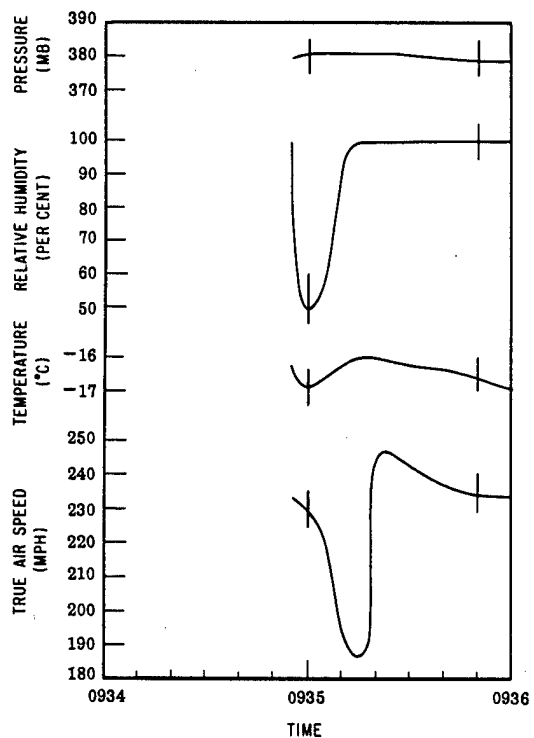


Fig. 5.37 Cross Section of George Cloud at 26,000 Ft, First Pass

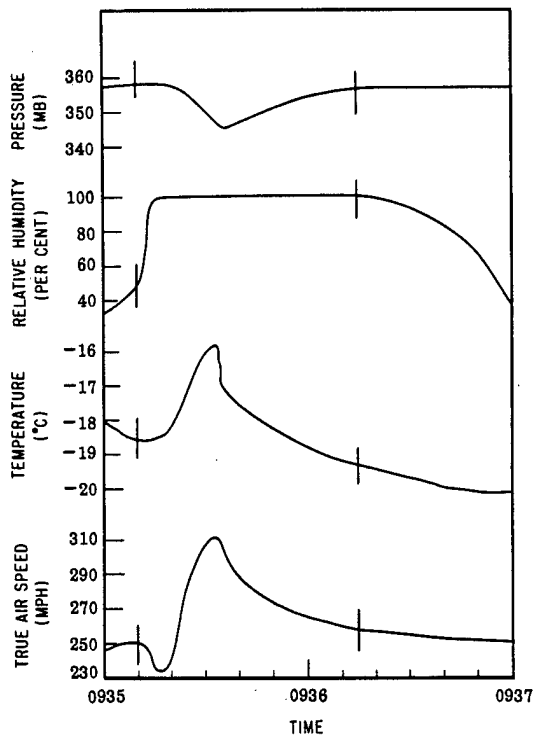


Fig. 5.38 Cross Section of George Cloud at 28,000 Ft, First Pass

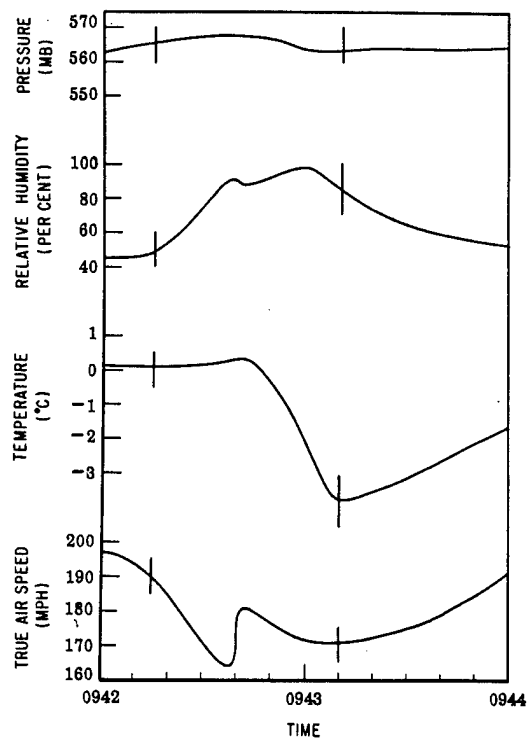


Fig. 5.39 Cross Section of George Cloud at 16,000 Ft, Second Pass

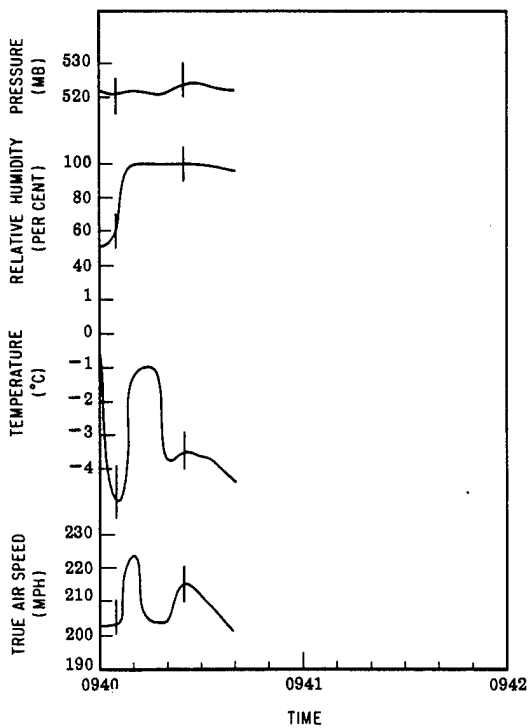


Fig. 5.40 Cross Section of George Cloud at 18,000 Ft, Second Pass

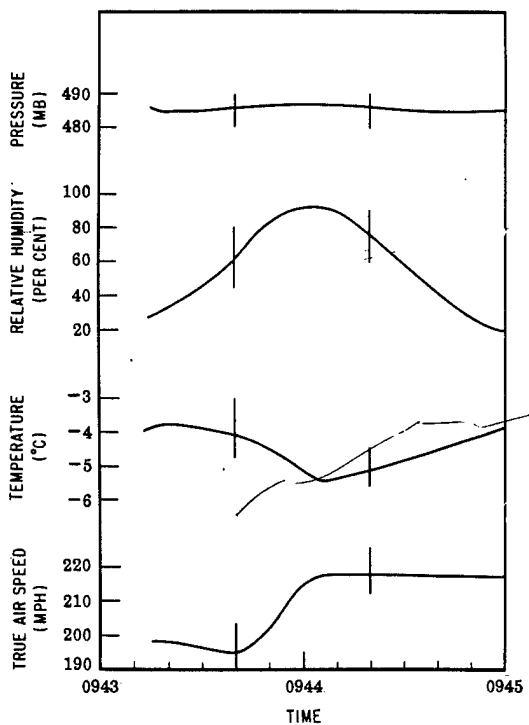


Fig. 5.41 Cross Section of George Cloud at 20,000 Ft, Second Pass

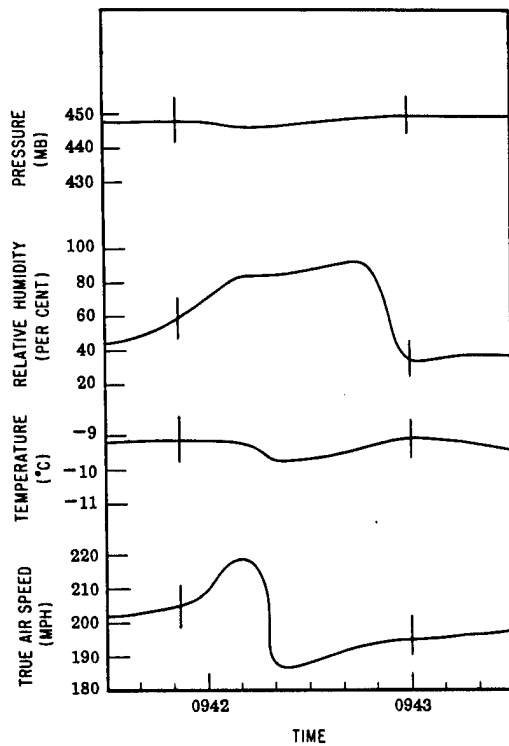


Fig. 5.42 Cross Section of George Cloud at 22,000 Ft, Second Pass

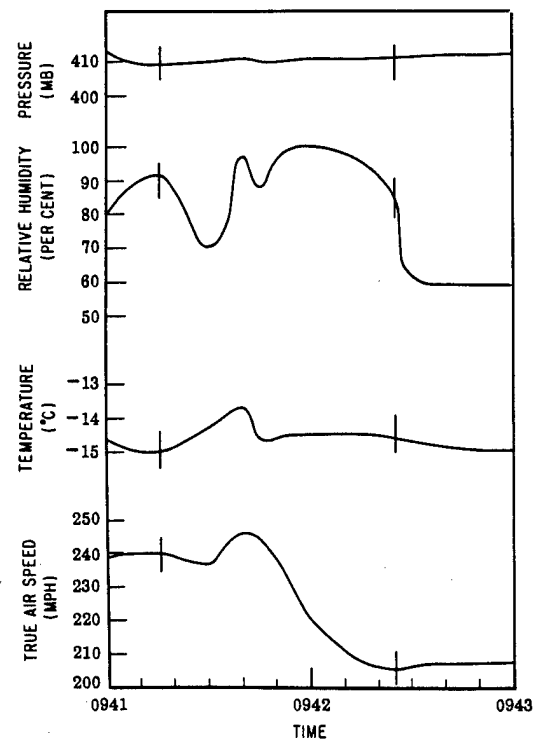


Fig. 5.43 Cross Section of George Cloud at 24,000 Ft, Second Pass

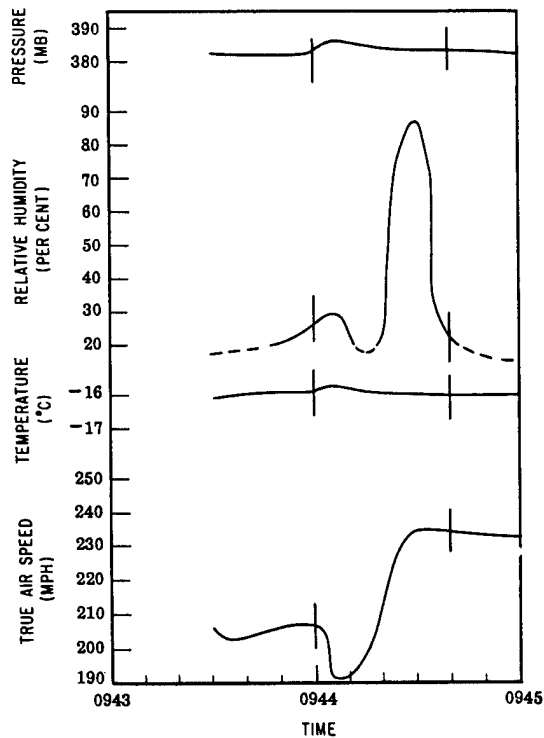


Fig. 5.44 Cross Section of George Cloud at 26,000 Ft, Second Pass

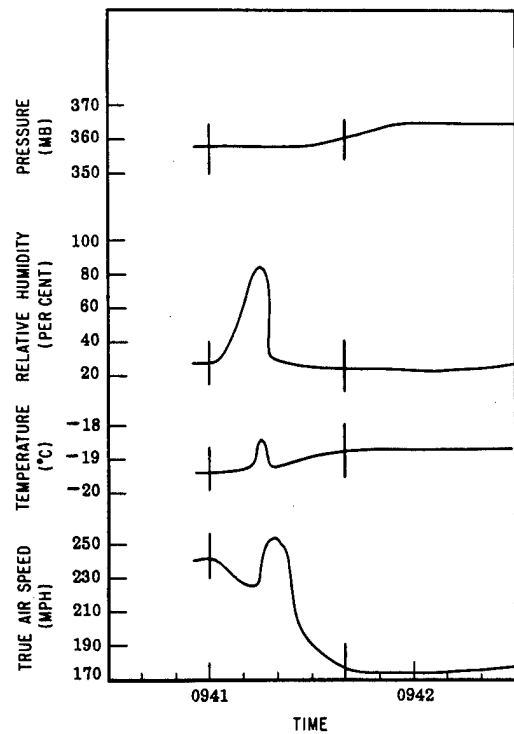


Fig. 5.45 Cross Section of George Cloud at 28,000 Ft, Second Pass

a lag in recovery of humidity would be experienced while the water evaporated.

The temperature traces resembled the textbook model for a growing cumulus cloud in that each trace was marked by an increase in temperature inside the cloud. A temperature rise due to the release of the latent heat of condensation would be the logical explanation of the observed effect. In Fig. 5.32 the 16,000-ft traverse indicated an increase and then a sharp decrease with recovery inside the cloud. A tentative explanation of the decrease may be had by assuming that the thermistor was wetted also by the

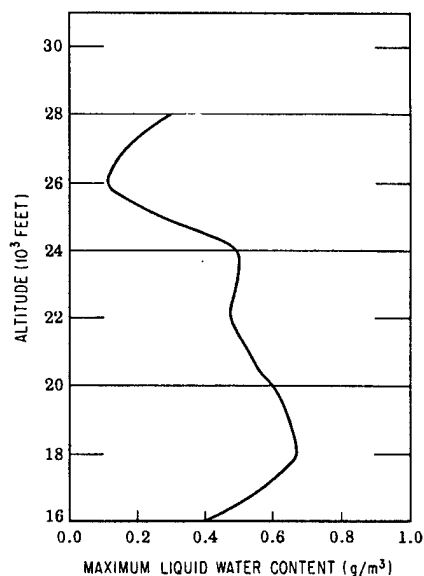


Fig. 5.46 Altitude Distribution of Liquid Water As a Function of Time of Penetration, George Cloud

liquid water, the rapid evaporation of the water giving rise to the sharp temperature drop. It may be noted that the relative humidity decreased below 100 per cent at about the same time that the temperature fell. Thus this hypothesis receives support since an unsaturated environment is required for evaporation.

The tails of the 18,000-ft pass (Fig. 5.33), the 20,000-ft pass (Fig. 5.34), the 24,000-ft pass (Fig. 5.36), and the 28,000-ft pass (Fig. 5.38) all show a strong temperature decrease. This is especially true of the 18,000-, 20,000-, 24,000-, and 28,000-ft passes, where the temperature actually fell to values considerably below the original environment value. Here again it is believed that evaporational cooling was the cause of the temperature fall. Reference to Fig. 5.46 lends weight to this surmise since

these traverses showed the high liquid-water content.

The pressure and airspeed patterns were similar to Dog cloud first passes. The true airspeed showed an abrupt increase on entering the cloud stem; this increase is believed to be due to strong updrafts inside the cloud. The pressure underwent a sharp decrease, reaching a minimum at about the center of the stem. In some of the passes symmetrical recovery was experienced, whereas in others the recovery was slower. It is felt that the model circulation discussed in Sec. 5.2.1 still offers the best explanation for the pressure drop, especially where a symmetrical recovery was found.

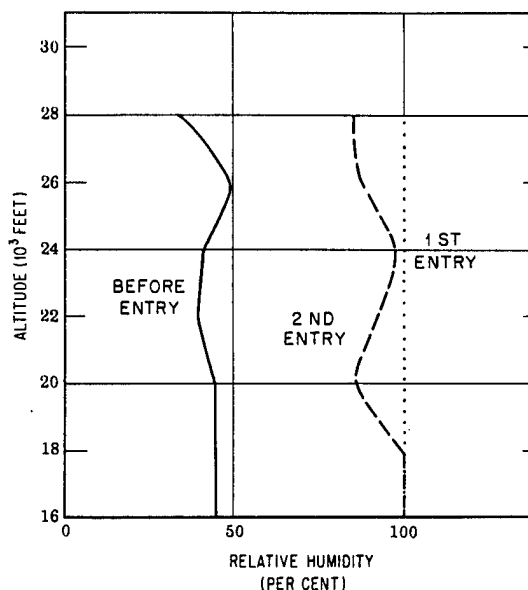


Fig. 5.47 Altitude Distribution of Relative Humidity As a Function of Time of Penetration, George Cloud

An alternate explanation of the pressure decrease might be made by assuming an increase of altitude of the drone. This explanation is attractive in those instances where the recovery was extremely slow (Figs. 5.33 and 5.35). However, the vertical acceleration of the drone required to account for the observed pressure drop must have taken place extremely rapidly (less than 10 sec). For this reason the model of the stem with a low-pressure center seems to be a more tenable explanation.

5.4.3 Effect of Aging on George Cloud

The results of the second penetrations are shown in Figs. 5.39 to 5.45. All the measured

parameters show less change than on the first penetrations. Table 5.6 indicates that all the second penetrations occurred after the mushroom had reached its maximum altitude. At the time of these penetrations the main cloud should have begun to deteriorate owing to spreading and shear, as well as to mixing with the free air. Portions of the stem cloud developed into swelling cumulus; this was observed in the lower part of the stem. That mixing was taking place is borne out by the change in observed relative humidity. The relative humidity decreased at all levels above 18,000 ft, as is seen in Fig. 5.47, as a result of mixing in drier outside air.

The temperature showed no general behavior during the second passes. In the 16,000-, 20,000-, and 22,000-ft traverses (Figs. 5.39, 5.41, and 5.42, respectively), the temperature decreased; the true airspeed was erratic, and the pressure showed little change. In the

18,000-, 24,000-, 26,000-, and 28,000-ft traverses, the temperature increased slightly, and the pressure remained fairly constant. The true airspeed varied in no set manner again, sometimes increasing, sometimes decreasing through the cloud. The fact that the stem was undergoing mixing with the free air meant that the various portions of the stem were in different stages of decay, and thus no over-all behavior patterns would be expected.

REFERENCES

1. H. B. Tolefson, NACA Advanced Restricted Report, ARR No. L5F27, July 1945.
2. H. R. Byers and R. Braham, The Thunderstorm, U. S. Weather Bureau, Dept. of Commerce.
3. W. Lewis, Meteorological Aspects of Aircraft Icing, Compendium of Meteorology, American Meteorological Society, Waverly Press, Baltimore, Md., 1951, p. 1197.

[REDACTED] 61

Chapter 6

Conclusions

6.1 SUMMARY OF AEROGRAPH RESULTS

6.1.1 Relation of Traverses to Cloud Geometry

One of the most significant findings of this study is that all the traverses, with the exception of one or two, were made through the stem of the atomic cloud and not through the main, or mushroom, cloud.

This fact should be borne in mind when examining the results of those projects having raw data furnished by drone-mounted equipment. Program 6 had a number of projects in this category. Thus the compilation of summaries of total radioactivity, types of radioactive particles, and similar studies on the general character of the atomic cloud, whose bases rest on drone data, must be understood to refer principally to the stem cloud.

Certainly the material in the stem cloud originated in the mushroom cloud, but it is not certain that the properties of the stem are entirely representative of the main mass of the atomic cloud.

6.1.2 Effect of State of Atmosphere on the Properties of the Atomic Cloud

The influence of the condition of the atmosphere at the time of detonation is clearly demonstrated in the case of moisture found in the stem. Easy and Dog clouds were formed in relatively dry air, whereas George cloud was formed from a rather deep moist layer. George was the only cloud to give 100 per cent relative humidity in its stem, and, in fact, it permitted a computation of reasonable values of liquid-water content. Both Easy and Dog clouds were found to have unsaturated stems.

It is thought that the only reason for this difference was the deep moist layer of air during George Shot.

6.1.3 Temperatures Inside the Atomic Cloud

It was found that the temperature inside the cloud was not very different from the free-air temperature. This statement is true for times as early as 2 to 3 min after detonation. In the case of Dog and Easy Shots, penetrations were made as early as this.

Apparently the cooling by radiation must be enormous and extremely rapid. As the fireball begins to rise, adiabatic expansion will cause additional cooling, but this is a secondary effect. From the aerograph data it appears that there is no danger of heat or high-temperature damage to aircraft if the atomic cloud is penetrated several minutes after detonation.

6.1.4 Turbulence Inside the Atomic Cloud

All penetrations showed sharp and extreme changes in true airspeed. These changes can be interpreted as the result of turbulence inside the cloud. From the amplitude and period of the changes, it might be surmised that the turbulence consisted mainly of drafts inside the cloud.

Since it is evident that the traverses were confined to the stem, turbulence in the main cloud would be expected to be of a different nature entirely. The origin of the turbulence in the stem was, of course, the inrush of air into the expanding mushroom. The mushroom itself was under toroidal circulation. Thus an aircraft penetrating an active, growing mushroom would be expected to encounter violent and severe turbulence.

6.2 FORMATION OF RAIN IN AN ATOMIC CLOUD

Since one of the original reasons for this study concerned the formation of rain, either

natural or artificial, from an atomic cloud, it would be worth while to discuss this aspect.

A model of the cumulus cloud, which develops rain, will be useful for comparison to the atomic cloud. The cumulus cloud, which grows into the cumulus congestus or cumulo-nimbus, both of which yield precipitation, does so by means of a succession of additions of air into the base of the cloud. The current concept of cumulus growth is that bubbles of air rise from the surface layers, penetrate the base of the cloud, and continue to rise until buoyancy forces are equalized. Bubbles are added continually, building up the cloud into a huge, towering mass. The path of the bubbles in the cloud is generally believed to be through a center shaft or core. This core is marked by updrafts. Mixing by entrainment with the free air can occur at all levels, but this process is believed to be taking place primarily at the edges of the cloud.

If the cloud is small in diameter, the entrainment process will interfere and modify the core, with the result that the general development of the cloud will be retarded and, in time, halted. The cores of larger clouds will not be affected in this way and will continue to receive additions of moisture to gradually build up appreciable liquid-water content in the form of water droplets. Coalescence among droplets

leads to the formation of large drops, or precipitation.

The atomic clouds differ in a number of respects. There is no mechanism for the continual addition of high moisture bearing bubbles to the atomic cloud. Thus the atomic cloud is itself a huge bubble.

Even in the cases of atomic clouds rising through deep moist layers, as in George Shot, the circulation pattern, which mixes outside air into the mushroom, will tend to soon halt the growth of the cloud. These clouds, therefore, do not have the time to establish the broad drop size spectrum required to initiate precipitation, even though the liquid-water content and turbulence compared favorably with shower clouds.

It would be expected, therefore, that little chance exists for the atomic mushroom cloud to develop into a shower or thunderstorm and thus yield radioactive rain.

On the other hand, the stem cloud was reported to have root clouds associated with it. These latter clouds are formed, presumably, by normal convective activity. There is no reason why this type cloud cannot develop into a shower or thunderstorm, provided the atmospheric conditions are favorable. In fact, the George cloud stem developed in just this manner into a cumulus congestus. Any rainfall from this cloud would be heavily contaminated.

Chapter 7

Recommendations

7.1 FUTURE INSTRUMENTATION

Since the accumulation of knowledge about the microstructure of atomic clouds must ultimately depend on the instrumentation, it is important to seek improved methods for measuring those parameters considered important.

One of the greatest needs on the Greenhouse tests turns out to be equipment that can measure directly the turbulence inside the cloud. The uncertainty about the interpretation of the pressure drop inside the stem would be easily resolved if the drones had been equipped with accelerometers and radar altimeters.

The lag in both the humidity and temperature sensing elements was too large to permit much detail. In future tests it would be helpful to use fine fast-response thermocouples for both temperature and moisture sensing.

A direct indicating device for measuring the condensed phase would be helpful in establishing the potentiality of atomic clouds for seeding. Liquid-water-content meters are being used in research at AFCRC, as well as icing-rate meters for supercooled water.

The dynamic heating of the probe due to ram pressure necessitated a large and uncertain correction to the measured values of temperature and humidity. A vortex housing like those housings currently being employed in aircraft thermometry should be used on future tests.

Finally, the location of the position of the drone aircraft from the navigator's log proved to be doubtful. A graph of a number of positions as shown in Table 4.1, 4.2, or 4.3 reveals incon-

sistencies when compared with photographic data. A more positive method of location would be gained by the use of radar tracking systems on the ground combined with beacon signals from the drone aircraft.

7.2 ADDITIONAL STUDIES ON THE ATOMIC CLOUD

1. The atomic cloud is an example of a bubble rising in the atmosphere. The behavior of the atomic cloud would make an excellent example for advancing meteorological concepts of the mechanism of bubble transport into cumulus clouds.

2. The atomic cloud processes can contribute to a better understanding of precipitation physics and thunderstorm electricity since a number of attributes are found in the atomic cloud which are normally associated with clouds that show precipitation and thunderstorm electricity.

3. The aging of the atomic cloud forms an excellent background to test general ideas concerning mixing and entrainment processes normally thought to be operating in convective clouds.

For these reasons it is felt that the data contained in this report should be released to the meteorological public. The subsequent interest among theoretical meteorologists will contribute greatly to a general understanding of convective processes in the atmosphere and will indirectly serve to better our appreciation of the development of the atomic cloud.

Part II

DEVELOPMENT OF THE ATOMIC CLOUD

by

WILLIAM W. KELLOGG

ROBERT E. McKOWN
Captain, USAF

and

DANIEL E. McPHERSON, JR.
1st Lt, USAF

Institute of Geophysics
University of California at Los Angeles
September 1951

Preface

The primary purpose of this report is to document the rise and development of the four Operation Greenhouse atomic clouds. All the observations were either visual or photographic, and therefore the records do not go much beyond 1 hr from shot time. The later stages of the cloud development, after the cloud was no longer clearly visible, are covered by Project 4.6 and Program 7, in which aircraft equipped with devices for detecting the atomic material directly or its ionization effects were used. Therefore a complete description of the cloud development should combine the results of this report, which gives the initial conditions, with the results of the more long-range projects.

Considerable interest has been expressed in the rate of rise of the atomic cloud since this is important to aircraft dropping atomic bombs and to sampling experiments in which rockets or aircraft are programmed to pass through specific parts of the rising cloud. Therefore this report not only gives the rates of rise of the Greenhouse clouds but also summarizes the measurements, such as they are, from other tests for which data were available.

An attempt is made in this report to develop theories and explanations for the effects observed. However, the report is mostly factual, and it is intended that enough facts be provided so that a more elaborate theoretical analysis can make use of them later.

Acknowledgments

The analysis of the features of the Operation Greenhouse atomic clouds contained in this report is based to a large extent on photographs taken by Edgerton, Germeshausen & Grier, Inc., under the direct supervision of 1st Lt Kenneth W. Cook, USAF. These photographs had to be taken under very poor lighting conditions, since the first two shots were predawn, and under conditions where the light level varied rather rapidly as the clouds moved up into the sunlight. Some of the pictures did not come out well, but the fact that the analysts had complete coverage of the cloud in time, except where cumulus clouds blocked the view, attests to the success with which the photographers solved the difficult problems.

Working with Lt Cook on the ground photography were Harry Smith and M/Sgt Melvin Lang, USAF, who helped in the establishment of the camera sites and in manning the cameras at shot time. The success of the photography was due to a large extent to their efforts.

The aerial movies were taken by Capt Millard E. Griffith and 1st Lt Raymond Hill. These pictures were taken with hand-held movie cameras and were excellent in showing certain features of the atomic clouds which could not be observed from the ground.

In the course of the writing of this report, much helpful advice on the theory of the rising cloud was given by Prof. Clarence Palmer of the Institute of Geophysics, who was in charge of Project 4.5.

Abstract

By means of a tracking and photographic network extending halfway around Eniwetok Atoll, the behavior of the first three Operation Greenhouse atomic clouds was observed and recorded. The rise of the fourth (and last) Greenhouse cloud was observed visually from only one site. The analysis of these observations, combined with information about the local weather conditions, gives a fairly complete picture of the development of each of the clouds. Particular emphasis has been placed on the earlier phases of the development, from about 20 sec after shot time to about 10 min after shot time, and

the heights and sizes of the cloud parts have been determined as functions of time.

For the sake of comparison and in order to make this report of more general use, a summary of important features of some previous atomic clouds has also been included.

Theoretical explanations for some of the phenomena involved in the development of an atomic cloud are given where possible, with particular attention being paid to quantitative calculations of the internal temperature, the rate of increase of mass due to entrainment, the height at which the cloud stabilizes, and the circulation pattern of the rising cloud.

Chapter 1

Observational Data

1.1 OBJECTIVES OF GREENHOUSE PROJECT 4.1B

The primary objective of Operation Greenhouse Project 4.1B was the documentation of the atomic cloud in its early stages while it was still clearly visible. It was not specified at first just which of the features of the cloud would be the most important, and therefore an attempt was made to cover as many features as possible with the facilities available. Since all the observations were either visual or photographic, it is clear that the features studied could only be those connected with the cloud appearance, such as size, position, shape, and color.

Although the observations of the cloud itself constitute the primary part of the program, the local weather conditions have a direct effect on the behavior of the cloud, particularly the winds and the atmospheric stability. Therefore an important secondary purpose of the program was to record the local weather conditions and to indicate their effect on the atomic cloud. The relations between the cloud and its surroundings could be the subject of a much more detailed analysis than is contained here, but many of the more obvious effects of the weather, especially of the winds and the atmospheric stability, are demonstrated.

1.2 SURFACE VISUAL OBSERVATIONS AT GREENHOUSE

As in the Operation Sandstone tests there were observers stationed at various sites with theodolites or nephoclinometers to record the development of the atomic cloud. However, this time there were certain improvements in the visual observations which made them somewhat more useful.

First, the sites were on land and were carefully aligned in order to allow triangulation on significant features. There were three manned sites in all, two on Eniwetok (Stations 190 and 191) and one on Japtan (see Fig. 1.1). The total

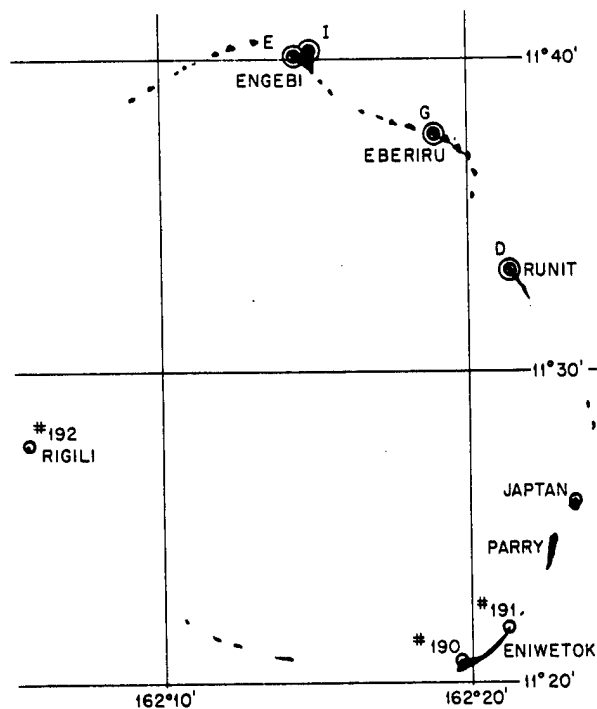


Fig. 1.1 Map of Eniwetok Atoll, Showing Observational and Camera Sites and Their Relation to the Shot Points

length of the base line between the three stations was 6.4 nautical miles, and, since this was at least one-third of the distance to the shot towers, fixes could be made wherever a distinct feature could be seen from all three sites.

A second innovation was the use of wire recorders to facilitate the recording of the infor-

mation. In the early stages of the atomic-cloud development, the changes occur rapidly, and it would be very difficult by writing or sketching alone to get the necessary observations unless a much larger crew were assigned to the task. With a wire recorder at each site, it was possible for one observer to read the theodolite angles as fast as they were made and to interject comments about the appearance of the cloud at the same time. Thus the volume of data obtained at each site was quite large.

It was found that the cloud changed less rapidly after the first 10 or 15 min, and therefore it was the practice of the observers to take time out at regular intervals to sketch the cloud as they saw it (as was done on Sandstone). These sketches proved very helpful in interpreting the wire-recorder records since it is often difficult to get a clear picture from a verbal description of a complicated shape. The desperate attempts of the observers to describe the cloud in its later stages resulted in such word pictures as, "It is now like a golf ball sandwiched between two cigars," or, "It looks like a marshmallow to me!"

Although the later stages, during the breakup of the cloud, may produce a variety of complicated shapes, during the rise and early drift the cloud has an orderly and well-defined shape. In order to be able to talk about the cloud in this stage, the observers agreed on a system of nomenclature that is worth recording here. The words were chosen from those that seemed to be in current use in other reports^{1,2} and are in nearly every case descriptive, everyday words. Figure 1.2 gives a summary of the nomenclature that was adopted.

1.3 SURFACE PHOTOGRAPHIC NETWORK AT GREENHOUSE

Since the tests were mostly predawn, the light level was generally too low to get pictures without specially rigged cameras. Therefore Edgerton, Germeshausen & Grier, Inc. (EG&G), designed and built three complete camera stations with a variety of cameras in each station to cover the entire course of the atomic cloud from the first few seconds on to the last visible traces. The coverage proved to be complete as far as the exposures were concerned, and the pictures actually served as the primary basis for the analysis in this report, rather than the

visual observations, which were generally less accurate (see Appendix A).

1.3.1 Location of Sites

Two of the three camera sites corresponded with the manned sites. Stations 190 and 191 on

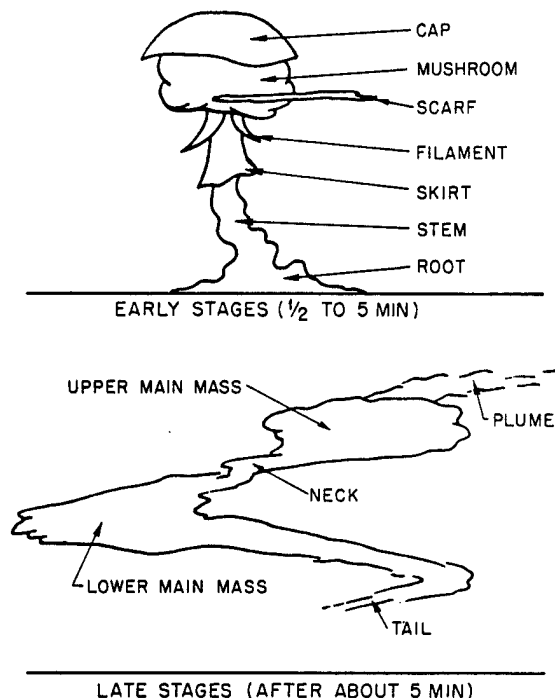


Fig. 1.2 Nomenclature of the Atomic Cloud

Eniwetok were manned by both observers and cameramen. The observers and the cameramen at these sites worked in close coordination, and therefore the wire recorders serve as a commentary to go with the pictures. The locations of these sites are shown in Fig. 1.1. The length of the base line between these two sites was 1.95 nautical miles.

The third camera site was on the island of Rigili, and, since this island is southwest of the firing points, it was considered unsafe to man it. (The prevailing winds are east in the lower layers, and, indeed, the fall-out on Rigili was very heavy following the first shot.) Therefore, although it had almost as many cameras as did the manned stations, it was operated completely automatically. Some difficulties were encountered in setting up and servicing this station, but it proved to be worth the effort. The total base line, from Station 191 to Rigili, was 16.25

nautical miles, and the difference in the angle of view between these two stations was from 55 deg to nearly 70 deg; therefore it was possible to get a good idea of the three-dimensional shape of the clouds.

One other advantage of having the site on Rigili proved to be the increased probability of getting a clear view between local cumulus clouds, which tend to lie in lines parallel with the prevailing surface winds. As it turned out, the Rigili site gave data on the atomic cloud for two periods when the cloud was obscured from the other two stations by local cumulus clouds (see results in Tables A.1 to A.3).

1.3.2 Description of Cameras

A more complete description of the camera sites is given in Part III of this report. It is enough here to give a general idea of the photographic coverage.

The greatest volume of material was obtained by banks of six K-8 aerial type cameras at each site. These cameras had 12-in. focal-length lenses and gave pictures that were 9 by 9 in. They were mounted in a rack in such a way that their fields of view just overlapped at the edges, and the total coverage was about 60 deg in elevation and about 116 deg in azimuth. This large total angular coverage was enough to ensure that the cloud would remain in the field of view for a reasonably long time (see Fig. A.1).

In addition, each of the three sites had one K-24 camera aimed directly at Ground Zero. These cameras have an f/2.5 lens with a 7-in. focal length, and they give 5- by 5-in. pictures. As will be explained, this was to cover a different time period by using different exposures.

Each of the manned stations (190 and 191) on Eniwetok had a Mitchell movie camera, which was directed by hand. The movies were taken steadily at first, and then intermittently as the camera was panned over distinguishing features of the cloud. The cameraman and the observer stood beside each other so that the footage on the camera and the directions to the cameraman would be recorded on the wire recorder. The recorder commentary, therefore, can be synchronized roughly with the movie, without which the films would be meaningless. Since no angles or times are recorded on the film, these movies cannot be used for precise measurements, except at the beginning when the horizon was still showing in the frame.

1.3.3 Photographic Exposures

The purpose of having so many cameras was to ensure that there would be complete photographic coverage, even with the adverse light conditions of a shot half an hour before dawn. This objective was achieved as far as the exposures were concerned.

The details of the camera operation are given in Part III of this report, but most of the facts are summarized in Tables A.1 to A.3. In noting exposures, keep in mind the fact that only Dog and Easy Shots were predawn shots, George Shot being in broad daylight. (Item Shot was also predawn, but it was not photographed for the project.)

No attempt was made to catch the first second or two since the study of the fireball is the domain of several other projects. Therefore all pictures were badly overexposed at shot time, although there was no damage to the film.

The K-24 cameras, centered on the shot tower, operated so as to get a fairly large number of pictures during the rise. The pictures covering the first minute or two were generally underexposed but were just readable. After the atomic cloud rose to 20,000 or 30,000 ft, it began to receive more indirect sunlight from the east, and from then on the pictures became progressively more dense. Total coverage time was 25 min for Dog Shot, 8 min for Easy Shot, and 6 min for George Shot.

The lower three and center top K-8 cameras were programmed to pick up the cloud from the time it reached 20,000 to 30,000 ft and to follow it for about 1 hr. Actually coverage was obtained for up to about 40 min. The exposures at the manned stations could be varied during this interval, but at Rigili they had to be the same throughout. The various apertures and exposure times are shown in Appendix A. The films turned out to be blank on the predawn firings from about 30 sec until the cloud reached the higher levels, and they were generally quite badly overexposed toward the end of the sequence; however, the pictures from about 3 min to about 20 min were generally excellent as far as exposures were concerned.

The Mitchell movie cameras were run at 8 frames/sec throughout, but the lens apertures and shutter angles were changed frequently to give the best pictures. No results were obtained with these during the early rise, after the fireball light died away, until about 5 min, when the

atomic cloud first became visible in the sunlight at a considerable altitude.

1.4 AERIAL OBSERVATIONS AT GREENHOUSE

As in some of the previous tests, an attempt was made to get photographic coverage from the air. Aerial photographs are unsatisfactory for accurate measurements owing to the uncertainty in the exact position of the aircraft when the photographs were taken. However, they did turn out to be helpful in getting a clearer idea of some of the features of the clouds which did not show up from the ground. (These were not released to the project scientists until one week before the report was due.)

The photographs that were taken specifically for Project 4.1B were all 35-mm movies taken with hand-held A-6 cameras from the two B-50D aircraft. The shots were continuous on the rising cloud, although little can be seen in the predawn shots until the cloud was well above the aircraft height and reached the more direct sunlight. Thereafter the practice was to take pan shots of the cloud at regular intervals while the aircraft circled the cloud at a distance of from 5 to 25 miles. These pictures were taken for 30 min to 1 hr from shot time.

The initial photographs of the rising cloud were taken with black-and-white film, and the later photographs were taken with color film. The reason for the shift was to get the greatest sensitivity at first, when the cloud was sharply defined but the light level was low (in the first two tests), and then to use color in order to be able to distinguish the atomic cloud from the other clouds by its characteristic brownish color.

Attempts were made to navigate carefully throughout the taking of the pictures and to tie the footage in with the navigator's log. This was not very successful owing partly to the fact that accurate navigation was made very difficult by the failure of the aircraft radar on several occasions and partly to the fact that the exact time of each shot was difficult to determine. Also, since the cameras were hand held, the bearings of the photographs with respect to the aircraft were not known.

1.5 AUXILIARY METEOROLOGICAL DATA

The meteorological program was under the direction of Task Unit 3.4.5, and the details of this program are contained in separate reports.

However, to understand the behavior of the atomic clouds, it is clearly necessary to have accessible all available information on the weather conditions at the times of firing. For this reason some of the meteorological data gathered at Eniwetok are included in this report for convenience.

The most significant meteorological data for the present study are the upper-air winds and temperatures. At Eniwetok an AN/GMD-1 Rawin set was in operation throughout the test and would have provided the necessary data if the radiosonde balloons had worked better. As it was, the data up to 40,000 or 50,000 ft are excellent, but above this height they become very sparse owing to frequent failure of the balloons, an unfortunate circumstance since it is of considerable importance to know the height of the tropopause at shot time and the winds above these levels.

The upper-air data are given for each shot (see Chap. 3).

1.6 DATA FROM PREVIOUS ATOMIC EXPLOSIONS

It is not the primary function of this report to summarize data from previous atomic explosions. However, it seemed worth while to include some of the results of former tests for the sake of comparison.

The most completely documented test, from the point of view of the study of the atomic cloud in its later stages, was Operation Sandstone. An excellent report by Humphrey² of the U. S. Weather Bureau summarizes the results of this test. However, at that time there was not the complete photographic coverage that was obtained at Operation Greenhouse, and the observations were almost all visual. Moreover, the observation sites were the decks of ships anchored in the lagoon, and therefore the azimuths could not be very accurately determined. Even so, the results were quite complete.

At the Trinity test the documentation was good for about the first minute and was reported by Mack³ in considerable detail. However, as soon as the cloud had moved upward to the point where the top of the cloud and the horizon were not in the same picture (which it did after about 1 min), it was no longer possible to make height measurements, which were done by measuring on 35-mm movie film from the horizon to the top of the cloud. A few points on the cloud were obtained at later times by observing with a search-

light beam, but it is not certain on what part of the cloud these sights were made.

There does not appear to have been any organized attempt to take measurements on the atomic clouds at Operation Crossroads after the first few seconds, although there were many pictures taken both from ships and from the air. General features are obtainable from these pictures, but measurements do not appear to have been made on the later stages.

In Chap. 2 (see Fig. 2.2), the data from Trinity and Sandstone on the rate of rise of the cloud

are presented for comparison with those from Greenhouse.

REFERENCES

1. "The Effects of Atomic Weapons," Chap. II, Government Printing Office, Washington, D. C., 1950.
2. Paul A. Humphrey, Classified Scientific Meteorological Information, Operation Sandstone, Annex 14, Sandstone SS-35, 1948.
3. J. E. Mack, July 16th Nuclear Explosion: Space-Time Relationships, Report LA-531, April 1946.

Chapter 2

Rise of the Atomic Cloud

2.1 MAIN FEATURES OF THE INITIAL GROWTH AND RISE OF A TOWER BURST

The most complete description of the initial stages of an atomic cloud is contained in the report of the Trinity test by Mack.¹ Other reports have also dealt with this subject in some detail.^{2,3} It will therefore be sufficient to define very briefly the various stages and to indicate where this report can contribute new information.

The photography for Project 4.1B was relatively slow speed, and the distances were so great and the overexposures so serious that little can be deduced from the pictures about the first few seconds of the atomic cloud. Indeed, these first few seconds are covered by a number of other observational programs, and therefore little or no attempt is made here to study them.

This report deals with the atomic cloud from the end of its "hover time" until it has dissipated visually. The hover time of an atomic cloud is not a very precise quantity but can best be defined as the time from burst to the time when the top of the atomic cloud begins to rise rapidly. There is a period of from 3 to 10 sec, presumably depending on the yield of the weapon, when the center of the fireball and cloud remains at roughly the same height, as determined from measurements of its top and sides. During this time the growth of the cloud in size becomes rapidly slower. Then quite abruptly the cloud begins to move upward as a whole, with a rate of rise that diminishes slowly with time.

There is one serious difficulty encountered in all blasts taking place in the Marshall Islands, where the humidity is always very high in the lower layers. The shock wave, as it moves out, trails a low-pressure wave behind it, and in

this low-pressure region a cloud of water vapor forms. This shock-wave cloud acts like a curtain and hides the atomic cloud from view during the critical time when the atomic cloud begins its rise. This was the case at Sandstone, as reported by Houghten,⁴ and seems to have been the case at Greenhouse, judging from the Project 4.1B photographs. For this reason the estimates of the hover time for the Greenhouse clouds cannot be at all accurate and are, in fact, based to a large extent on an extrapolation of the observations at Trinity, using a scaling factor of the yield to the one-third power, as suggested by Gallentine.⁵ It can only be said that the results so obtained appear to be consistent with hover times deduced by extrapolating the height of top vs time curves back down to a height corresponding to the approximate radius of the cloud when it started its rise.*⁶

This large uncertainty in the hover times due to the lack of observations led to an inquiry about the mechanism for the hovering. It was felt that the third-power-of-the-yield scaling factor used by Gallentine had little more than very general arguments to justify it, and nowhere could any ready explanation be found for the fact that the atomic cloud hovered at all. Considerable help in this matter was given by Frederick Reines in a personal discussion, however, and some preliminary suggestions are given in Appendix C to account for the phenomenon of hovering. It will be clear to anyone,

*Preliminary results obtained by Lewis Fussell of EG&G indicate that on George Shot the hover time was 4 to 5 sec and on Easy and Item Shots, 2 to 3 sec. These are shorter than those predicted by Gallentine, but there is little doubt about the reality of the phenomenon.

after reading Appendix C, that we are dealing with a very poorly understood subject.

Following the end of the hovering time, the fireball rises and breaks away from the ground, leaving only the stem below it. The fireball, now referred to as the "mushroom," rapidly loses its brilliance as it rises and, after rising to a few thousand feet, does not show up as a light source on the photographs from Greenhouse, although under clearer conditions it might have been seen longer. However, just before the light dies away, it is possible to see in the movies the strong upward draft in the stem below it and the indraft along the ground. This suggests that a good way of determining the indraft or afterwind might be to study the rate of motion of the flying dust and debris as seen on the photographs. This was not done here because the detail in the Project 4.1B photographs was generally too poor because of the great range.

2.2 RATE OF RISE

Figures 2.1 and 2.2, giving the height of the top of the atomic cloud as a function of time, are self-explanatory. It is believed that, where there were no obscuring cumulus clouds, the observations on the first few minutes of the atomic cloud are very precise since during this time the cloud went practically straight up and there is no deviational effect due to the wind. Moreover, the assumption that the top of the cloud is spherical is probably still quite good during this interval, and therefore little error is introduced by the fact that the sightings were made on the edges of the clouds rather than on the top (corrections for this were made, assuming the cloud to be a hemisphere of known radius, as described in Appendix B).

Unfortunately, during the three tests that were photographed, there was serious obscuring of the cloud by cumulus, and therefore the data are not at all complete for some of the shots. For Dog Shot the atomic cloud disappeared in a strato-cumulus deck at about 2000 ft before the shock-wave cloud lifted and remained obscured until it appeared above the cumulus at about 44,000 ft, as seen from the unmanned site on Rigili. The cloud did not reappear to the observers at Eniwetok in time to get any measurements on its rise. The observer on Japtan got a few shots after $4\frac{1}{2}$ min. Easy Shot was better, but here again the low cumulus was in the way

for part of the time. The cloud was momentarily visible from about 10 to 16 sec after shot time, and after that the next sight on the cloud was from Rigili when the top was at 12,000 ft. George Shot was even better, with the earliest observation on the top when the cloud was at 3600 ft, but in this case it was lost again at about 23,000 ft. (The last shot, Item, would have given perfect coverage right from the beginning, but there were no cameras set up for it. Theodolite observations were made, however.)

During the rise the upper part of the atomic cloud, or mushroom, preserves a roughly hemispherical shape,¹ and the size grows rapidly, as shown in Figs. 2.4 and 2.5. To test the assumption that the mushroom was hemispherical (as required for the reduction method described in Appendix B), a plot of the ratio of the observed horizontal semidiameter to the observed depth of the mushroom was made. If it is close to unity, the assumption is justified. Figure 2.5 shows how these plots turned out.

It should be added that the depth was determined by subtracting from the corrected height of the top of the cloud the observed height of the base of the mushroom, taking into account only the change in horizontal range to determine the latter. The elevation angle of the base was sometimes difficult to determine since there is probably some latitude in interpreting just which part of the bottom should be called the base. Therefore some of the spread of the points in Fig. 2.5 may be due to this uncertainty in the observations of the mushroom depth.

2.3 MAXIMUM ALTITUDE

The rise of the atomic cloud is obviously due to the fact that the air inside the cloud is initially much warmer than the environment. However, as the cloud rises, it cools, at first by losing heat through radiation and then, after 5 or 10 sec, by adiabatic expansion as it rises to levels of lower pressure. If these were the only two factors involved in cooling the cloud, it would rise far into the stratosphere before it was cooled to the same temperature as the environment. Actually, the cloud barely reaches the base of the stratosphere in most cases. The extra loss of buoyancy is due to the fact that the cloud entrains air from the outside from the very start and dilutes itself. For example, the George cloud grew in volume by a factor of

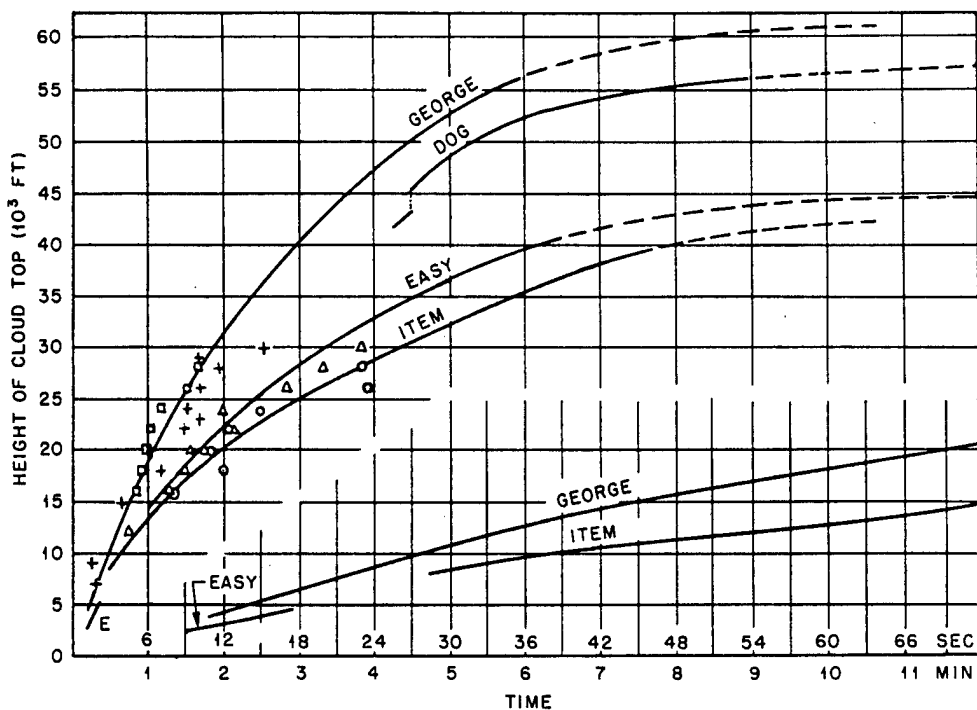


Fig. 2.1 Height of Tops of Clouds As a Function of Time, Operation Greenhouse. The plotted points were determined by the times when the pilots of the "mother" aircraft estimated that the top was at their flight altitude. +, Dog Shot. Δ , Easy Shot. \square , George Shot. \circ , Item Shot.

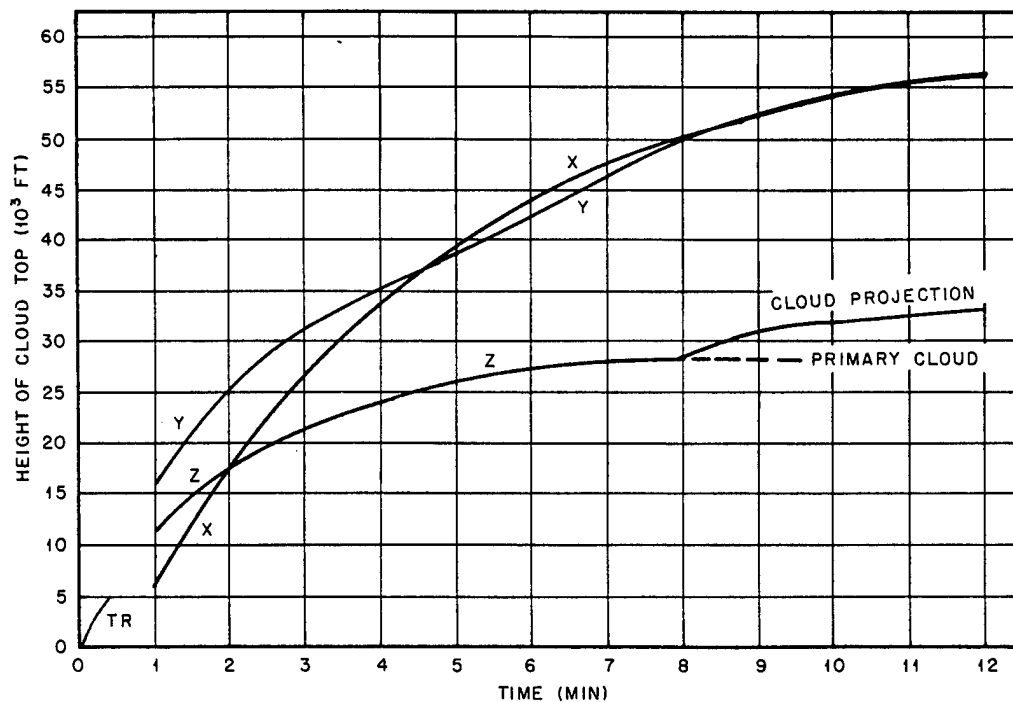


Fig. 2.2 Height of Tops of Clouds As a Function of Time, Operations Sandstone and Trinity

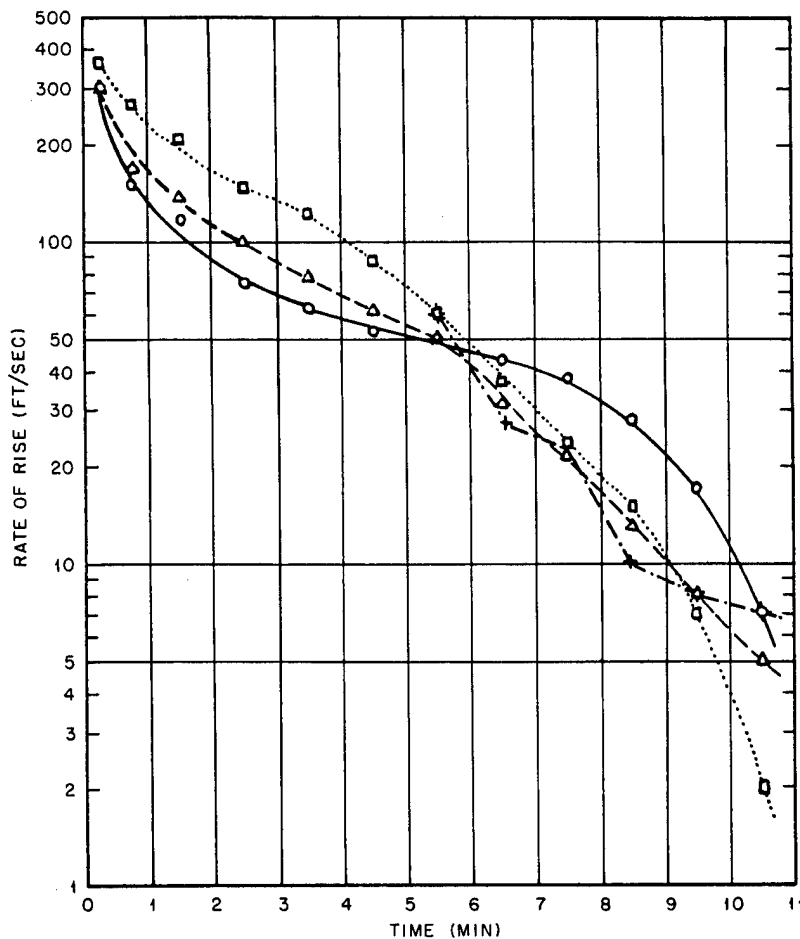


Fig. 2.3 Rate of Rise of Tops of Clouds As a Function of Time. +, Dog Shot. Δ, Easy Shot. □, George Shot. O, Item Shot.

about 220 in rising from 5000 ft to its ceiling, and it probably gained in mass by a comparable, though smaller, factor. The Easy cloud increased in volume 57 times in its rise from 5000 ft to its ceiling.

There is still another factor involved in the heat balance of the cloud. The air entrained into the cloud and carried upward has a certain amount of moisture, and, as it is carried aloft and cooled, the moisture condenses out in the form of a cloud. In so doing, the latent heat of vaporization of this water is added to the atomic cloud and so allows it to rise higher than it would in a completely dry atmosphere.

These introductory remarks suggest that the heat budget of the rising atomic cloud is fairly complicated. However, to get an idea of the magnitude of some of the factors involved, some calculations were made on the Easy and George clouds for which data were quite complete. By

use of a modification of a method suggested by Machta,⁷ the entrainment of air into the cloud was taken into account, and the temperature inside the cloud was calculated assuming negligible loss by radiation and negligible gain by condensation of water vapor. The details are given in Appendix D.

It will be seen, from Table D.1, that neglecting the effects of radiation and condensation leads to the requirement of an absurdly large initial temperature as the cloud starts upward since a 10,000°K (or higher) temperature at 5000 ft would mean that the atomic cloud was still very brilliant and losing heat rapidly by radiation at this level,⁸ which is not the case. The fact of the matter is, clearly, that the release of heat into the cloud by the condensation of water vapor is an important factor and should be taken into account in calculating its heat balance. This can probably be done with the

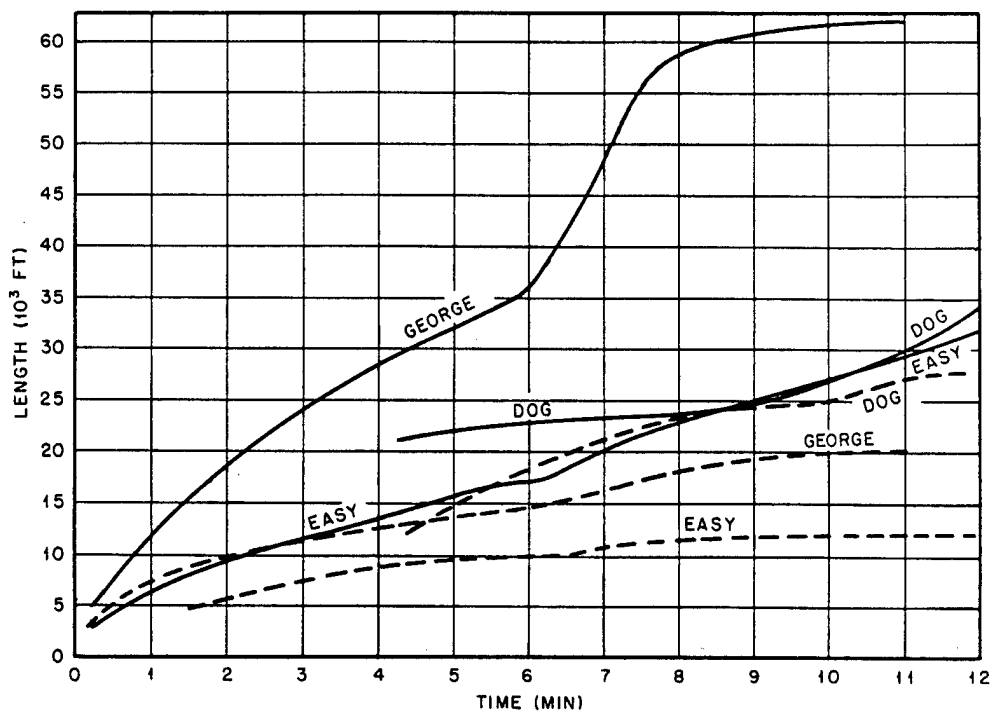


Fig. 2.4 Diameter (——) and Depth (-----) of Mushroom Clouds As a Function of Time

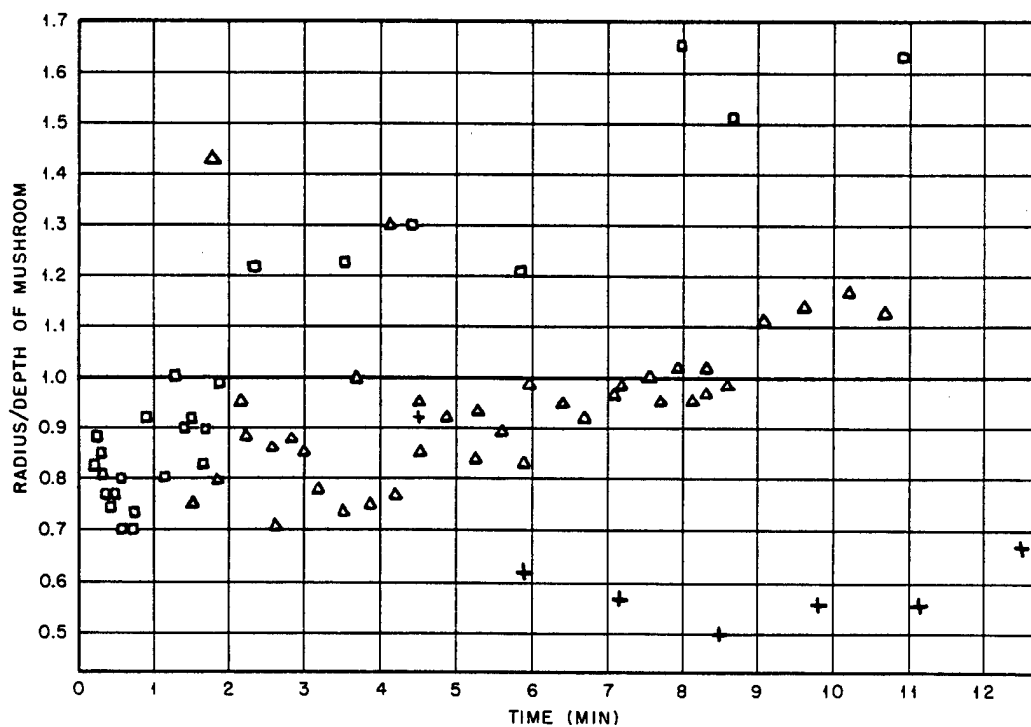


Fig. 2.5 Ratio of Observed Radius to Observed Depth of Mushrooms As a Function of Time. +, Dog Shot. Δ , Easy Shot. \square , George Shot.

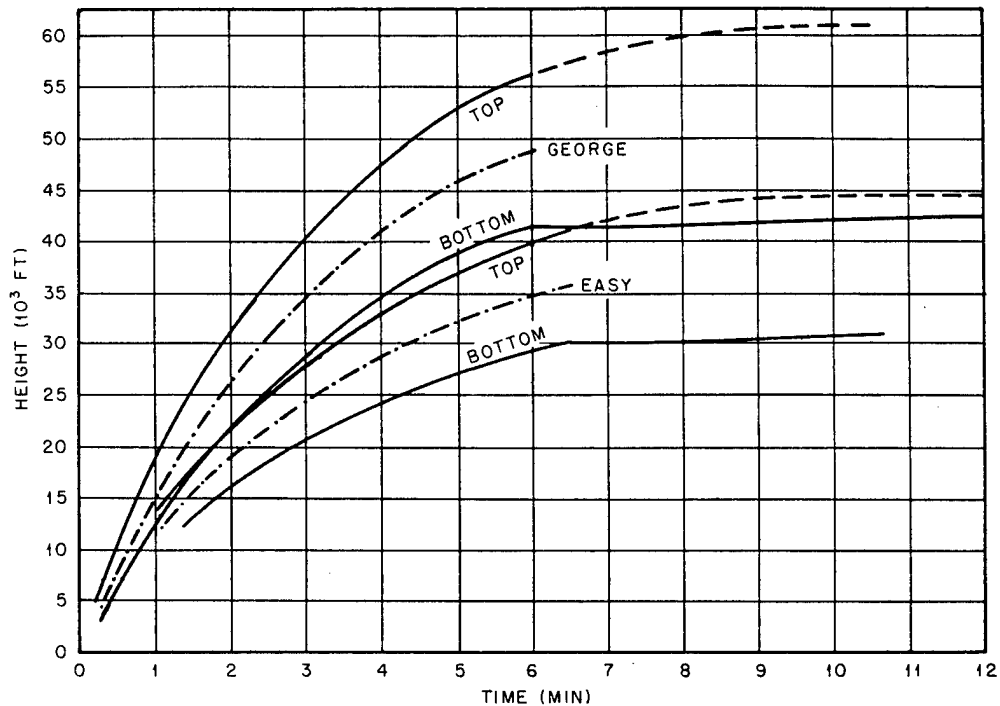


Fig. 2.6 Rise and Vertical Growth of the Easy and George Clouds

present data, although it would involve some laborious calculations.

This result also suggests that the relatively straightforward "dry adiabatic" treatment discussed in Appendix D would work quite well in the Nevada tests where the moisture content is often very low.

When the atomic cloud reaches its ceiling, there is a rather sudden and pronounced flattening of the cloud. Although this has been predicted,⁹ it had apparently not been reported on previous tests, the reason being that one cannot see it by observing only the top of the cloud from the ground. As is pointed out in Appendix B and elsewhere, the observer on the ground cannot actually see the top at all and can only guess at its location by observing the edge and making assumptions about the shape of the top. The arrival of the cloud at its ceiling is marked by two observable features: (1) a sudden increase in the diameter of the cloud and (2) a stabilization of the bottom of the cloud. It is as if the cloud actually hit a solid "ceiling" which prevented the top from rising any further and the turbulence still left in the cloud then acted to spread the cloud out sideways. The abruptness of this transition, where local clouds allowed it to be observed, leaves little doubt as to its reality (see Figs. 2.4 and 2.6).

It has been supposed that atomic clouds usually rise to the tropopause and stop there since that is the level where the stability of the atmosphere suddenly increases. (This was assumed as the basis for the height calculations in the analysis of the Sandstone X-ray and Yoke clouds.¹⁰) However, the Zebra, Easy, and Item clouds did not rise that high, and very large yield weapons will probably go considerably higher. Table 2.1 summarizes the maximum heights of the Sandstone and Greenhouse clouds as compared to the heights of the tropopause. It will be seen that predicting the ceiling of an atomic cloud on the basis of the height of the tropopause is a rather good "rule of thumb" for weapons with yields of around 100 kt or more, but the smaller weapons often fall short of the tropopause. As a surmise, it would be likely that atomic clouds exploded in drier places would be even more likely to fall short of the tropopause because of the smaller help given by the condensation of water vapor.

2.4 INTERNAL CIRCULATION OF THE CLOUD

In Sec. 2.3 it was pointed out that all the rising atomic clouds grew in size and mass by en-

TABLE 2.1 MAXIMUM HEIGHTS OF ATOMIC CLOUDS

Designation of cloud	Yield (kt)	Estimated ceiling (ft)	Height of tropopause (ft)	Remarks
X-ray	38	56,000	56,000	Possible error of 2000 ft
Yoke	47	56,000	56,000	Possible error of 6000 ft*
Zebra	20	33,000	54,000	
Dog	83-90	56,000	56,000	
Easy	50	41,000	52,000	
George	225-350	56,000	55,000	
Item	45	40,000	54,000	Possible error of 3000 ft

*Observations based on observed winds indicated a ceiling of 50,200 ft, but then it was assumed that the winds were in error by an amount such that the observations should have given 56,000 ft.

training air from the environment. Anyone watching a rising atomic cloud can see the general pattern of the circulation, and it is fairly clear that the entrainment is into the bottom of the mushroom. The pattern that is usually visualized¹¹ is a simple toroidal one, almost like the circulation in a fat smoke ring, in which the air rises faster in the middle, diverges at the top, and then curls back down on the outside and rises up in the middle again.

This simple pattern seems acceptable except for two features which it does not explain. First, there is no way for the radioactive material in the mushroom to break out of this spiral, streamline pattern. The original material would be trapped and all carried aloft (as is the case in a smoke ring). This is clearly not the case since it is well established that the stem contains fairly large quantities of radioactive material all the way up it, and the brownish color of the stem must be due to the nitrogen dioxide formed in the fireball stage. This cannot be explained as coming up from the ground or falling down by gravity, but it must be left behind by the rising atomic cloud.

A second feature that should be considered in the circulation pattern is the observed twist of the stem, which suggests a vortex in the center of the system. That this is almost surely present can be seen by considering that the convergence at the base of the mushroom is comparable to that around a tornado or a waterspout, and, where there is convergence, there is certain to be a conservation of vorticity and an increase in the angular velocity (as in the time-worn example of the water running out of a bathtub). The direction of this spin depends on the direction of the absolute vorticity in the air at the start and therefore will usually be cyclonic

at middle to high latitudes. However, it turns out to have been anticyclonic (like a left-handed screw) in the two cases where it was most marked, in Trinity and George clouds.

A strong vortex in either direction will cause a low pressure to develop at the center owing to the centripetal force. Thus, along the lower part of the axis of the atomic cloud, there must be a relatively low pressure. At the very top of the atomic cloud, as it moves rapidly upward, there must be a considerable increase in pressure due to the "ram" effect of the moving mass, this pressure being a maximum at the center of the top, which is a sort of stagnation point. Thus there is a low pressure along the lower part of the axis and a high pressure at the top, and this pressure gradient might be expected to force the air downward along the axis.

Figure 2.7 shows this more clearly. It is important to separate the absolute velocity field from the relative velocity field. Part a of Fig. 2.7 will be recognized as the circulation pattern that one sees, with the upward convergence at the base of the cloud. Part b of Fig. 2.7, however, gives the velocity field relative to the top of the cloud. (The second is obtained from the first by subtracting the vector representing the motion of the top of the cloud from the absolute velocity vector at each point in the field.) In the relative field it can be seen that the pressure gradient at the top forces some air down along the axis, and therefore there is actually some outflow downward at the base.

This must be the explanation for the fact that parts of the atomic-cloud material are left behind in the stem, although there is some absolute upward motion in the base of the cloud.

This circulation pattern also helps to explain some other features of rising atomic clouds.

For example, in the Easy cloud there seemed to be a flattening of the top, which gave the impression that the cloud was quite doughnut shaped during the later part of its rise. Another common feature is the formation of filaments

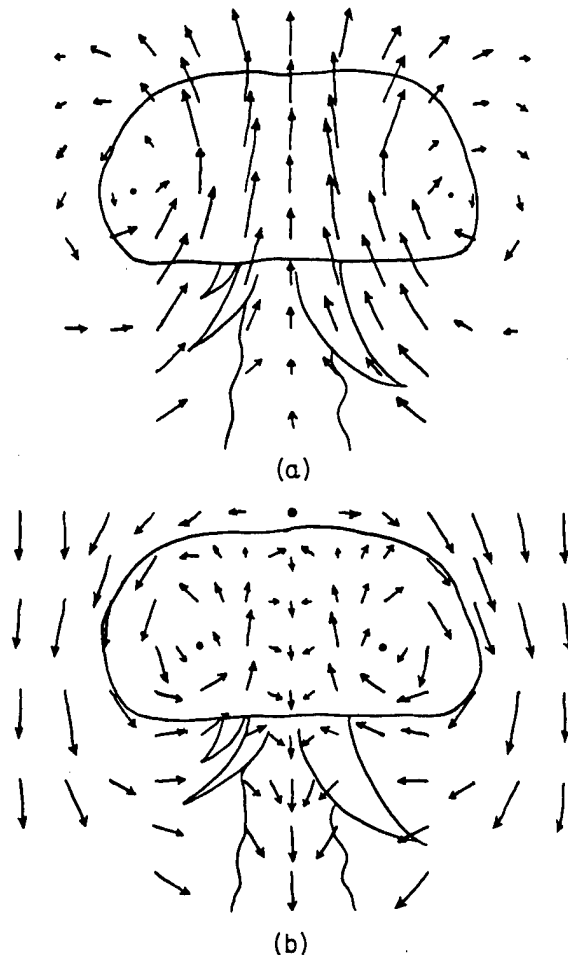


Fig. 2.7 Schematic Representation of the Velocity Field of a Rising Atomic Cloud. The absolute velocity field can be obtained from the relative velocity field by adding vectorially the motion of the cloud to the relative velocity at each point. These are only the meridional velocities, to which are added the rotation of the gas around the axis. (a) absolute velocities; (b) relative velocities.

and skirts around the base of the cloud; this would be expected since the entrained air is lifted as it is sucked in at the bottom. Still another feature is the gradient in color often seen in the cloud, which is usually whiter on top than around the base. As the circulation pattern suggests, the cloud material, which is a mixture

of orange smoke and cloud droplets, rises toward the top of the cloud, causing an increase in the density of the cloud droplets, and then pauses or even descends slightly at the sides as the cloud rushes on past. This slight descending motion causes the cloud fraction to dissipate partly, and therefore the orange smoke becomes more visible around the base.

There is general agreement concerning the upward motion in the stem. In all the Marshall Island tests swelling cumulus clouds were observed to form above the root cloud, and the dense appearance of the stem is certainly due to cloud droplets formed by the upward motion. In the case of George Shot this upward motion was strong enough to actually form its own cap or scarf cloud part way up the stem, which can only be formed when the air is forced upward rapidly.

An attempt was made to determine the values of some of these vertical motions in the stem and around the base of the mushroom, but it was abandoned because it was obvious that the clouds did not move with the air currents but were continually dissipating and re-forming. Clouds can be used to measure horizontal motions, but they are completely useless in measuring vertical motions because of their instability. Vertical motions can probably best be measured by aircraft actually flying through the various parts of the cloud, using the techniques developed by the National Advisory Committee for Aeronautics for the exploration of the vertical currents in thunderstorms.

REFERENCES

1. J. E. Mack, July 16th Nuclear Explosion: Space-Time Relationships, Report LA-531, April 1946.
2. Paul A. Humphrey, Classified Scientific Meteorological Information, Operation Sandstone, Annex 14, Sandstone SS-35, 1948.
3. "The Effects of Atomic Weapons," Chap. II, Government Printing Office, Washington, D. C., 1950.
4. R. A. Houghten, Technical Photography Measurements: Space-Time Relationships Measured from the Sandstone Photographs, Annex 7, Part II, Sandstone SS-28, September 1950.
5. P. G. Galentine, An Approximate Method for Computing Cloud Rise at Early Times, Report LA-1184, December 1950.

6. Lewis Fussell, Preliminary Measurement of Early Cloud Rise, EG&G Report 1062.
7. Lester Machta, Entrainment and the Maximum Height of an Atomic Cloud, Bull. Am. Meteorol. Soc., 31: 215-216 (1950).
8. "The Effects of Atomic Weapons," p. 32, Government Printing Office, Washington, D. C., 1950.
9. "The Effects of Atomic Weapons," p. 33, Government Printing Office, Washington, D. C., 1950.
10. Paul A. Humphrey, Classified Scientific Meteorological Information, Operation Sandstone, Annex 14, Sandstone SS-35, 1948, p. 30.
11. Paul A. Humphrey, Classified Scientific Meteorological Information, Operation Sandstone, Annex 14, Sandstone SS-35, 1948, p. 73.

Chapter 3

Dispersion of the Atomic Cloud

3.1 EFFECTS OF WIND, WIND SHEAR, AND DIFFUSION

It is useful to think of the atomic cloud, immediately after it has stabilized in height, as a nearly vertical trail of smoke. As has been mentioned in Chap. 2, it will have a slight slant due to the action of the winds during the 5 to 10 min of its rise, but this slant is obviously small relative to the horizontal displacements that occur during the next hours and days.

The factors that operate on the cloud are easily defined but difficult to isolate observationally. The most obvious factor is the wind. The small cloud particles will be carried along the trajectories of the atmospheric flow and, following these trajectories, will travel all the way around the world. The long-term travel of the cloud is reported elsewhere (Projects 4.5 and 4.6 and Program 7). The first hour or two after the shot, while the cloud was still visible, is of foremost concern here; during this period the wind primarily determined the shape of the cloud.

Figures 3.4, 3.9, 3.14, and 3.18 show plan views of the four Greenhouse clouds after one-half hour. The displacement at each level is just that due to the wind, the trajectories for such short displacements being assumed straight.

The second factor is the wind shear, which tends to distend the cloud at certain levels where there is a rapid change of wind with height. The wind shear seems to behave capriciously, and it causes the cloud to develop into shapes that cannot be explained in terms of the measured upper winds alone. Thus, in the Sandstone Zebra cloud, there was a curious plume that shot out of the top, and, in the case of the George cloud, the upper part spread out in a smooth fan shape, which appeared to cover

the whole eastern part of the atoll. Such large motions must be due to the action of the wind and the wind shear in both direction and speed, and an analysis of them is made doubly complicated by the inaccuracy of the wind observations, the variability of upper-level winds, and the difficulties in fixing the diffuse cloud in three dimensions.

One cloud was notable for the lack of shear in a part of it. On Dog Shot the observer at Japtan had a good view of the cloud, and the Eniwetok observers had intermittent views. All agreed that most of the cloud seemed to be concentrated in a thick brown mass that moved off to the northeast, and it was reported at first that this was where most of the radioactive cloud material must have been. A more detailed analysis later showed that the thick brown mass that persisted for so long was indeed a lower part of the mushroom at between 35,000 and 40,000 ft (the top was at between 50,000 and 55,000 ft when it stabilized), but the reason that it appeared to be so dense for so long was that it was in a region of almost no shear (as shown by the local Rawin observations). In other words, a part of the cloud with only a nominal amount of material persisted as a fairly dense mass for 2 or 3 hr simply because it was not torn apart by the wind shear as were the other parts of the cloud. On no other occasion did a part of a cloud persist so clearly.

The third factor, and the least susceptible to analysis, is eddy diffusion. The qualitative picture of eddy diffusion, as given by Sutton,¹ Kolmogoroff,² Batchelor,^{2,3} Weizsäcker,⁴ and others, portrays the general circulation of the atmosphere as a source of large-scale eddies, the cyclonic vortexes that are studied on weather maps, and these vortexes as the source of other smaller vortexes, and so on down to the rela-

tively small-scale turbulence that is felt as "bumps" by aircraft flying in the free air, and thence finally down to the smallest scale motion that is possible in the atmosphere, the motion of the molecules themselves. The mechanism is one whereby the energy of the atmospheric circulation is dissipated by turbulence and finally ends by warming the atmosphere, analogous to the action of friction on a moving object.

This picture of turbulence suggests that everywhere in the atmosphere there will be a certain amount of random eddy motion. Whatever the scale or the speed of this motion, it will act on a smoke cloud in such a way as to spread it out in all directions. The statistical laws of eddy diffusion are difficult to apply to smoke-cloud observations, and, even if it were possible to apply these laws theoretically, in practice it would be difficult because shear is also operative and it is hard to separate the effects of shear from those of eddy diffusion.

It was thought, at first, that it might be possible to get an idea of the magnitude of the eddy diffusion from the observations of the growth of the atomic cloud. To test this, careful measurements were made on the three-dimensional shape of the section of the Dog Shot cloud between 35,000 and 40,000 ft, where, as indicated above, there was a minimum of wind shear and diffusion might be considered the dominant factor in the growth. Figure 3.5 shows the successive stages in the growth of this section of the cloud and also shows the wind vectors in this altitude range. It will be seen that, although the wind is remarkably constant in this layer, it is not perfectly so, as shown by the Rawin observations. It will be seen also that the small observed variations of the wind are nearly enough to account for the observed increase in the size of the cloud. Thus any attempt to deduce the magnitude of the eddy diffusion from even this "ideal" case would lead to an inconclusive result.

One therefore gets the impression that the wind shear is the dominant factor in pulling the cloud apart and "diffusing" it throughout the atmosphere. However, this statement is misleading since it is actually impossible to distinguish here between observed wind shear and the variations in the wind produced by the eddies in the atmosphere. One is led to ask the questions: At what point do we draw the line between wind gradients in the world-wide wind pattern and local eddies? Is not the scale of our

pattern of winds really a function of the closeness of the observational network? The answer to the second question is certainly yes.

3.2 DOG SHOT

3.2.1 General

The first test of Operation Greenhouse took place at 0634M (local time) on 8 April 1951, which was half an hour before sunrise. The tower was located on the north end of Runit Island. At the time of the firing there was enough light to see the local clouds and the horizon, but there was not enough to permit photographs to be taken without long exposures.

The cloud was observed by the two observers on Eniwetok and the observer on Japtan, and all three camera sites were operated, but the automatic site on Rigili did not start operations until 4 min after shot time.

The yield of the weapon was reported as being between 83 and 90 kt, making it the second largest of the four tested at Greenhouse.

3.2.2 Meteorological Conditions

At the time of the firing there was between 0.3 and 0.5 strato-cumulus over the atoll, and there was apparently a deck of clouds with bases at about 2000 ft almost directly over Ground Zero when the shot occurred. Showers were reported in the area both before and after shot time.

The wind structure was fairly typical, as can be seen in Fig. 3.1, with east winds at low levels, up to about 20,000 ft, backing through north to west winds at between 30,000 and 45,000 ft, and then veering back to north winds at 50,000 ft and above. The temperature structure is given in Fig. 3.2, showing a typical lapse rate and moisture distribution and a tropopause at a little above 55,000 ft.

3.2.3 Rise and Development

The local strato-cumulus clouds that hung close to Ground Zero at shot time had bases at about 2000 ft, and so, by the time the shock-wave cloud lifted, the fireball had already disappeared into the overcast, as seen from the sites on Eniwetok and Japtan, and no measurements could be made on its early rise from Project 4.1B observations. The movie film does show the stem and root cloud, however, illuminated by the last glow of the fireball as it disappeared, and it is worth noting that the strong

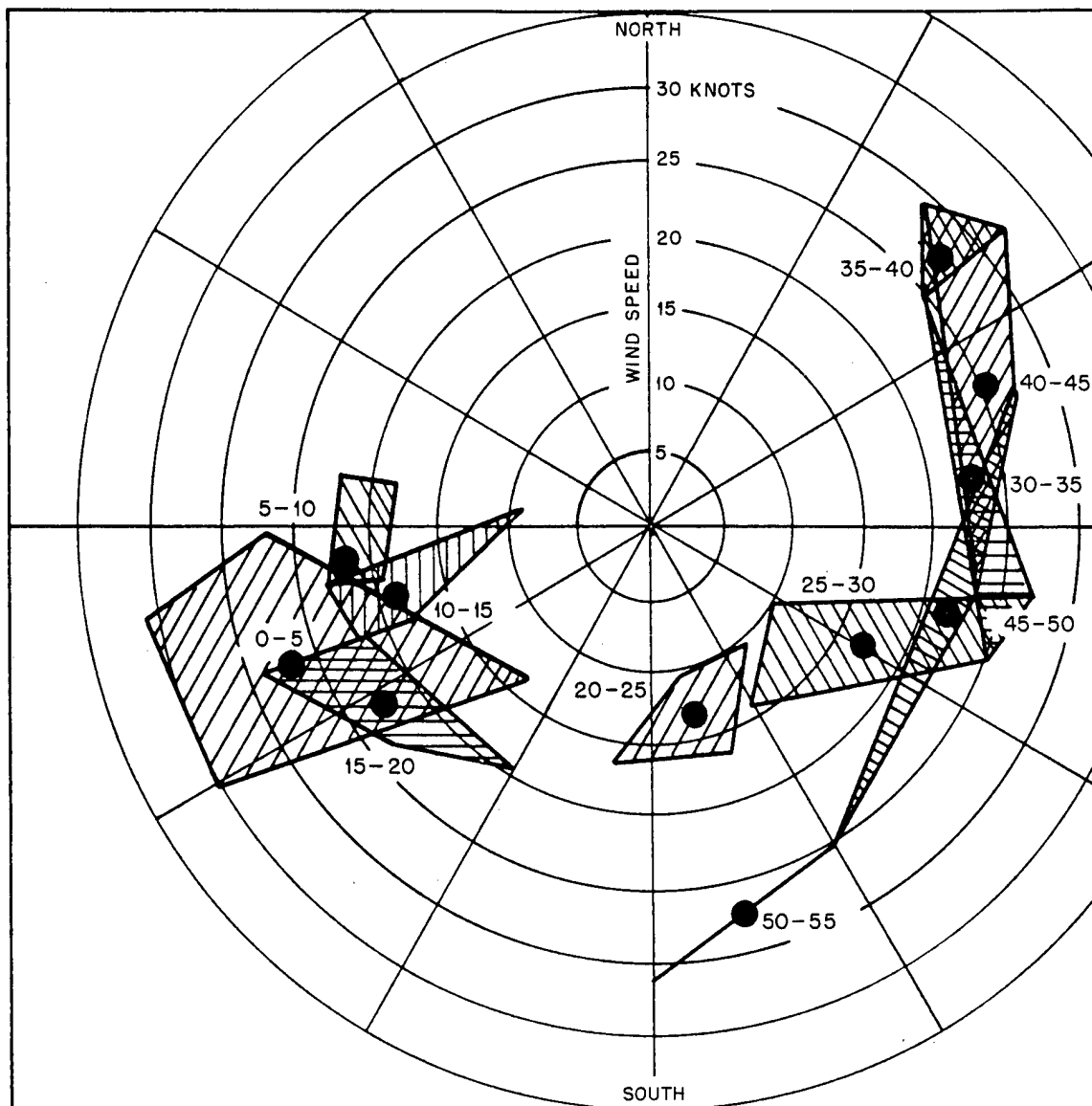


Fig. 3.1 Wind Diagram for Dog Shot (8 April 1951). The hatched areas include the ends of all the wind vectors for each 5000-ft interval.

convergence at the surface can be easily seen in the motion of the smoke and debris kicked up by the blast.

The sound of the explosion, as reported by all three observers, was very sharp, like the crack of a pistol. Note the sharp inversion in the temperature structure at 5500 ft.

After its disappearance into the overcast the atomic cloud was completely hidden from view from all the sites until 4 min 30 sec after the shot. At this point the Rigili camera site picked it up emerging above the local clouds, and at about the same time the observer on Japtan

caught a fairly complete view through a gap. From then on it was possible to keep track of it and follow its development.

A little information on the location of the top of the cloud during the first couple of minutes was obtained from pilot reports, but, as can be seen from Fig. 2.1, these do not appear at all consistent.

The inspection of the photographs from Rigili revealed an interesting feature which has apparently not been reported in other tests, i.e., the presence of a triple cap. Five minutes after the shot the top of the mushroom was covered

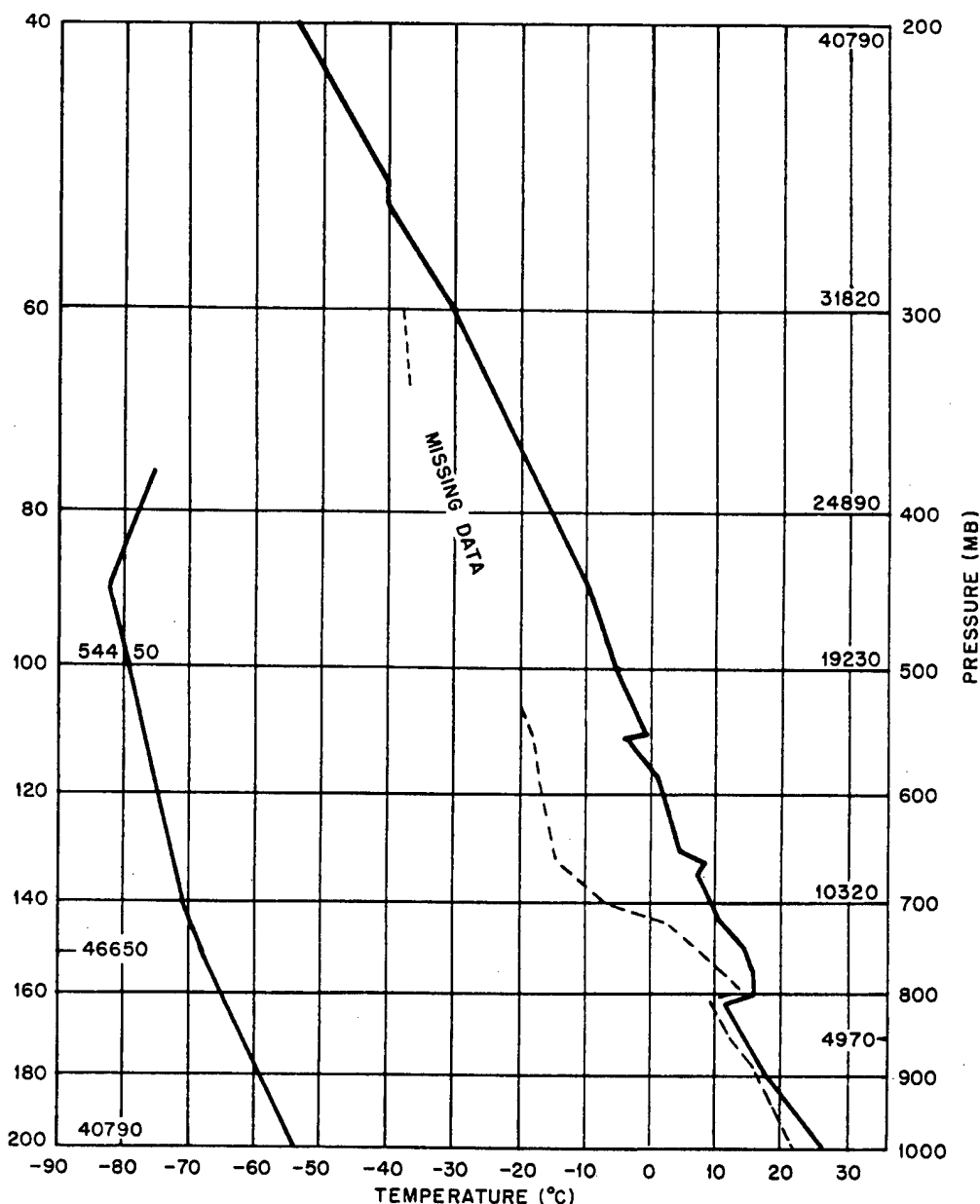


Fig. 3.2 Radiosonde for Dog Shot (8 April 1951, 0900M). Heights of standard pressure surfaces are given in feet. ----, dew-point curve.

by a smooth cap with a top at 43,000 ft, the next cap had a top 1000 ft higher, and the top cap was at 47,500 ft. Each cap was less extensive than the one below it, giving the top of the mushroom an appearance a little like a Chinese pagoda (see Fig. 3.3d). Thirty seconds later all the caps had become denser and had merged (or the top one had become so dense that the others could not be seen through it).

Little can be determined from the photographs after this time because local clouds

kept moving across the fields of all the cameras. However, a combination of the photographs and visual observations permits a fairly good reconstruction of what happened. The Japtan site, although it had no camera, had a better view than any of the other sites, and therefore much of the data came from the observer's records there.

It appears that Dog cloud continued rising for a longer time than the other clouds and did not reach its ceiling of 56,000 ft until about 8 min

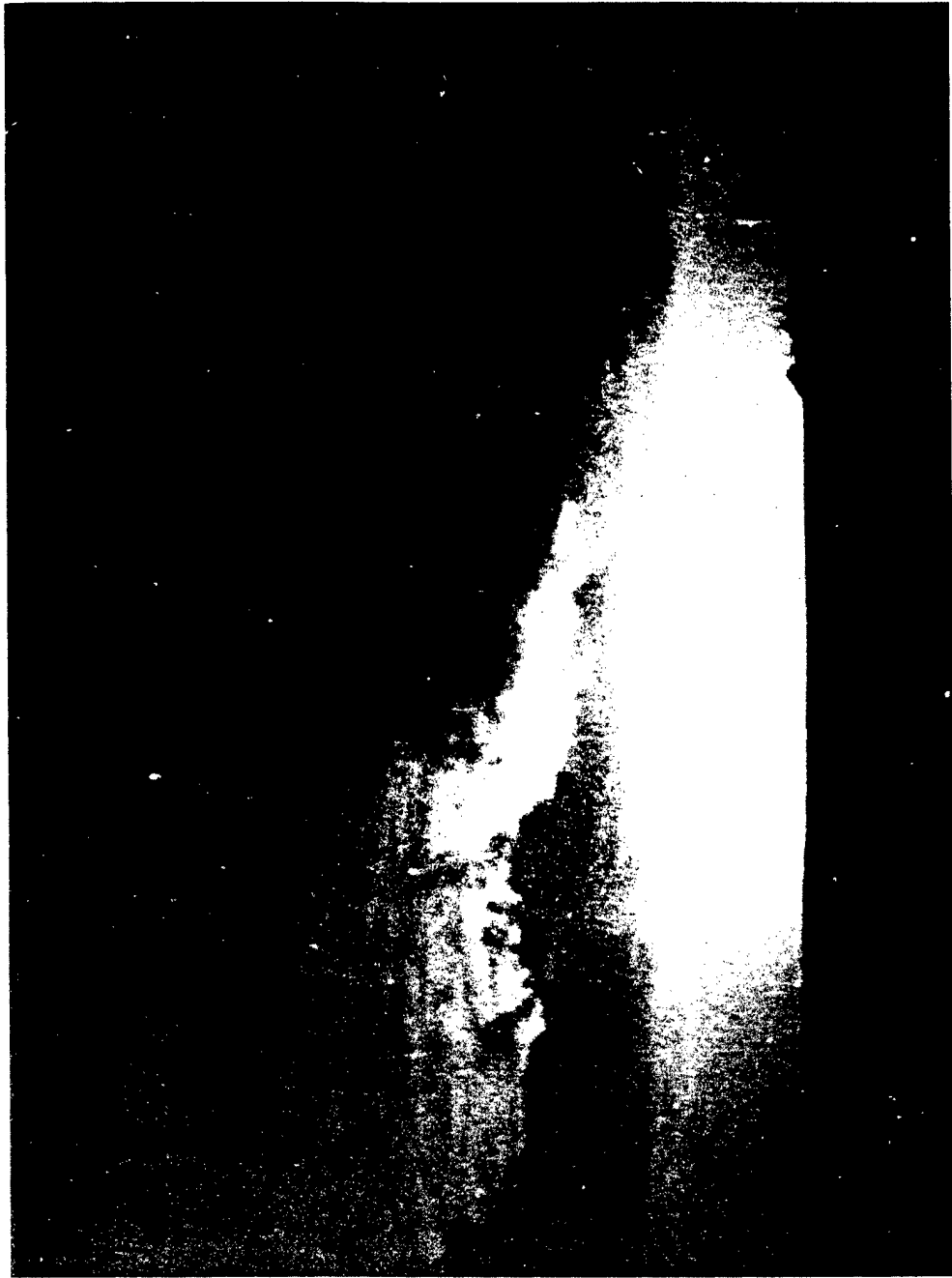


Fig. 3.3a Dog Cloud at 5 Sec from Station 190. The shock-wave cloud still hides the atomic cloud.

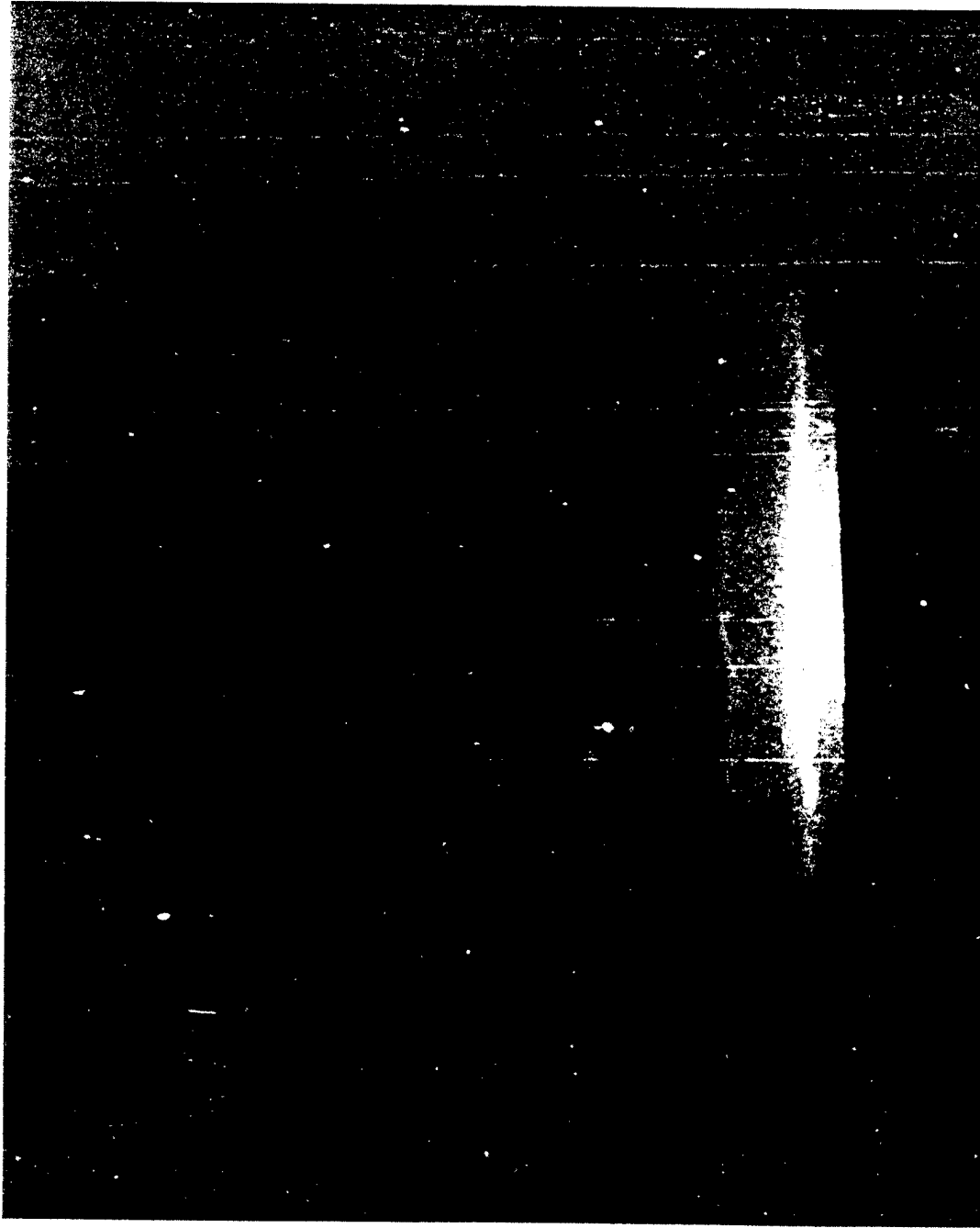


Fig. 3.3b Dog Cloud at 8 Sec from Station 190. The shock-wave cloud has just lifted, but the atomic cloud has already started to rise and is behind the cloud deck. The root and stem are clearly visible.

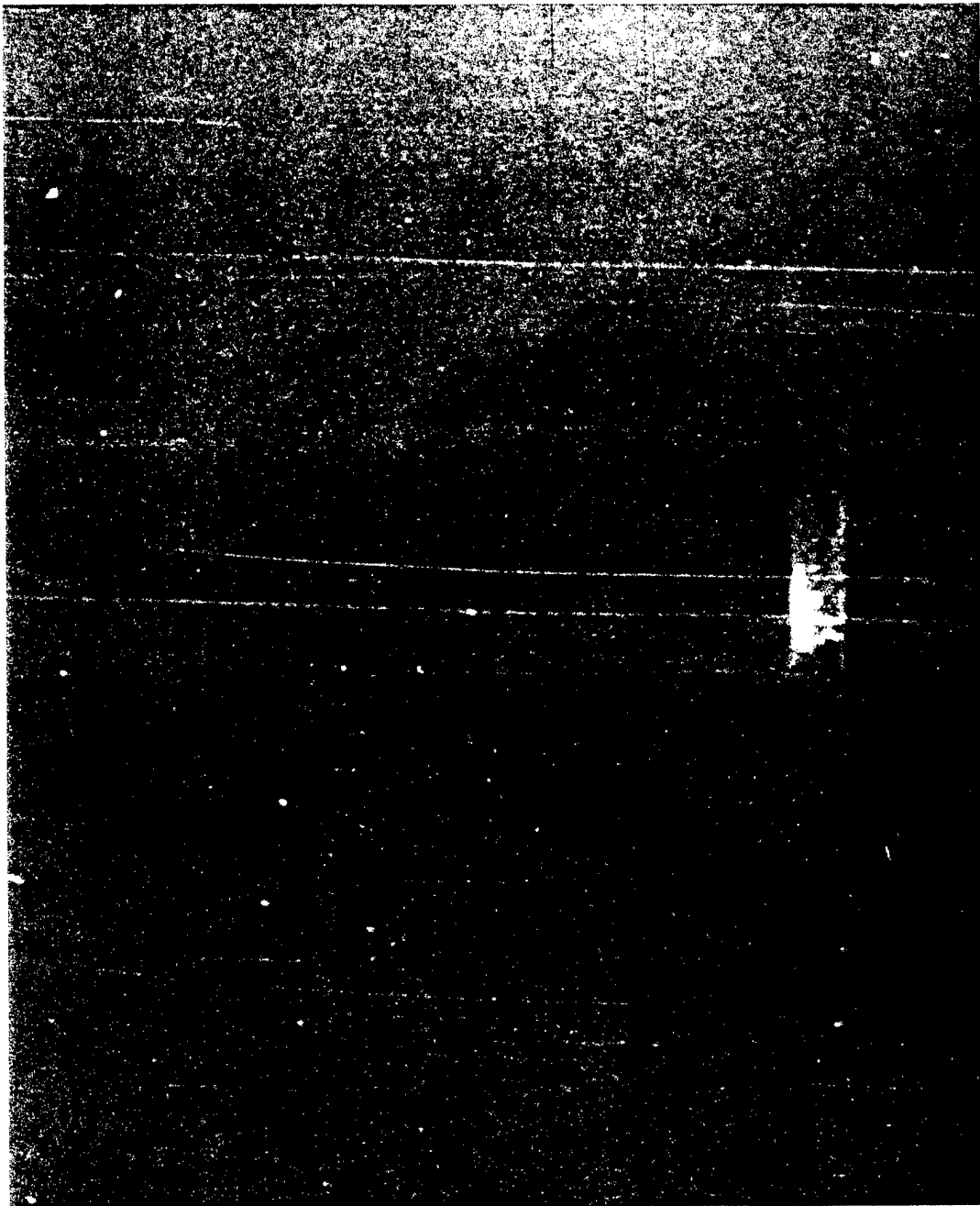


Fig. 3.3c Dog Cloud at 10 Sec from Station 190



Fig. 3.3d Dog Cloud at 5 Min from Station 192. Note the triple cloud cap.



Fig. 3.3e Dog Cloud at 10 Min from Station 192. Shortly after this, the atomic cloud was hidden by low clouds.

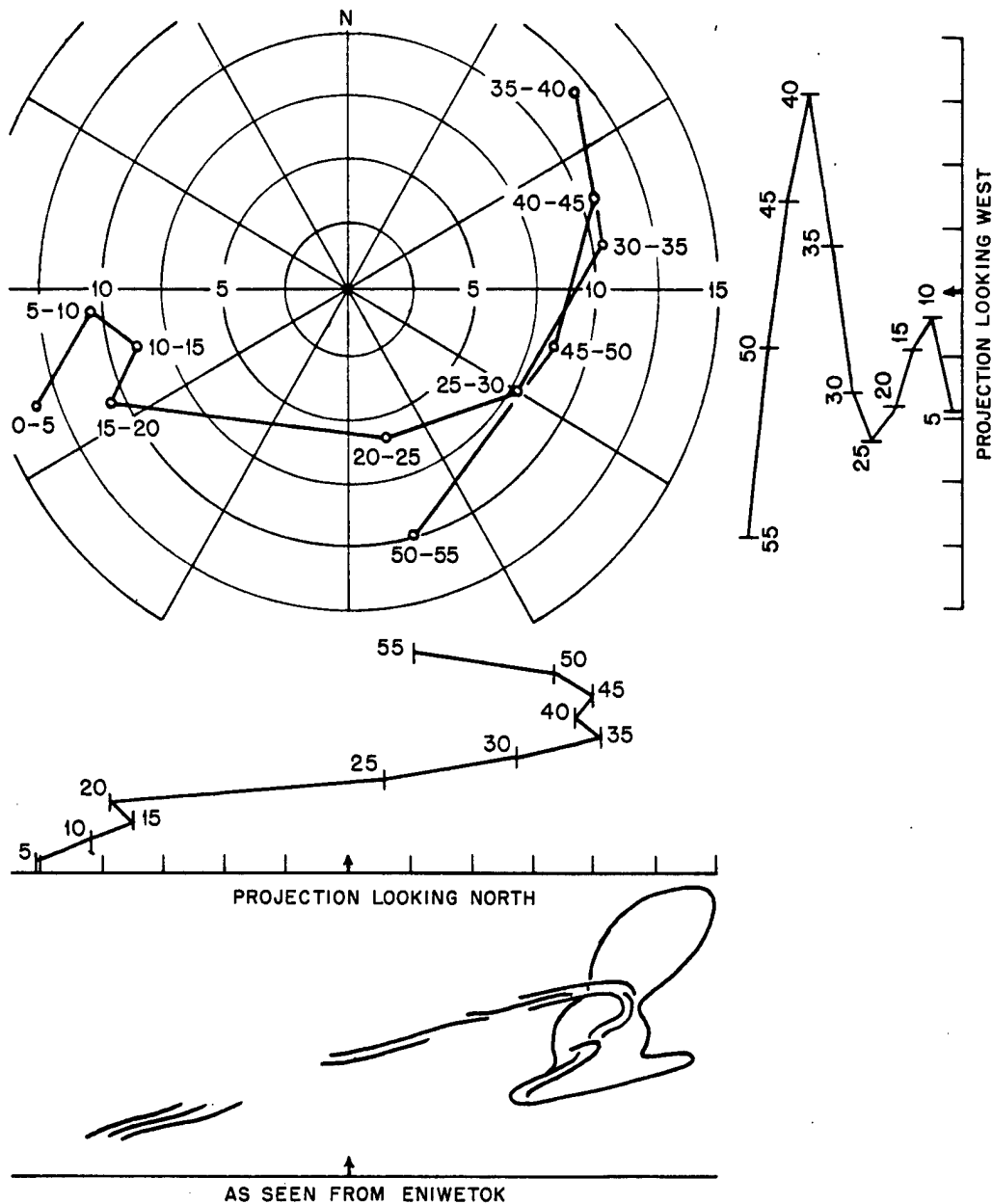


Fig. 3.4 Shape of Dog Cloud at One-half Hour. The construction is based on the winds aloft, and the sketch at the bottom of the figure is based on the observers' descriptions.

after shot time (see Fig. 2.1). At this time the bottom stopped rising, and the characteristic spreading of the width took place. The appearance of the cloud at this time was similar to George cloud, with a heavy stem, becoming narrower near the top, and a well-formed mushroom cloud.

After it stabilized, it moved with the winds at each level and was torn apart by 30 min, as

shown in Fig. 3.4. Its appearance as seen from all the manned sites was that of the letter "Z," with the most dense part at the lower left corner. It was not until the wind pattern was studied in detail that the observers realized that the upper left part of the Z was really the bottom part of the stem moving off to the west-southwest at an elevation of about 15,000 to 20,000 ft and appearing to merge continuously with the upper

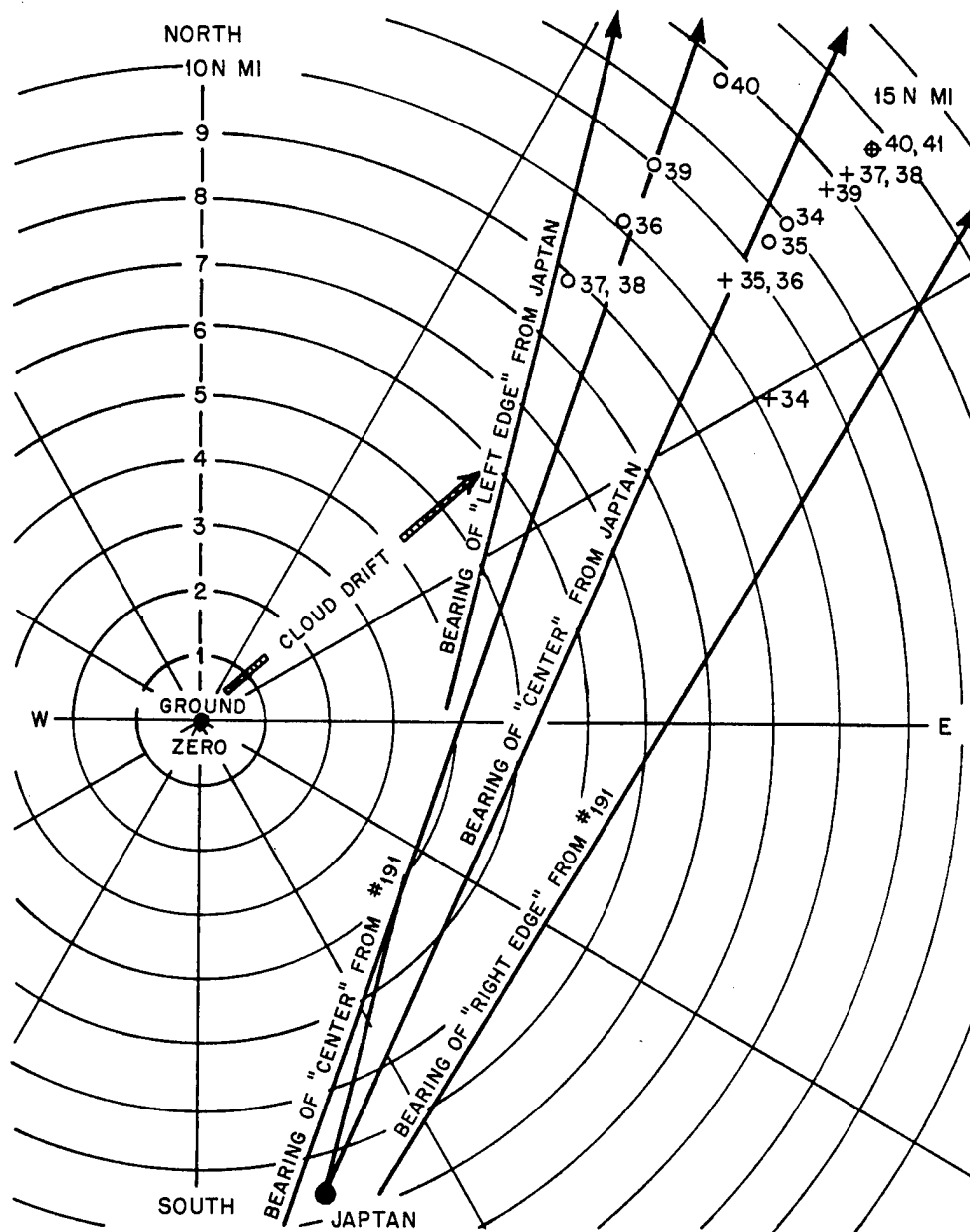


Fig. 3.5 Detail of the Development of Dog Cloud Between 35,000 and 40,000 Ft. The points show the computed half-hour positions of the cloud at each elevation (elevation given beside each point in thousands of feet), based on 0615M (+) and 0845M (O) upper winds. These are compared with the bearings of the edges and center of the cloud as seen from Japtan and Eniwetok after half an hour.

right part of the cloud, which was really the topmost extension, at an altitude of some 50,000 to 60,000 ft. This therefore represents a good example of the confusion that may arise from observing an atomic cloud from the ground.

By far the most persistent part of the cloud was the main mass located at the lower left part

of the Z, which could still be clearly seen 3 hr after shot time as an orange-colored cloud low in the northeast sky. This part was actually only the bottom portion of the mushroom since it appears to have been at an elevation of between 35,000 and 40,000 ft, and it persisted because it was in a region of very little shear. Figure 3.5

gives a detail of this part of the cloud and shows its growth in size as measured from the observers' records. It will be noted that the growth seems to agree quite well with the small spread in the wind values in this 5000-ft layer, a point that was stressed in Sec. 3.1.

An observation that was not anticipated was made by the observer at Japtan, who recorded the remarks of the people standing around him at 44 min after shot time to the effect that there was a very noticeable odor, similar to that of burnt gunpowder, in the air. The odor did not persist or was not noticed again after this time. The wind pattern was such as to make any horizontal advection of the stem cloud along the surface impossible from Runit to Japtan. However, there were clearly discernible showers to windward (northeast) of Japtan, and it is possible that some smoke was carried down by the showers from the material embedded in the antitrades.

The fall-out that occurred on the atoll following Dog Shot is discussed in other reports. However, it is worth mentioning here that the trajectory of a heavy particle falling from about 40,000 ft would be such as to cause it to land due south of Runit, in the direction of the inhabited islands. Moreover, it can be seen from Fig. 3.1 that the uninhabited island of Rigili was directly in line with the winds in the first few thousand feet. It is not surprising, then, that Rigili experienced a strong fall-out of radioactive material from the root and stem. This contamination was enough to partially fog all the films at the automatic site on Rigili, even though the cameras were in a shelter.

3.3 EASY SHOT

3.3.1 General

The second atomic test of Operation Greenhouse took place at 0627M (local time) on 21 April 1951, which was 31 min before sunrise.

The test site was a tower on the island of Engebi, the northernmost island in the Eniwetok Atoll. The yield of the weapon was 50 kt, approximately one-half that of Dog Shot.

All personnel connected with the cloud-physics project (discussed in Part I of this report) profited greatly from their experiences with the technical problems of Dog Shot, and this was reflected in the amount of data collected on the Easy cloud. The fixed cameras at each of the

three sites operated without incident and produced excellent photographic coverage of the atomic-cloud rise and development (see Table A.2).

3.3.2 Meteorological Conditions

Scattered low clouds with bases at 2000 ft and tops variable from 6500 to 8500 ft prevailed at shot time and during the period of consideration thereafter. These local cumulus clouds varied between 0.2 and 0.4 in sky coverage and were of sufficient amount to obscure the observers' vision during a portion of their recording time. Fortunately, with the unmanned camera racks at Station 192 on Rigili Island functioning properly, a continuous view of the cloud was afforded the analysts after 1 min.

Thin high clouds estimated at or above 30,000 ft persisted throughout the period. Varying between 0.7 and 1.0 sky coverage, this cirrostratus deck constituted the ceiling but was of little concern to the observers; later analyses of the films proved that these high clouds produced little or no obstruction to visibility.

There was no measurable precipitation during the period; scattered showers, however, were present. One of these showers passed over Station 191 at about 0700M; later, a 5-min shower was recorded at the Eniwetok Weather Central, producing a trace of precipitation at 0902M. Surface visibility was unrestricted at all times in spite of the widely scattered showers.

The trade-wind layer (moderately strong easterly winds) existed to approximately 5000 ft. The transition from the lower easterlies to the upper westerlies was very gradual, and light winds (average speed of 4 knots) prevailed from 5000 to 25,000 ft. Above 25,000 ft the wind was from a westerly direction at a speed of 20 to 30 knots, and this condition extended through the tropopause and into the stratosphere up to a known level of at least 75,000 ft. Figure 3.6 shows the vectorial wind diagram for Easy Shot. This vertical wind structure of strong shallow easterlies below strong upper westerlies with a deep (20,000-ft) transition layer was the atmospheric flow into which the Easy Shot cloud was to develop.

A temperature inversion existed at about 9000 ft, and above this level the moisture content of the atmosphere was negligible (see Fig. 3.7). The tropopause was at approximately 53,000 ft.

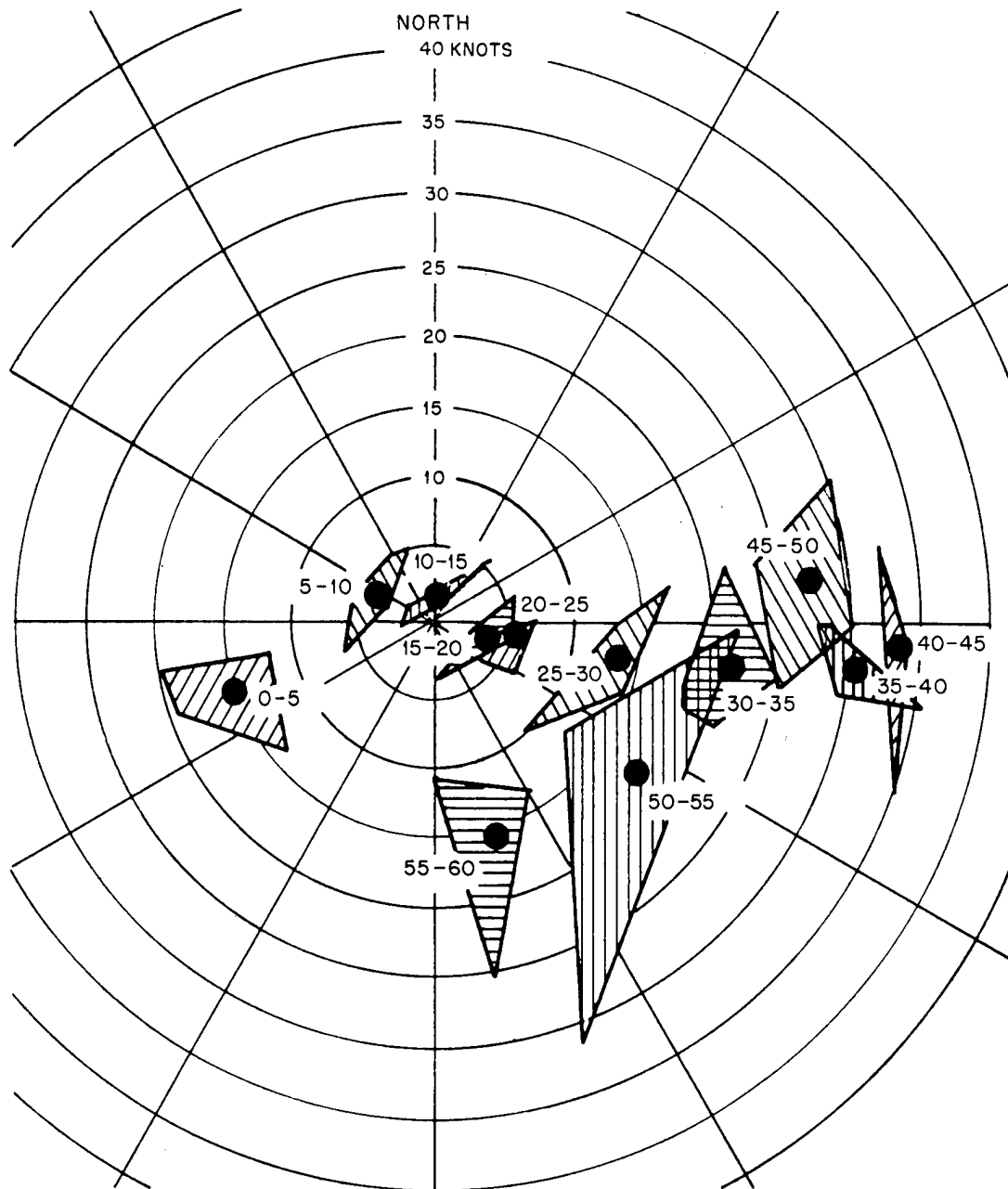


Fig. 3.6 Wind Diagram for Easy Shot (21 April 1951, 0600M and 0900M). The hatched areas include the ends of all the wind vectors for each 5000-ft interval.

3.3.3 Rise and Development

From the first minute after shot time until well over an hour later, a multitude of visual and photographic observations were made on the Easy Shot cloud. The total number of individual observations made on the rise of this cloud and

on the size and shape that it assumed is believed to be the maximum of all atomic tests. Furthermore, it is considered that, as a consequence of this dense coverage, the data presented concerning the Easy Shot cloud rise and development are the most accurate possible under the system employed.

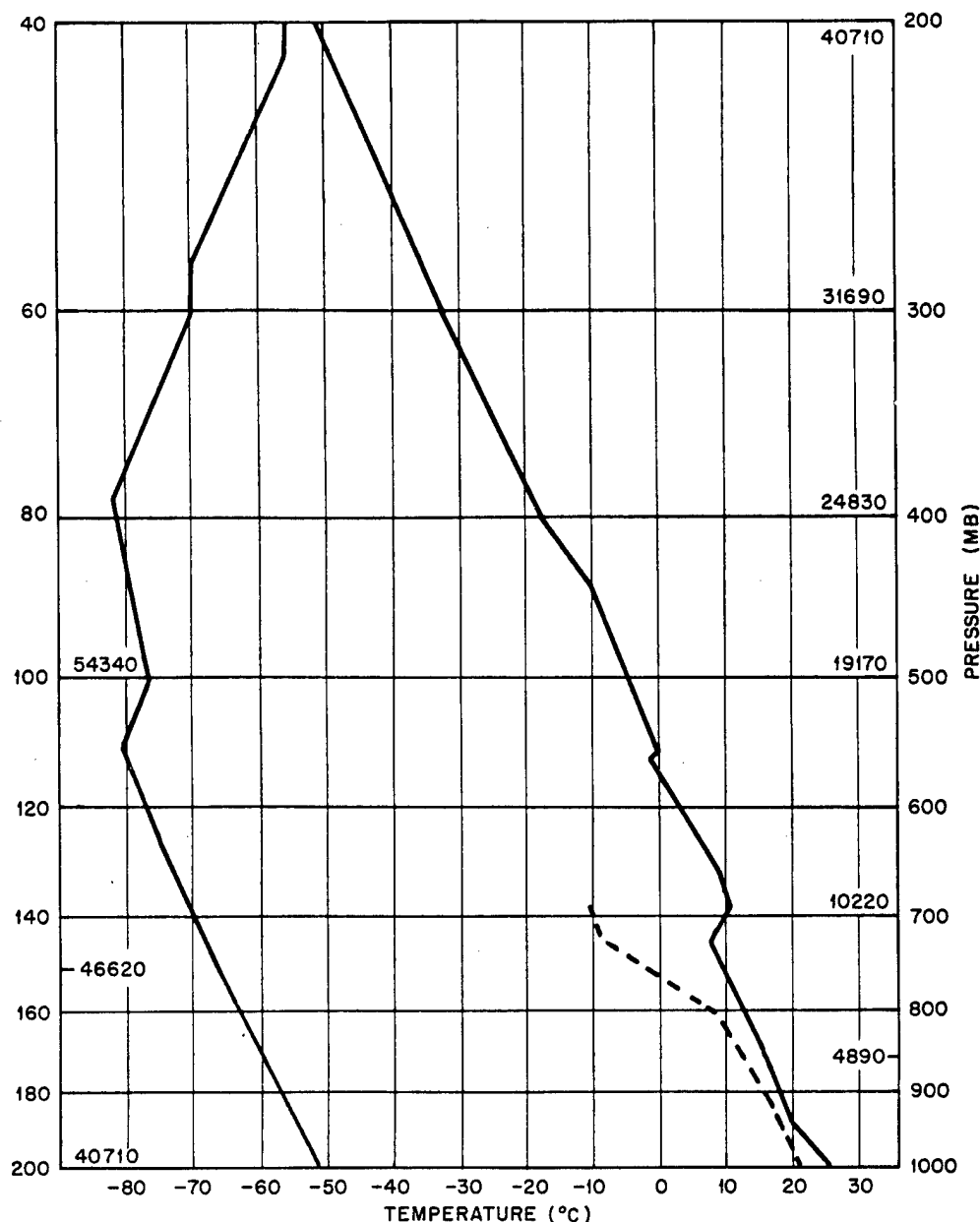


Fig. 3.7 Radiosonde for Easy Shot (21 April 1951, 0600M). Heights of standard pressure surfaces are given in feet. ----, dew-point curve.

The shock wave reached Eniwetok Island about 1 min 45 sec after the shot was fired. The pressure change was not noticeable to the observers, although a sharp 0.08-in. deflection was recorded in the Weather Central barograph trace. The sound accompanying the wave was soft and rumbling, instead of the sharp report of the Dog Shot blast.

The observations of the height of the top of the cloud as a function of time are plotted in

Fig. 2.1. Since there were many observations and the internal consistency of these observations was good (to a few hundred feet for the first 6 min), the curve is probably quite representative.

The visual observations of the top by the pilots of the B-17 aircraft agree, in general, with the surface observations, but it is obvious that there are serious inconsistencies between the various pilot reports. It was probably difficult for the

pilots to tell just when the top of the rapidly moving atomic clouds reached their level, especially when the aircraft were in every case several miles away from Ground Zero.

The Easy cloud probably reached its ceiling at about 6 min 30 sec, at which time its top was at about 41,000 ft. This was well below the tropopause, and it was perhaps for this reason that the flattening was not so pronounced here as for the clouds that did reach the tropopause, although Fig. 2.5 shows that some flattening did take place. Figure 2.6 shows how the bottom leveled off at this time.

As early as 2 min 30 sec after shot time, the main mass of the cloud began to be sheared away from the stem, and by 5 min it began to break into several main masses. As the mushroom ascended, it appeared as if two pistons were operating inside the upper main mass; that is to say, on a series of photographs two points on either side of Ground Zero appeared to be of nearly equal height on the top of the mushroom. On alternate photographs the right-hand bulb appeared to be the higher point, and on the intervening pictures the left-hand bulb appeared to be higher. This feature was more apparent from the Rigili site photographs and suggests that the highest point of the cloud was actually a ring around the top of the mushroom.

There was no cap cloud during the rise of the Easy cloud; this was probably because the air was quite dry above 5000 ft.

After 8 min the upper main mass was disintegrating and being swept into the strong westerly current aloft. This shearing off of the top resulted in the atomic cloud being distorted into rapidly changing shapes. After 11 min, looking north from Eniwetok, the appearance was described as "a seal's head facing eastward." The top of the seal's head was then the highest point of the cloud, and the nose constituted the leading edge of the diffusing upper main mass.

The top continued to be pulled farther to the east and the stem farther to the west, and the shape could best be described from all observing points as a laterally elongated reverse "Z." The lower horizontal elongation had many orange wisps, and the upper horizontal elongation developed a series of S-shaped waves ranging in color from yellow to purple. The vertical connection of the two elongated, stratiform developments remained a dark brownish color,

the left apex of the upper horizontal cloud being above the Ground Zero point.

After 1 hr 20 min, no main mass was discernible as such, and the upper portion of the atomic cloud spread across the sky from the tower area eastward in an indefinite cirro-stratus appearance. After 2 hr 30 sec the cloud was still faintly visible because of its orange tinge, but it was drawn out in a tangle of fine wisps of cirrus. No accurate measurements of the main mass of the cloud could be made after the first hour.

3.4 GEORGE SHOT

3.4.1 General

The most important test of Operation Greenhouse, from many viewpoints, was the third test, known as George Shot. This test took place at 0930M (local time) on 9 May 1951. This particular shot was the only one fired during daylight hours. Originally scheduled as a pre-dawn shot (about 31 min before sunrise), George Shot was delayed for approximately 3 hr owing to the probability of early-morning showers.

The test site was a 200-ft tower located on Eberiru Island, a small island about 16 nautical miles from the camera stations in the northeast sector of Eniwetok Atoll. The yield of the weapon was 225 to 350 kt, the largest of the Operation Greenhouse tests and presumably the largest ever fired up to that time.

Although the observers were well prepared for this test and had the advantage of daylight for taking more pictures, some of the equipment did not function properly, which resulted in less data than for Easy Shot. As explained in Appendix A, the light differential was probably not sufficient to actuate the Blue Box at the Rigili site, and the use of these cameras was lost. The loss of the Rigili site at this time was unfortunate since the normal lines of cumulus were fairly extensive. One such line lay between the Eniwetok sites and Japtan and continually obstructed the view from the former. From Japtan the view was splendid, but unfortunately this site was not equipped with specially aligned cameras; therefore no films were available for measurements. The observer, however, was equipped with a theodolite, wire recorder, and sketch pad and was able to collect enough data to augment and fill in the void spots from other sources.

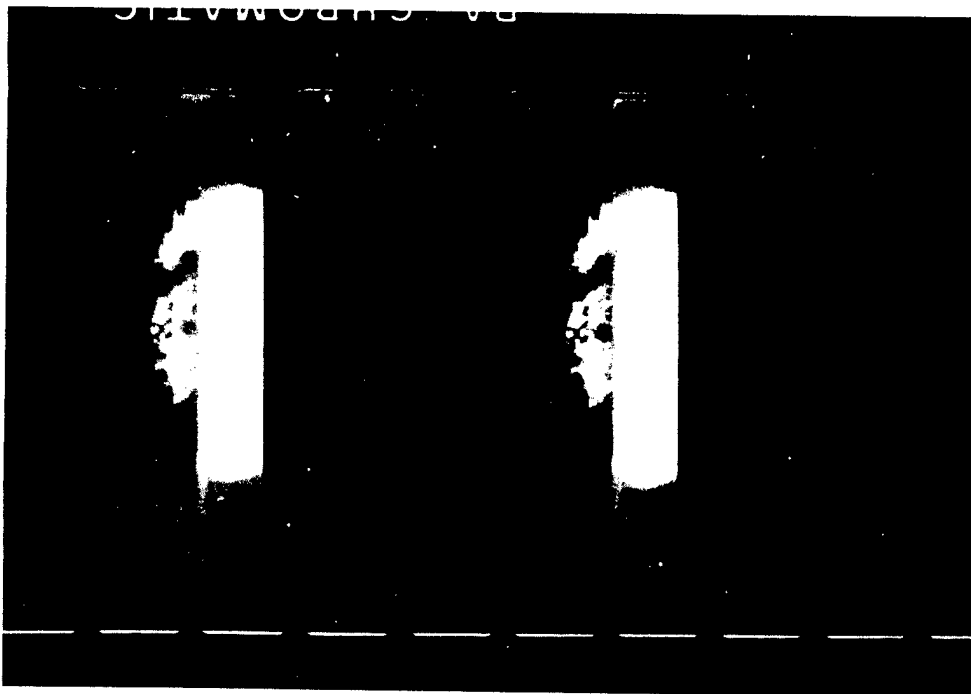


Fig. 3.8a Easy Cloud at 5 Sec from Station 191. The shock-wave cloud still hides the atomic cloud.

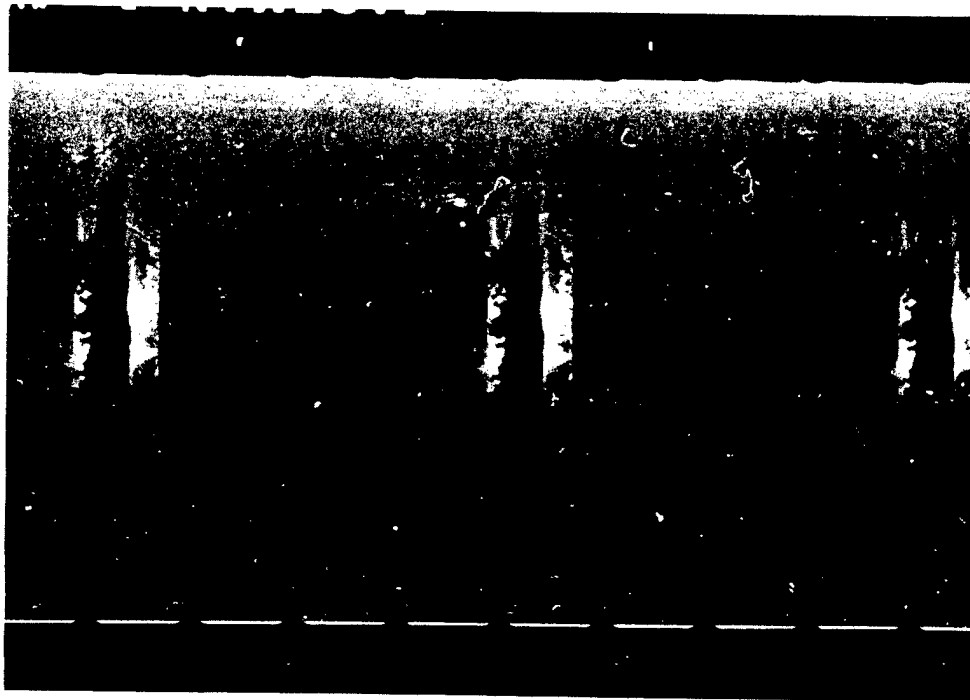


Fig. 3.8b Easy Cloud at 10 Sec from Station 191. The shock-wave cloud has just lifted, and the ball of fire can be seen just starting to rise.

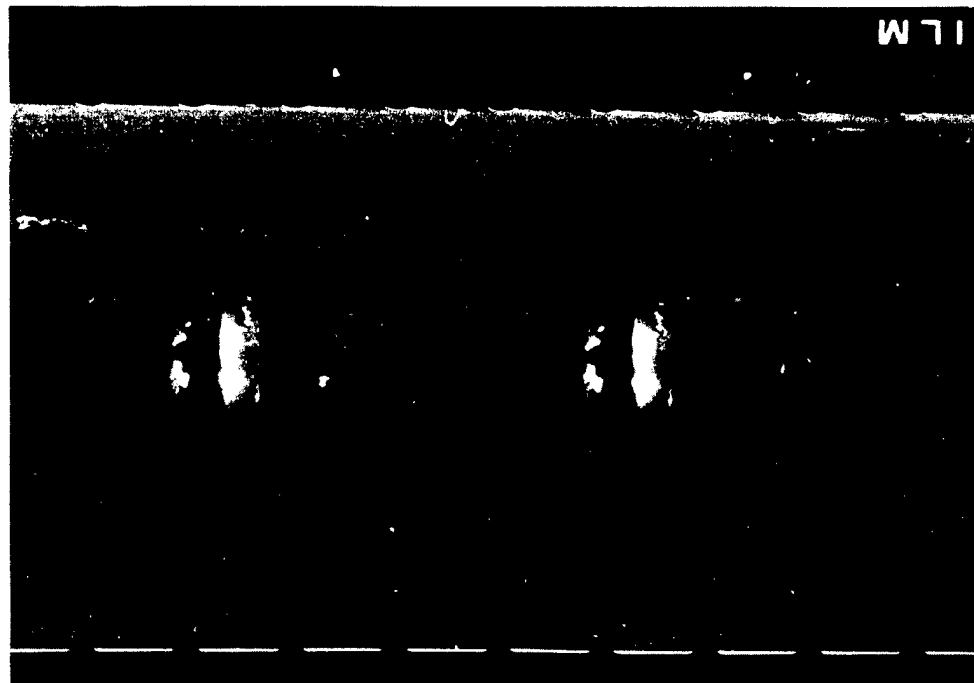


Fig. 3.8c Easy Cloud at 12.5 Sec from Station 191.
The ball of fire can be seen rising above the first low
deck of clouds, which is partly the remains of the
shock-wave cloud.

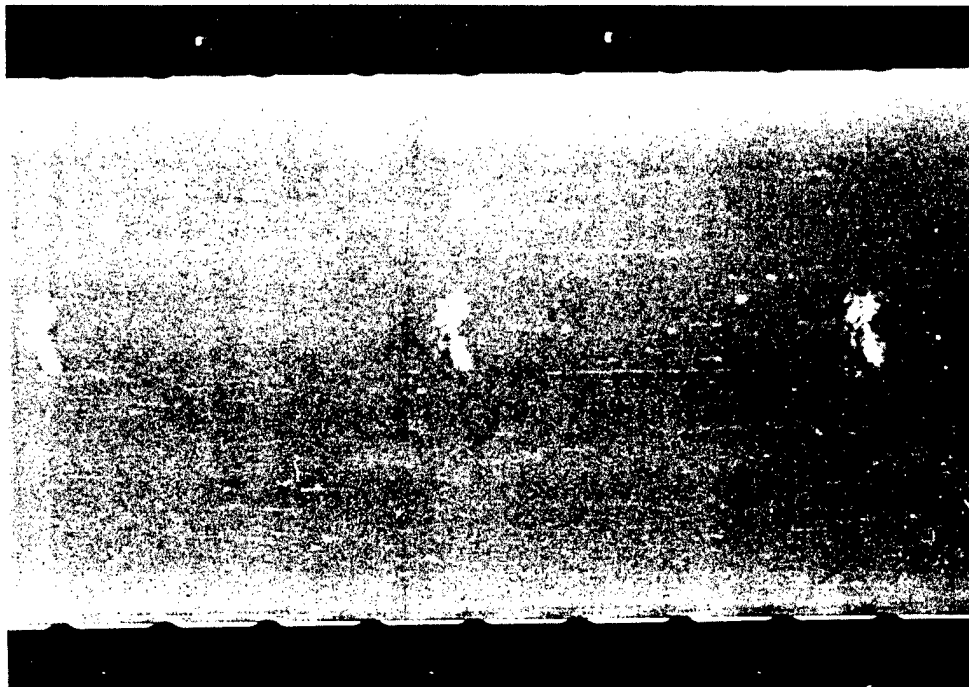


Fig. 3.8d Easy Cloud at 15 Sec from Station 191. A
last glimpse of the atomic cloud before it disappeared
behind the strato-cumulus.



Fig. 3.8e Easy Cloud at 1 Min from Station 191. The atomic cloud is just appearing above the strato-cumulus deck.

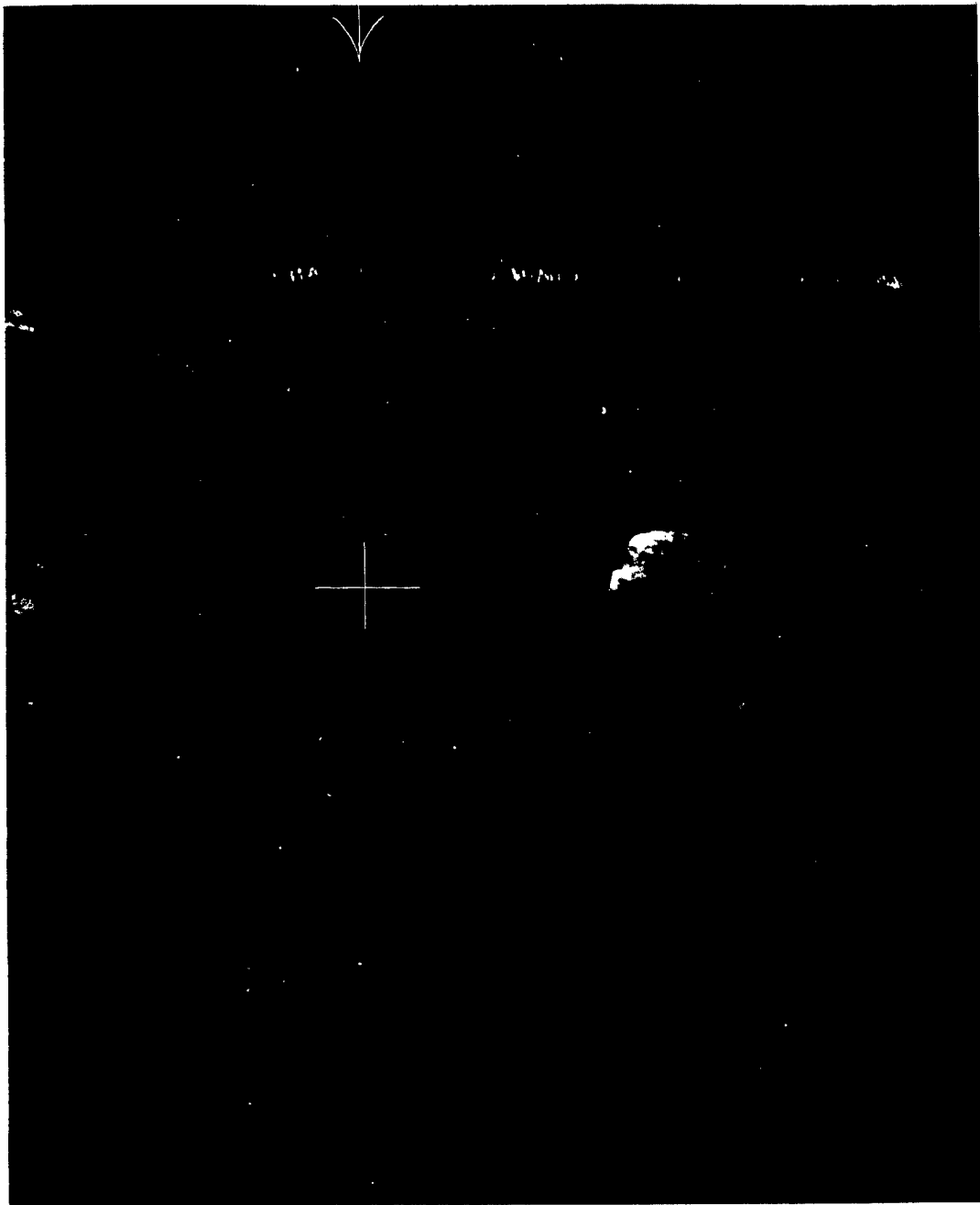


Fig. 3.8f Easy Cloud at 2 Min from Station 191. The internal circulation of the cloud is very rapid.



Fig. 3.8g Easy Cloud at 3 Min from Station 191

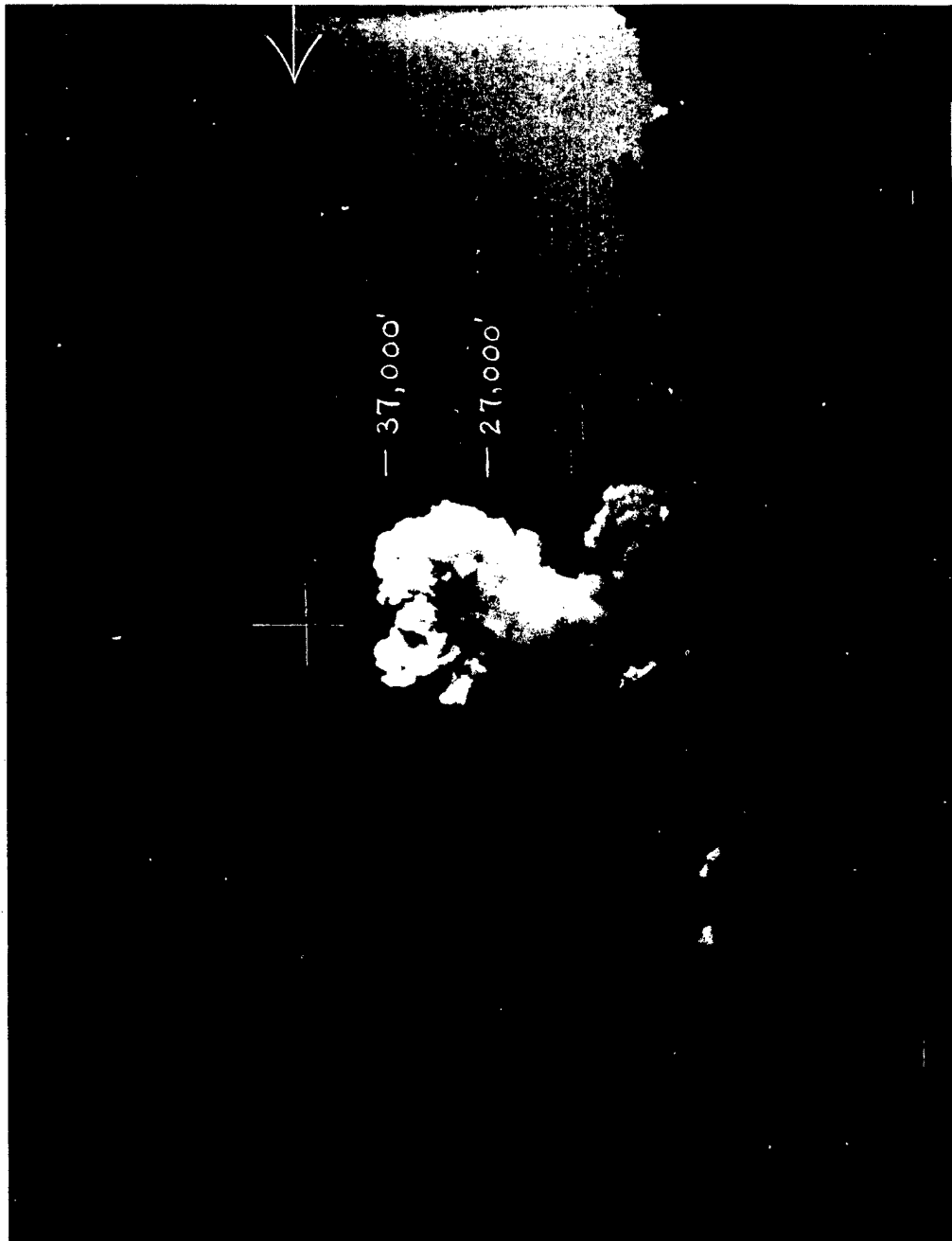


Fig. 3.8h Easy Cloud at 5 Min from Station 191. Cloud is slowing down and will reach its ceiling in about 1 min more.
The circulation is still visible.



Fig. 3.81 Easy Cloud at 10 Min from Station 191. The cloud has stabilized, the internal circulation has practically died out, and the stem is being bent to the east by the wind shear.



Fig. 3.8j Easy Cloud at 15 Min from Station 191. The cloud is drifting with the winds at each level and is becoming thinner and more wispy at the edges. The top part is being carried eastward, and the bottom part of the stem is nearly stationary.



Fig. 3.8k Easy Cloud at 20 Min from Station 191. The thinning of the cloud continues, but it still has the characteristic reddish color of an atomic cloud. The sun is now shining directly on the top part.

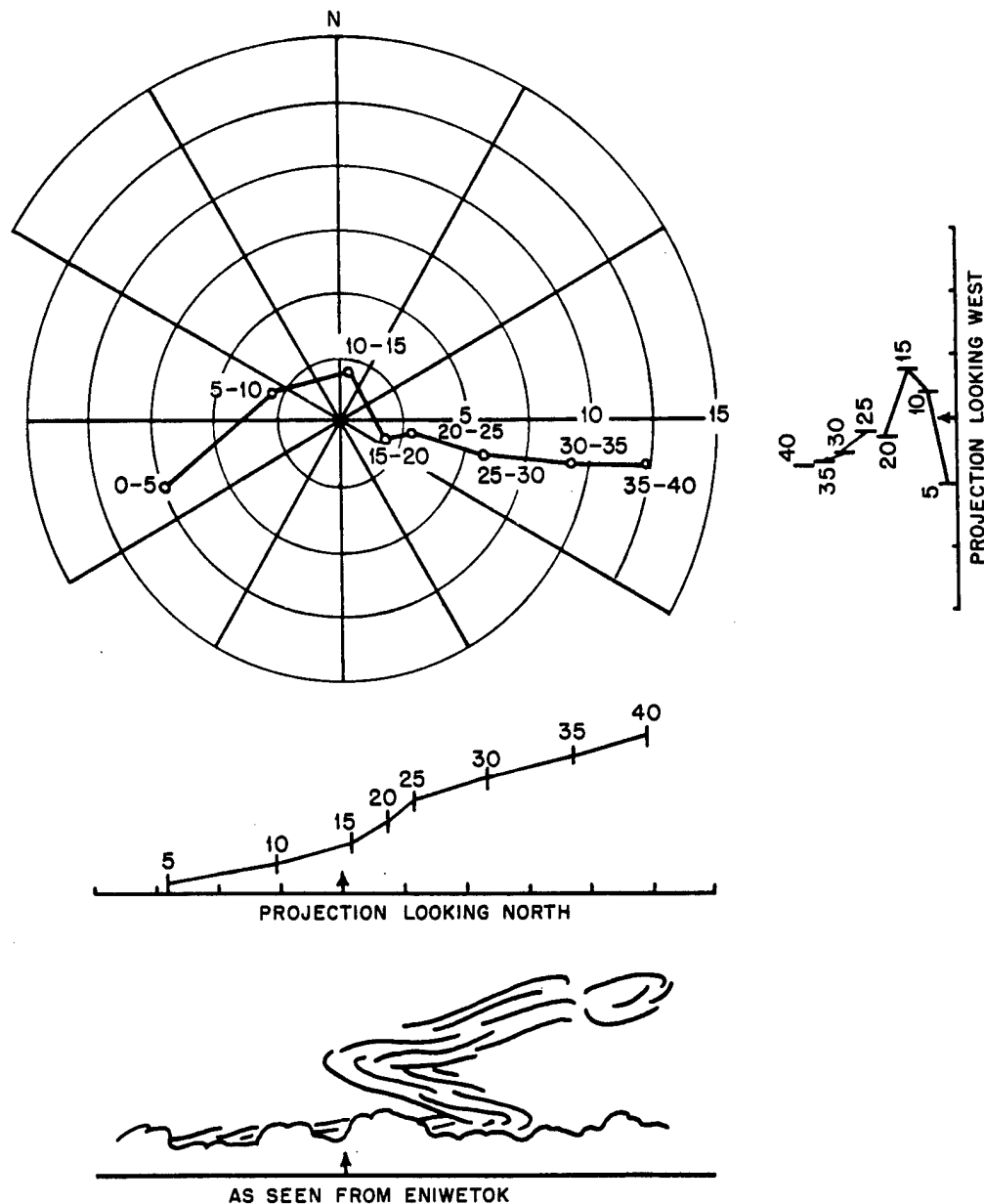


Fig. 3.9 Shape of Easy Cloud at One-half Hour. The construction is based on the winds aloft, and the sketch at the bottom of the figure is based on the observers' descriptions.

3.4.2 Meteorological Conditions

At the time of George Shot the Eniwetok area was under the influence of the late stages of a tropical storm (Joan) of typhoon intensity. From 8 May to 10 May the path of this storm was concentrated in an area about 200 miles northwest of Eniwetok. The storm had passed about 4 deg to the west of Eniwetok 36 hr before shot time, and at H-hour the center was located

about 250 miles north-northwest (340 deg) of the atoll.

The excessive rainfall and greater amount of cloud coverage preceding H-hour were due to the passage of the typhoon. At the time of firing the local cumulus clouds lay in widely scattered lines moving toward the east and amounted to 0.3 to 0.5 coverage. The middle clouds, alto-cumulus at 14,000 ft, were less than 0.3 and did not obstruct the initial view. The cirrus

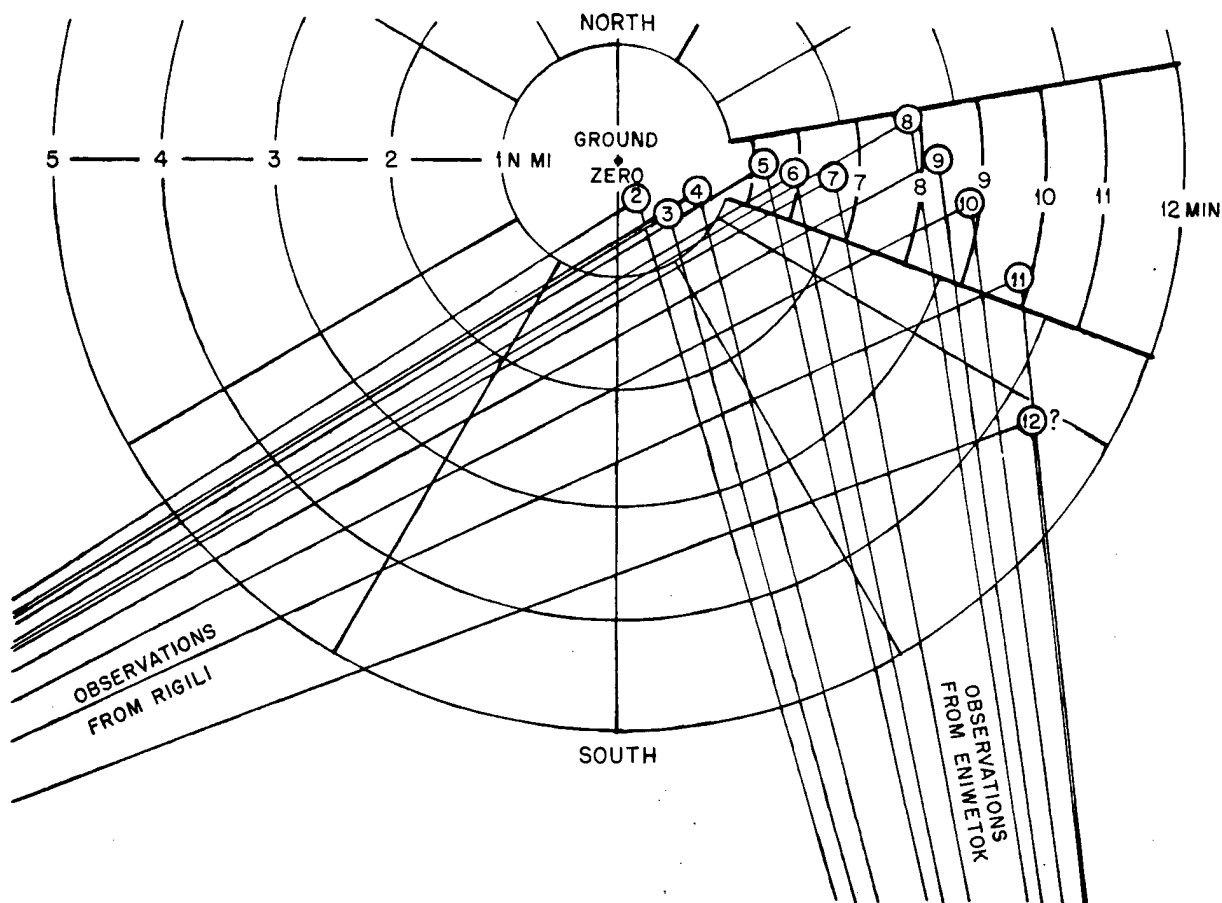


Fig. 3.10 Comparison Between the Actual Movement of the Top of Easy Cloud and the Movement Predicted on the Basis of the Upper-wind Observations. The numbers in circles are the times of the triangulations on the top of the cloud. The numbers set into the arcs are the times of the computed positions, using the range of winds between 41,000 and 45,000 ft.

cloud was quite extensive, covering the entire sky at a height exceeding 40,000 ft.

Although there had been heavy rain and rain showers in the early morning, there were no showers in the immediate area at H-hour. The other weather data seemed quite normal: temperature, 81°F; dew point, 77°F; relative humidity, 88 per cent; and visibility, 8 miles.

The cyclonic circulation of the typhoon dominated the entire area, replacing the normal low-level easterly flow with southwest winds at all levels up to 40,000 ft. The surface wind was west-southwest at 16 knots, and the average upper winds were from the southwest at 30 knots at 5000 ft, decreasing to less than 5 knots at 40,000 ft. Above 40,000 ft the winds were northerly at about 10 knots.

The radiosonde taken at 0900M indicated a steady decrease of temperature up to a height of 50,000 ft, which was the end of the run. (The extension of the run above 50,000 ft in Fig. 3.12 is from the sounding 12 hr later.) The temperature at 114 mb was -78°C, and the tropopause was estimated to be at 54,000 to 55,000 ft.

The weather conditions during George Shot were for most purposes excellent for an atomic test in this locality.

3.4.3 Rise and Development

Except for the curtaining effect of the shock wave, the fireball and formation of the mushroom were well documented during the first minute (0 to 32 sec at Station 190 and 0 to 1

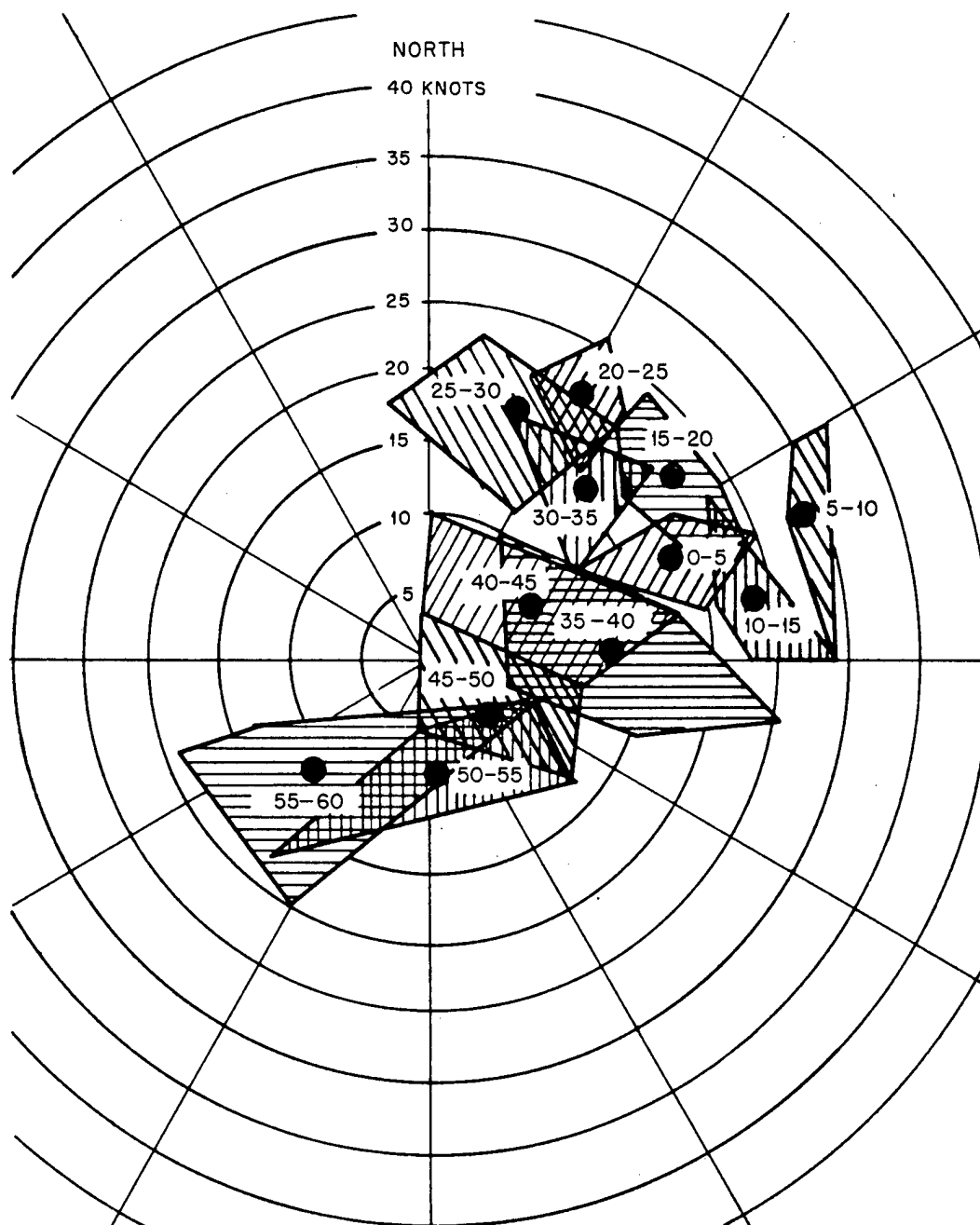


Fig. 3.11 Wind Diagram for George Shot (9 May 1951, 0900M and 1000M). The hatched areas include the ends of all the wind vectors for each 5000-ft interval.

min 18 sec at Station 191). For this initial period the maximum amount of data was obtained, including clear pictures of the top and shape of the atomic cloud.

The shock wave passed Japtan at 1 min 10 sec and Eniwetok at 1 min 28 sec. There was a

large depression on the barograph trace of 0.24 in. The sound as heard on Japtan was a loud report similar to Dog Shot, but on Eniwetok it had become less sharp, rather a loud rumble.

The second period, covering the time interval from 1 min 21 sec to 1 min 41 sec, contains few

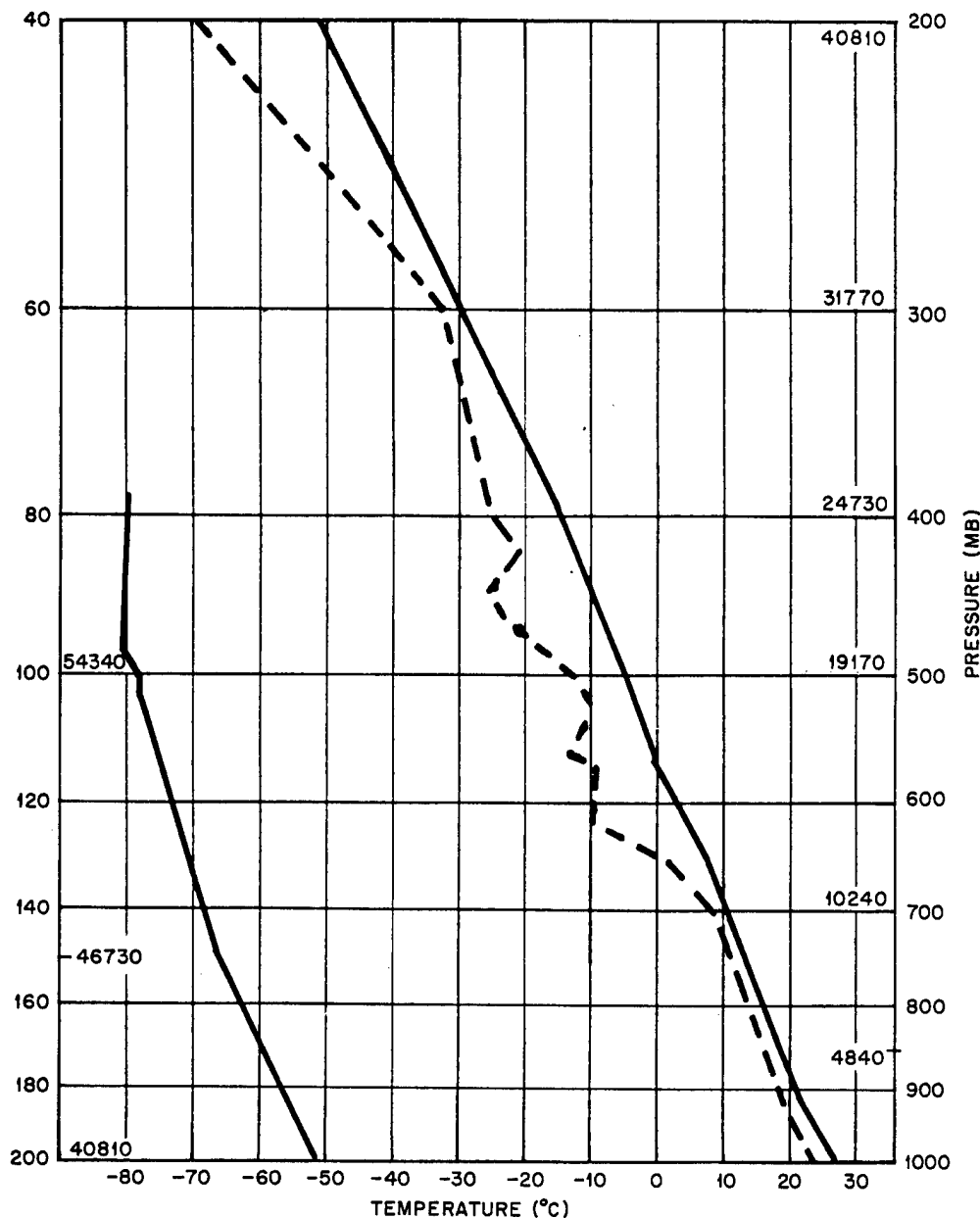


Fig. 3.12 Radiosonde for George Shot (9 May 1951, 0900M). Heights of standard pressure surfaces are given in feet. ----, dew-point curve.

readings of the cloud top but rather good measurements of the diameter and bottom of the cloud.

Between 1 min 41 sec and 4 min, the main mass was not discernible in the photographs, but the observers were able to make some observations that give reasonable results when compared to the graph (Fig. 2.1) of the top of the cloud.

After 4 min the cloud became more discernible on the films, and enough points were

calculated to complete the diagrams. After the cloud stabilized, the corrections applied to the height of the top seemed inadequate since they are difficult to determine owing to the large diameter of the cloud and the inaccuracy or lack of wind data. In the late stages (after about 10 min), the cloud top was dissipating and spreading out into a fan shape. This spreading was toward the south (which corresponds with the winds above 40,000 ft), and, as the cloud moved overhead, the observers' view of the actual top

was obscured. It might be possible to determine the real top from photographs taken from aircraft that were flying at 30,000 ft and 20 miles or more from Ground Zero. Owing to the yield of George Shot, it is conceivable that the circulation was strong enough to place the actual top above the estimates here, but it is likely that the top went no higher than Fig. 2.1 indicates. By studying the graphs of several tests, it is seen that a stabilization generally occurs between 6 and 8 min. This stabilization took place at 6 min and was marked by the leveling off of the bottom of the George cloud (see Fig. 2.6) and a sudden spreading of the top (see Fig. 2.4). This spreading was much more rapid than that in any of the other Greenhouse clouds, and so the George cloud probably stopped abruptly within a thousand feet or so of the tropopause.

The pilot reports of the top of the atomic cloud during the first few minutes show good agreement with the readings obtained from the ground observations.

Although George cloud had the same general appearance as the other clouds in Operation Greenhouse, it had certain characteristics worth mentioning. Because of the rather uniform structure of the wind field, there were no large-scale shear effects until the cloud rose above 40,000 ft. The shear resulting from the gradients in the wind-speed field was gradual, giving the stem a continuous bending shape rather than splitting or tearing it into sections, as in the case of Dog and Easy Shots.

The radiosonde showed that the moist level of the lower atmosphere extended above 12,000 ft. As the air was raised through this level, a skirt cloud began forming at about 14,000 ft (between 49 and 57 sec) and gradually built downward to join the rising root cloud. The cap cloud that formed above 30,000 ft was seen by the observer at Japtan. This height corresponds to a second moist level near the 300-mb surface (see Fig. 3.15).

There was a noticeably high concentration of colored smoke in the mushroom cloud as it rose, and this concentration was evident even after the cloud reached its maximum height, as indicated by a dark purplish color in the center of the cloud top, which appeared to be located over Ground Zero.

The stem was well defined throughout the time of observation. After about 1 min there was a thickening of the stem as the root cloud built up to join the lower skirt. About this same

time there was an apparent anticyclonic twist or spiral in the circulation of the stem. At 7 min the stem was quite massive and had a light brownish tinge where the sun struck it. Also, a scarf cloud appeared which was associated with the top of the stem. Although the lower stem cloud moved to the east of Ground Zero, it remained intact, and the strong circulation in it could still be seen after 21 min. As it tilted, owing to the action of the shear, small swelling cumulus clouds could be seen emerging from the top of the stem, and even 2 hr after shot time the remains of the root cloud and lower stem were marked by a mass of cumulus congestus far to the northeast.

The atomic cloud continued to hold the same general formation after 1 hr. This pattern was the fan-shaped cloud, which was thin and white with quite diffuse edges, stretching out from the center dark mass of grayish purple. The upper stem now lay in a diffuse pattern of thin wisps of light brownish cloud extending for about 30 deg across the sky to the north and northeast.

3.5 ITEM SHOT

3.5.1 General

Item Shot, the fourth and last test of Operation Greenhouse, took place at 0617M (local time) on 25 May 1951. Item Shot was originally scheduled to be a daylight test, following the experience of George; however, on 23 May 1951 final decision was made in favor of a predawn test, as had been the custom previous to George Shot. The time of firing was synchronized to be approximately 31 min before the time of actual sunrise, the same time interval employed on Dog and Easy Shots.

The site chosen for the Item test was the same as that for Easy Shot, i.e., a tower located on the island of Engebi, the principal northern island in the Eniwetok Atoll. The yield of the weapon compared closely with Easy Shot also, being 45 kt.

Although no specific requirements, per se, were established by Project 4.1B for photographic coverage of Item Shot, two observers nevertheless availed themselves of the opportunity to gather these additional data. The two men manned Station 190 (see Fig. 1.1) and were equipped with a mounted nephoclinometer, such as was used for visual observations on the previous three Greenhouse tests. No pictures were taken of the Item cloud for Project 4.1B; neither

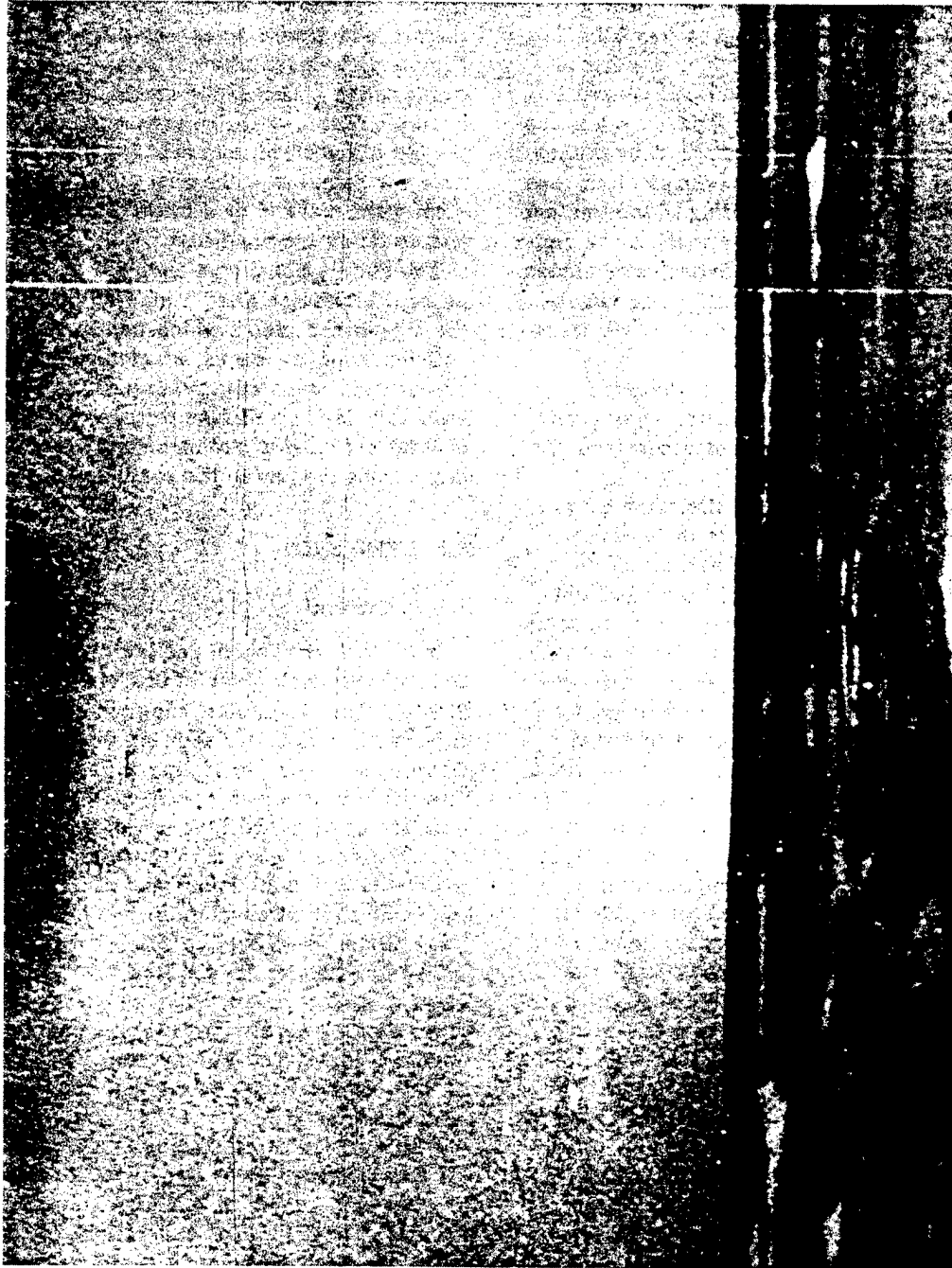


Fig. 3.13a. George Cloud at 5 Sec from Station 191. The shock-wave cloud hides everything.



Fig. 3.13b George Cloud at 10 Sec from Station 191. The shock-wave cloud is beginning to thin out in places.

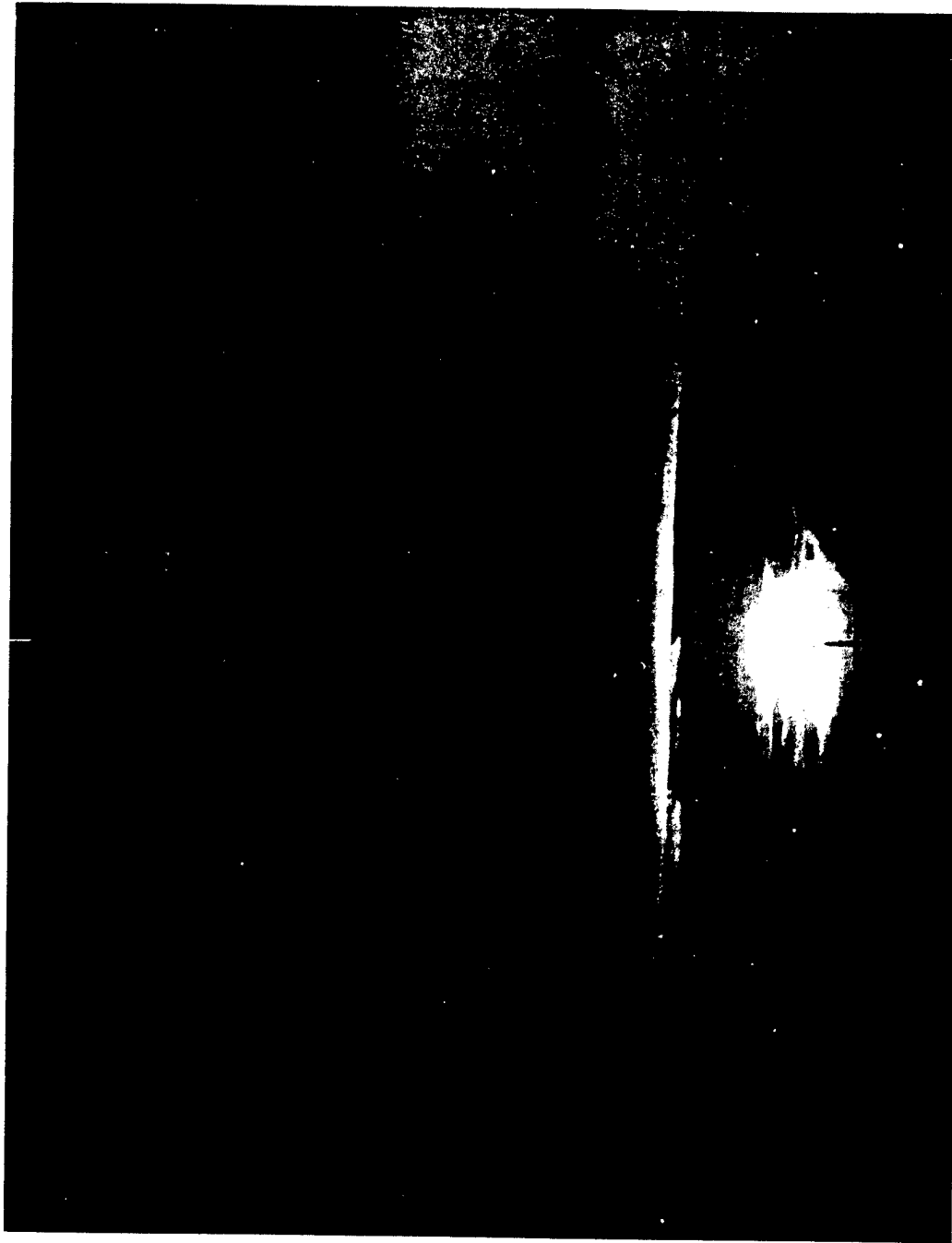


Fig. 3.13c George Cloud at 16 Sec from Station 191. The atomic cloud rises above the lower clouds.

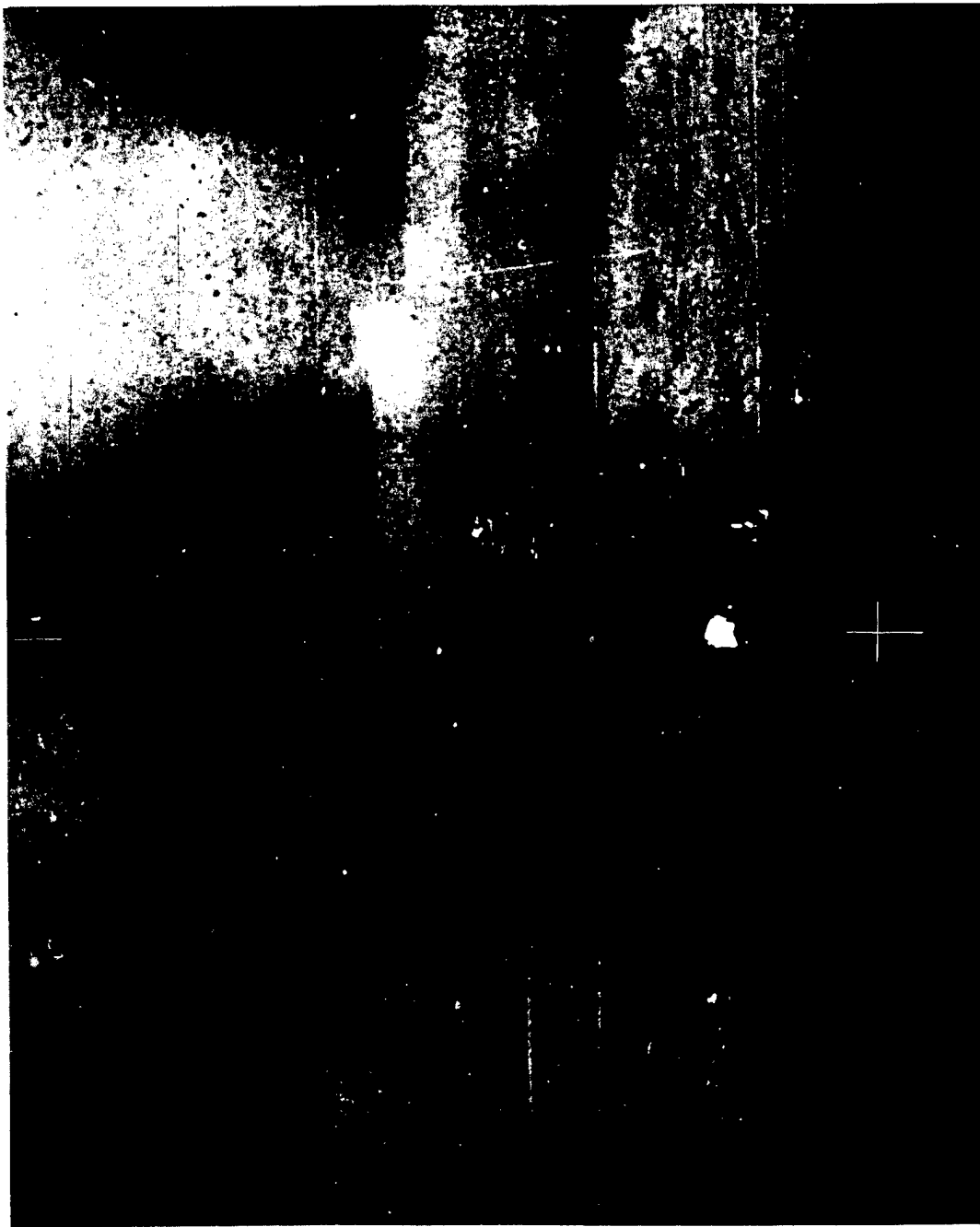


Fig. 3.13d George Cloud at 30 Sec from Station 191. The stem is still hidden, but the mushroom is clearly visible.



Fig. 3.13e George Cloud at 1 Min from Station 191. Note the dense skirt cloud (starting at about 7000 ft) caused by the air drawn upward around the stem.



Fig. 3.13f George Cloud at 2 Min from Station 191. The skirt has thickened and is building downward. The ice cap has formed at this stage, though hidden from Eniwetok.

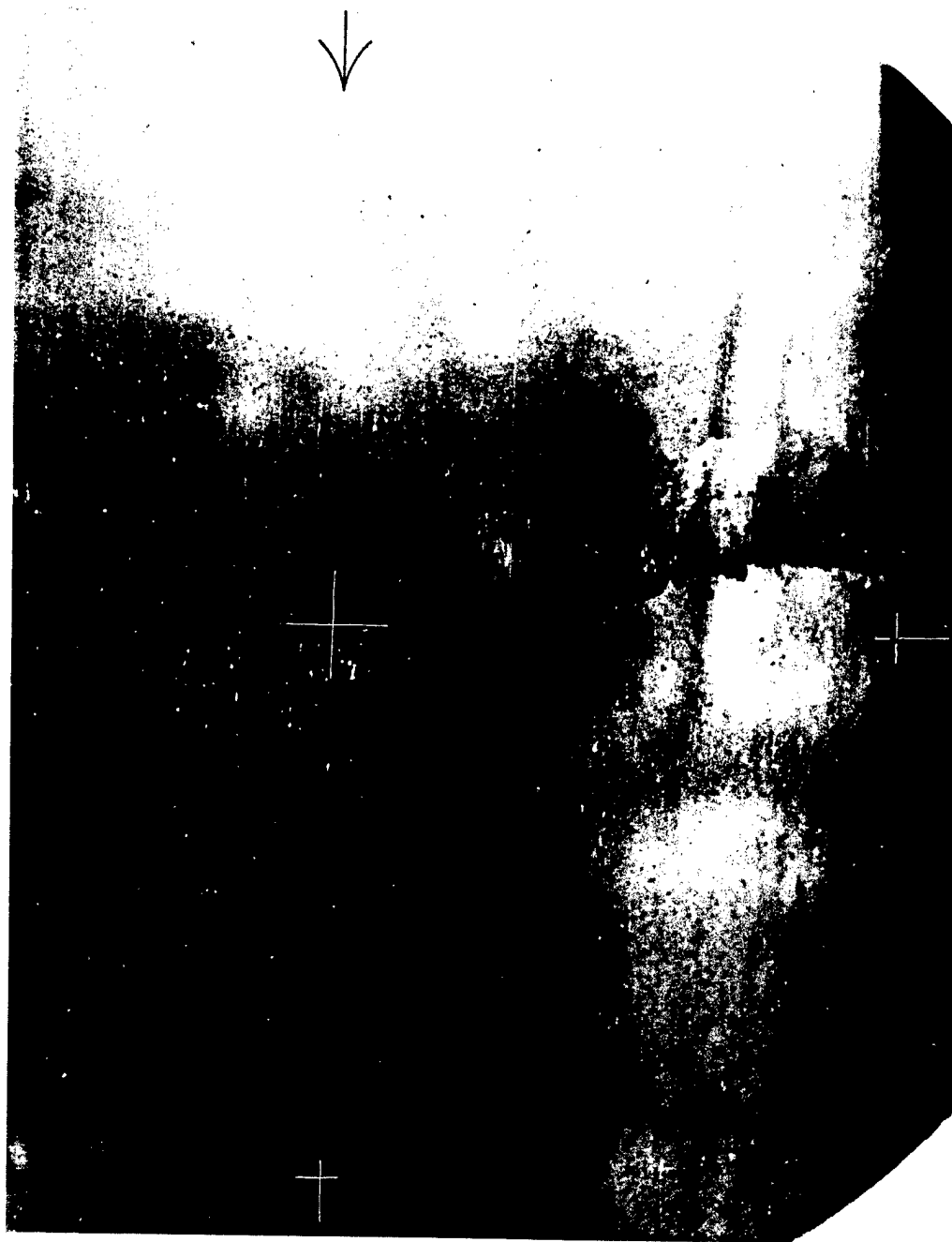


Fig. 3.13g George Cloud at 3 Min from Station 191. The screwlike shape of the stem suggests a clockwise circulation.



Fig. 3.13h George Cloud at 5 Min from Station 191. The internal circulation in stem and mushroom is still very pronounced.



Fig. 3.13i George Cloud at 10 Min from Station 191. The top has stabilized and most of the circulation has died out in the mushroom. However, note the active cumulus growing out of the root and lower stem.

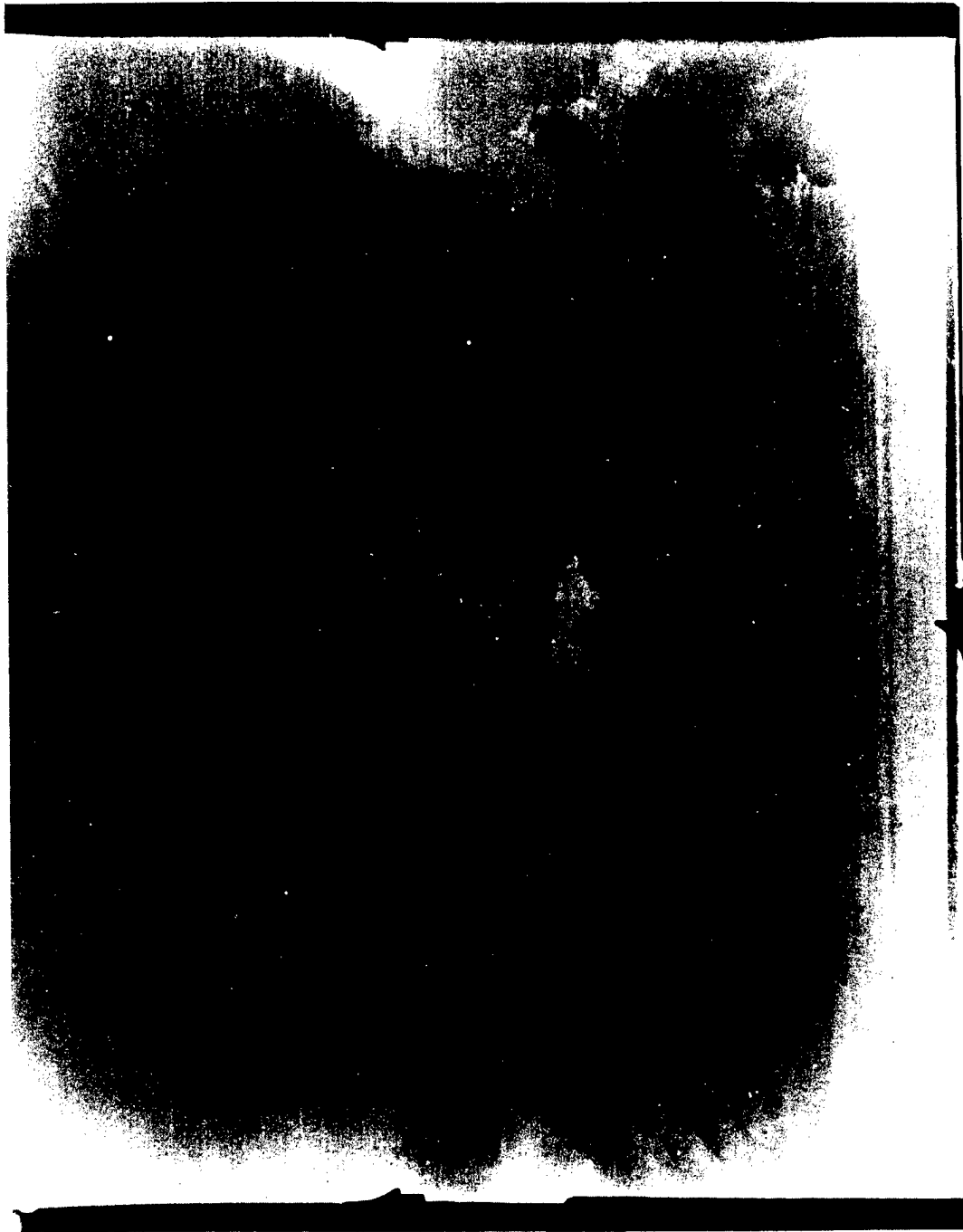


Fig. 3.13j George Cloud at 15 Min from Station 191. The mushroom has spread upward, and in another 15 min it will pass the zenith at Eniwetok. The root cloud is still dense and shows signs of cumulus development.

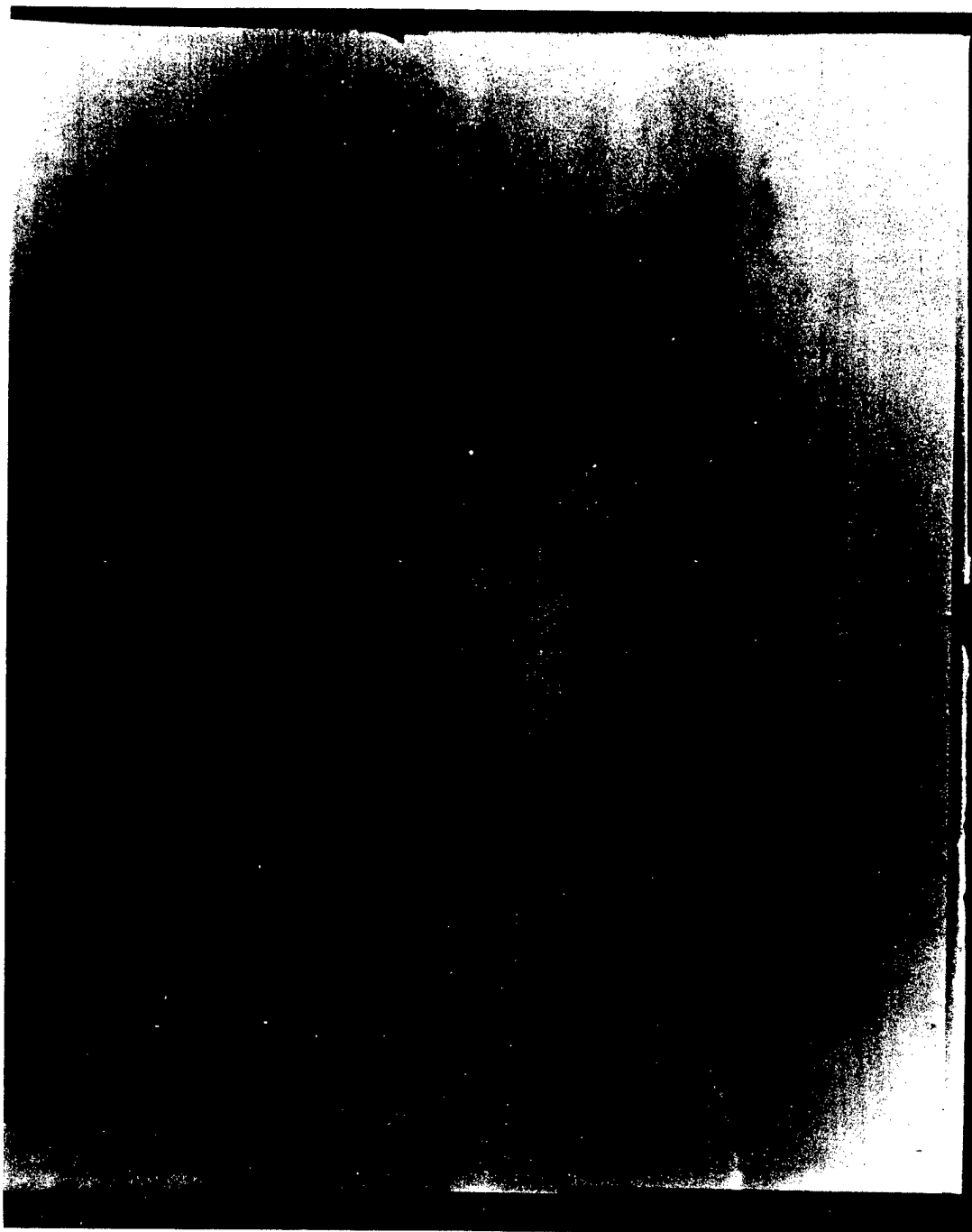


Fig. 3.13k George Cloud at 20 Min from Station 191

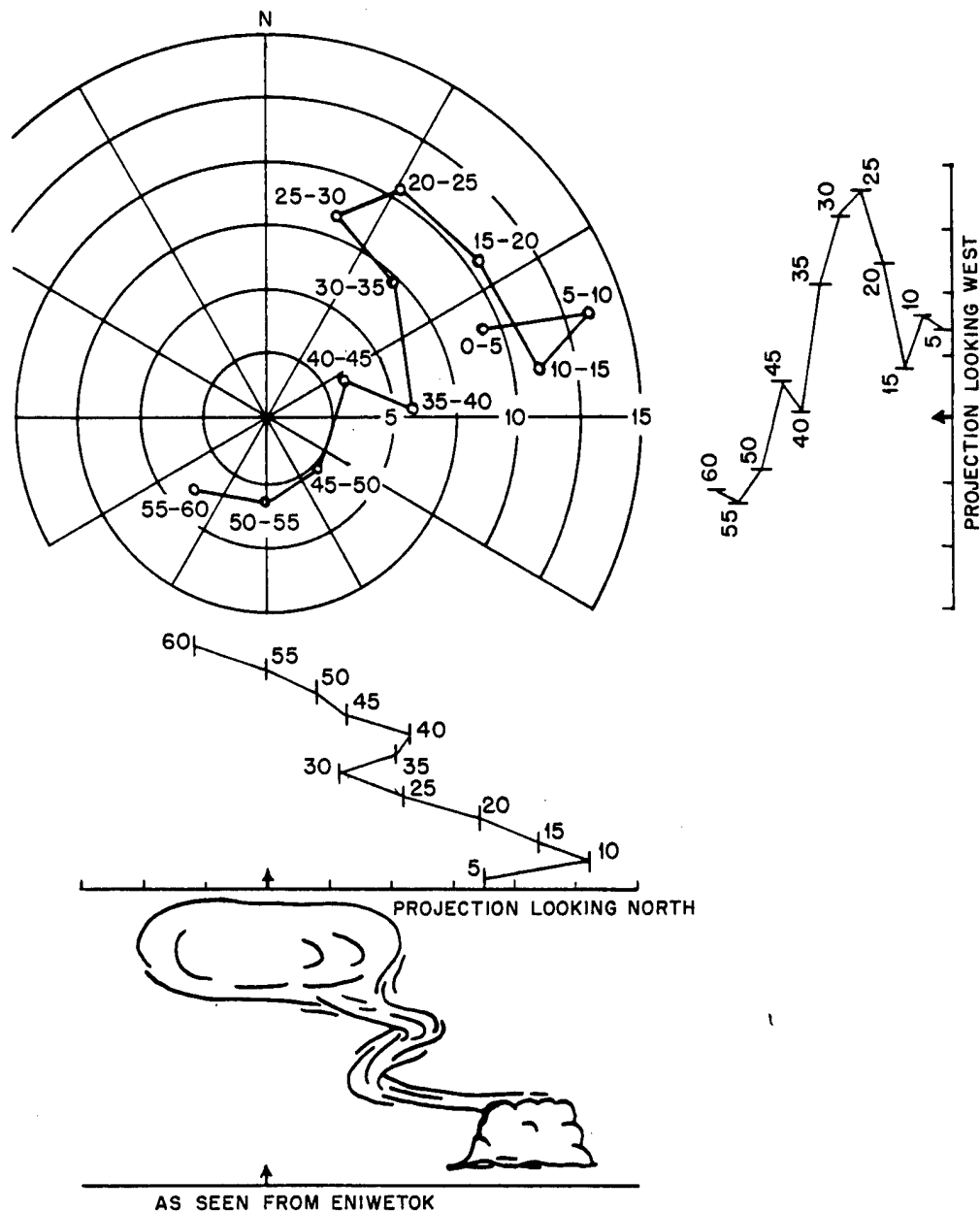


Fig. 3.14 Shape of George Cloud at One-half Hour. The construction is based on the winds aloft, and the sketch at the bottom of the figure is based on the observers' descriptions.

was a wire recorder available for the use of the observers.

Visual observations were, therefore, made on the top of the cloud from 17 sec to 30 min after shot time. Some additional measurements were taken of the sides for volume computations at 6, 14, and 19 min after shot time.

Twelve individual observations were recorded in the first 3 min of the cloud rise.

Notwithstanding the fact that the possibility of triangulation was eliminated and that no photographs were available to check the visual observations, it is believed that the measurements and computations made in connection with Item

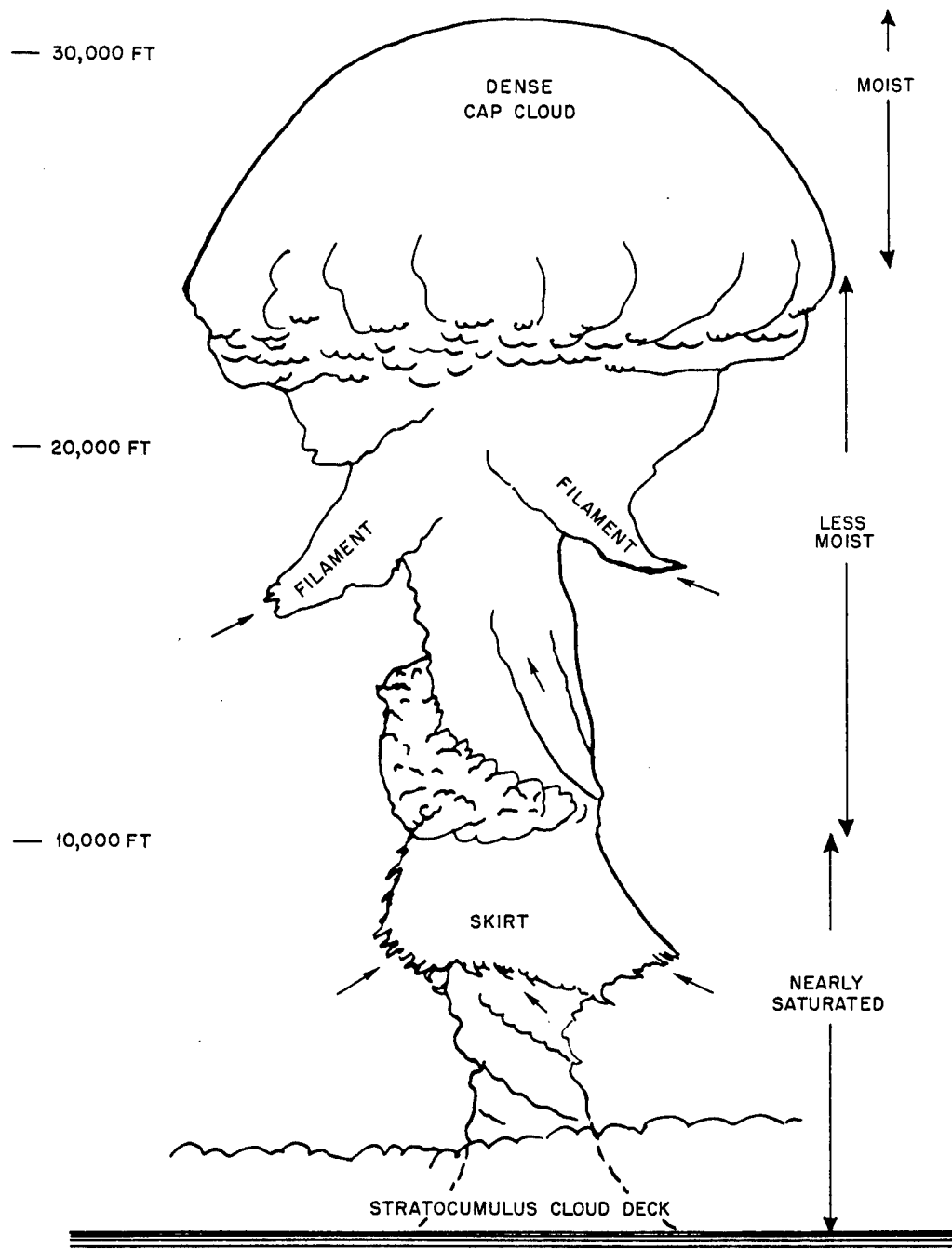


Fig. 3.15 Detail of the Development of the Skirt, George Shot. This is at about 2 min (see Fig. 3.13f). The dense skirt cloud appears to originate in the upper part of the lower moist layer. The cap cloud appeared on the top of the mushroom shortly after the mushroom reached an upper moist layer.

Shot approach the degree of accuracy claimed by this project for the first three tests. The completely unobstructed view afforded the observers made Item Shot unique among the Greenhouse tests.

3.5.2 Meteorological Conditions

As far as the meteorological conditions were concerned, Item Shot proved to be the best of the four tests for observational purposes. Less

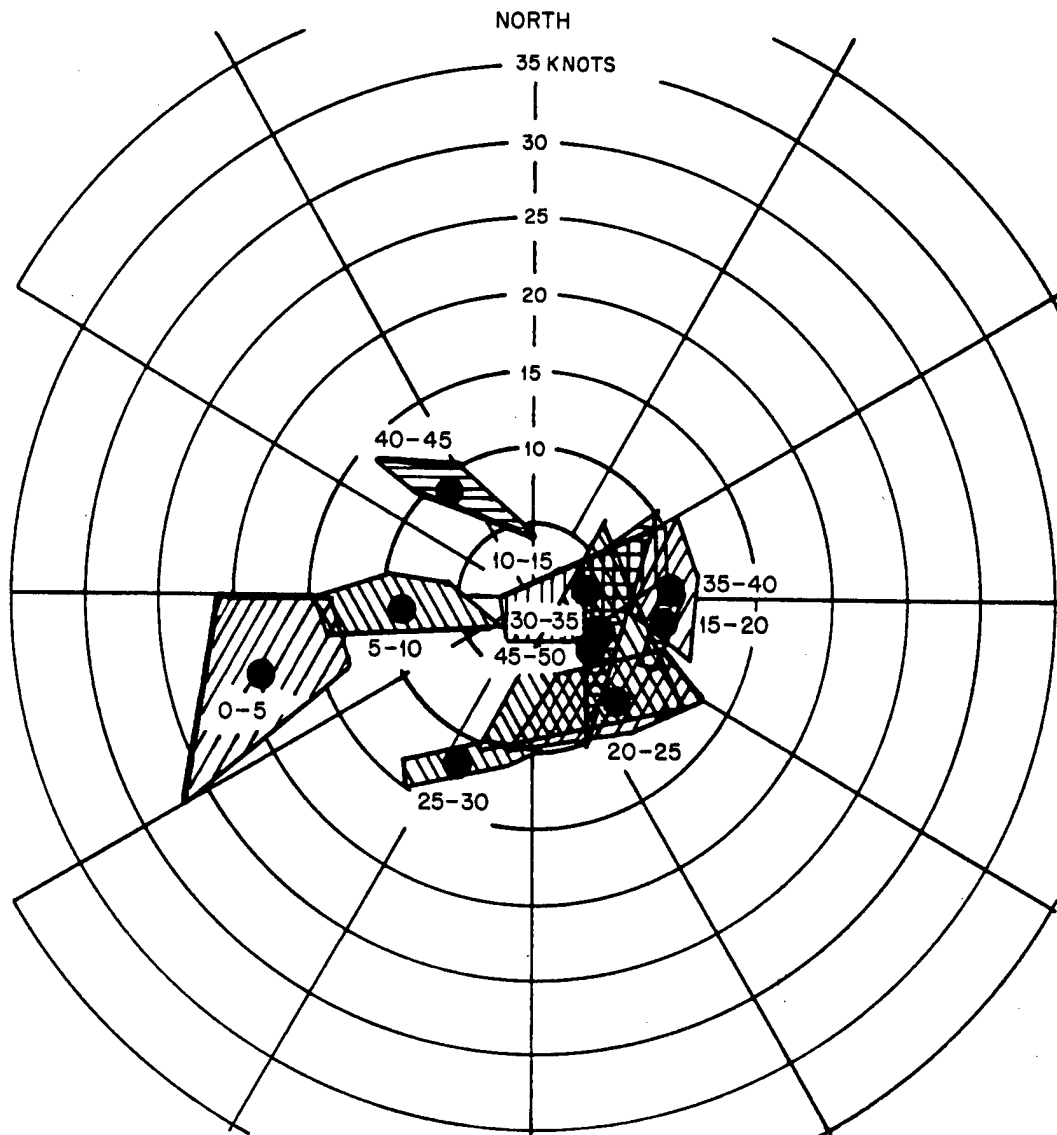


Fig. 3.16 Wind Diagram for Item Shot (25 May 1951, 0600M and 0845M). The hatched areas include the ends of all the wind vectors for each 5000-ft interval.

than 0.1 of the sky was covered with scattered shallow-depth trade cumulus at shot time and during the period of the cloud rise and development following. There was no precipitation in the entire area, and visibility was unrestricted from all points of observation.

The vertical wind structure as determined from the Eniwetok Rawin observations is shown in Fig. 3.16. The wind shear produced by changes in both speed and direction is worthy of attention. The layer of no shear near 27,000 ft is of particular interest and will be referred to later in the description of the atomic-cloud development.

An inspection of the radiosonde for Item Shot (Fig. 3.17), coupled with the diagram of the vertical wind structure (Fig. 3.16), offers a ready physical explanation for the lack of clouds at all levels near the Eniwetok area on 25 May. It will be noted that, at any layer in which the wind structure would permit the growth of local clouds, the moisture content in that layer was insufficient to form a cloud structure and, conversely, in layers through which the moisture was present in measurable quantity, the shears in both speed and direction of the wind were of sufficient strength to preclude the development of local clouds.

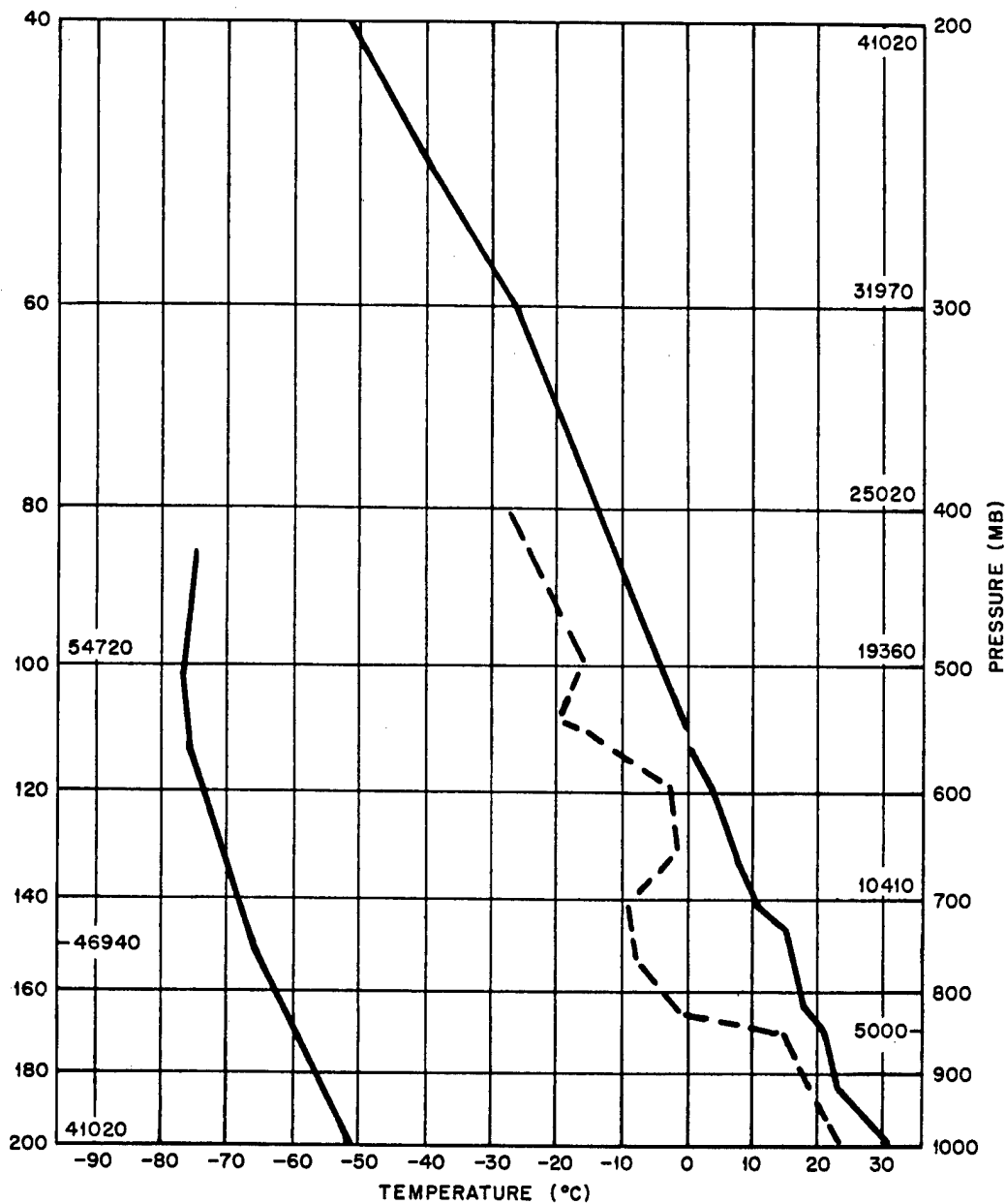


Fig. 3.17 Radiosonde for Item Shot (25 May 1951, 1500M). The heights of the standard pressure surfaces are given in feet. ----, dew-point curve.

The height of the tropopause was about 53,000 ft, although not clearly defined.

3.5.3 Rise and Development

Item Shot was a brilliant display throughout its course. Sufficient predawn light shone in the clear air aloft after the fireball illumination had dissipated to provide continuous vision of the predominant features of the atomic cloud through its rising, developing, and spreading stages.

The shock wave was heard by the observers at Station 190 at 1 min 44 sec. The sensible effects of the shock wave were nonexistent, except for the sound resembling far-distant thunder. The sound waves apparently were not reflected back to earth in concentration by an atmospheric inversion in the lower layers, as was the case during Dog Shot; neither was the energy yield of the test of the same order that produced the reverberating roar during George Shot. The passage of the shock wave at Station

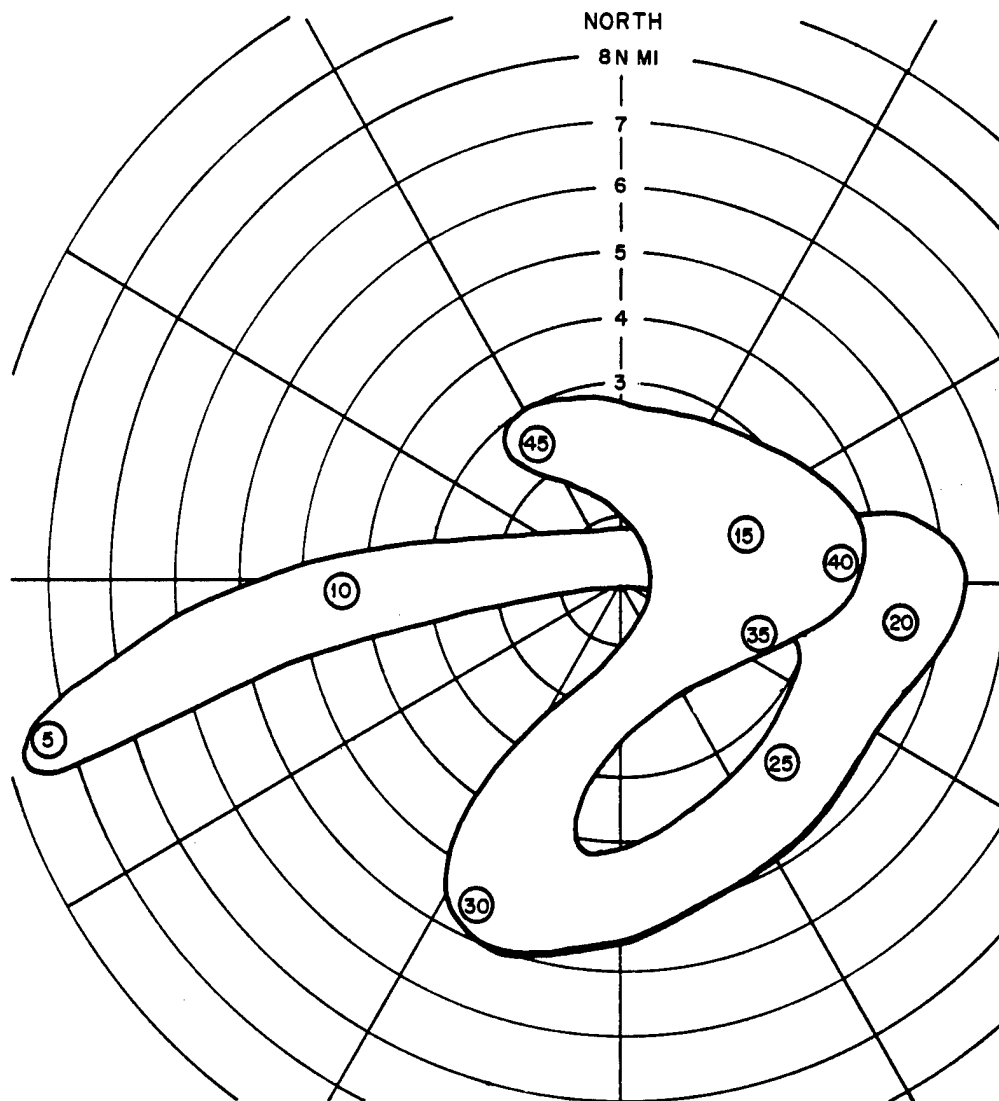


Fig. 3.18 Shape of Item Cloud at One-half Hour. The small circles are the mean wind vectors for a 5000-ft interval, and the numbers refer to the height of the top of the interval. The cloud outline as shown is schematic.

190 was, in fact, very similar to that associated with Easy Shot.

The observations showed that the top of the cloud rose regularly with time. After about $2\frac{1}{2}$ min the rate of rise had appreciably decreased, and by about 7 min the cloud top had become fairly stabilized.

It should be noted at this time that the heights of the tops as given in Fig. 2.1 were corrected for both the wind factor and the shape of the cloud. The correction applied for the size and shape of the cloud in later stages was per-

formed in the same fashion as that described in Appendix B and demonstrated in Figs. B.1 and B.3. Since it was difficult to apply corrections for the shape of the cloud owing to the lack of good observations of the diameter of the cloud, it was decided that the diameters previously computed for Easy Shot could be used as a first approximation for these corrections. It was felt that this assumption was valid and yet maintained the desired degree of accuracy; however, the computations were not carried out beyond 10 min after shot time to ensure meaningful results.

The arguments supporting the validity of this assumption are as follows:

1. Both Easy and Item Shots had approximately the same yield.
2. Neither Easy nor Item Shot reached the tropopause before ceasing to rise.
3. The width and depth measurements of Item cloud agreed closely with those obtained from Easy cloud, especially during the cloud rise.
4. The magnitude of the correction on Easy Shot (and, by the same argument, Item) was small compared to Dog and George Shots because Easy cloud (and Item) did not ascend to the heights attained by Dog and George clouds.

At 8 min 30 sec, as the cloud reached to approximately 41,000 ft, a cap cloud developed above the main cloud top. This cap cloud never assumed the multicap appearance that was observed at the 5-min mark during Dog Shot. The cap possessed hazy, cirrus-filose characteristics and persisted as a separate entity for over 3 min.

At 11 min 43 sec the cloud top was again clearly defined and appeared to be at nearly 46,000 ft. The cap cloud never reappeared.

A measurement at 15 min 32 sec indicates that the top had completely stabilized by that time and all subsequent measurements of the cloud-top height up to one-half hour after shot time showed no change.

Up to about 22 min after shot time, when the cloud top was in enough sunlight aloft to show detailed features of the structure, some internal circulation was visible. It is regrettable that no photographs are available to verify this observation. However, immediately following this time, the top of the cloud and the upper main mass were being torn apart. By 24 min the top and the sides of the upper main mass were spreading laterally and had indefinite edges.

After 20 min variations in color were noted in the various sectors of the cloud. The top of the cloud and the upper main mass had a dark gray tinge. A transition in the color existed through the neck to the lower main mass, which was a definite pinkish-brown sparkling color. The lower main mass extended from about 20,000 to 33,000 ft. Below this the trail of the cloud and the distorted traces of the stem had a dark brownish-pink color, dull compared to the brilliance of the colors above. Naturally, the rays of the sun aloft were the principal contributing factors to the relative brilliance of the upper cloud sectors.

The lower main mass retained its identity for the longest period. This level, well-defined by the vertical wind profile (Fig. 3.16), was centered at about 27,000 ft. It was in a region of small shear. Below and above this layer the wind was from a west of north sector at a speed of less than 10 knots; but throughout this layer the wind had an east of north component in excess of 10 knots. As the top of the cloud and the upper main mass spread and diffused and the stem in the shallow trade flow rapidly moved off to the west in a weirdly distorted trail, the lower main mass remained relatively unchanged in shape for over 1 hr.

REFERENCES

1. O. G. Sutton, A Theory of Eddy Diffusion in the Atmosphere, *Proc. Roy. Soc.*, 135A: 143 (1932).
2. G. K. Batchelor, Kolmogoroff's Theory of Locally Isotropic Turbulence, *Proc. Cambridge Phil. Soc.*, 43: 553-570 (1947).
3. G. K. Batchelor, The Application of the Similarity Theory of Turbulence to Atmospheric Diffusion, *Quart. J. Roy. Meteorol. Soc.*, 76: 133-145 (1950).
4. C. F. v. Weizsäcker, Das Spektrum der Turbulenz bei Grossen Reynoldsen Zahlen, *Z. Physik*, 124: 614-627 (1947).

Chapter 4

Summary and Conclusions

4.1 SUMMARY

The photographic and visual coverage of the later stages of the Operation Greenhouse clouds was better than that for any of the previous tests, and the resulting measurements of heights, sizes, etc., are therefore probably more accurate than any previously obtained. However, it must be admitted that even here there were serious gaps in the coverage due to local cloudiness, which often obscured the early stages of the rise, and the precision of the measurements during the later stages of the clouds' development is not very great owing to the diffuseness of these clouds. For example, the spread in the measurements of the heights of the top of the clouds as seen from different sites increased from a few hundred feet during the first 5 min to about two or three thousand feet after some 8 to 10 min, clearly showing the decrease in accuracy with time (and elevation of the clouds).

In addition to giving quantitative data on the development of the clouds, the good photographic coverage permitted a study of special features of the development, and this has thrown new light on such matters as the internal circulation of the rising cloud, the motion of the air around the cloud, and the growth of the cloud due to entrainment.

It is likely that more theoretical work remains to be done in connection with the analysis of the Greenhouse atomic clouds than has been done in this report. Wherever possible such analysis has been anticipated, and the data are provided in an accessible form.

One negative result of the analysis is the lack of further information on rates of eddy diffusion in the free air. Several approaches were made to the problem, but each time it had to be concluded that wind shear completely masked the

effects of eddy diffusion. A tentative conclusion may therefore be that the effects of eddy diffusion are indeed small compared to the effects of wind and wind shear and that the cloud particles follow the large-scale streamline flow very closely, although here the "scale" is largely a matter of the spacing of the upper-air observational network.

4.2 CONCLUSIONS AND RECOMMENDATIONS

The following specific conclusions and recommendations are made as a result of the experience gained in Project 4.1B:

1. It is possible to obtain measurements on an atomic cloud by means of trained observers with theodolites or nephoclinometers, but the increase in accuracy and detail of the measurements when photographs are also available is very great. The reasons for this are fairly obvious. The most important is that the cloud develops rapidly at first, and the observers can only get a few hurried readings per minute. Moreover, there is no way to go back and find an error in a measurement once it is made. The proof of the superior accuracy of the photographic measurements lies in the relatively good agreement between observations made from photographs from different sites, whereas there were occasionally serious discrepancies between the visual observations made from different sites.

It is therefore recommended that every effort be made to provide photographic coverage from fixed camera sites for any future cloud-physics program.

2. Eniwetok is not a good place to study the atomic cloud owing to the frequency of low cloudiness which hinders observations. How-

ever, if such cloud observations are to be undertaken in future tests in the Marshall Islands, the probability of success might be increased by making the tests earlier in the year. The short climatological record that is available for Eniwetok suggests that the cloudiness starts to increase markedly in May and June. The spring of 1951 may not have been too representative since there were a number of tropical disturbances passing close to the area during the tests, and it will be impossible to make any very definite statements until a few more years of records have been obtained for Eniwetok.

3. Another way of increasing the probability of getting good cloud coverage under Eniwetok weather conditions is the establishment of a number of widely separated sites in order to increase the chances of catching a glimpse between the cumulus clouds. In particular, a site either upwind or downwind appears to have a very good chance of seeing the atomic cloud because the cumulus clouds tend to line up in rows aligned with the wind. This was probably the reason that Rigili, the automatic camera site located downwind to the southwest of the firing points, saw considerably more of the first two clouds than did the sites on Eniwetok.

It is therefore recommended that the site on Rigili be used again, in spite of the difficulties in maintaining it, and that a camera site be set up on Japtan. One of the Eniwetok sites could be abandoned since the views from Stations 190 and 191 are so similar.

4. The photographic coverage for Easy Shot was excellent, and the exposures, frequency of taking pictures, film type, etc., seem to have been close to optimum for a one-half hour predawn shot. However, in the analysis it turned out that it is absolutely necessary to have some indication of the times directly on the films. The K-8 cameras did have such indications, and it was necessary to determine the times of other cameras (K-24 and Mitchell) by careful comparisons between them and the K-8 pictures from the same site. Relying on the intervalometer settings as reported in the camera log books would have introduced errors of about 20 per cent in the time of the K-24 pictures on two occasions.

5. In none of the Greenhouse tests was it necessary to use the entire angular coverage of the fixed cameras, which was about 60 deg in elevation and 116 deg in azimuth. The most im-

portant portion of the photographic record is that obtained during the early rise and spread, up to about 15 min, and the cloud never moved out of the field of the center low-elevation K-8 cameras (with an angular view of 40 by 40 deg) until 9 or 10 min had passed. In other words, if only the low-elevation center cameras had been used (one K-24 and one K-8), complete coverage would have been obtained for at least 9 or 10 min, and usually for 15 min. After 15 min the cloud is often hard to see on the negatives anyway, particularly where there are other cumulus clouds in the field, and the drawings and accounts of the visual observers are almost as useful as the photographs.

It is therefore recommended, for the sake of economy and reliability, that, in addition to increasing the number of sites (see item 3), the camera installation at each site consist of more cameras pointed at Ground Zero and fewer off at large angles from Ground Zero. One suggested setup to be used at the old sites on a future test would be one fast-operating K-24, as before, to cover the first few minutes, and only two low-elevation K-8 cameras, each pointing 10 to 15 deg on each side of Ground Zero and about 19½ deg above the horizon. This would give three cameras covering the early rise and a total angular coverage of 40 deg in elevation and 60 to 70 deg in azimuth. Such a system would eliminate four K-8 cameras at each site. If a site is set up at Japtan, it would be necessary to add another bank of two K-8 cameras covering a higher elevation angle since Japtan is considerably closer than any of the other sites.

6. The movie footage taken with the Mitchell cameras proved to be by far the best for the first 15 to 20 sec, even during the predawn shots. However, it is recommended that these be taken with longer focal-length lenses in order to get the biggest image of the initial cloud and that the cameras be left perfectly stationary until all light has died away. This will serve to give detailed coverage of the early rise of the fireball, until it has risen to about 10,000 ft, and will show the development and motion of the root cloud. After this time the other cameras with their longer exposures will provide the coverage.

7. The use of voice recorders by the observers proved to be of great value and should be repeated in any future observation program. The long playing time of the wire recorders

(about 1 hr) was an asset, but they are inconvenient to play back because of the long time required to rewind.

8. The photographic coverage from the air was useful in studying general features of the cloud and in seeing the details of the top of the cloud. Color film should be used for this where possible. A better determination of camera orientations and aircraft positions would help in the analysis of these pictures, although this

appears to be difficult to achieve in practice.

9. The importance of obtaining high-altitude upper-air soundings and winds cannot be over-emphasized. The failure of the sounding balloons at Greenhouse was unfortunate, and it is recommended that special efforts be made on future tests to provide better balloons. The tracking equipment (AN/GMD-1) appears to have worked very well except for some minor maintenance difficulties.

Appendix A

Record of Camera Exposures, Orientations, and Operating Results

The data presented in Tables A.1 to A.3 are intended to be for the use of those planning future photographic coverage of atomic clouds.

Figure A.1 shows the field of vision encompassed by the various cameras in a camera rack. As is pointed out in Sec. 1.3, the three camera sites had identical racks and each had seven fixed cameras mounted in these racks. The field of vision of each of the seven cameras was 40 by 40 deg. They were arranged in the rack frame to provide an overlapping coverage of 60 deg in elevation and 116 deg in azimuth. The lower four cameras (positions 1, 2, 3, and 7) were sighted so that their axes were approximately 19 deg above the horizon. The elevation coverage in the lower three cameras, therefore, was from 1 deg below the horizon to 39 deg above the horizon. The three cameras in the upper bank of the racks (positions 4, 5, and 6) were arranged so that their axes were at an elevation angle of approximately 39 deg. The range of elevation angles in the upper three cameras, therefore, was from 19 to 59 deg above the horizon. Thus the total elevation coverage existed from 1 deg below the horizon to 59 deg above the horizon with an overlap in the interval between 19 and 39 deg.

In azimuth the middle cameras in each bank (positions 2, 5, and 7) were aligned directly on the shot towers, providing an azimuthal coverage of 20 deg on both sides of the shot towers. The two cameras facing to the left of the shot towers (positions 1 and 4) were positioned at an azimuth angle 38 deg to the left, thus covering the azimuths between 18 and 58 deg to the left of the shot towers. The two cameras facing to the right (positions 3 and 6) had similar arrangements. The total camera coverage in

azimuth was, therefore, from 58 deg right to 58 deg left of the shot towers.

In Fig. A.1, it will be noted that camera positions 2 and 7 were sighted identically in both elevation and azimuth. However, these two positions held two different type cameras operating at different exposure rates and timed to cover different periods of the cloud development in detail.

K-8 aerial type cameras were mounted in positions 1 to 6. These cameras had 12-in. focal-length lenses and gave pictures that were 9 by 9 in. Cameras of the K-24 type were mounted in position 7 at each site. These cameras have an f/2.5 lens, with a 7-in. focal length, and gave pictures that were 5 by 5 in.

As explained in Sec. 1.3.2, two of the three camera sites were manned, and they also included Mitchell movie cameras. Data pertaining to these Mitchell cameras are also included in Tables A.1 to A.3 for completeness.

All the K-8 cameras were equipped with Tri-X film, the K-24 cameras used Super-XX film, and the Mitchells used Superior No. 2 film.

For the fixed cameras no filter was used during Dog Shot, but a yellow filter was used with the K-8 and K-24 cameras on both Easy and George Shots. The filters on the Mitchells were changed on all three shots covered by the camera operators as discretion dictated.

No special attempts were made to photograph the fireball stage, and the shot pictures were invariably completely overexposed.

All the cameras were started together and ran until all the film was exhausted. The only exception to this was during Easy Shot, when cameras in positions 4 and 6 were preset to start late at Stations 190 and 191, but the opera-

TABLE A.1 CAMERA DATA FOR DOG SHOT

Position*	Exposure	Aperture	Frames/min	Shot time (min)			Remarks
	(sec)	(f)		Operating	Readable	Atomic cloud	
Station 190							
1	13	5	4	0-36½	2-8½	None	0-2, streaks; 8½-36½, overexposed
2	13	5	4	0-38	0-16	0-½	16-38, overexposed
3	13	5	4	0-38	0-16	None	16-38, overexposed
4	1/50	5	4	0-38	14-38	None	0-14, underexposed
5	13	5	4	0-36	0-14	None	14-36, overexposed
6	1/50	5	4	0-38	12-38	None	0-12, underexposed
7	8	4	3.8	1-25	1-15	None	15-25, overexposed
M	Var.	Var.	480	24	23	1/2	
Station 191							
1	13	5	4	1-46½	1-28	None	28-46½, overexposed
2	13	5	4	1-47½	0-16	0-¼	16-47½, overexposed (streaks throughout)
3	13	5	4	1-44½	1-21	None	21-44, overexposed
4	1/50	5	4	½-46	1-8½	None	8½-46, overexposed
5	13	5	4	1-46	2-17	None	17-46, overexposed
6	1/50	5	4	1-42	15-42	None	1-15, underexposed
7	8	4	3.8	1-25	1-15	None	15-25, overexposed
M	Var.	Var.	480	39	24	1/2	0-15, underexposed
Station 192†							
1	13	5	4	4¼-40	4¼-25	None	25-40, overexposed
2	13	5	4	4¼-42	4¼-20	4¼-13½	20-42, overexposed
3	13	5	4	4¼-42	4¼-25	None	25-42, overexposed (streaks throughout)
4	1/50	5	4	4¼-42	30-42	None	4¼-30, underexposed
5	13	5	4	4¼-40	4¼-25	4¼-13½	25-40, overexposed
6	1/50	5	4	4¼-42	25-42	None	4¼-25, underexposed
7	8	4	3.8	4½-30	4½-15	4½-12	15-30, overexposed

* M refers to the Mitchell cameras.

† All cameras at Station 192 apparently were not activated by the clocks until 4 $\frac{1}{4}$ min after shot time. All films from Station 192 were fogged considerably by radioactivity.

TABLE A.2 CAMERA DATA FOR EASY SHOT

Position*	Exposure	Aperture	Frames/min	Shot time (min)			Remarks
	(sec)	(f)		Operating	Readable	Atomic cloud	
Station 190							
1	13; 4†	22	4; 10†	0-29½	11-29½	None	0-11, underexposed
2	13; 4†	22	4; 10†	0-29	4-29	4-29	0-4, underexposed
3	13; 4†	22	4; 10†	0-29	0-29	15-29	
4	1/50	22	4; 10†	6½-30½	None	None	Completely unexposed
5	13; 4†	22	4; 10†	0-26	9½-26	None	0-9½, underexposed
6	1/50	22	4; 10†	6-30‡	19-30	None	6-19, underexposed
7	2	5.6	13	0-8¼	0-8¼	0-8¼	
M	Var.	Var.	480	48	39	21	Excellent
Station 191							
1	13; 4§	22	4; 10§	0-28	0-28	None	
2	13; 4§	22	4; 10§	0-28½	3½-28½	3½-27½	0-3½, underexposed
3	13; 4§	22	4; 10§	0-29	0-29	14-29	
4	1/50	22	4; 10§	35-53‡	35-53	None	Mostly unexposed
5	13; 4§	22	4; 10§	0-14	0-14	8-14	Double exposure after 14 min
6	1/50	22	4; 10§	0-29‡	23-29	None	0-23, underexposed
7	2	5.6	13	0-8½	0-8½	1-8½	0-1, underexposed
M	Var.	Var.	480	42	15	6	Extreme density contrast
Station 192							
1	13; 4¶	22	4; 10¶	0-26½	4-16	None	0-4, underexposed
2	13; 4¶	22	4; 10¶	0-26	0-26	1-13½	
3	13; 4¶	22	4; 10¶	0-14	0-14	None	Mostly unexposed
4	1/50	22	4; 10¶	0-25	None	None	Completely unexposed
5	13; 4¶	22	4; 10¶	0-26	4½-26	4½-12½	0-4½, underexposed
6	1/50	22	4; 10¶	0-31	26-31	None	0-26, underexposed
7	2	5.6	18½	0-6	0-6	1-6	0-1, underexposed

* M refers to the Mitchell cameras.

† A 13-sec exposure and 4 frames/min for first 9 min only.

‡ Preset to start late.

§ A 13-sec exposure and 4 frames/min for first 7 min only.

¶ A 13-sec exposure and 4 frames/min for first 5 min only.

TABLE A.3 CAMERA DATA FOR GEORGE SHOT*

Position†	Exposure	Aperture	Frames/min	Shot time (min)			Remarks
	(sec)	(f)		Operating	Readable	Atomic cloud	
Station 190							
1	1/180	22	‡	0-38½	0-38½	None	Film broke
2	1/180	22	‡	0-39	0-39	0-39	
3	1/180	22	‡	0-39	0-39	17-39	
4	1/180	22	‡	0-39	0-39	None	
5	1/180	22	‡	0-½	0-½	None	
6	1/180	22	‡	0-40	0-40	8-40	
7	1/450	16	15	0-6	0-6	0-6	Excellent coverage
M	Var.	Var.	480	36	36	27	
Station 191							
1	1/180	22	‡	0-30	0-30	None	Double and overexposed throughout
2	1/180	22	‡	0-30	0-30	0-30	
3	1/180	22	‡	0-30	0-30	9½-30	
4	1/180	22	‡	Ind.	None	None	
5	1/180	22	‡	0-30	0-3½	None	3½-30, double exposed
6	1/180	22	‡	0-29	0-29	10-29	
7	1/450	11	15	0-6	0-6	0-6	Overexposed last 9 min
M			480	39	30	29	

* Station 192 did not operate owing to control-system malfunction.

† M refers to the Mitchell cameras.

‡ 20 frames/min from 0 to 3 min; 6.7 frames/min from 3 to 23 min; 4 frames/min from 23 to 40 min.

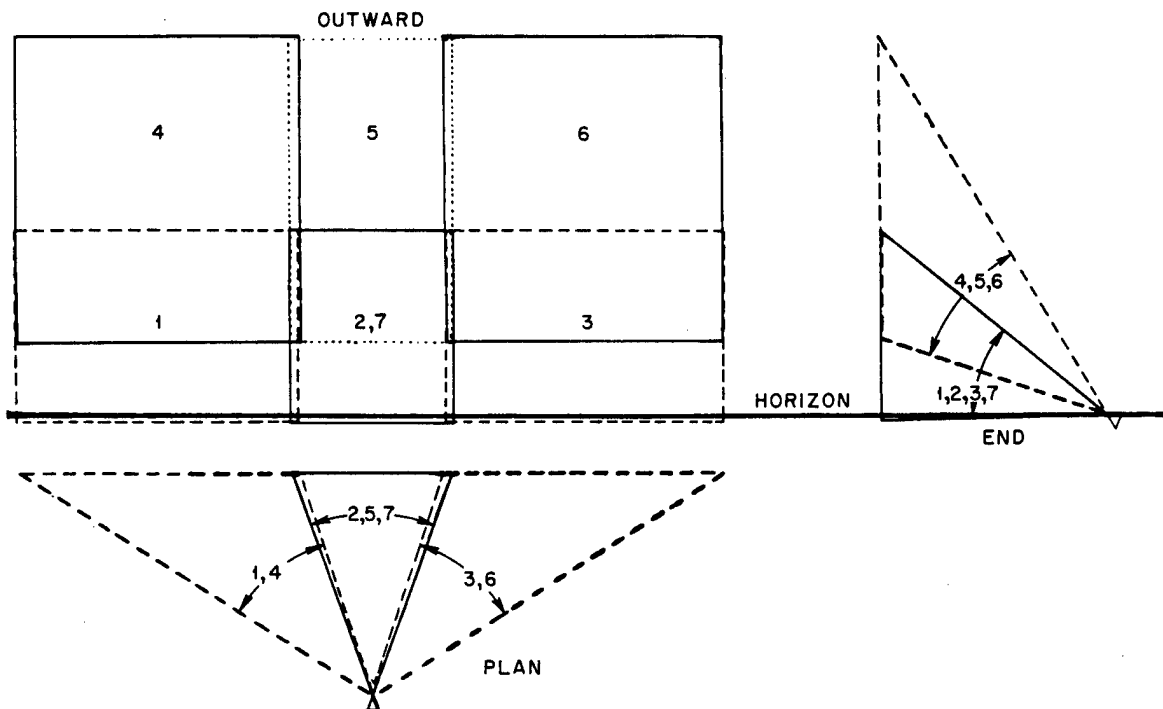


Fig. A.1 Diagram of Camera Orientations. The numbers refer to the rack positions.

tional results were erratic (see Table A.2). Since some cameras were set to catch the early rise and some the later stages, this necessarily produced some wasted film because of underexposures at the start or overexposures at the end of the strip of film for predawn tests. With the system employed this was unavoidable.

George Shot, a daytime test, presented no particular problems as far as exposures were concerned, and these pictures all came out well. However, since George was a daytime shot, the light differential between the light of day and the fireball was not sufficient to actuate the station control system at the unmanned camera site, Station 192, and therefore no pictures of George Shot were obtained from this site.

Although it is regrettable that conditions of low-level cumulus blocked vision of the rise and development of the atomic cloud, it is noteworthy and a tribute to the professional talents of the personnel of EG&G that only three of 52

reels (Easy, Station 192, position 4; Easy, Station 190, position 4; and George, Station 191, position 4) were completely useless because of exposure or film jamming in the camera.

Tables A.1 to A.3 are designed to give a rather complete summary of the results obtained from the camera sites.

The "operating" time in column 5 is the interval during which the cameras were running, in minutes from shot time, as determined by the camera clocks. The "readable" time in column 6 is the interval during which the exposures were such as to allow readable cloud pictures. In the next column the time interval in which the atomic cloud was actually observable (and hence measurable) is tabulated; the actual time during which the atomic cloud was photographed was usually less than the readable, either because local cumulus clouds blocked the vision or because the atomic cloud did not move into the field of view of the camera immediately.

Appendix B

Method of Determining Distances and Heights from the Photographs

B.1 DETERMINING ANGLES FROM THE PHOTOGRAPHS

The basic parameter that is determined from the photographs is the angle. It is not possible to scale proportional distances directly from the photographs in this case because the distances to the various parts of the cloud vary from point to point and there is no one scaling factor as there is, for example, in certain aerial photographs. Therefore the process of reduction of the photographs is just one of obtaining angles.

Figure B.1 is a schematic drawing of the optical system of one of the cameras. It will be seen that, assuming the object at an infinite distance,

$$\frac{X}{\text{Focal length}} = \tan (\epsilon - \alpha)$$

where X = the vertical distance measured from the center of the plate to the image of the point

ϵ = the elevation angle of the camera's axis

α = the elevation angle of the point above the horizon

Since the focal length and ϵ are quite precisely known for each camera, it is a simple computation to determine α from the measured values of X .

The same is true in determining azimuth angles, of course, where a corresponding measurement on the plate gives the tangent of the angle between the azimuth of the point and the orientation of the camera's axis.

B.2 DETERMINING HEIGHTS FROM THE ANGLES

To determine any side of one of the right triangles in Fig. B.1, it is only necessary to know the angle α and one other side. The angle is obtained from the photographs, as explained above, but the various ranges are sometimes not so precisely known.

During the early stages of the cloud's rise it appears that the top of the cloud goes almost exactly straight upward. This is verified by studying the photographs taken from various azimuths and also seems to be reasonable when the observed winds are considered. Figure B.2 shows the trajectories of the tops of the clouds, calculated by combining the observed heights of the clouds with the observed upper-air winds in each layer, the time that each wind operated on the cloud being proportional to the time that the cloud top spent in that layer. (The layers were arbitrarily taken as being 5000 ft thick.) It will be seen from these trajectories that the drift away from Ground Zero of the top of the cloud was usually less than a mile for the first 4 or 5 min.

Thus the computations for the early rise are simplified by the fact that the horizontal range is constant, equal to the range from the camera to Ground Zero. The height of any part of the cloud is then just

$$\text{Range} \times \tan \alpha = h$$

As the cloud rises and grows, it is necessary to make two corrections, however. One is for the change in the horizontal range due to the drift, which is made by plotting the trajectories

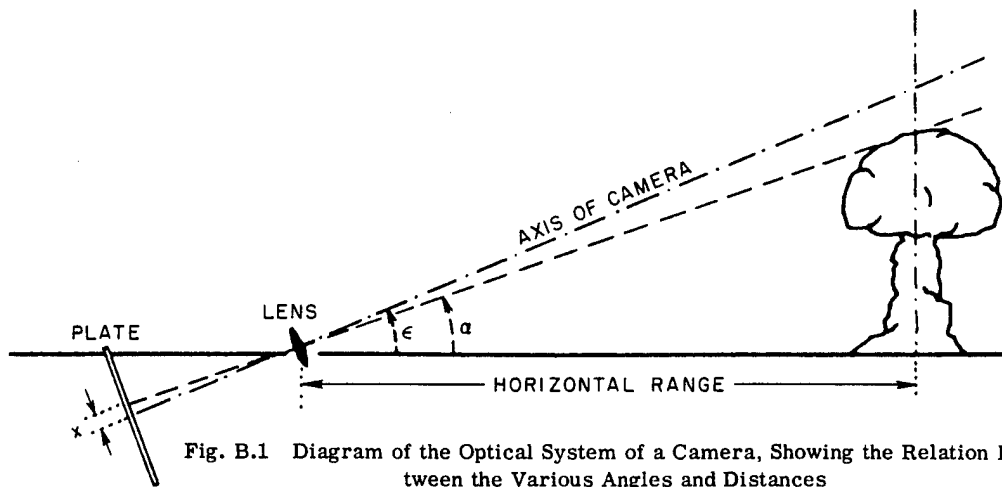


Fig. B.1 Diagram of the Optical System of a Camera, Showing the Relation Between the Various Angles and Distances

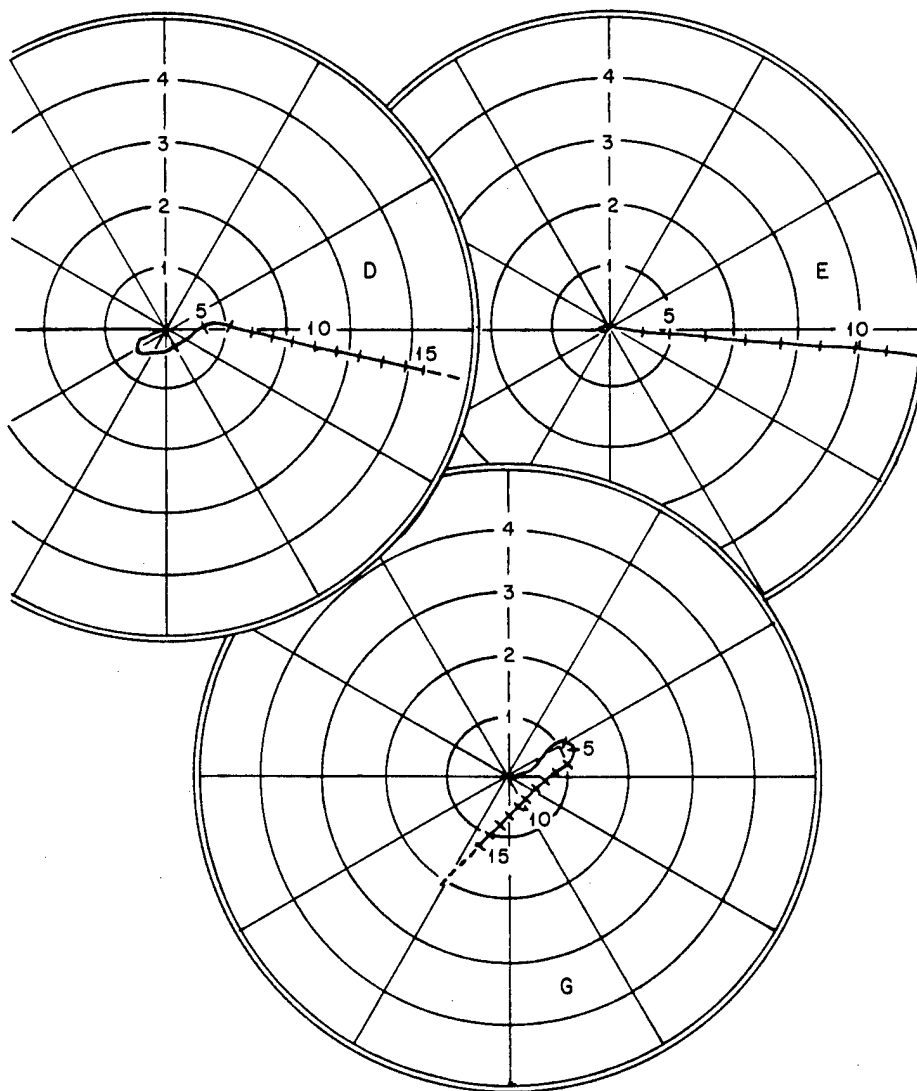


Fig. B.2 Trajectories of the Tops of the Rising Clouds Determined from the Observed Heights and the Observed Upper Winds

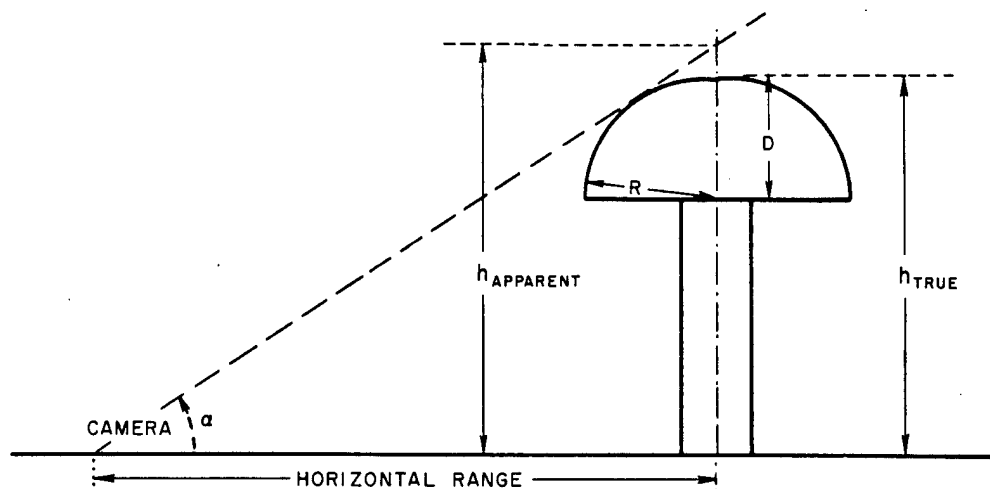


Fig. B.3 Idealized Sketch of the Atomic Cloud, Showing the Method of Correcting for the Angle of View

based on the upper winds, and the other is the correction for the size of the cloud itself. Figure B.3 indicates how the latter can be done. The actual method used was to draw the picture to scale, with the variable horizontal range and the angle α known. Then the radius of the mushroom, assumed to be a hemisphere, was determined from the angular width of the mushroom and the slant range by the relation

$$\text{Radius} = \text{slant range} \times \tan \frac{\theta}{2}$$

where θ is the angular width. The mushroom can then be drawn in to scale as a hemisphere, and the true heights can be measured from the drawing.

Although this is not a very elegant way of making the correction, it has the advantage that the drawing of the mushroom can sometimes be altered to take into account irregularities in the cloud, as shown on the photographs. In other words, the assumption of a perfect hemisphere can be modified to fit the evidence where necessary.

The corrections for the size of the cloud and the fact that the observer must look up at a rather steep angle sometimes amount to several thousands of feet, and there is naturally some uncertainty as to just what shape the top does have. Aerial photographs taken at some distance away indicate that the assumption of a spherical cloud is quite good until the cloud reaches its maximum height, and then it flattens somewhat at the top. This suggests that the method used is good during the rise of the

cloud but may be subject to more error after the cloud stabilizes.

B.3 OBTAINING FIXES ON THE CLOUD

As a check on the calculated drifts, based on the upper-air winds, fixes were obtained on certain parts of the cloud by triangulation from the four sites. These fixes generally agree with the calculated trajectories, but they are not precise because of the difficulty of picking a particular feature of the cloud which could be identified at two or more sites.

The most reliable fixes were obtained on the "leading edge" of various parts of the cloud which moved toward the observation network. At each site it was possible to say, during the first hour or so, which part of the cloud was farthest to the right or left of the field of view. The fixes obtained on these leading edges agreed quite well but never perfectly (see Fig. 3.10).

After a number of attempts to delineate the entire three-dimensional figure of the cloud by triangulation methods, the idea was abandoned. The reasons for this were, first, that the results appeared to be very unprecise because of the difficulty in telling where the cloud was and which features were being seen from various sites and, second, that the determinations based on the winds gave the same results much more easily. Therefore detailed three-dimensional studies were made only on certain features that were of special interest. Where these studies were made, they are described in detail in the individual write-up of each cloud.

Appendix C

Tentative Explanation of the Hover of an Atomic Cloud

C.1 OBSERVATIONS

At the time of writing (see footnote on page 78), the best observations available to the author are those from the Trinity tests.¹ (On the Sandstone tests the shock-wave cloud prevented observations² beyond about 2.4 sec.) In this case the top of the cloud rose to a height of 360 meters in the first second, apparently went down by 5 meters in the next second, rose to about 375 meters at 3 sec, and at 3.5 sec started upward at a steady rate of about 115 meters/sec.

Movies of some of the Operation Ranger shots, which were air bursts, indicate that for these tests, too, there was a certain period during which the cloud did not rise and that then it started upward quite suddenly.

C.2 GENERAL CONSIDERATIONS

The facts suggest that something was going on inside the cloud during the period of hovering and that the motion made itself suddenly visible when it pierced the top of the cloud. This seems entirely reasonable, and the purpose of this section is to indicate what might have taken place in the white-hot core of the fireball.

During the first few milliseconds the fireball is thought of as an isothermal sphere since the radiation density is such that only small temperature gradients could exist. After a second or so, however, the temperature has fallen considerably, and the flow of heat is such as to cause the outside of the cloud to be cooler than the center. Thus there is initially a spherically symmetrical temperature field with the gradient directed outward (part a of Fig. C.1).

At the same time there is a strong spherically symmetrical pressure field produced by the sudden expansion, and superimposed on this is the normal upward pressure gradient produced by gravity in the surrounding atmosphere (part b of Fig. C.1). It does not matter for the moment whether the spherical pressure field has a gradient inward or outward since it will not enter into the calculations that follow. This separation of the pressure field into two components, one the transient (spherical) field and one the permanent (linear) field, permits a mathematical analysis of the forces that cause the initial circulation inside the cloud.

Following the treatment of Bjerknes,³ we can say that the simple equation of motion of a particle in a fluid, neglecting viscous and Coriolis forces, is

$$\dot{\mathbf{v}} = -\alpha \nabla p + \mathbf{g} \quad (\text{C.1})$$

where $\dot{\mathbf{v}}$ = the vector acceleration

α = the specific volume (the reciprocal of the density)

\mathbf{g} = the acceleration of gravity

Then the total acceleration of the circulation around a circuit in the fluid, such as that shown in part c of Fig. C.1, is

$$\dot{c} = \oint \dot{\mathbf{v}} \cdot \delta \mathbf{c} \quad (\text{C.2})$$

which is the integral of the component of the acceleration of the fluid along the circuit. (We will take $\delta \mathbf{c}$ as being along the circuit in part c of Fig. C.1 in a clockwise direction.)

Substituting Eq. C.1 in Eq. C.2 and using Stokes's theorem,

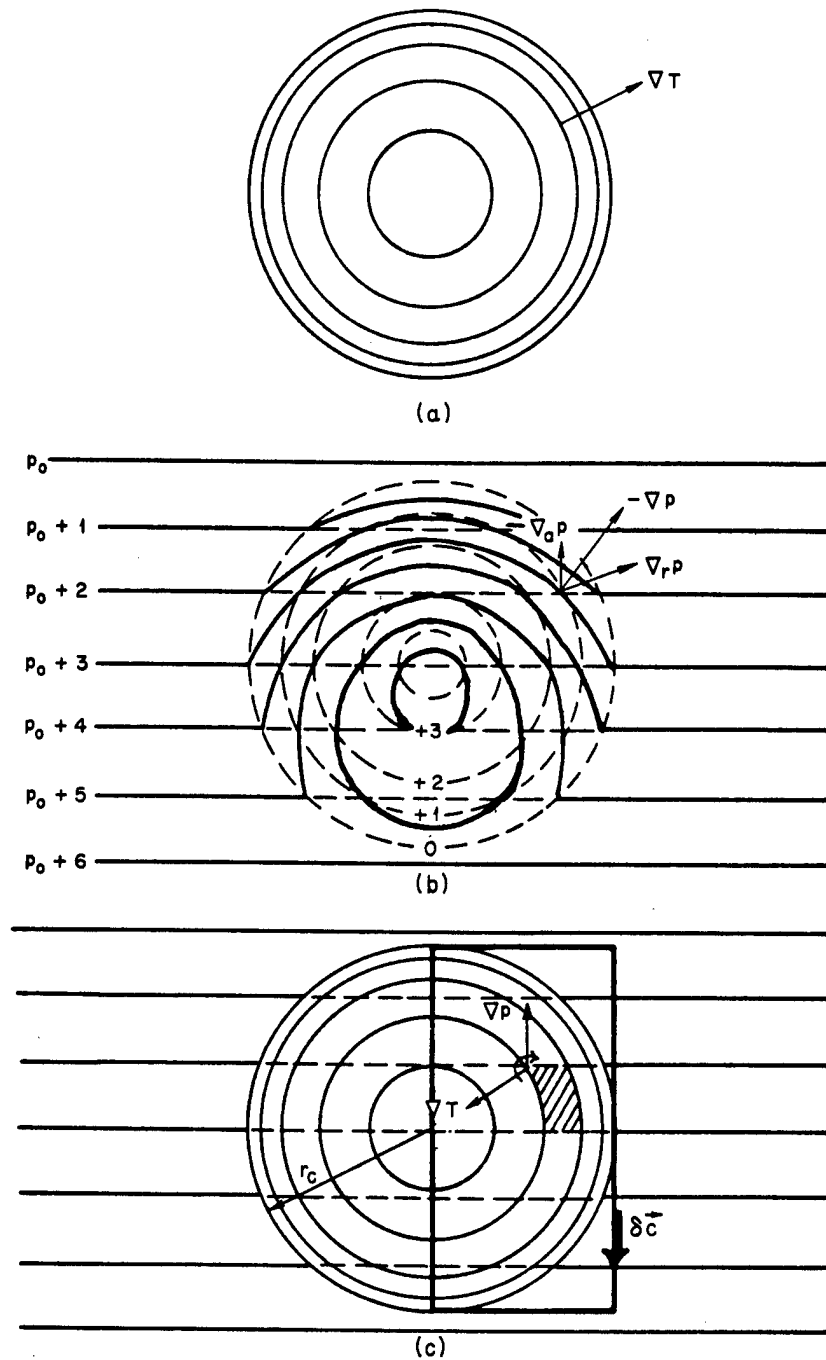


Fig. C.1 Schematic Representation of Fields of (a) Temperature, (b) Pressure, and (c) Circulation in the Fireball

$$\dot{c} = \int_a \nabla \times (-\alpha \nabla p) \cdot \delta a \quad (C.3)$$

where δa is an element of area, with a vector direction into the paper.

Substituting from the equation of state,

$$\alpha = \frac{RT}{p}$$

and rearranging, Eq. C.3 becomes

$$\dot{c} = R \int_a \nabla T \times \left(-\frac{\nabla p}{p} \right) \cdot \delta a \quad (C.4)$$

Now, as shown in part b of Fig. C.1, the total pressure gradient is

$$-\nabla p = -\nabla_r p - \nabla_a p$$

where $\nabla_r p$ is the purely radial vector, and $\nabla_a p$, the pressure gradient due to gravity in the surrounding atmosphere, is

$$-\nabla_a p = g \rho_a = \frac{g p_a \nabla z}{RT_a} \quad (C.5)$$

where T_a = the outside air temperature

R = the gas constant for air

∇z = a unit vector directed upward

In using the hydrostatic equation for the gravity pressure field inside the fireball, it is implied that there are no blast accelerations except those which are purely radial, and the effect of these can be thought of as being included in the $\nabla_r p$ field (which will disappear).

Substituting this in Eq. C.4,

$$\begin{aligned} \dot{c} &= R \int_a \nabla T \times \left(-\frac{\nabla_r p}{p_a} - \frac{\nabla_a p}{p_a} \right) \cdot \delta a \\ &= \frac{g}{T_a} \int_a \nabla T \times (\nabla z) \cdot \delta a \end{aligned} \quad (C.6)$$

where the radial pressure term disappeared because both it and ∇T are radial vectors. Using the fact that

$$\nabla z = \nabla x \times \nabla y$$

in a Cartesian coordinate system, we can substitute and expand in Eq. C.6 to get the final form

$$\dot{c} = -\frac{g}{T_a} \int_a (\nabla T \cdot \nabla x) \nabla y \cdot \delta a$$

$$\dot{c} = -\frac{g}{T_a} \int_a \frac{\partial T}{\partial x} \delta a \quad (C.7)$$

C.3 ESTIMATES OF THE INTERNAL ACCELERATIONS IN A FIREBALL

To see what sort of accelerations should exist inside the fireball, it is necessary to solve Eq. C.7 with a few numbers in it. It was already postulated that the temperature field was initially spherically symmetrical; therefore it is possible to write some reasonable expression for T as a function of r alone. Take

$$\begin{aligned} T &= T(r) = T_0 - Kr^2 \\ &= T_0 - K(x^2 + z^2) \end{aligned}$$

Then

$$\frac{\partial T}{\partial x} = -2Kx$$

and

$$\begin{aligned} \dot{c} &= \frac{gK}{T_a} \iint_a 2x \, dx \, dz \\ &= \frac{gK}{T_a} \iint_a d(x^2) \, dy \end{aligned}$$

The limits as seen from part c of Fig. C.1 are: x from 0 to r_c and y from $-r_c$ to $+r_c$, where r_c is the cloud radius. Thus

$$\dot{c} = \frac{2gKr_c^3}{T_a} \quad (C.8)$$

and the mean acceleration at each point in the path is

$$\begin{aligned} \bar{\nu} &= \frac{\dot{c}}{6r_c} = \frac{gKr_c^2}{3T_a} \\ &= \frac{g(T_0 - T_a)}{3T_a} \end{aligned} \quad (C.9)$$

It is interesting to note in passing that the resulting mean acceleration along the path, which includes the vertical axis of the cloud, is dependent only on the temperatures inside and outside and not on the dimensions of the cloud. This same general result would be obtained if we used the simple parcel method to calculate the upward acceleration of a cloud as a whole. The net buoyant force on a parcel of volume V and mean density $\bar{\rho}$ is

$$F = \rho_a Vg - \bar{p}Vg = \dot{v}\bar{p}V$$

where ρ_a is the density of the environment and \dot{v} is the upward acceleration. If the pressures are equalized between the parcel and the environment,

$$\begin{aligned}\dot{v} &= \frac{g(\rho_a - \bar{\rho})}{\bar{\rho}} = \frac{g[(1/T_a) - (1/\bar{T})]}{1/\bar{T}} \\ &= \frac{g(\bar{T} - T_a)}{T_a} = \frac{2}{3} g \frac{T_0 - T_a}{T_a}\end{aligned}\quad (C.10)$$

In other words, according to these results the internal acceleration along the axis of the fireball would be about the same as the mean upward acceleration of the fireball as a whole. However, this is not very helpful in explaining how the fireball hovers and then suddenly moves upward.

TABLE C.1 ACCELERATIONS INSIDE THE FIREBALL

Central temperature, T_0 (°K)	Vertical acceleration along the axis, \dot{v} , (meters/sec ²)
500	2.2
1000	7.7
2000	19
3000	30
5000	51

Table C.1 gives accelerations corresponding to some temperatures at the center (T_0), based on Eq. C.9. Recall now that the velocity with which the top of the Trinity cloud suddenly moved upward was about 115 meters/sec, and this was after 3 to 3.5 sec, implying a mean acceleration inside the cloud of about 35 meters/sec². Thus the range of internal temperatures generally considered for the 0.5- to 3-sec period is of the right order of magnitude to give this mean acceleration to the gas along the axis of the fireball.

This explains the appearance at the top after 3 sec of a mass of gas moving at the right

speed, but it does not explain why the top was stationary for so long. Two suggestions are made in the hope that they will eventually lead to the correct explanation. First, the internal circulation pattern started by the radial temperature gradient is such as to carry the hot central gas to the top. Here its loss by radiation is greatly increased, and therefore it contracts rapidly. Thus, although there is a mass convergence below the top, the contraction of the gas may be enough to prevent any motion of the boundary upward until the core has been "scavenged" by cooler air from below. The time and dimensions are about right for this since, with a mean acceleration of 35 meters/sec², the gas that was initially at the center of the cloud, the initial core, would reach the top of the cloud at about 3 sec. This must be the hottest gas, and therefore after this there would be an advection of cooler gas and hence less contraction at the top.

A second explanation may be that the whole fireball is actually beginning to collapse after about 1 sec owing to loss of heat by radiation and contraction of the gas. The dust skirt makes it hard to see what the sides of the fireball are doing in this period, but it may be that the contraction is taking place just fast enough to compensate for the upward acceleration of the center. Lest it be said that the fireball cannot be contracting, because it is observed to grow bigger as it moves above the dust skirt, recall that the rate of entrainment after the breakaway is very great, and therefore the expansion after it leaves the ground is due to this fact alone.

REFERENCES

1. J. E. Mack, July 16th Nuclear Explosion: Space-Time Relationships, Report LA-531, April 1946.
2. R. A. Houghten, Space-Time Relationships Measured from the Sandstone Photographs, Annex 7, Part II, Sandstone SS-28, Sept. 1, 1950.
3. V. Bjerknes, J. Bjerknes, H. Solberg, and T. Bergeron, "Physikalische Hydrodynamik," Verlag Julius Springer, Berlin, 1933.

Appendix D

Calculations on the Rise and Growth of an Atomic Cloud

D.1 ASSUMPTIONS AND DERIVATIONS OF THE EQUATIONS

Following Machta,¹ consider that the potential temperature* of the cloud at a height $z + dz$ is equal to the weighted mean value of the potential temperature of the cloud at z and the potential temperature of the air entrained between z and $z + dz$. Thus

$$\theta_{z+dz} = \frac{M\theta_z + \frac{\partial M}{\partial z} dz \theta'_z}{M + \frac{\partial M}{\partial z} dz} \quad (D.1)$$

where θ_z = the potential temperature inside the cloud

θ'_z = the potential temperature of the environment

M = the mass of the cloud

When the potential temperature of the environment is subtracted from this and terms of higher order infinitesimals are neglected in the expansion,

$$\theta_{z+dz} - \theta'_{z+dz} = (\Delta\theta)_{z+dz}$$

* The potential temperature of the air at a given level in the atmosphere is defined as the temperature which a parcel of air at that level would attain after being compressed adiabatically to sea-level pressure (1013.7 mb). This parameter is a convenient one to use in this type of calculation since it does not change when a parcel is lifted (without condensation of water vapor) from one level to another, i.e., it is a conservative property of a parcel of air undergoing vertical motion.

$$\theta_{z+dz} - \theta'_{z+dz} = \frac{M(\theta_z - \theta'_z) - M \frac{\partial \theta'}{\partial z} dz}{M + \frac{\partial M}{\partial z} dz} \quad (D.2)$$

and this can be rewritten as

$$\frac{\partial \Delta\theta}{\partial z} + \Delta\theta \frac{1}{M} \frac{\partial M}{\partial z} + \frac{\partial \theta'}{\partial z} = 0 \quad (D.3)$$

A solution for this differential equation is obtainable when the quantities $(1/M) dM/dz$ and $d\theta'/dz$ are constant, this solution being

$$(\Delta\theta)_z = \left[(\Delta\theta)_0 + \frac{\frac{\partial \theta'}{\partial z}}{\frac{1}{M} \frac{\partial M}{\partial z}} \right] \times e^{-\frac{1}{M} \frac{\partial M}{\partial z} (z-z_0)} - \frac{\frac{\partial \theta'}{\partial z}}{\frac{1}{M} \frac{\partial M}{\partial z}} \quad (D.4)$$

Equation D.4 was obtained by Machta and was then applied to the entire course of the Trinity cloud to determine its maximum height. However, notice that the quantities $(1/M) dM/dz$ and $d\theta'/dz$ must be constant throughout in order to make this meaningful. Moreover, to find the maximum height, a value for $(\Delta\theta)_0$ and $(1/M) \times dM/dz$ must be assumed, and these are not known at all well, as will be shown.

To avoid this objection, it seems more reasonable to use the same equation as is applied to a limited layer where $(1/M) dM/dz$ and $d\theta'/dz$ are really very nearly constant and to start from the top and work down toward the ground, since it can be assumed with some certainty

that $(\Delta\theta)_z$ at the point where the cloud stabilizes is very nearly zero. In other words, Eq. D.4 would be used stepwise, beginning at the top, and applied to successive layers small enough so that the constants really would be constants. The reverse equation is

$$(\Delta\theta)_{n-1} = \left[(\Delta\theta)_n + \frac{\frac{\partial\theta'}{\partial z}}{\frac{1}{M} \frac{\delta M}{\delta z}} \right] \times e^{-\frac{1}{M} \frac{\delta M}{\delta z} (z_n - z_{n-1})} - \frac{\frac{\partial\theta'}{\partial z}}{\frac{1}{M} \frac{\delta M}{\delta z}} \quad (D.5)$$

where $(\Delta\theta)_n$ is the potential difference at the top of the n th layer and z_n is the height of the top of the n th layer. One of the boundary conditions of the problem is then that the $(\Delta\theta)_n$ for the topmost layer, where the cloud stabilizes, must be nearly zero.

It would appear, from a superficial look at Eq. D.5, that the stepwise solution would lead explicitly to a value for the $(\Delta\theta)_0$ at the bottom of the last layer. However, it turns out that the equation cannot be solved for $(\Delta\theta)_{n-1}$ explicitly because the calculation of M (the cloud mass) depends on a knowledge of the temperature inside the cloud and hence of $(\Delta\theta)_{n-1}$ itself.

This can be seen more clearly when it is recalled that the observable feature of an atomic cloud is its volume, and this is related to the mass by

$$M = \rho V$$

Therefore

$$\frac{1}{M} \frac{\delta M}{\delta z} = \frac{1}{V} \frac{\delta V}{\delta z} + \frac{1}{\rho} \frac{\delta \rho}{\delta z} \quad (D.6)$$

The last term can be put in terms of temperatures alone by the hydrostatic equation in the form

$$\frac{1}{\rho} \frac{\delta \rho}{\delta z} = -\frac{g}{RT_a} - \frac{1}{T} \frac{\delta T}{\delta z} \quad (D.7)$$

where T is the temperature inside the cloud and T_a is the ambient temperature. The assumption is made here that during the rise the pressures

inside the cloud are approximately those outside at the same level. Thus

$$\frac{1}{M} \frac{\delta M}{\delta z} = \frac{1}{V} \frac{\delta V}{\delta z} - \left(\frac{g}{RT_a} + \frac{1}{T} \frac{\delta T}{\delta z} \right) \quad (D.8)$$

allowing one to calculate the mass change, but only if the temperature inside the cloud is known. Unfortunately the last term involving T is far from negligible.

D.2 CALCULATIONS OF TEMPERATURES INSIDE THE CLOUD

Equation D.5 does not give $(\Delta\theta)_{n-1}$ explicitly; therefore, to solve the equation numerically, it is necessary to use a method of successive approximations, so that the solution in each layer agrees with the value for $(1/T) dT/dz$. This process is laborious and inaccurate but serves to show the orders of magnitude of the result. These are shown in Table D.1 for Easy and George Shots, for which the most complete data exist.

It will be noted that the temperatures obtained for the lower two layers appear to be too large since at these temperatures (5000 to 10,000°K) the cooling process is far from adiabatic owing to the loss of heat by radiation. Therefore something must be wrong with the assumptions involved in the calculations. Loss of heat by radiation cannot be the factor overlooked since taking radiation into account would lead to the conclusion that one ought to have even higher initial temperatures in order to provide a balance in the heat budget.

The trouble undoubtedly lies in the assumption that the cloud as it rises cools dry adiabatically, i.e., without any release of heat by condensation of water vapor. This is especially not true in the Marshall Islands since the cloud clearly has a great deal of condensed water vapor in it. This release of heat of vaporization would explain why a cloud with an initial $(\Delta\theta)_0$ of only a few thousand degrees could rise to the tropopause with the observed expansion.

The entrainment of moist air into an ordinary cumulus cloud can be treated quantitatively,^{2,3} but the analysis would be very complicated if extended to the atomic cloud. This must probably be done before the rise can be described properly.

As a partial check on the observed values of the volume of the Greenhouse clouds (which are

TABLE D.1 EXPANSION AND ENTRAINMENT OF EASY AND GEORGE SHOTS

Height of layer (10 ³ ft)	Time center of cloud reached top of layer (min:sec)		Volume at top of layer (km ³)		$\frac{1}{V} \frac{dV}{dz}$ (10 ⁻⁵ m ⁻¹)		$\frac{1}{M} \frac{dM}{dz}$ (10 ⁻⁵ m ⁻¹)		$(\Delta\theta)_h$ at top of layer (°K)	
	Easy	George	Easy	George	Easy	George	Easy	George	Easy	George
0-5	0:26	0:16	0.75	1.35	102	45.0	155	?	9600	?
5-10	0:55	0:36	2.00	5.91	59.6	82.5	85	178	130	6500
10-15	1:25	0:56	3.77	13.6	40.0	51.5	39.9	73.8	66.2	433
15-20	2:10	1:20	8.2	24.8	48.5	38.2	46.2	38.5	26.4	140
20-25	3:05	1:50	14.8	43.4	37.4	35.8	30.1	30.0	13.6	39.3
25-30	4:25	2:24	28.1	65.5	41.0	26.6	32.4	18.7	4.4	25.2
30-35	6:15	3:05	43.0	98.7	27.5	26.4	18.8	18.4	-3	13.9
35-40		3:50		147		25.7		17.3		8.1
40-45		4:46		208		22.2		13.4		3.2
45-50		6:00		300		24.0		12.1		-3

TABLE D.2 EXPANSION OF TRINITY CLOUD

Height of center (10 ³ ft)	Time (sec)	Volume (km ³)	$\frac{1}{V} \frac{dV}{dz}$ (10 ⁻⁵ m ⁻¹)
0.82	3.5	0.051	
1.05	5.0	0.102	980
1.58	10	0.23	510
2.22	15	0.30	140
3.12	20	0.37	75
5.74	30	0.87	100
7.3	40	1.1	48
11.2	60	2.0	51
13.5	75	2.8	48

not very accurately known for the early times), Table D.2 shows some values for Trinity Shot, where the early observations were probably as good as could be obtained since there was no shock-wave cloud to obscure the fireball.

It appears that the agreement here is fairly good with the Greenhouse values after the center moves above about 5000 ft. There is no way to check the Greenhouse values from Project 4.1B pictures for the very early times. The large initial values for $(1/V) dV/dz$ obtained at Operation Trinity should be checked in some

way because they may be misleading since the dust skirt or "torus" was included in the volume calculations. The dust skirt did mark the boundary of the visible cloud, but the theory concerns itself with the volume of the heated air associated with the fireball itself, and this cannot be seen except at the top.

One conclusion to be drawn, then, is that such a temperature analysis as this should not be carried below about 5000 ft until better early volume observations are available.

A second conclusion is that, whereas a dry adiabatic analysis gives temperatures inside the cloud which are too high in the Marshall Islands clouds, it might work quite well in some of the Nevada clouds, where there is much less moisture.

REFERENCES

1. Lester Machta, Entrainment and the Maximum Height of an Atomic Cloud, Bull. Am. Meteorol. Soc., 31: 215-216 (1950).
2. C. E. Palmer, The Precipitation and Formation Movements of Clouds in the Central Pacific, Greenhouse Report, WT-40(Ref), 1951.
3. H. Stommel, Entrainment of Air into a Cumulus Cloud II, J. Meteorol., 8: 127-129 (1951).

Part III

CLOUD-TRACKING PHOTOGRAPHY

Edgerton, Germeshausen & Grier, Inc.
Boston, Massachusetts

July 1951

Cloud-tracking Photography

1 DOCUMENTATION OF THE CLOUD

The formation, rise, and dispersion of the cloud for a nominal 20 min after zero was photographed with aerial type K cameras from the north and south stations on Eniwetok and the Back Bay station on Rigili (herein referred to as Stations 191, 190, and 192, respectively, Fig. 1). In addition, one Mitchell camera at Station 190 and one at Station 191 provided motion-picture coverage up to 1 hr after zero.

The photographs are of three types: 9- by 9-in. size and 5- by 5-in. size taken on aerial roll film and 35-mm size taken on motion-picture 1000-ft rolls. The aerial roll film was processed at Lookout Mountain Laboratory, Hollywood, Calif. The 35-mm film was processed by Edgerton, Germeshausen & Grier, Inc. (EG&G). The processed film was then delivered to William W. Kellogg, Institute of Geophysics, University of California, Los Angeles, Calif., of the cloud-physics group for analysis, after which the film was routed to EG&G.

Figures 2 to 5 show the fields of view for the eighteen 9- by 9-in. K-8A-B cameras, in three groups of six each, one group at each triangulation station. Three 5- by 5-in. K-24 cameras, Fig. 6, one at each triangulation station, were used to augment the coverage of the K-8 cameras. Each group of six K-8 cameras, as shown in Figs. 7 and 8, had a total overlapped field of view sufficient to cover the conduct of the cloud drifting for 20 min in a 20-knot wind of any direction and up to an altitude of 60,000 ft. The K-24 camera was set at an angle that covered the cloud at the early stages of growth (0 to 7 min). This was necessary on predawn shots because of the exposure-time limitations of the K-8 cameras. The 35-mm Mitchell motion-

picture cameras (Fig. 9) were used to obtain general documentary information of the cloud and adjacent areas. A closely coordinated tape recording was made by a meteorologist directing the Mitchell operator's coverage of the phenomenon.

2 CALIBRATION

The aerial cameras were focalscoped and tested by EG&G and were oriented in the field to ± 1 min of arc by sighting into the camera lens at the focal plane with a Wild T-1 theodolite.

3 ASPECTS OF CLOUD-TRACKING ANALYSIS

To utilize these pictures for cloud-volume determinations, it is necessary to be able to determine scale factors for each camera, which means determining effective focal length and gross distortions in the laboratory and determining cloud range from the photographs by triangulation techniques. The triangulation process involves knowing the space orientation of the "optical axis." The field note data for each shot, giving the elevation and azimuth settings of the K-series cameras, refer to this axis. Figure 10 shows the schematic positioning of the two banks of three K-8 cameras. The difference between ψ and ϵ is due to a $\frac{1}{2}$ -in. intelligence strip across the bottom of the film plate (a 9- by 8.5-in. image plane results instead of a 9- by 9-in. image plane).

The position on the image plane from which the theodolite measurements are referenced is obtained by drawing intersecting lines from the fiducial markers on the edge of the image plane.

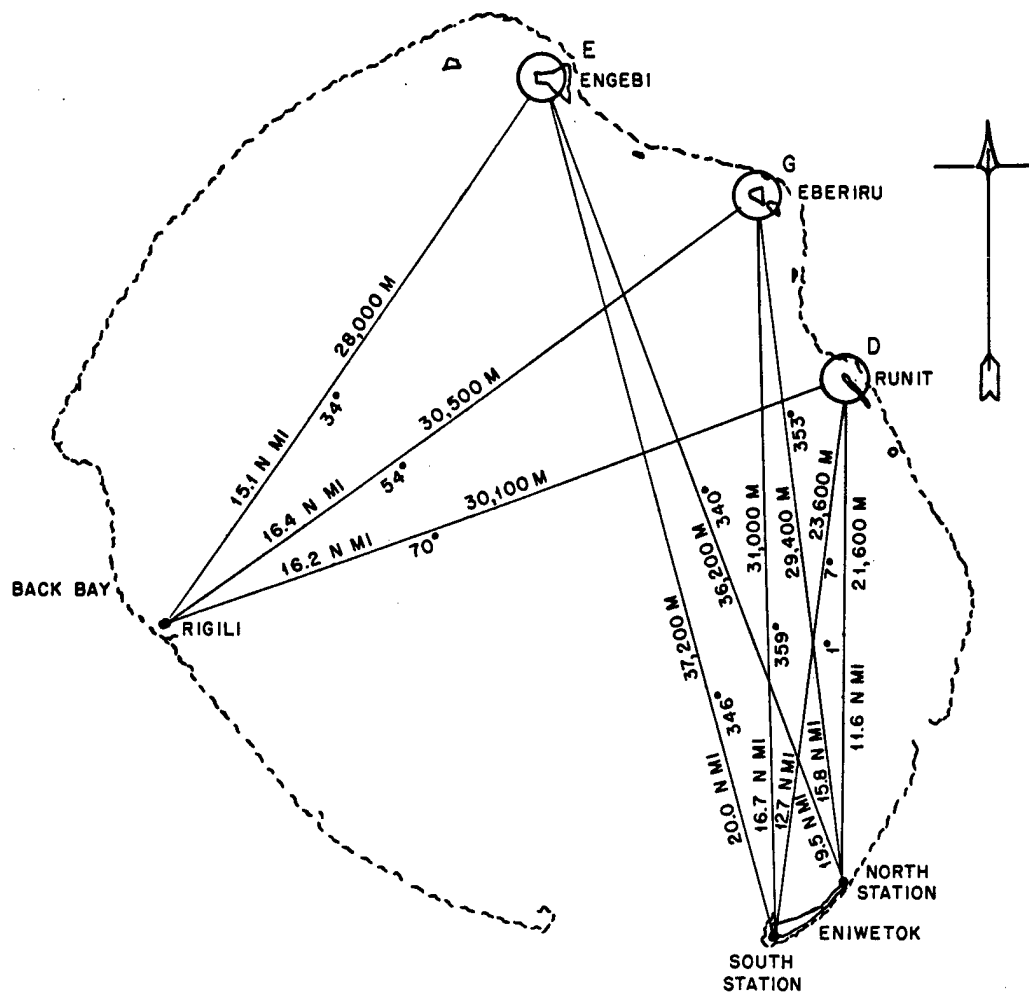


Fig. 1 Cloud-tracking Stations

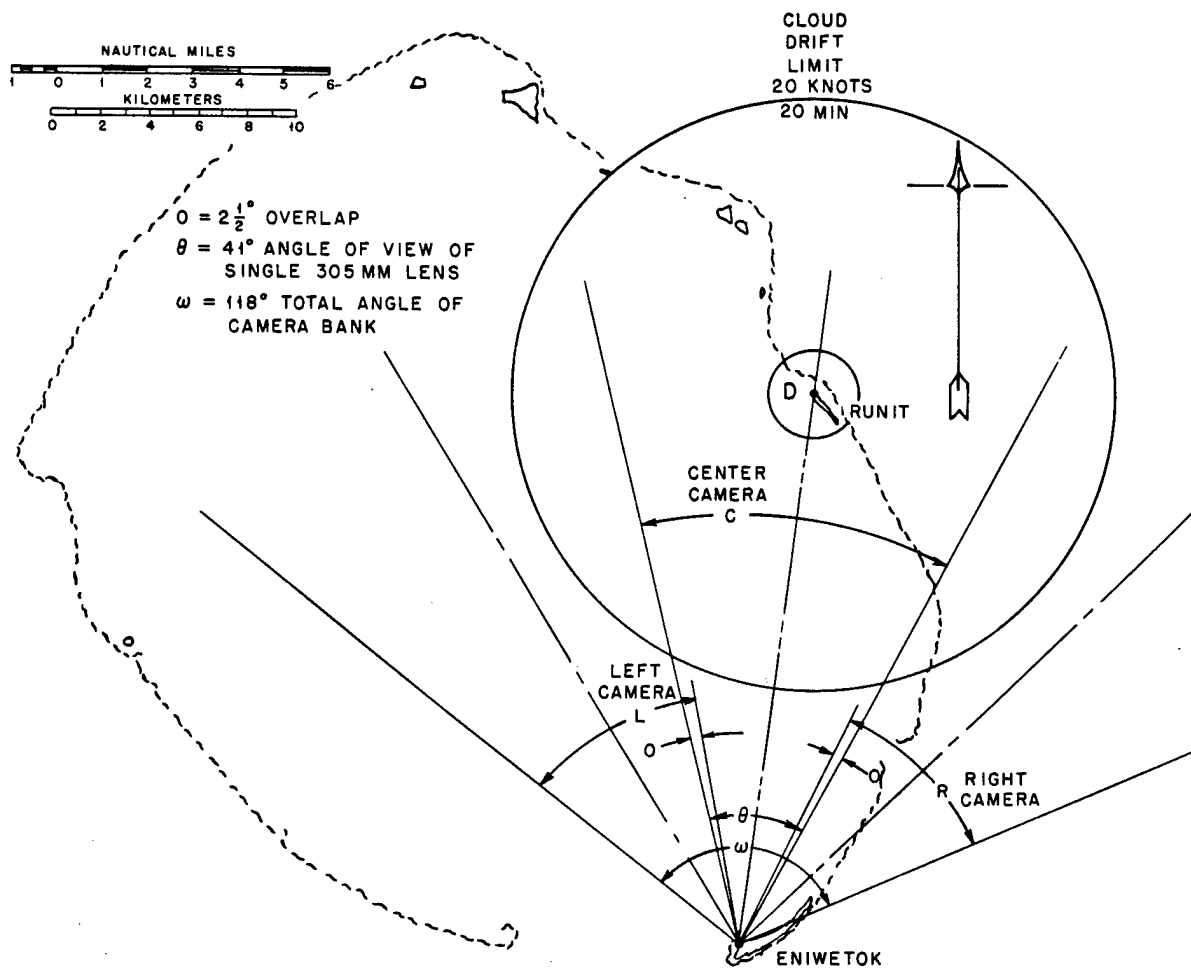


Fig. 2 Horizontal Angular Coverage

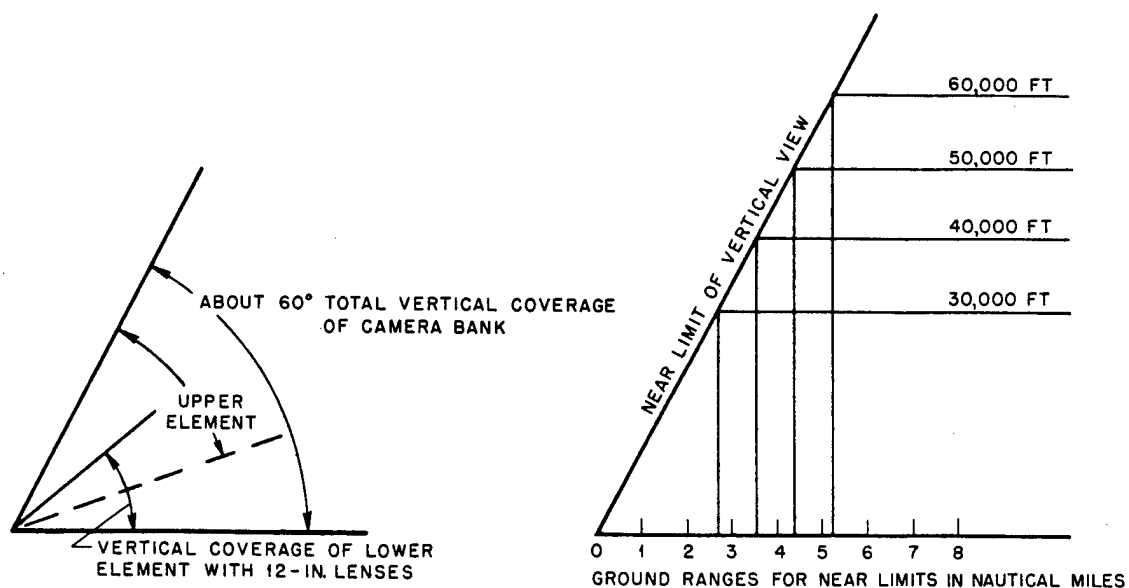


Fig. 3 Vertical Angular Coverage

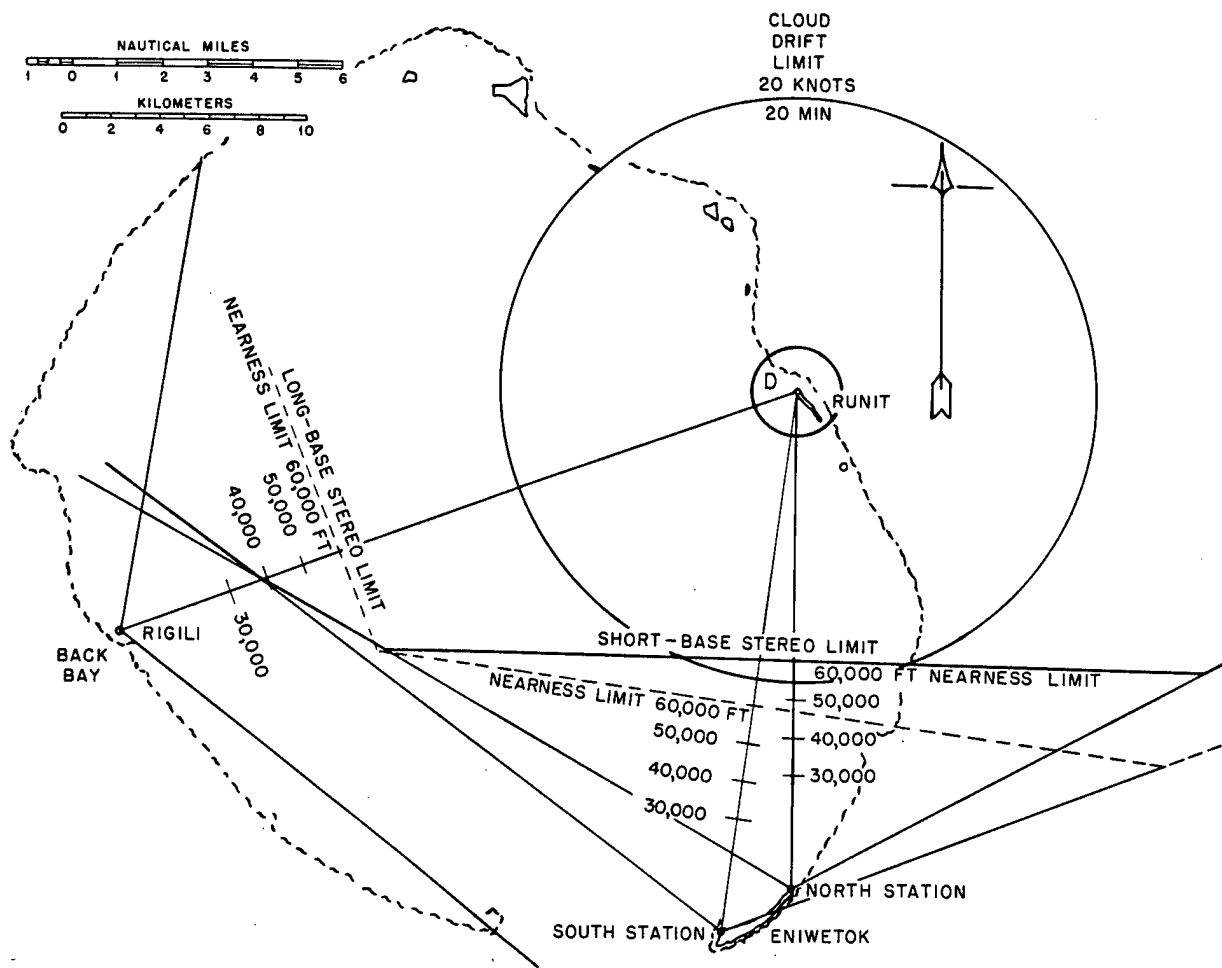


Fig. 4 Stereo Nearness Limits

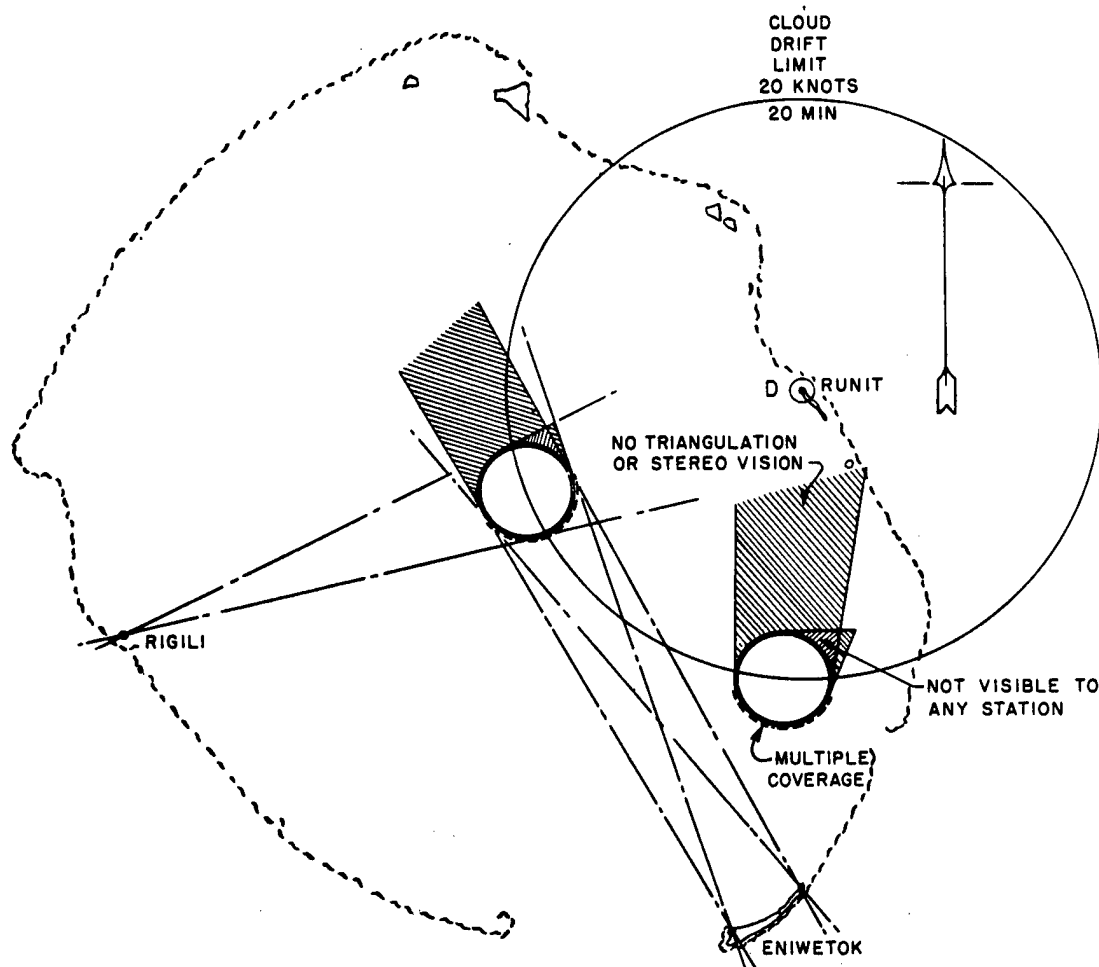


Fig. 5 Composite Visibility Diagram

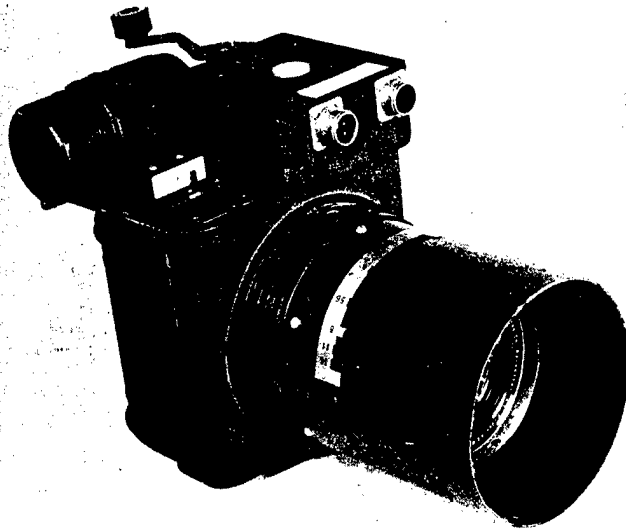


Fig. 6 K-24 Camera

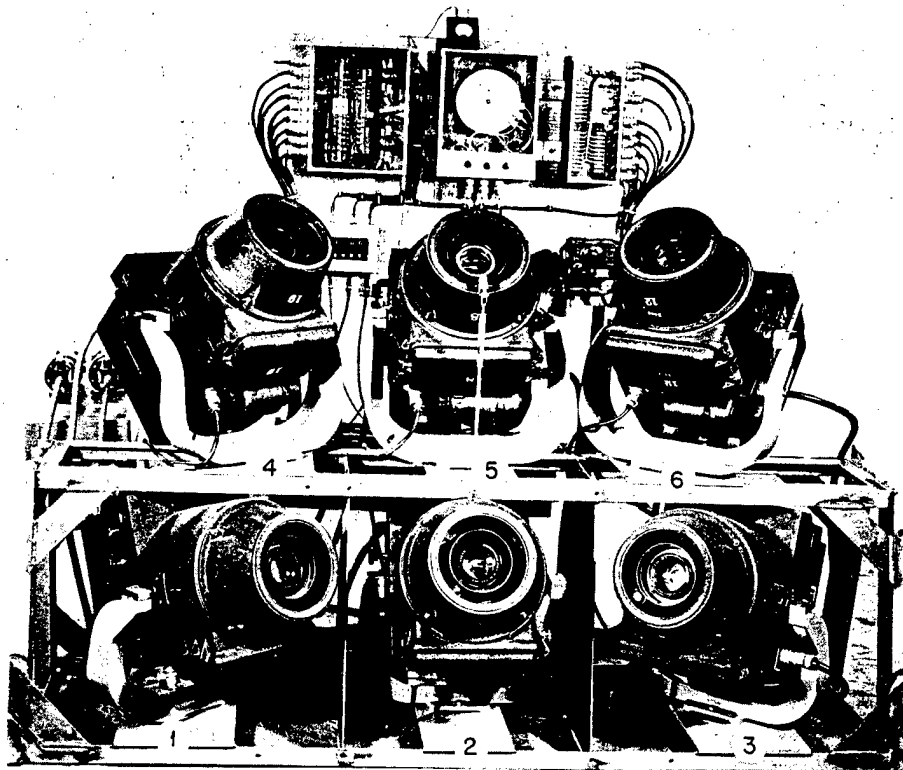


Fig. 7 K-8A-B Camera Station

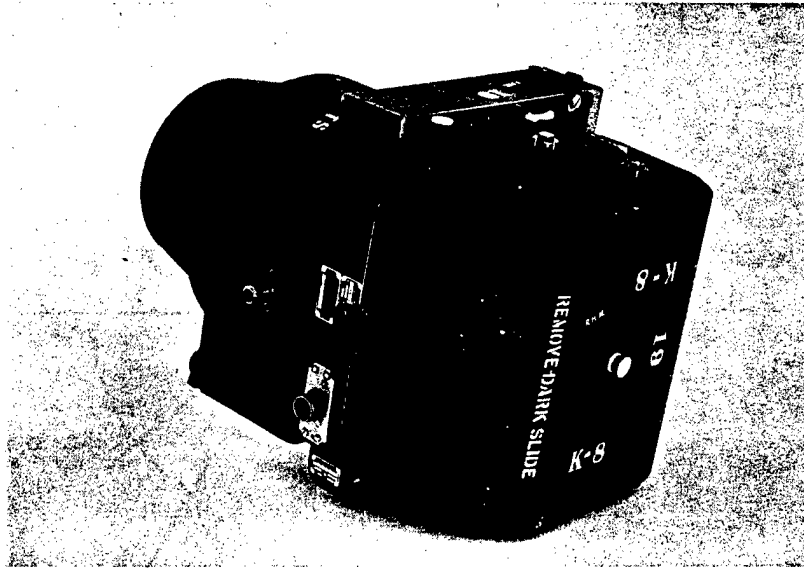


Fig. 8 K-8A-B Camera

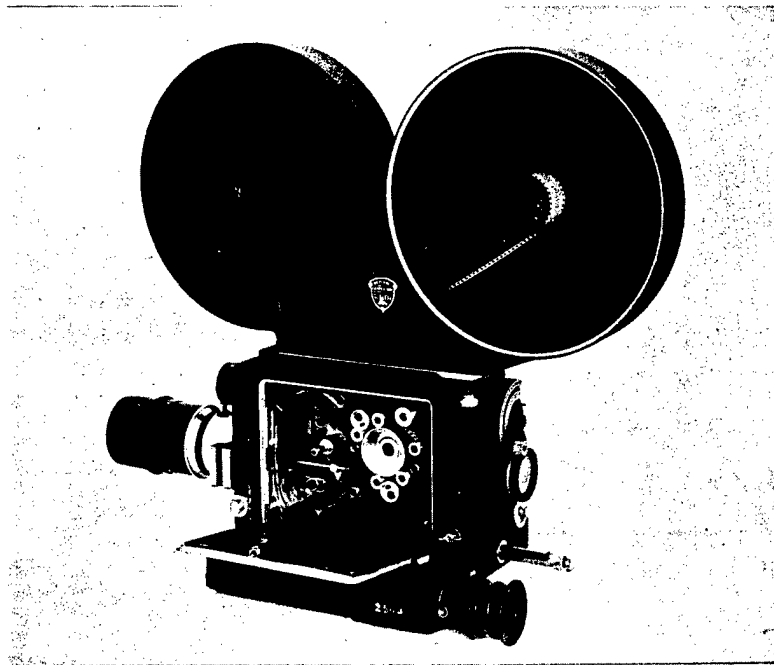


Fig. 9 Standard-speed Mitchell 35-mm Camera

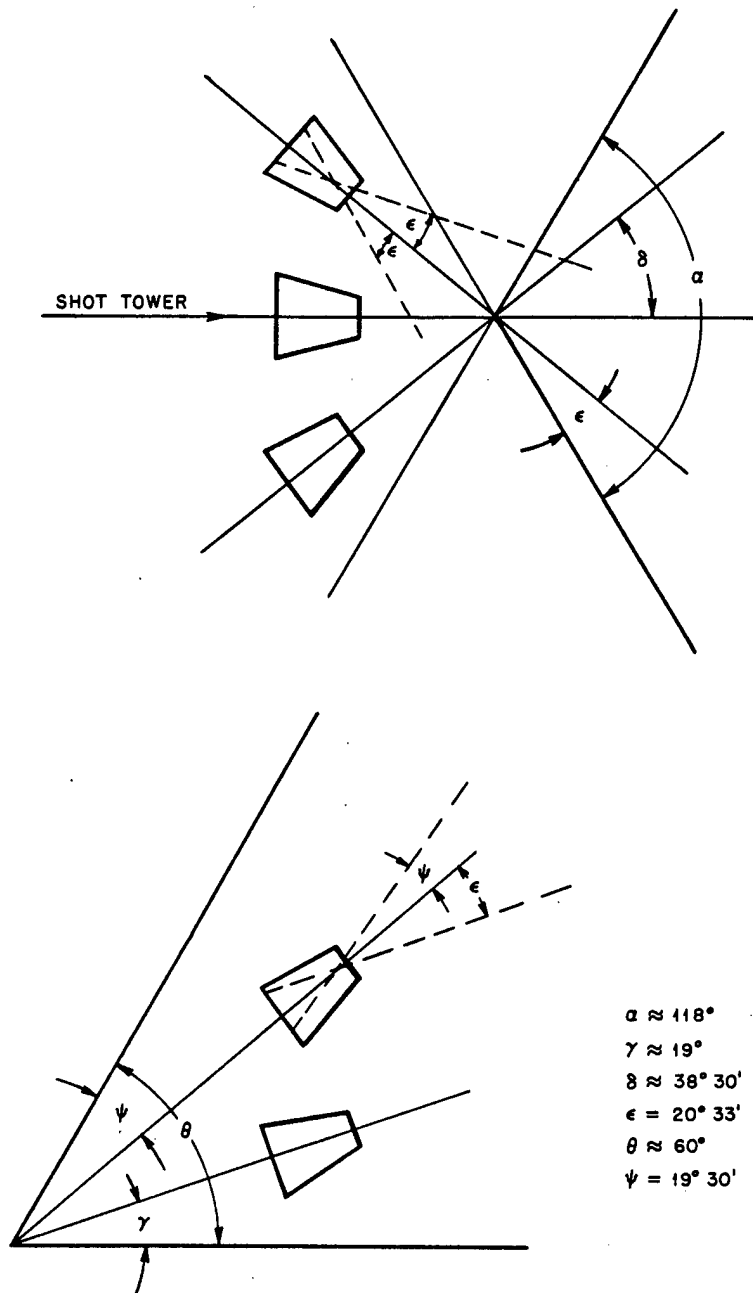


Fig. 10 Positioning of Camera Banks

The rack positions of the K-8 cameras are shown in Fig. 7.

The K-8 cameras have a clock image on each negative which provides an accurate time relation. The K-24 photographs can be evaluated by using the fireball image as zero and thereafter using the intervalometer setting as a time base.

The length of the base line between Station 190 and Station 191 is 11,843.47 ft. The direction of this line is south 54°44'41" west. The specific location of shot towers and triangulation stations can be determined from the following Holmes & Narver drawings:

Sheet No.	F.S. 75
Sheet No.	F.S. 92
Sheet No.	13A-211
Sheet No.	13A-212
Sheet No.	13A-213
Sheet No.	13A-214
Sheet No.	13A-215
Field book 106	H.N. 2085

The azimuth settings of the cameras at Stations 190 and 191 are with reference to the zero tower for each shot. The cameras at Station 192 have their azimuth settings with reference to true north. The elevation settings for the cameras are with respect to the horizon.

4 OPERATION

The exact manner of photographing each shot was determined by the time of the shot, the weather, and the lighting. A detailed discussion of each shot appears in Sec. 5. Stations 190 and 191 were manually operated, each having two photographers and one meteorologist. Station 192 was automatically operated by means of a specially designed clock. Figures 11 and 12 give the circuitry employed at these stations. Station 192 (Fig. 13) differed also from Stations 190 and 191 in that it had its protective canvas door secured by a bomb rack, which released the canvas at the time of the shot.

5 DATA AND DISCUSSION

5.1 Dog Shot

The low cumulus cloud coverage at the time of the shot completely obscured the primary mass.

The K-8 cameras in rack positions 1, 2, 3, and 5 at each triangulation station, oriented for the early stages of cloud development, were set at an f/5 lens opening, and the mechanical shutter system was deactivated. The intervalometer that controlled the interval at which the pictures were taken was set at 15 sec. This resulted in a 13-sec exposure, the remaining 2 sec being used for the transfer of film by the film drive motor. The extremely low level of light on this predawn shot permitted the shutterless operation, and the 2-sec movement of the film in comparison to the 13 sec in which the film was stationary resulted in no marked blurring of the negative. This deactivating of the shutter on the K-8 cameras was necessary since $\frac{1}{50}$ sec is the slowest speed at which the shutter can be operated. The K-8 cameras in rack positions 4 and 6 at each station were set at $\frac{1}{50}$ sec. These positions were oriented for the later stages of cloud drift.

The K-24 cameras at each triangulation station were set in such a manner that the focal-plane shutter would remain open for 8 sec and remain closed for the next 8 sec. A B-7 intervalometer supplied the signal every 8 sec.

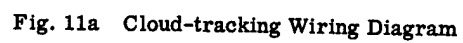
The Mitchell cameras at Stations 190 and 191 were operated at 8 frames/sec. The later stages of the cloud development were manifest occasionally through the omnipresent mass of closely knit clouds as scattered brownish-orange streaks which the Mitchell cameras tracked.

The complete technical data on Dog Shot are included in the field book. Tables 1 and 2 give data on airborne cloud-tracking photography.

5.2 Easy Shot

The prevailing sky condition for cloud tracking was excellent, and the entire coverage, after the primary mass cleared a low bank of cumulus clouds near the shot tower, was free from transient cloud obstructions.

The shutters of the K-8 cameras at all three stations were operated in the same manner as on Dog Shot for the first 5 min. The K-8 cameras in rack positions 1, 2, 3, and 5 after the first 5 min were changed from a 15-sec intervalometer setting (13-sec exposure) to a 6-sec intervalometer setting (4-sec exposure). The K-8 cameras in rack positions 4 and 6 were operated with the shutters in time at $\frac{1}{50}$ -sec exposures.



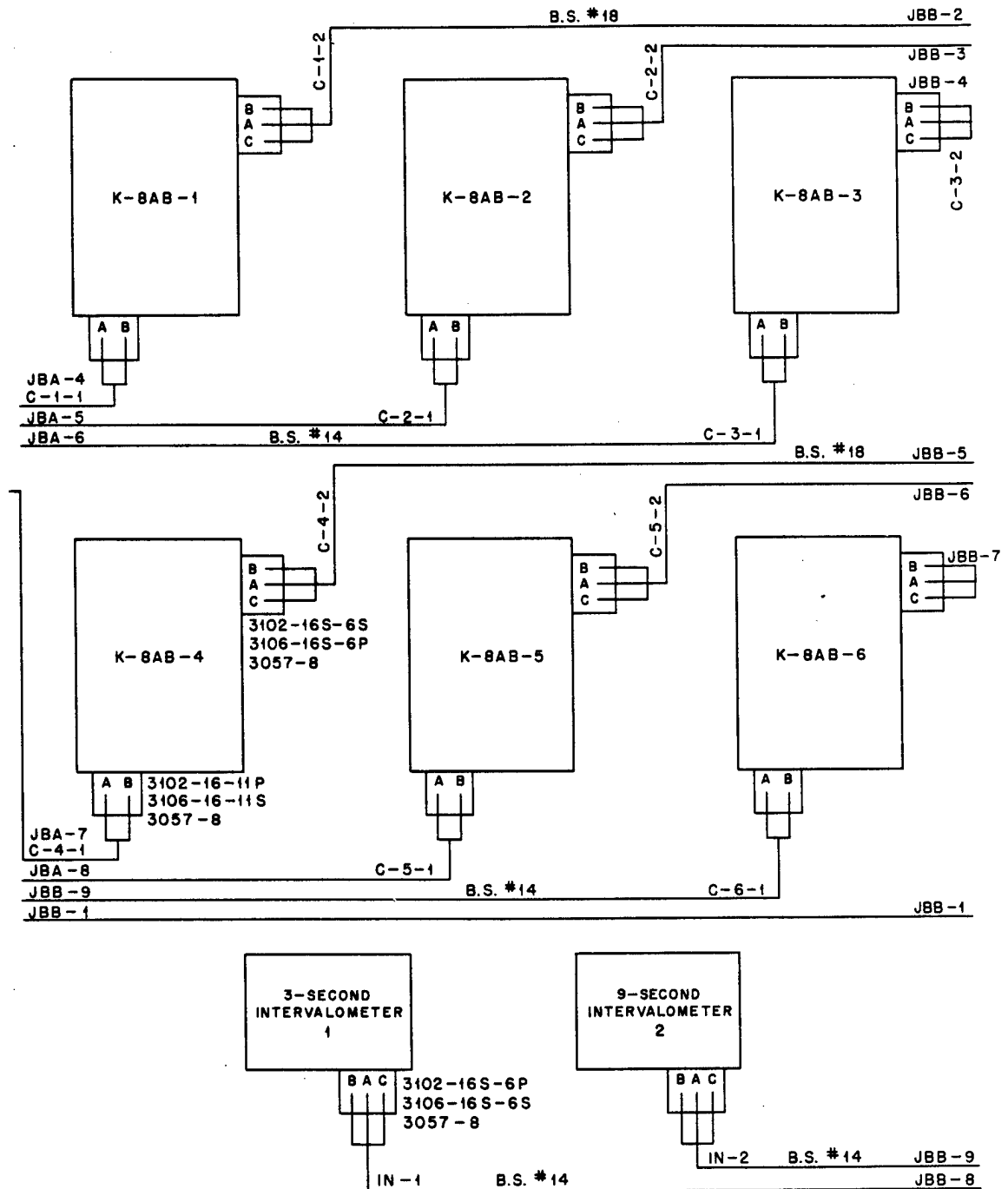


Fig. 11b Cloud-tracking Wiring Diagram

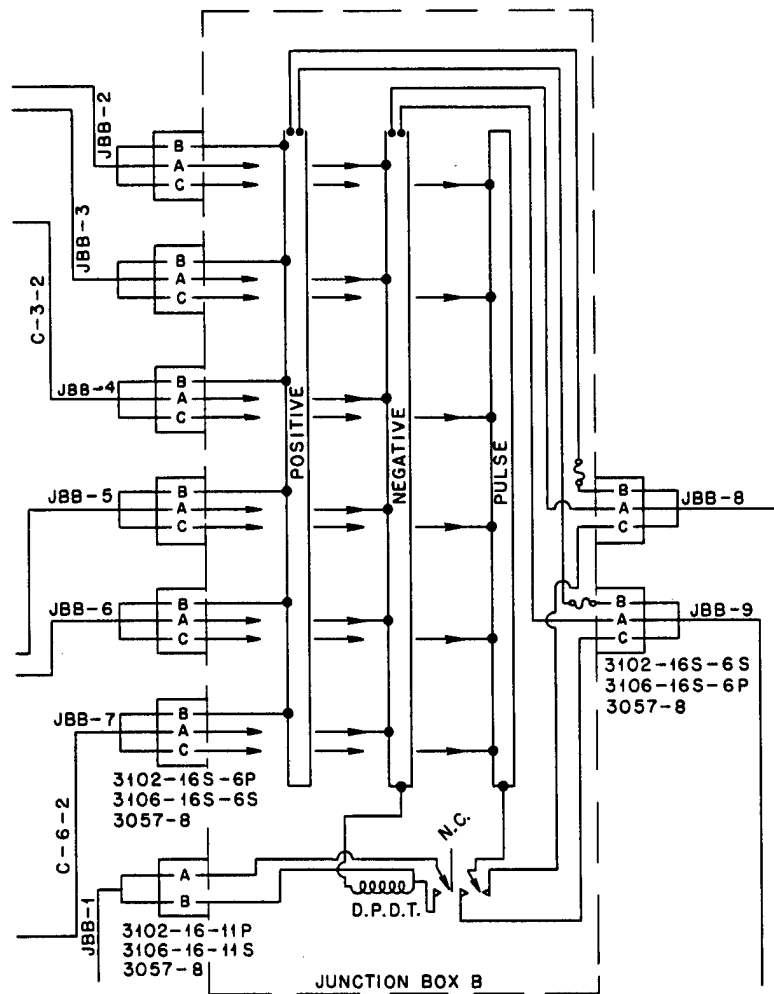
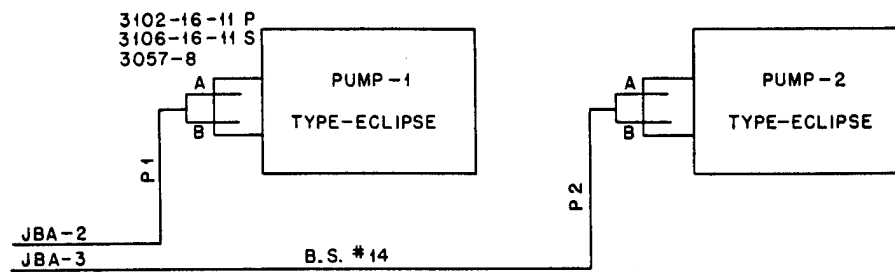


Fig. 11c Cloud-tracking Wiring Diagram

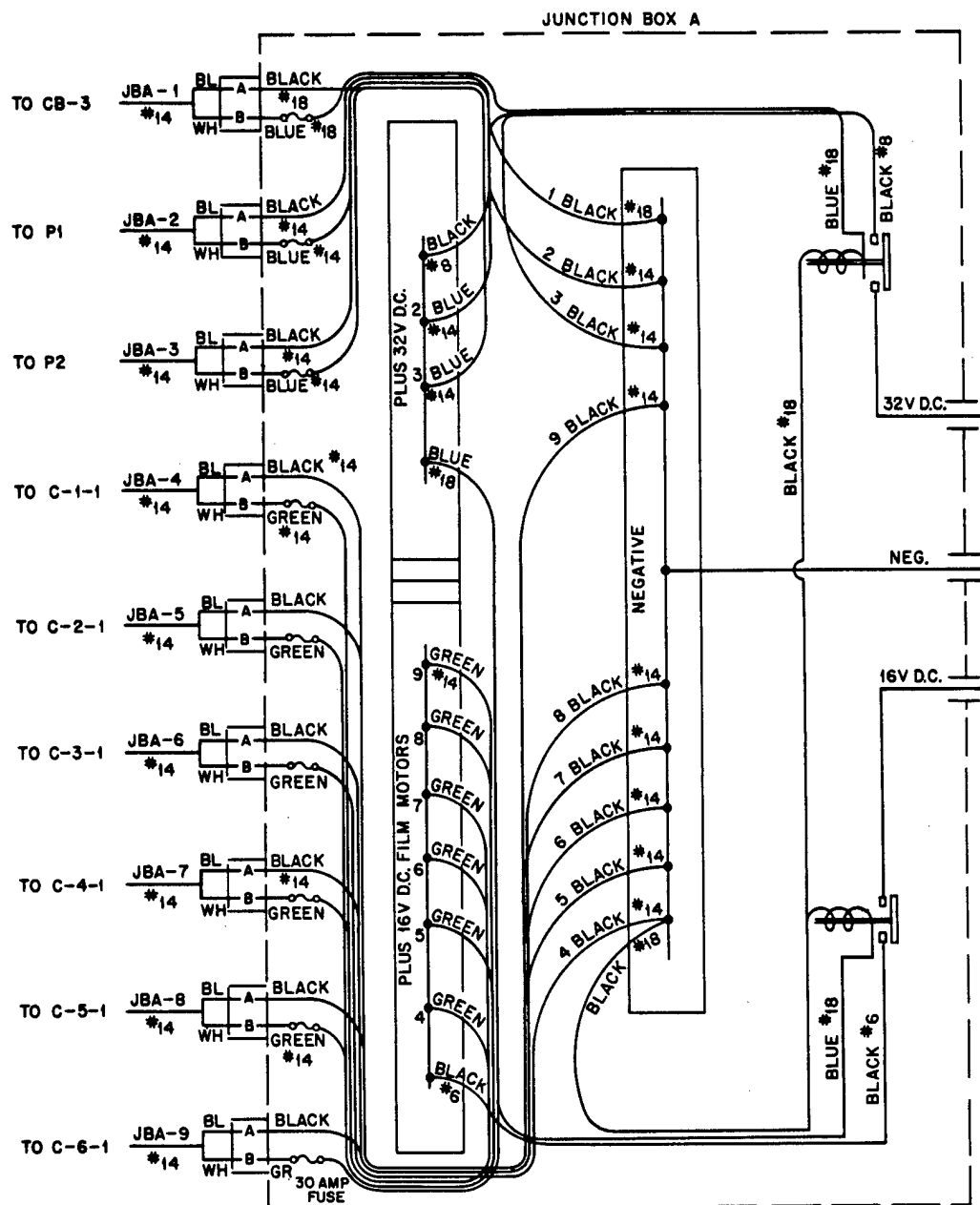


Fig. 12a Cloud-tracking Control Panel

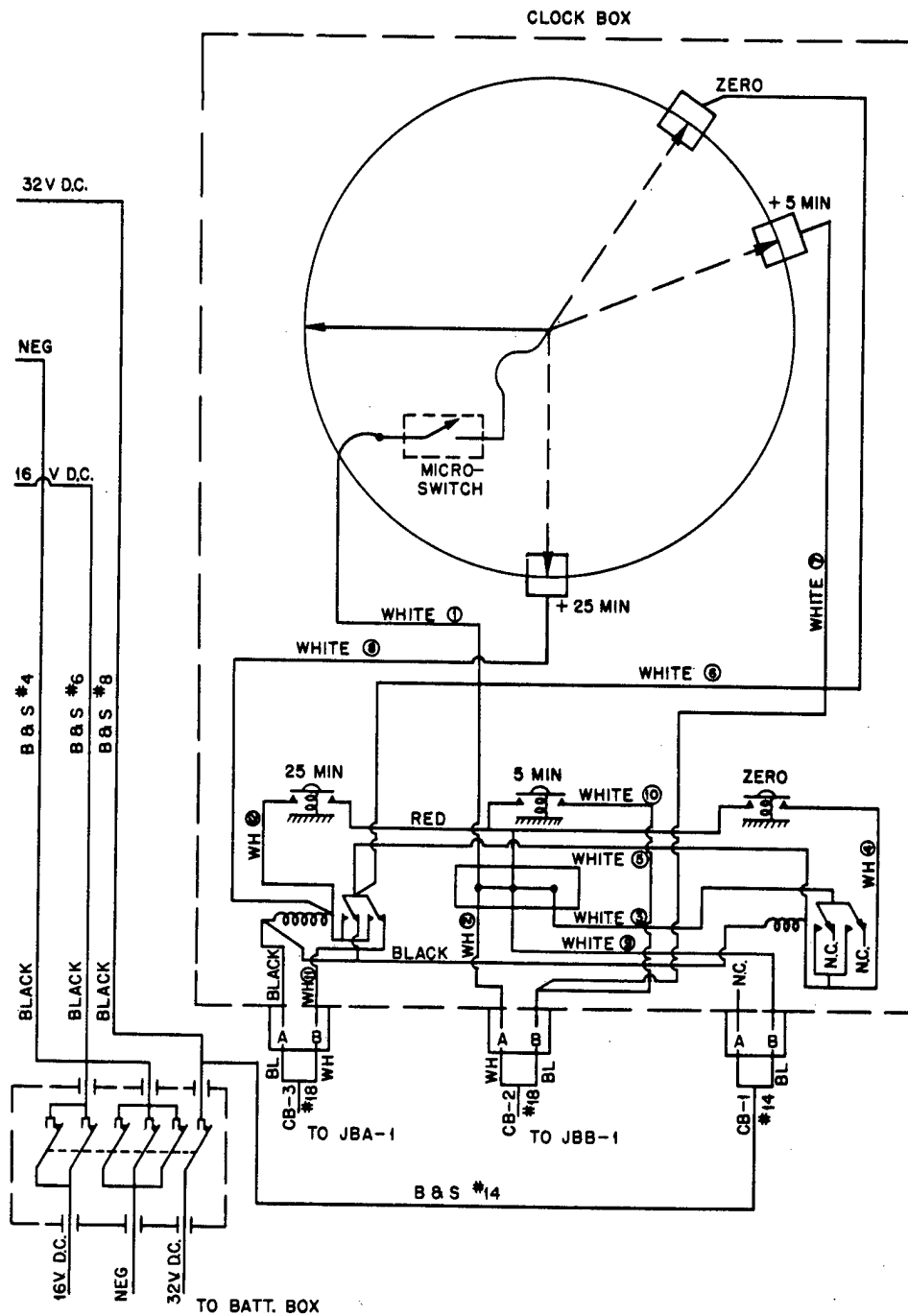


Fig. 12b Cloud-tracking Control Panel

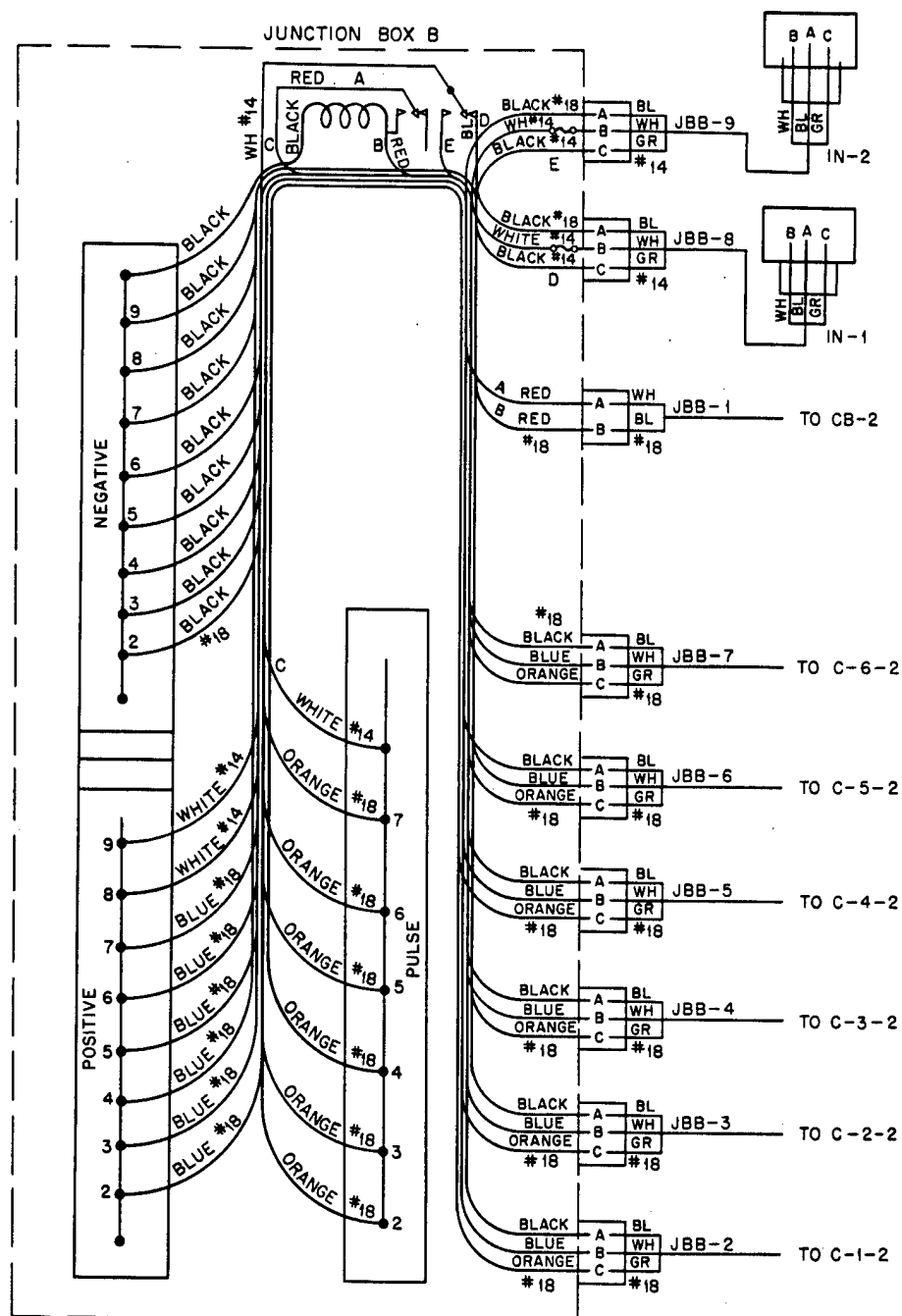


Fig. 12c Cloud-tracking Control Panel

TABLE 1 AIRBORNE CLOUD-TRACKING PHOTOGRAPHY, DOG SHOT (Left waist position, B-50 No. 290 Grace, 35-mm A-6 cameras, yellow filter)

EG&G film code RD-I:::A	Local time	Mag. No.*	Lens stop	Focal length (in.)	Aircraft heading (deg)	Film type	Footage Begin	End
324	0650	7B	f/2.5	2	14	S-2	400	270
324		7B	f/2.5	1	308	S-2	270	175
324		7B	f/2.8	1	243	S-2	175	50
324		7B	f/2.8	1	243	S-2	50	0
315		2A	f/2.8	1	128	S-2	400	
329		5B	f/2.5	1	128	Color	275	230
315		2A	f/4.0	1	128	S-2		290
329		5B	f/2.8	1	47	Color	230	170
315	0715	2A	f/5.6	1	Turn	S-2	290	218
315	0721	2A	f/5.6	1	307	S-2	218	42
315	0726	2A	f/5.6	4		S-2	42	0
329	0735	5B	f/5.6	1		Color	170	
329	0736	5B	f/5.6	1		Color		100
329	0737	5B	f/5.6	1		Color	100	75
329	0738	5B	f/5.6	1		Color	75	40
329	0741	5B	f/5.6	1		Color	40	0

*Magazines 7B and 2A, camera A-6 10, 48 frames/sec; magazine 5B, camera A-6 2, 24 frames/sec, A-2 filter.

TABLE 2 AIRBORNE CLOUD-TRACKING PHOTOGRAPHY, DOG SHOT* (Left waist position, B-50 No. 340 Frances, 35-mm camera No. A-6 6, 24 frames/sec, yellow filter; all bursts panned from left to right)

Burst No.	Local time		Burst No.	Local time	
	Start	Stop		Start	Stop
1	0703	0703:20	14	0724:12	0724:30
2	0705:10	0705:18	15	0725:12	0725:25
3	0707:45	0707:52	16	0726:33	0726:45
4	0710:30	0710:45	17	0727:32	0727:43
5	0711:15	0711:35	18	0728:40	0728:55
6	0712:08	0712:20	19	0729:05	0729:19
7	0712:55	0713:08	20	0730:25	0730:40
8	0714:05	0714:15	21	0731:35	0731:55
9	0715:25	0715:45	22	0733:00	0733:17
10	0717:30	0717:45	23	0737:02	0737:37
11	0720:55	0721:25	24	0744:23	0744:35
12	0722:02	0722:18	25	0754:25	0754:38
13	0723:15	0723:34			

*EG&G film code RD-I:::A327 in magazine No. 6A, S-2 film type; EG&G film code RD-I:::A328 in magazine No. 6B, S-2 film type; lens stop and aperture as required; footage not specified; for aircraft heading vs time, see flight log.

TABLE 3 AIRBORNE CLOUD-TRACKING PHOTOGRAPHY, EASY SHOT
(Left waist position, B-50 No. 290 Frances, 35-mm A-6
cameras, 24 frames/sec, yellow filter)

EG&G film code RE-I:::A	Local time	Mag. No.*	Lens stop	Focal length (in.)	Aircraft heading (deg)	Film type	Footage Begin End	
578	0630	9A	f/2.8	1		S-2	400	375
578	0633	9A	f/5.6	4		S-2	375	300
578	0635	9A	f/4	1		S-2	302	295
578	0638	9A	f/4	1		S-2	295	275
578	0640	9A	f/5.6	1		S-2	275	220
578	0642	9A	f/5.6	1		S-2	220	150
578	0644	9A	f/5.6	2		S-2	150	120
578	0646	9A	f/5.6	2		S-2	120	40
578	0620	9A	f/5.6	2		S-2	40	20
578	0652	9A	f/5.6	1	339	S-2	20	0
579	0655	9B	f/5.6	1	270	S-2	400	370
579	0700	9B	f/8	1	270	S-2	370	310
579	0702	9B	f/8	1	196	S-2	310	300
579	0704	9B	f/22	1	196	S-2	300	290
579	0706	9B	f/11	1	133	S-2	290	275
579	0708	9B	f/11	1	133	S-2	275	260
579	0710	9B	f/11	1	052	S-2	260	245
579	0712	9B	f/11	1	339	S-2	245	230
579	0714	9B	f/16	2	339	S-2	230	195
579	0716	9B	f/16	2	339	S-2	195	145
579	0718	9B	f/16	2	270	S-2	145	60
579	0720	9B	f/16	2	270	S-2	60	0

*Magazine No. 9A on camera No. A-6 6; magazine No. 9B on camera No. A-6 7.

UNCLASSIFIED

TABLE 4 AIRBORNE CLOUD-TRACKING PHOTOGRAPHY, EASY SHOT
(Left waist position, B-50 No. 340 Grace, 35-mm
A-6 cameras, 24 frames/sec)

EG&G film code RE-I:::A	Local time	Mag. No.*	Lens stop	Aircraft heading (deg)	Film type	Footage Begin End	
576	0635	14A	f/2.8†	267	S-2	140	Jam
575	0636	13B	f/2.8	267	S-2	400	338
575	0640	13B	f/4.0	179	S-2	338	270
575	0642	13B	f/4.0	179	S-2	270	250
575	0643	13B	f/4.0	122	S-2	250	200
569	0651	3A	f/2.8	046	Color	225	175
575	0652	13B	f/4.0	046	S-2	200	160
575	0658	13B	f/5.6	339	S-2	160	100
569	0657	3B	f/2.8	339	Color	175	145
575	0704	13B	f/8.0	259	S-2	100	70
569	0703	3A	f/5.6	259	Color	145	110
575	0706	13B	f/8.0	190	S-2	70	40
575	0712	13B	f/16.0	‡	S-2	40	30
575	0712	13B	f/16.0	120	S-2	30	End

*A-2 filter used with magazine No. 3A, camera No. A-6 11; yellow filter used with other magazines, camera No. A-6 12.

†One-inch focal length.

‡Into sun, doing left turn.

TABLE 5 AIRBORNE CLOUD-TRACKING PHOTOGRAPHY, GEORGE SHOT
(Left waist position, B-50 No. 340 Grace, 35-mm camera
No. A-6 11, 24 frames/sec, K-2 filter)

EG&G film code RG-I:::A	Local time	Mag. No.	Lens stop	Focal length (in.)	Aircraft heading (deg)	Film type	Footage Begin End	
754	0935	13A	f/8	1	338	S-2	400	250
753	0939	4A	f/4	1	280	Color	250	150
754	0941	13A	f/11	1	226	S-2	250	220
753	0943	4A	f/5.6	1	226	Color	150	100
753	0946	4A	f/5.6	2	176	Color	100	75
754	0947	13A	f/11	2	176	S-2	220	200
753	0950	4A	f/5.6	2	138	Color	75	40
753	0952	4A	f/5.6	1	138	Color	40	0
754	0954	13A	f/16	2	138	S-2	200	150
754	0955	13A	f/16	1	138	S-2	150	0

UNCLASSIFIED

The shutters of the K-24 cameras were supplied pulses every 2 sec by the B-7 intervalometers so that the shutters were open for 2 sec and closed for 2 sec. This procedure corresponds to a picture every 4 sec for each K-24 camera.

The light level was a great deal higher for the predawn Easy Shot than for Dog Shot; and therefore the f stops on all cameras were stopped down, and yellow filters were used for better contrast.

The complete technical data on Easy Shot are included in the field book. Data for airborne cloud-tracking photography are given in Tables 3 and 4.

5.3 George Shot

The necessary changes were made in the shutter operation of the camera at Stations 190 and 191 after George Shot time was changed from predawn to daylight. The K-8 cameras were operated with the shutters in time and set at the fastest speed available, $\frac{1}{180}$ sec. The frequency was varied from 3-sec intervals for

the first 3 min to 9-sec intervals for the next 20 min to 15-sec intervals for the remaining film (about 15 min).

The K-24 cameras at Stations 190 and 191 were changed from a night-shutter operation (which was used on previous shots) to $\frac{1}{450}$ -sec focal-plane shutter. The intervalometer was set at 2-sec intervals. This resulted (since the daylight setting was used) in an exposure every 2 sec (on night setting, which was used on Dog and Easy Shots, the camera required 2 pulses from the intervalometer to take one exposure; the first pulse would open the shutter, and the second pulse would actuate the capping shutter and energize the film transfer motor). In figuring the time basis for each negative on this shot, the frequency is one picture every 2 sec.

The gross light from the daytime test was apparently insufficient at the remote Station 192 on Rigili to actuate the controls, and therefore these cameras did not run.

The complete technical data on George Shot are included in the field book. Data on airborne cloud-tracking photography are given in Table 5.